

RAMAN RESEARCH INSTITUTE
THEORETICAL PHYSICS

DOCTORAL THESIS

**Fluctuations and large deviations in
non-equilibrium systems**

Deepak Gupta

*A thesis submitted to the Jawaharlal Nehru University
for the degree of Doctor of Philosophy*

January 2, 2019

Dedicated to my family.

Declaration

I, Deepak Gupta, hereby, declare that this thesis is the result of my original work at Raman Research Institute, Bangalore, India, under the guidance of Prof. Sanjib Sabhapandit. The content presented in this thesis has not previously formed the basis for the award of any degree, diploma, associateship, fellowship or any other similar title in any other University. I also declare that I have run this thesis through the Turnitin plagiarism software.


Prof. Sanjib Sabhapandit

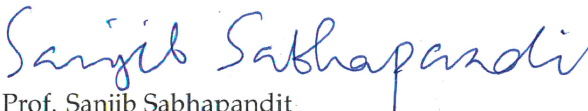

Deepak Gupta

Raman Research Institute
Bangalore 560080
India

Certificate

This is to certify that the thesis entitled "*Fluctuations and large deviations in non-equilibrium systems*" submitted by Deepak Gupta for the award of the degree of Doctor of Philosophy of Jawaharlal Nehru University is his original work. This has not been published or submitted to any other University for any other Degree or Diploma.

Prof. Ravi Subrahmanyam
Director
Raman Research Institute
Bangalore 560080
India


Prof. Sanjib Sabhapandit
Thesis Supervisor

Acknowledgements

Though this work will bear my name, without the unconditional support of many people, this would never have been possible.

Firstly, I would like to thank my thesis supervisor Prof. Sanjib Sabhapandit for his constant support over the past five years. His approach to tackling physics problems is always admirable. His valuable guidance and calm led me in finishing this work in the shape of a thesis. I learnt a lot from him, especially, patience when nothing is going well while solving a problem. His creative thinking always motivated me in understanding problems by considering simple systems which turned out to be very effective in certain cases. I was fortunate to have discussions with him.

I am thankful to Prof. Abhishek Dhar and Prof. Joseph Samuel for being part of my annual committee. Their valuable feedback and criticism motivated me to understand the problem from a different perspective. I am happy that I had the opportunity to discuss various scientific problems with them during the course of time. While working in theoretical physics student room, I was next door to Prof. Joseph Samuel, I had a great time discussing physics and mathematical problems with him.

I am also thankful to Prof. Supurna Sinha for many delightful discussions. She always taught me how to make an analogy of different problems in a very elegant ways. I would like to acknowledge Dr. Dibyendu Roy with whom I always enjoyed discussions on some specific physical systems that helped me to broaden my understanding towards areas which I was not aware of.

I do not want to forget Dr. Arnab Pal and Dr. V.V. Prasad who always helped me in academic and non-academic issues of my life. I always loved to discuss with them.

I would like to thank RRI sports committee for providing us useful resources. I am thankful to all cricket and football players with whom I spent beautiful time on the ground. Apart from that, I would like to acknowledge Nomaan, Santanu, Raj, Shivam, Anirudh, Alkesh, Rahul with whom I had constant discussion about studies and sports.

I am also thankful to Siman, Varun, and Nomaan who taught me swimming.

I have had a great time at RMV hostel. I can't forget late night parties, birthday celebrations, Sunday cookings, etc., which always cheered me up. I would like to acknowledge some of my friends who helped me in many aspects, namely, Nazma, Lijo, Mayuri, Reena, Manasa, Adhip, Sanjay, Deepshikha, Ayyapan, Sreyas, Sagar, Anidya, Nancy, Palak, Amrita, Chaitra, Shafi, Neha, Urbashi, Karam, Kartick, Abir, Swami, JK, Mari, Chandan, Venu, Irla, Ashwath, Pramod, Buti, Meera, Srija, Madhukar, Surya, Raj Prince, Sugandha, Shivani, Prachi, Sujit, Gayathri, Manasi, Radhika, Swati, Shanky, Athul, Abhishek, Ion, and many more.

I would like to acknowledge our group secretary Mr. Manjunath in assisting me for various administrative and accounts related issues.

I am also thankful to RRI library for providing me with scientific journals, books, xerox, scan, etc.

I would like to thank computer section which helped to resolve computer related problems.

It is worth mentioning the names of two beautiful institutes, RRI and ICTS, that always encouraged us to participate in several programs like short-term schools, workshops, meetings etc. These kind of discussion meetings and schools always helped me to understand various interesting physical problems.

I am also thankful to the Department of science and technology for providing the travel grant to visit Bruneck (Italy) to attend a summer school on "Fundamental Problems in Statistical Physics XIV (2017)".

I thank the Nordic Institute for Theoretical Physics (Nordita) for providing travel grant and accommodation support to attend the scientific program "Current and Future trends in Stochastic Thermodynamics" at Stockholm (Sweden).

I thank International Centre for Theoretical Physics (ICTP) for providing travel grant and accommodation support to attend the workshop "Advanced Workshop on Nonequilibrium Systems in Physics, Geosciences, and Life Sciences" at Trieste (Italy).

Finally, and most importantly, I want to thank Ms. Anjali Sharma for her constant love, support, and encouragement. I admire her positive and clear thoughts about life. I always love to discuss various issues and problems in the society, and most importantly, how can we resolve them using our economical and educational

supports with her. From the academic perspective, she is an excellent researcher. She is always a cheering friend of mine. I am very fortunate to have such a friend. I thank Mr. Yogendra Sharma and Mrs. Geeta Sharma for their wishes. I am grateful to my father and elder brother who have always given me the freedom to choose my path.

Synopsis

Equilibrium thermodynamics is one of the successful theories of all time. It encapsulates the phenomena of large macroscopic systems which are in thermal equilibrium. When two systems are in equilibrium with each other, and a third system is brought in contact with either of these two by a diathermal wall, then, all of them will reach in an equilibrium state. This principle is referred to as the *zeroth law of thermodynamics*. As a consequence, it helps to define an empirical temperature such that systems are in an equilibrium state will have the same temperature. In terms of conservation of energy, the *first law of thermodynamics* states that change in the internal energy is the sum of the amount of work done on the system and the heat supplied to the system. There are several processes which obey the first law of thermodynamics, but they do not occur in nature. For example, heat never flows from a cold body to a hot body. The *second law of thermodynamics* incorporates such observations in the thermodynamics and defines a state function called *entropy* which characterizes the irreversibility of a process. For an isolated system in the equilibrium, the entropy attains a maximum value. These laws of thermodynamics are well understood from the microscopic degrees of freedom of a system in a well-established framework known as *equilibrium statistical mechanics*. In this context, the probability of the system to find in a given configuration is expressed as Gibbs-Boltzmann weight. Moreover, the macroscopic properties can be evaluated, in principle, from a normalization constant called the *partition function*. In contrast to equilibrium picture, non-equilibrium phenomena cover a much larger class of problems in science. These phenomena can be seen in biology, chemistry, physics, mathematics, ecology, financial markets, etc. Because of driving fields such as temperature or chemical potential gradient, shear flow, external time-dependent fields, etc., these systems are not in the equilibrium state. Such driving fields are known as affinity or generalized force. There is no such general theory present which describes the methodology to study the observable properties of the system away from equilibrium. Nevertheless, linear irreversible thermodynamics is a very helpful tool to understand the physics of systems which

are close to equilibrium. The foundation of linear irreversible thermodynamics is based on time-reversal invariance principle and the postulates of equilibrium thermodynamics. Within this context, one can write the rate of entropy production as the sum of the product of each flux with its associated affinity (generalized force). For *purely resistive systems*, each local flux depends upon instantaneous values of *all* affinities. If affinities are so small, each local flux is related to all of them through *kinetic coefficients* linearly. These kinetic coefficients depend upon the local intensive parameters of the system. Moreover, in the linear regime, one can study Thomson effect, Peltier effect, Seebeck effect, etc. In the case of *non-purely resistive systems*, local flux depends upon the value of affinities at the instantaneous as well as the previous times, i.e. systems have memory. Here, one can study the properties of the system using the fluctuation-dissipation theorem or Kubo formula. When these systems are far away from equilibrium, there is no such non-equilibrium counterpart of the equilibrium partition function with which one can compute the observable properties.

This thesis compiles a set of physical problems where the systems under observation are in microscopic scale. These small systems can be biopolymers (like DNA, RNA, protein molecules), enzymes, Brownian particle, Brownian motors, small scale heat engine, small electronic systems, etc. As the system size reduces, fluctuations present in the surrounding bath perturb the deterministic behaviour of the system. Nevertheless, the probabilistic nature of these small systems can be exactly understood by Fokker-Planck or master equation. These equations play an essential role to write down the evolution of the probability of each configuration visited by the system.

For a generic irreversible process, work done on the system is bounded below by the change in free energy of the initial and final states. Similar bound one can see for the entropy change between two states. *Fluctuation relations* extend these bounds into exact equalities. These identities are proven to be remarkable results in the area of non-equilibrium statistical mechanics. For example, Jarzynki's equality helps in the computation of free energy difference between two equilibrium states using work done in a non-equilibrium protocol. Fluctuation theorem relates the

probabilities of positive and negative entropy production in both steady and transient state. Earlier, it was assumed that the total entropy production is only due to the heat exchange by the system to the environment (*medium entropy production*) in a non-equilibrium process. This entropy production is found to be the ratio of path probabilities of the forward to that of the reverse process when the dynamics of the system is *microscopically reversible*. But later, it was found that the fluctuation theorem for total entropy production in the steady state is valid once we incorporate the entropy production of the system to the total entropy production. The entropy production of the system is called *entropy change* which occurs due to configurational change between the initial and final states. This theorem is independent of the driving protocol and is valid for all time.

While fluctuation relations display exciting results in the realm of non-equilibrium statistical physics, they do not give the insight of the individual probability distribution of stochastic quantities such as work done, heat flow, entropy, efficiency, etc. In particular, one is also interested in the large time statistics of these observables. In this thesis, we will focus on both the fluctuation theorem as well as the probability density of these stochastic quantities.

Fluctuation theorem for partial entropy production

Consider a system where a large number of degrees of freedom are interacting with each other. This given system is connected to a heat bath of constant temperature. Evidently, the total entropy production is zero, i.e. the system is in equilibrium. Suppose the whole system is driven by some external forces (these forces are explained above), then the total entropy production is not zero. Therefore, the total entropy production characterizes the non-equilibrium system and the measurement of it is quite essential. In the steady state, it satisfies the fluctuation theorem as mentioned above. In some experiments, it is possible to have some setup where entropy production is to be observed. In such settings, we have to understand the clear time-scale separations among the degrees of freedom. Based on time-scales of relaxation, we classify degrees of freedoms as *fast* or *slow* variables. In some earlier experimental

and theoretical studies, it was observed that the fluctuation theorem for total entropy production would hold once we observe *all* slow degrees of freedom. If one may not succeed to observe *all* relevant slow degrees of freedom of the system, the exact estimate of the total entropy production would be difficult. Thus, the fluctuation theorem for the total entropy production based on partial information may not hold. In some earlier studies, the order of violation of fluctuation theorem was observed to be proportional to the interaction parameter between the observed degrees of freedom and the hidden ones (which we cannot observe). When such an interaction parameter is taken to be very small called the *weak coupling limit*, the fluctuation theorem restores its form which is also a naive guess one can think of. On the contrary to that, in this thesis, we have considered some simple analytically tractable model systems where we estimate the violation of the fluctuation theorem even in the weak coupling limit. Therefore, it is essential to consider the hidden degrees of freedom even though these are weakly coupled to the observed ones. Moreover, we have given a recipe with which one can nullify the effect of the weak coupling of the hidden variables on the observed ones.

- A given system A is coupled to another system B of the same kind (both systems have same time-scale of relaxation), jointly called system C. The system C is in contact with the heat bath of a constant temperature. External forces (these forces can be correlated as well as uncorrelated with each other) are used to drive system C out of equilibrium and entropy is generated. Total entropy production by the coupled system C satisfies the fluctuation theorem in the steady state. The entropy production due to system A in the coupled system C is computed and shown that this entropy production does not obey steady state fluctuation theorem even in weak coupling limit which is a remarkable result.
- In one more setup, we have considered two Brownian particles (A and B) coupled via harmonic interaction. One of the particles (say A) is connected to a temperature gradient while the other one B is connected to one heat bath of a constant temperature. In general, all of these heat baths do not have same temperature. In the steady state, we compute the entropy production due to

particle A in the coupled system and show that it does not satisfy the fluctuation theorem in weak coupling limit.

- Consider two Brownian particles A and B and these particles are coupled by harmonic interaction. Both particles are confined in a harmonic trap. The whole system is immersed in the heat bath of a constant temperature. Both of these particles are driven by some external forces. It is shown that the entropy production by one of the particles in the coupled system in steady state, satisfies the fluctuation theorem in weak coupling limit.
- Suppose a Brownian particle is connected to two heat baths (B_1 and B_2) of different temperatures. Then, we couple the given particle to one more heat bath B_3 of a distinct temperature weakly. The observable is the total entropy production by the particle due to baths B_1 and B_2 in the steady state, and we show that it satisfies the fluctuation theorem when bath B_3 is weakly coupled to the particle.

Stochastic efficiency of an isothermal work-to-work converter engine

In thermodynamics, a heat engine is a machine used to do work by consuming energy in a cyclic process. The efficiency of any macroscopic engine (working substance $\sim 10^{23}$ particles) is limited by the Carnot's theorem. This bound is universal and does not depend on the nature of constituents of the engine. Recently, there has been a lot of research going on to investigate the nature of these heat engines in the microscopic scale. On this scale, thermal fluctuation predominates, and hence, observables such as work done, heat flow, entropy, efficiency, etc. become stochastic quantity. Therefore, the probability density function of the efficiency (ratio of output power to the input power) of a microscopic heat engine becomes a good candidate to examine. In this thesis, we extend this study by giving two simple model systems of such a microscopic engine which converts the input work to the output work.

- A Brownian particle is immersed in a heat bath of a constant temperature. For this system to function as an engine called *isothermal work-to-work converter engine*, we apply stochastic external forces. These forces are called drive and load forces. The function of the drive force is to drive the particle against the load force. Since the system is in the microscopic regime, work done by these forces are random variables. The efficiency of such engine defined as the ratio of output work to the input work, is also a stochastic variable. Using this setting, we analytically obtain the large but finite time probability density function of the stochastic efficiency.
- Consider an isothermal machine composed of two Brownian particles (say particle A and B) connected by a harmonic spring. A constant load is attached to particle A, and particle B is trapped in harmonic confinement whose minimum is dragged with a constant velocity. The distribution of work done on particle A, particle B, and on both particles together is obtained, and the corresponding transient fluctuation theorem is tested. Furthermore, the probability density function for the stochastic efficiency (output work/input work) of this machine is computed for all time.

Briefly, in this thesis, we have explored the problems where the system size is very small and is driven away from the equilibrium using some driving protocol. In the steady state (except Chapter 7), we computed the large deviation function as well as the probability density function of stochastic observables such as work done, heat flow, entropy, efficiency, etc. In Chapter 7, the probability density functions for work done and stochastic efficiency are studied in the transient regime.

Prof. Sanjib Sabhapandit

Deepak Gupta

Raman Research Institute

Bangalore 560080

India

Publications

1. Fluctuation theorem for entropy production of a partial system in the weak coupling limit, Deepak Gupta and Sanjib Sabhapandit, EPL 115, 60003 (2016).
2. Fluctuation theorem for partial entropy production in a coupled Brownian particle system, Deepak Gupta and Sanjib Sabhapandit, Manuscript in preparation.
3. Partial entropy production in heat transport, Deepak Gupta and Sanjib Sabhapandit, J. Stat. Mech. (2018) 063203.
4. Entropy production for partially observed system in a harmonic trap, Deepak Gupta and Sanjib Sabhapandit, arXiv:1710.11339.
5. Stochastic efficiency of an isothermal work-to-work converter engine, Deepak Gupta and Sanjib Sabhapandit, Phys. Rev. E 96, 042130 (2017).
6. Exact distribution for work and stochastic efficiency of an isothermal machine, Deepak Gupta, J. Stat. Mech. (2018) 073201.

Contents

Declaration	v
Certificate	vii
Acknowledgements	ix
Synopsis	xiii
Publications	xix
1 Introduction	1
1.1 Thermodynamics	2
1.2 Equilibrium statistical mechanics	2
1.3 Non-equilibrium statistical mechanics	4
1.4 Fluctuation relations	6
1.4.1 Fluctuation theorem	7
1.4.2 Jarzynski's equality	9
1.4.3 Crooks relation	10
1.4.4 Hatano-Sasa relation	11
1.5 Stochastic thermodynamics	11
1.6 Large deviation theory	13
1.6.1 Coin tossing experiment	13
1.7 Theoretical investigations on probability density function and fluctuation relations	17
1.8 Experimental investigations on probability density function and fluctuation relations	21
1.9 Outline of the thesis	23

2	Fluctuation theorem for partial entropy production in a coupled Brownian particle system	27
2.1	Introduction	28
2.2	Model	30
2.2.1	Total entropy production from particle A: partial and apparent entropy production	32
2.3	Steady state distribution $P_{ss}(U)$	34
2.4	Fokker-Planck equation and its general solution	37
2.5	Calculation for moment generating function	38
2.6	Probability distribution function and the fluctuation theorem	46
2.7	Single Brownian particle	47
2.8	Analysis for cumulant generating function $\mu(\lambda)$	48
2.9	Large deviation function and asymmetry function	55
2.9.1	Large deviation function	55
2.9.2	Second order discontinuity of the large deviation function	58
2.9.3	The asymmetry function and its discontinuity	59
2.10	Numerical simulation	65
2.11	Summary	66
3	Partial entropy production in heat transport	69
3.1	Introduction	69
3.2	Model	71
3.2.1	Partial entropy production	73
3.2.2	Apparent entropy production	74
3.3	Fokker-Planck equation	76
3.4	Calculation for moment generating function $Z(\lambda)$	78
3.5	Probability distribution function	85
3.6	Single Brownian particle in contact with two heat baths ($\delta = 0$)	86
3.7	Analysis for prefactor $g(\lambda)$ for $\delta \neq 0$	89
3.8	Analysis for cumulant generating function $\mu(\lambda)$ for $\delta \neq 0$	90
3.8.1	Gallavotti-Cohen symmetry for cumulant generating function $\mu(\lambda)$	95

3.9	Large deviation function, fluctuation theorem and asymmetry function	100
3.10	Numerical simulation	101
3.11	Summary	102
4	Entropy production for partially observed system in a harmonic trap	103
4.1.	Introduction	103
4.2.	Model	105
4.2.1.	Partial entropy production	106
4.2.2.	Apparent entropy production	108
4.3.	Fokker-Planck equation and its general solution	111
4.4.	Calculation of moment generating function	114
4.5.	Single Brownian particle in a harmonic trap	122
4.6.	Probability distribution function	123
4.7.	Large deviation theorem and fluctuation theorem	128
4.8.	Numerical simulation	130
4.9.	Summary	130
5	Effect of weakly coupled fast degrees of freedom on fluctuation theorem	133
5.1.	Introduction	133
5.2.	Model	134
5.3.	Fokker-Planck equation	137
5.4.	Probability distribution function	140
5.5.	Large deviation function and fluctuation theorem	142
5.6.	Summary	143
6	Stochastic efficiency of an isothermal work-to-work converter engine	145
6.1.	Introduction	145
6.2.	Model	149
6.2.1.	Example	152
6.3.	Fokker-Planck equation	153
6.4.	Joint Probability density function $P_t(W_1, W_2)$	157
6.4.1.	Analytic behavior of the correction term $g(\lambda_1, \lambda_2)$	159
6.4.2.	Case 1: Singularity contour is absent	163

6.4.3. Case 2: Singularity contour is present	163
6.4.4. Large deviation function and FT for joint distribution $P_t(W_1, W_2)$	164
6.5. Probability density function of Stochastic efficiency $P(\eta, t)$	165
6.5.1. Case 1: $g(\lambda_1, \lambda_2)$ does not have singularities	165
6.5.2. Numerical simulation	166
6.5.3. Case 2: $g(\lambda_1, \lambda_2)$ has singularities	166
6.5.4. Numerical saddle-point integration	169
6.5.5. Numerical simulation: Possibility I	170
6.5.6. Numerical simulation: Possibility II	170
6.6. Summary	170
7 Exact distribution for work and stochastic efficiency of an isothermal machine	173
7.1. Introduction	173
7.2. Model	175
7.3. Joint distribution $P_\tau(W_A, W_B)$	177
7.4. Transient fluctuation theorem for work done W_A and W_B	182
7.5. Transient fluctuation theorem for total work done on coupled system	186
7.6. Probability density function for stochastic efficiency $p_\tau(\eta)$	187
7.7. Summary	191
A Simulation technique	193
Bibliography	195

Chapter 1

Introduction

A macroscopic system obeys the laws of thermodynamics which are very well understood within the framework of equilibrium statistical mechanics. A system with a large number of degrees of freedom is characterized by a small number of macroscopic variables such as pressure, volume, entropy, magnetization, etc. When a system is in equilibrium with the surrounding environment, the probability of the system to be in a given configuration follows the Gibbs-Boltzmann distribution in which the normalization factor called the partition function is used to obtain the macroscopic variables. In contrast to the equilibrium system, non-equilibrium systems cover a broader area of science and can be seen in biology, physics, mathematics, ecology, chemistry, etc. Here, systems are constantly driven, and there does not exist a general platform from which the properties of the system can be understood. Instead, a large variety of methods can be seen for specific situations. For such a system, there arise several questions such as what is the analogue of the equilibrium probability measure or equivalently the partition function for non-equilibrium case, what are relevant observables to characterize the system, how to compute such observables, whether the system reaches a steady state, and if it does, what is the distribution of each configuration, can one find the distribution of the observables and associated the large deviation function, and do these distributions follow some universal behaviour? The answers to these questions will give us the basic understanding of the non-equilibrium system, and the development of a general theory which captures the methodology to tackle such problems is still in progress.

1.1 Thermodynamics

Thermodynamics [15, 58, 147] is the phenomenological theory to understand the properties of macroscopic systems of a large number of degrees of freedom. These macroscopic bodies are characterized by thermodynamic coordinates or state functions such as pressure, temperature, mass, volume, composition, magnetization, etc. Note that these state functions are well defined in the *equilibrium*. In general, thermodynamics provides the fundamental laws of the macroscopic system based on empirical observations. For example, the *zeroth law* states that when two systems are separately in equilibrium with the third one, all of them are in equilibrium with each other, i.e. they have the same empirical temperature. In terms of conservation of energy, the *first law of thermodynamics* defines a state function called *internal energy* which changes by addition of heat to the system and the amount of work done on the system. There are several processes which obey the law of conservation of energy, but they do not occur in nature. For example, heat flows from the hotter to the colder body, but the reverse process is never seen. Similarly, a book resting on the table does not jump from it by absorbing heat from the environment. These textbook examples show that certain processes run only in one direction. Therefore, the aim of the *second law* is to incorporate such observations in thermodynamics. It defines a state function called *entropy* which never decreases over time for an isolated system, i.e. entropy characterizes the irreversibility of processes. Can one understand these thermodynamic laws from a microscopic point of view? Why does some specific system show certain thermodynamic characteristics? Such questions can be understood within the framework of *statistical mechanics* [58, 78, 74]. It uses probability theory with the classical or quantum mechanical equations of motion of the microscopic degrees of freedom.

1.2 Equilibrium statistical mechanics

When a system is either isolated or in contact of reservoirs such as a heat reservoir, particle reservoir, pressure reservoir etc., *equilibrium statistical mechanics* is generally

applicable. Within this context, the macrostate of a system is specified by state variables such as number of particles, volume, temperature, internal energy, chemical potential, etc., depending upon the constraints imposed on the system. For a given constraint, one can write the probability of a configuration of the system, and the observable properties can be evaluated, in principle, from it. For example, *micro-canonical ensemble* is the collection of a large number of identical copies of an isolated system composed of N particles in a volume V . Since the system is not interacting with the surroundings, its energy U remains fixed. The postulate of *equal a priori probabilities* states that any member of the ensemble is equally likely to be in any one of the microstate. Therefore, the probability of the system to be in a given microstate is given as $P = \Omega^{-1}$, where Ω is the number of microstates. In practice, energy of the system is difficult to keep under strict control. Instead, a temperature T is a suitable quantity which can be measured accurately using a thermometer, and can be controlled by keeping the system in contact with a thermal bath of the constant temperature T , resulting ensemble is called *canonical ensemble*. Here, the probability of the system to be in a configuration of energy E_S is given by the Gibbs-Boltzmann distribution $P(E_S) = e^{-\beta E_S} / Z(\beta)$, where $\beta = 1/T$ and $Z(\beta)$ is the partition function. However, in some physical systems, there may arise a situation where the system not only exchanges energy E_S from the heat bath but also the number of particles N from the surrounding particle reservoir. Consequently, both E_S and N become fluctuating quantities. In such case, the probability of a system to be in a configuration having energy E_S and number of particles N is given by $P(E_S, N) = e^{-\beta(E_S - \mu N)} / Z_G(\beta, \mu)$, where $Z_G(\beta, \mu) = \sum_{N=0}^{\infty} \sum_{E_S|N} e^{-\beta(E_S - \mu N)}$ is the grand canonical partition function and μ is the chemical potential of the system.

In general, there can be a number of ensembles depending upon the constraints imposed on the system. Relaxing certain constraints allows the system to exchange extensive quantities such as volume, energy, number of particles, etc., with the surrounding environment. After a long time, the system and the surrounding achieve a constant value of intensive variables such as temperature, pressure, chemical potential, etc., and extensive variables still fluctuate around the equilibrium values. Thus, equilibrium statistical mechanics enables us not only to compute the ensemble average of the fluctuating extensive variables but also the magnitude of the fluctuations.

1.3 Non-equilibrium statistical mechanics

Consider an electrical conductor whose extremities are connected to a voltage source. When the voltage is non-zero, the electrical current flows through the electrical conductor. The analogy of this setup in the context of heat conduction is a thermal conductor whose ends are at different temperatures, and heat current flows across the thermal conductor. These are the simplest examples of the system away from equilibrium. In general, non-equilibrium phenomena cover a broader class of problems in science. These phenomena can be observed in biology, chemistry, physics, mathematics, ecology, financial markets, etc. Here, the systems are driven out of equilibrium by a continuous supply of energy from external agents such as temperature gradient, chemical gradient, shear flow, electric or magnetic fields, etc. The external field which drives the system is called *affinity* or generalized force. Within this context, one is interested in the processes occurring between states of the system under consideration. Equilibrium thermodynamics provides two methods where limited information about such a system can be deduced: (1) one can study the initial and final equilibrium states of the system, and understand the affect of the process, and (2) extremely slow processes are compared with quasi-static processes where the system is assumed to be in equilibrium at each point of the process (i.e. thermodynamic variables can be defined). But both of these methods do not furnish proper information about the rate of the physical processes. Nevertheless, *linear irreversible thermodynamics* (extension to equilibrium thermodynamics) is the framework where one can deduce the properties of the system close to equilibrium for which we can define thermodynamic variables *locally* [15]. It is based on the postulates of equilibrium thermodynamics and time-reversal invariance. Here, the rate of entropy production is found to be the sum of the product of each affinity and its associated flux. The nature of the flux depends upon the type of the system studied, i.e. purely or non-purely resistive system. In the case of purely resistive systems (for example, resistor), the local flux depends upon the instantaneous value of all affinities. When the affinities are small, the local flux is related to the *kinetic coefficients* which itself depends upon the intensive parameters. Moreover, the symmetry of kinetic coefficients is given by the *Onsager reciprocity theorem* using time-reversal symmetry. In the

linear regime, one can study Seebeck effect, Thomson effect, Peltier effect, thermoelectric effect, etc. For non-purely resistive system (for example, a circuit containing inductance or capacitance), the local flux depends on the instantaneous value of the affinities as well as their value in previous times. Here, the system properties can be obtained using the fluctuation-dissipation theorem or the Kubo formula [75, 86].

When the system is driven far away from equilibrium, the theoretical understanding of it is rather poor. However, for a subset of non-equilibrium systems obeying the *Markov property*, the time evolution of the probability of the system to be in each configuration is given by the master equation (e.g. discrete state system) and the Fokker-Planck equation (e.g. continuous state system) [70, 107, 45].

Consider a system characterized by a set of configurations $\{C_1, C_2, \dots, C_n\}$. Let the probability of the system to be in configuration C_j at time t to be $P(C_j, t)$. The given system makes a random transition from a given configuration to the other (i.e. stochastic evolution). Suppose at time t the system is in configuration C_j and jumps to the configuration C_i at time $t + dt$. Under the Markov property, the transition rate from C_j to C_i does not depend upon the previous history of the process, and is denoted by $W(C_j \rightarrow C_i) = W(C_i, C_j)$. For simplicity, we have considered time-independent transitions rates. The evolution of probability of the system to be in C_i is described by the following master equation

$$\frac{d}{dt}P(C_i, t) = \sum_{j \neq i} [W(C_i, C_j)P(C_j, t) - W(C_j, C_i)P(C_i, t)], \quad (1.1)$$

$$= \sum_{j \neq i} [J(C_j \rightarrow C_i) - J(C_i \rightarrow C_j)], \quad (1.2)$$

where in Eq. (1.1), the first term on right hand side is the *gain-term* due to the transition from all configurations C_j (where $j \neq i$) to C_i whereas the second term on the right hand side is the *loss-term* due to the transition from the configuration C_i to all C_j (where $j \neq i$). In Eq. (1.2), $J(C_i \rightarrow C_j) = W(C_j, C_i)P(C_i, t)$ is the probability current from configuration C_i to C_j . Equation (1.1) can be rewritten in the matrix form:

$$\frac{d|P(t)\rangle}{dt} = M|P(t)\rangle, \quad (1.3)$$

where the column vector is $|P(t)\rangle = [P(\mathcal{C}_1, t), P(\mathcal{C}_2, t), \dots, P(\mathcal{C}_n, t)]^T$ and the matrix M is called the *Markov* or *stochastic matrix* whose matrix elements are $M_{ii} = -\sum_{j \neq i} W(\mathcal{C}_j, \mathcal{C}_i)$, and $M_{ij} = W(\mathcal{C}_i, \mathcal{C}_j)$ for $i \neq j$. The Markov matrix has two important properties: (1) the off-diagonal and diagonal matrix elements have positive and negative values, respectively, and (2) the sum of the column matrix elements is equal to zero which indicates the conservation of probability. It also implies that the stochastic matrix has a left eigenvector $\langle \chi | = (1, 1, \dots, 1)$ with eigenvalue zero, i.e. $\langle \chi | M = 0$. Therefore, there also exists a right eigenvector $|\Phi\rangle$ with same eigenvalue (i.e. zero) for which $M|\Phi\rangle = 0$, i.e. $|\Phi\rangle$ is the stationary solution of the master equation which represent the stationary state of the system.

In the stationary state, the left hand side of Eq. (1.1) is identically zero. This implies that

$$\sum_{j \neq i} [J(\mathcal{C}_j \rightarrow \mathcal{C}_i) - J(\mathcal{C}_i \rightarrow \mathcal{C}_j)] = 0. \quad (1.4)$$

Two possibilities can be drawn from the above equation: either (1) the probability current between any pair of configurations is same, i.e. $J(\mathcal{C}_i \rightarrow \mathcal{C}_j) = J(\mathcal{C}_j \rightarrow \mathcal{C}_i)$ for all $\mathcal{C}_i, \mathcal{C}_j$ or (2) although the probability current between any pair of configuration is not same yet the total probability current vanishes (see above equation).

It follows from possibility (1) that

$$W(\mathcal{C}_i, \mathcal{C}_j)P_{eq}(\mathcal{C}_j) = W(\mathcal{C}_j, \mathcal{C}_i)P_{eq}(\mathcal{C}_i). \quad (1.5)$$

The above equation expresses the *detailed balance* property of the equilibrium system with the probability measure $P_{eq}(\mathcal{C}_i)$ of the configuration \mathcal{C}_i . On the other hand, possibility (2) indicates that the detailed balance does not hold, and there exists a stationary probability current between any two configurations in the stationary state and the respective state is called a non-equilibrium steady state.

1.4 Fluctuation relations

Equilibrium systems are well studied within the framework of equilibrium statistical mechanics. Linear irreversible thermodynamics deals with the system close to equilibrium. However, *fluctuation relations* go beyond the linear regime and are valid

for systems driven arbitrary far away from equilibrium. These relations include transient fluctuation theorem, steady state fluctuation theorem, Jarzynski equality, Crooks work-fluctuation theorem, Hatano-Sasa relation, etc. In the following subsections, we briefly discuss these fluctuation relations.

1.4.1 Fluctuation theorem

Evans et al. [32] performed molecular dynamics simulation of a certain number of disks in a shearing fluid in two-dimension, interacting with Weeks-Chandler-Anderson potential :

$$\Phi(r) = \begin{cases} \Phi_{\text{LJ}}(r) + \epsilon & \text{for } r < 2^{1/6}\sigma, \\ 0 & \text{otherwise.} \end{cases} \quad (1.6)$$

In the above equation, $\Phi_{\text{LJ}} = 4\epsilon[(\sigma/r)^{12} - (\sigma/r)^6]$ is the Lennard-Jones potential in which r is the inter-particle separation, σ is the value of r at which $\Phi_{\text{LJ}}(r) = 0$, and $-\epsilon < 0$ is the depth of the potential. The boundary conditions were taken to be Lees-Edwards periodic boundary conditions [33]. They analyzed the ratio of probability of induced shear stress in the direction and opposite to externally applied shear rate in the non-equilibrium steady state. These induced stresses are related to entropy production. The probability distribution function for entropy production is computed. The distribution follows a remarkable symmetry property where the probability of positive entropy production is found to be exponentially higher than that of the negative one. This relation ensures that the violation of the second law of thermodynamics appears for small intervals of time, and this violation decreases as time progresses, i.e. the system will appear as time-irreversible as the observation time increases. The above symmetry relation is called the *steady state fluctuation theorem*.

When the initial condition is chosen from a microcanonical ensemble, an anisotropy in the temporal evolution of reversible deterministic system is observed by Evans and Searles [34]. They found the ratio of weight of the trajectory segment to that of the anti-trajectory segment using similar type of molecular dynamics simulation as

in Ref. [32]. This observation concluded how irreversibility emerges with the observation time. It is shown that the entropy production follows the same symmetry property as that of the steady state fluctuation theorem with the difference that the present symmetry relation holds for any arbitrary time, and this theorem is called the *transient fluctuation theorem*.

Gallavotti and Cohen [39] theoretically studied a model of a shear fluid in two-dimensions, driven by a shearing rate into the non-equilibrium steady state. The whole system was coupled to a heat bath of constant temperature. While the boundary condition along the horizontal direction was chosen to be periodic, reflected boundary condition was taken along the vertical axis. Using the chaotic assumption for dynamics and time-reversal invariance, they proved the fluctuation theorem in the steady state. Moreover, the consistency of the chaotic hypothesis was tested by Gallavotti [40] by showing that the fluctuation theorems valid at an arbitrary driving field are the extension of the Green-Kubo formula and the Onsager reciprocity theorem in the limit of zero driving field.

Later, fluctuation theorem for a system obeying Langevin dynamics was proved by Kurchan [77], and the extension to this fluctuation theorem for the Markov process was proposed by Lebowitz and Spohn [82].

In contrast to the earlier study on transient fluctuation theorem where the initial ensemble was microcanonical and the dynamics was isoenergetic, Searles and Evans [118] generalized this theorem for an arbitrary initial equilibrium ensemble such as isokinetic ensemble, isothermal-isobaric, isoenergetic boundary-driven flow, etc. They argued that the transient fluctuation theorem converges to the steady state fluctuation theorem asymptotically in the large time limit, provided the system has a unique steady state. Numerical results were also given by them to support the possibility of the convergence.

In all of the above cases, fluctuation theorem has been understood when the system under investigation was in contact with a thermostat, and the given system was driven using mechanical fields. Later, Searles and Evans [117] considered a cell maintained out of equilibrium using a thermal gradient. For this system, they derived a fluctuation relation in terms of the logarithm of the ratio of the probability density function of the total time-average entropy production having positive and

negative values corresponding to the direction of thermal gradient and opposite to it, respectively, in the transient regime. Furthermore, they argued that if the steady state exists and is unique, the corresponding steady state fluctuation theorem will be satisfied asymptotically (in the large time limit). Some of these results are given in Ref. [35].

In brief, when a certain dissipation function A satisfies the fluctuation theorem, the ratio of the probability of A having values $+a$ to that of $-a$ is given by

$$\frac{P(A = +a\tau)}{P(A = -a\tau)} \sim e^{a\tau}. \quad (1.7)$$

In the above equation, the quantity A is an extensive quantity that scales with the observation time τ . Therefore, it is clear from Eq. (1.7) that as the observation time gets longer, the system will appear time irreversible which is consistent with the second law of thermodynamics. In the case of the transient fluctuation theorem, the sign \sim is replaced by the sign $=$ whereas for the steady state fluctuation theorem, the sign \sim implies the logarithmic equality:

$$\lim_{\tau \rightarrow \infty} \frac{1}{\tau} \ln \frac{P(A = +a\tau)}{P(A = -a\tau)} = a. \quad (1.8)$$

1.4.2 Jarzynski's equality

When some work is performed on a system (e.g. gas, rubber band, spins, etc.) by changing a parameter (e.g. length of the rubber band, volume of the cylinder constraint by a piston, external electric or magnetic field, etc.) with a finite rate, from standard thermodynamics we find that the average work done on the system is

$$\langle W \rangle \geq \Delta F, \quad (1.9)$$

where the angular brackets show the average over many realizations for a fixed protocol of variation of the parameters, and ΔF is the change in the free energy between the initial and final state. The difference between $\langle W \rangle$ and ΔF is the dissipated work during an irreversible process. Jarzynski [61, 60, 62] replaced the above inequality

with the following relation

$$\langle e^{-\beta W} \rangle = e^{-\beta \Delta F}, \quad (1.10)$$

where β is the inverse temperature of the heat bath. Equation (1.10) is independent of the path over which the protocol is being carried out as well as the rate of change of the parameter. One can utilize the above relation to compute the equilibrium free energy difference ΔF from the non-equilibrium work done. Notice that Eqs. (1.9) and (1.10) are related to each other by the Jensen's inequality: $\langle e^x \rangle \geq e^{\langle x \rangle}$.

1.4.3 Crooks relation

Jarzynski proved the relation (1.10) for systems obeying deterministic dynamics, and stochastic dynamics. The generalization of Jarzynski's equality was given by Crooks for microscopically reversible systems having Markovian dynamics [24, 25, 26]. He proved the following relation

$$\frac{P(i_0|\lambda_0)P_F(i_0 \xrightarrow{\lambda_1} i_1 \xrightarrow{\lambda_2} i_2 \xrightarrow{\lambda_3} i_3 \dots i_{t_f-1} \xrightarrow{\lambda_{t_f}} i_{t_f})}{\tilde{P}(i_{t_f}|\lambda_{t_f})P_R(i_0 \xleftarrow{\lambda_1} i_1 \xleftarrow{\lambda_2} i_2 \xleftarrow{\lambda_3} i_3 \dots i_{t_f-1} \xleftarrow{\lambda_{t_f}} i_{t_f})} = e^{\beta(W-\Delta F)}, \quad (1.11)$$

where i_t and λ_t label the internal state of system and the value of the externally controlled parameter at time t , respectively, and subscripts F and R correspond to the forward and reverse process, respectively. The probabilities of an initial equilibrium state for the forward and reverse process, respectively, are $P(i_0|\lambda_0)$ and $\tilde{P}(i_{t_f}|\lambda_{t_f})$ for a given parameter. Utilizing the above expression, Crooks found a remarkably beautiful symmetry relation for the work done called the *Work-Fluctuation Theorem*:

$$\frac{P_F(W)}{P_R(-W)} = e^{\beta(W-\Delta F)}. \quad (1.12)$$

Further, Crooks proved the Jarzynski equality by taking the ensemble average of $e^{-\beta W}$ using the above relation. Equation (1.12) is similar to the Evans-Searles fluctuation theorem [34]. While the former case corresponds to asymmetry in the distribution of forward and reverse trajectories emanated from respective initial equilibrium distributions, the latter relates the probability of trajectories to that of anti-trajectories starting from the same initial equilibrium distribution.

1.4.4 Hatano-Sasa relation

Oono and Paniconi [92] gave a framework called the *steady state thermodynamics*, to study the transitions between different non-equilibrium steady states. Using this framework, Hatano and Sasa [57] generalized the Jarzynski relation for transition between non-equilibrium steady states to $\langle e^{-\beta Q_{ex} - \Delta\phi} \rangle = 1$, where the angular brackets show the average over the set of all paths from the given initial steady state distribution $\rho_{ss}(x_0; \alpha_0)$ in which x_0 is the state of the system and α_0 is the set of control parameters at time t_0 . The quantity $\Delta\phi = -\ln \rho_{ss}(x_t; \alpha_t) + \ln \rho_{ss}(x_0; \alpha_0)$, and $Q_{ex} = Q_{tot} - Q_{hk}$ is the excess heat associated with the transition between different steady states due to the variation of the parameter α , Q_{hk} is called the *house keeping heat* which continuously dissipates to maintain the non-equilibrium steady state at a fixed parameter α , and Q_{tot} is the total heat. Note that in equilibrium, the house keeping heat vanishes and the excess heat becomes the total heat [57, 116].

1.5 Stochastic thermodynamics

Consider a gas of classical particles confined in a cylinder. The evolution of these particles is governed by the *Newton's equation of motion*. In principle, properties of the system can be derived from the solutions of the Newton's equations or from the deterministic trajectories of the system. Since these equations of motion are time-reversible, there do exist anti-trajectories which obey the same equations of motion. For a reversible system, probability of trajectories and that of anti-trajectories should be equal, and the ratio quantifies the irreversibility of a system. According to the second law of thermodynamics, the probability of anti-trajectories should be equal to *zero*. Therefore, one of the central questions in statistical mechanics is how does irreversibility emerge from the reversible dynamics of the system? One of the successful attempts in this direction are the fluctuation relations. These relations shed light on the irreversibility of a system which emerges when the system size or observation time is large. At these observation scales, the probability of trajectories violating the second law is vanishingly small, i.e. the second law holds for large system or at large observation time.

As the system size reduces, fluctuations become predominant, and the trajectories violating the second law of thermodynamics appear more frequently as compared to a large scale system. Therefore, a lot of research is going on in understanding fluctuation relations using small-scale systems such as a Brownian particle (colloidal particle), DNA molecules, proteins chains, enzyme molecules, small chemical networks, molecular motors, etc. Within this context, *stochastic thermodynamics* [123, 125, 3] extends the notion of work, heat, etc., for small-scale system at the level of stochastic trajectories of a non-equilibrium ensemble where the change in the internal energy, heat dissipation, and the work done follow the energy conservation principle (first law of thermodynamics).

For a macroscopic system, the second law of thermodynamics sets a bound on the entropy change between two states, i.e. it always remains non-negative. The fluctuation theorem extends this bound into an exact equality. It gives the symmetry relation between the probability of positive entropy production and that of negative entropy production. Positive entropy production corresponds to those trajectories which obey the second law of thermodynamics while trajectories violating the second law belong to negative entropy production. It suggests that there should also be a notion of entropy at the level of a single trajectory. Seifert [121, 120, 122] identified the entropy production along a single stochastic trajectory of the non-equilibrium process. This entropy production consists of two parts: the entropy production in the bath ΔS_{med} due to the heat exchanged by the system and the bath, and the entropy production of the system ΔS_{sys} . The sum of these two parts is called the *total entropy production* $\Delta S_{tot} = \Delta S_{sys} + \Delta S_{med}$. In the initial derivations of the fluctuation theorem, it was assumed that the total entropy production is only due to ΔS_{med} . This is because the entropy production of the system ΔS_{sys} does not scale with time and hence it does not contribute to ΔS_{tot} for a system having bounded energy in the long time limit. Therefore, the fluctuation theorem for ΔS_{med} tends to hold as observation time increases. When both of these parts (ΔS_{sys} and ΔS_{med}) are considered, the total entropy production ΔS_{tot} in the non-equilibrium steady state obeys the following fluctuation theorem

$$\frac{P(\Delta S_{tot})}{P(-\Delta S_{tot})} = e^{\Delta S_{tot}} \quad (1.13)$$

for all time. From the above equation, one can recover the *integral fluctuation theorem*: $\langle e^{-\Delta S_{tot}} \rangle = 1$ which also implies $\langle \Delta S_{tot} \rangle \geq 0$. It implies that on average, the second law of thermodynamics is valid.

In the following section, we give a brief introduction to a framework which is helpful in obtaining the probability density function of stochastic quantities.

1.6 Large deviation theory

In this thesis, we focus on small systems driven out of equilibrium. Since fluctuations play a significant role, the value of an observable varies from one realization to the other. Hence, they have a probability distribution function instead of a sharp peak at the most probable value. Unlike equilibrium statistical mechanics, there is no general rule to obtain the probability distribution of observables of the driven system. Therefore, one has to compute them from first principles. Within this context, *Large Deviation Theory* [136] is a remarkable framework where one may obtain them. This theory was initiated by Cramér in 1930, and developed by Donsker and Varadhan and by Freidlin and Wentzell. The framework deals with the exponential decay of the probability distribution of the stochastic processes, and is the extension or refinement of the *Central Limit Theorem*, the law of large number, etc. In the following, we give an example to understand the connection between large deviation theory and the central limit theorem.

1.6.1 Coin tossing experiment

Consider an experiment where N unbiased coins are tossed. Let N_H and N_T be the number of heads and tails, respectively, such that $N = N_H + N_T$. Since the coins are unbiased, the probability of getting either a head or a tail for a single coin is equal, i.e. $P_H = P_T = 1/2$. Now, the question is, what is the probability of getting H number of heads?

We associate a random variable x_i with the i th coin such that $x_i = 1$ when head appears, and 0 otherwise. Thus, the total number of heads is $N_H = \sum_{i=1}^N x_i$. The mean number of heads μ and variance σ^2 are given by $\mu = \langle N_H \rangle = N/2$ and $\sigma^2 = \langle N_H^2 \rangle - \langle N_H \rangle^2 = N/4$.

The distribution of the number of heads in the large N limit is given by the central limit theorem [136]

$$P_{CLT}(N_H = H, N) \approx \frac{1}{\sqrt{2\pi\sigma^2}} \exp\left[-\frac{(H - \mu)^2}{2\sigma^2}\right]. \quad (1.14)$$

However, the exact probability of getting $N_H = H$ number of heads is given by the binomial distribution:

$$P_{BD}(N_H = H, N) = \frac{N!}{2^N H!(N - H)!}. \quad (1.15)$$

The probability of exactly N heads (large fluctuations) obtained from Eqs. (1.14) and (1.15) are $P_{CLT}(H = N, N) \approx e^{-N/2}$ and $P_{BD}(H = N, N) = e^{-N \ln 2}$, respectively. Therefore, it is clear that the central limit does not give the correct result far from $H = \mu + O(\sqrt{N})$.

In the large N limit, we can use the Stirling formula ($N! \approx N^N e^{-N} \sqrt{2\pi N}$) to approximate Eq. (1.15) which gives the probability density function for a fraction of heads $r = H/N$

$$p(r) \approx \frac{\sqrt{N}}{\sqrt{2\pi r(1-r)}} e^{NI(r)}, \quad \text{where} \quad (1.16)$$

$$I(r) = -[r \ln r + (1-r) \ln(1-r) + \ln 2] \quad (1.17)$$

is the *large deviation function* [136] in which $r \in (0, 1)$. It can be seen that $I(r^*) = I'(r^*) = 0$ at $r = r^* = 1/2$. The expansion of the large deviation function $I(r)$ about $r = r^*$ yields $I(r = r^*) = -2(r - 1/2)^2 + \dots$. Therefore,

$$p(r) \approx \sqrt{\frac{2N}{\pi}} e^{-2N(r-1/2)^2}. \quad (1.18)$$

The above equation is the same as given by Eq. (1.14). In Fig. 1.1(a), we show the comparison of the analytical results given by Eq. (1.16) and analytical results obtained from the central limit theorem (1.18) with the numerical simulation. From the figure, it is clear that the result obtained from the central limit theorem is valid for $r = 1/2 + O(1/\sqrt{N})$. One more observation one can draw from Fig. 1.1(b) is that as the number of coins N increases, the fraction of heads r converges to a typical value $r^* = 1/2$. This implies $N_H/N \rightarrow 1/2$ as $N \rightarrow \infty$ (*Law of large number*).

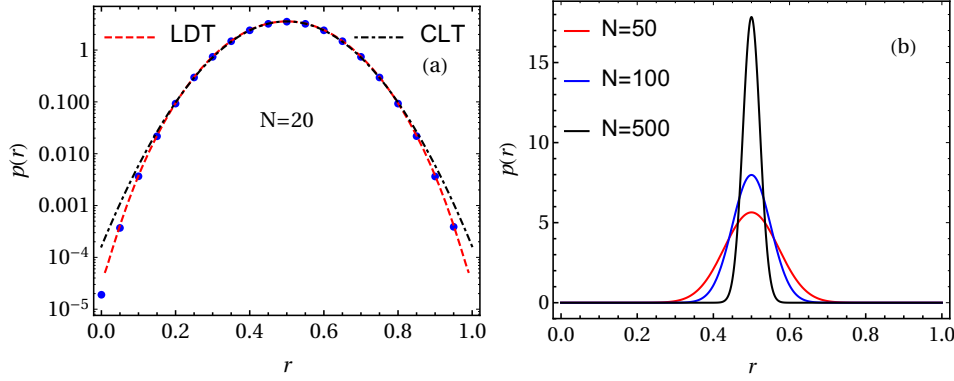


FIGURE 1.1: (a): The probability density functions $p(r)$ given by Eq. (1.16) (red dashed line) and Eq. (1.18) (black dotdashed) are plotted against the fraction of heads r . Blue dots are obtained from numerical simulation. In figure, LDT and CLT represent the large deviation theory and central limit theory results, respectively. (b): Figure indicates that the probability density function $p(r)$ given in Eq. (1.16), concentrates around the typical value of the fraction of heads, i.e. at $r^* = 1/2$, as the number N increases.

The probability $p(r) \approx e^{NI(r)}$ for large N , is an example of the large deviation form of the distribution in which the large deviation function $I(r)$ captures both typical as well as atypical fluctuations of r around its most probable value.

In the above example, we knew the exact distribution, and were also able to write down the large deviation form of distribution using the Stirling approximation. In general, it may not be possible to obtain the probability distribution of certain stochastic observables which involve continuous random variables, non-IID (independent and identical) random variables (discrete and continuous), etc., by either computing directly or using of approximation formulae such as the Stirling formula. Nevertheless, Gärtner-Ellis theorem [136] provides a platform to obtain the large deviation form of distribution which is summarized as follows.

For a random variable Ω , the scaled cumulant generating function is given by

$$\mu(\lambda) = \lim_{N \rightarrow \infty} \frac{1}{N} \ln \langle e^{-\lambda \Omega} \rangle, \quad \text{where} \quad \lambda \in \mathbb{R} \quad (1.19)$$

and

$$\langle e^{-\lambda \Omega} \rangle = \int e^{-\lambda \Omega} P(\Omega) d\Omega. \quad (1.20)$$

If $\mu(\lambda)$ exists and is differentiable for all λ , then Ω satisfies the large deviation principle, i.e. $P(\Omega = \omega N) \approx e^{NI(\omega)}$. The *large deviation function* $I(\omega)$ is related to the

scaled cumulant generating function $\mu(\lambda)$ using the Legendre transform

$$I(\omega) = \mu(\lambda^*) + \lambda^* \omega, \quad (1.21)$$

where $\lambda^*(\omega)$ is the saddle point solution of the following equation

$$\left. \frac{\partial \mu(\lambda)}{\partial \lambda} \right|_{\lambda=\lambda^*} + \omega = 0. \quad (1.22)$$

In the following, we compute the probability distribution of the number of heads N_H of the above given problem of the coin tossing experiment using the large deviation theory. The scaled cumulant generating function corresponding to $N_H = \sum_i x_i$ is given by [using Eq. (1.19)]

$$\mu(\lambda) = \lim_{N \rightarrow \infty} \frac{1}{N} \ln \langle e^{-\lambda \sum_i x_i} \rangle. \quad (1.23)$$

Since the x_i 's are independent of each other, we write

$$\mu(\lambda) = \lim_{N \rightarrow \infty} \frac{1}{N} \ln \prod_i^N \langle e^{-\lambda x_i} \rangle. \quad (1.24)$$

In our case, x_i^s are drawn from an identical distribution, and attain values 0 and 1 with equal probability (i.e. probability for each outcome is equal to 1/2). Thus, we get

$$\mu(\lambda) = \ln \langle e^{-\lambda x} \rangle = \ln \frac{1 + e^{-\lambda}}{2}. \quad (1.25)$$

Therefore, the large deviation function $I(r)$ given in Eq. (1.17) can be obtained using Eq. (1.21), where the saddle point $\lambda^*(r) = \ln \frac{1-r}{r}$ in which $r = N_H/N$. Thus, the large deviation form of the distribution is given by $p(r) \approx e^{NI(r)}$.

In equilibrium statistical mechanics, properties of many particle systems are described at the probabilistic level by statistical ensembles such as microcanonical ensemble, canonical ensemble, etc. In the thermodynamic limit, the probability of outcome of a macrostate concentrates around the *typical* value. Within the framework of large deviation theory, the probability of outcome of a macrostate follows the large deviation principle as it attains a sharp peak at the most probable or equilibrium

value in the limit of large number of constituents particles. Moreover, the probability of departure from the equilibrium value is exponentially small as the number of particles increases. Therefore, the study of equilibrium states and their fluctuations in an ensemble is reduced to the study of large deviation functions. It turns out that the entropy functions and the free energies are actually the large deviation function and scaled cumulant generating function, respectively, and both of them are related by the Legendre transform.

The analogy of equilibrium and non-equilibrium statistical mechanics can be made by identifying an extensive parameter such as number of particles, volume of the container, etc. as in the equilibrium picture. For dynamical systems, *time* serves as an extensive parameter which controls the large deviation principle. Driven systems can be of two types: (1) the state of the system has non-stationary probability distribution function for all time, and (2) the system reaches the steady state in the long time limit. In this thesis, we focus on systems of type (2) and compute the observables in the steady state (except in Chapter 7 where we compute the observables in the transient regime). Even for this type of system, a general principle to obtain the state's probability from the knowledge of system invariants or external constraints is not known. To understand the observable statistics of a driven system, we first need to find the probability of state of a system from first principles. Once this is known, using the large deviation principle, one can obtain the large deviation form of the probability density function of the observable that are functionals of state of a system.

In the following, we give a brief overview of both recent theoretical and experiment studies on the fluctuations of stochastic quantities in non-equilibrium systems.

1.7 Theoretical investigations on probability density function and fluctuation relations

Mazonka and Jarynski [88] proved the non-equilibrium work relation for free energy differences, transient fluctuation theorem, steady state fluctuation theorem, and detailed fluctuation theorem for time average entropy production using a Brownian particle in a harmonic trap whose center was moved with constant velocity in a heat

bath of constant temperature. Farago [36] identified injected and dissipated powers to a Brownian particle from the Langevin equation, and computed the probability density function for these powers using the path integral formalism. Moreover, the large deviation functions were also computed, and it was shown that the large deviation function does not depend on the pinning potential to the Brownian particle. In Ref. [150], stationary and transient work fluctuation theorems were investigated for a Brownian particle trapped in a harmonic confinement whose center was moved with a given velocity in a heat bath. Subsequently, an extension to the steady state fluctuation theorem for heat absorption by a Brownian particle was given in Refs. [151, 149]. For non-equilibrium chemical reactions with time-independent rates, the fluctuation theorem was studied by Gaspard [42]. Similarly, a fluctuation theorem for an enzyme was shown in Ref. [119]. Speck and Seifert [128] used a model of a colloidal particle in a periodic potential, driven by a time-dependent force. The periodic potential was modulated by an externally controlled time-dependent parameter. They have shown that the house keeping heat satisfies an integral fluctuation theorem: $\langle e^{-\beta Q_{hk}} \rangle = 1$. Gomez-Marín and Sancho [47] studied a model of a Brownian transducer to observe the heat flow, and analyzed the exchange fluctuation theorem. In Ref. [143], the probability density function and the large deviation function for a heat flow from the hot bath to a Brownian particle is studied by Visco in a model of a Brownian particle coupled to two heat baths of distinct temperatures. It was shown that tails of the large deviation function are strongly influenced by the initial conditions (either fixed initial condition or drawn from a steady state distribution) even in the infinite time limit. Consequently, a modification of the fluctuation theorem for time average flux was observed. Touchette and Cohen [135] studied the statistics of work done on a Brownian particle confined in a harmonic trap whose minimum was moved with constant velocity in the fluid having Lévy noise. In this case, authors computed the distribution of work done in the stationary state, and showed that it has *fat* power law tails which cause the violation of the conventional fluctuation theorem. Taniguchi and Cohen [134] used a Brownian particle confined in a harmonic trap as a model. The system was maintained in a non-equilibrium steady state by moving the trap with constant velocity in the fluid at a constant temperature. Using this model, they extended the Onsager-Machlup

theory in the non-equilibrium domain and the entropy production rate was introduced using path probability. Moreover, the energy conservation law and second law of thermodynamics were derived by them in non-equilibrium thermodynamics, and the extended fluctuation theorem for heat flow was also studied for this model. Jayannavar and Sahoo [63] considered a model of a charged particle confined in a two-dimensional harmonic trap in the presence of a magnetic field. This setup was in contact with a heat reservoir at a constant temperature. The work distribution was computed using two non-equilibrium protocols: the minimum of the potential was dragged with constant velocity, and an AC field was applied to the charged particle in one direction. For both cases, Jarzynski's equality was verified, and they showed that this equality is consistent with the Bohr-van Leeuwen theorem which states that there will be no diamagnetism for a classical statistical system. For Markovian dynamics, Harris and Schütz [56] proved fluctuation relations such as integral fluctuation relation for entropy, Jarzynski equality, Crooks fluctuation theorem, Evans-Searless fluctuation relation, etc. In contrast to earlier work by Taniguchi and Cohen where only the transient fluctuation theorem was discussed [134], in Ref. [132], authors studied the fluctuation theorem in the non-equilibrium steady state of work done on a harmonically confined Brownian particle dragged in a fluid, and the effect of an inertial term (ratio of mass to friction constant) is also studied. Subsequently, using the extended Onsager-Machlup theory for a non-equilibrium steady state, authors identified work done and heat flow in the non-equilibrium process [133, 22]. Saha and Jayannavar [111] studied Jarzynski equality and Crooks fluctuation theorem using a model of a charged particle in a two-dimensional harmonic trap in the presence of a time-dependent magnetic field. Mehl et al. [90] used a model of a colloidal particle driven along the toroidal geometry into a non-equilibrium steady state using a constant force. In addition to that, a periodic potential was also introduced. The large deviation function for entropy production in the bath was studied in this model, and they showed that the large deviation function has the *kink* behaviour at *zero entropy production* for an appropriate choice of external force and amplitude of the periodic potential. Baule and Cohen [4] extended the work given in Ref. [135] by considering the statistics of noise from the bath to be an asymmetric Poissonian shot noise. They computed the large deviation of work distribution and

the corresponding fluctuation theorem in the non-equilibrium steady state. Using a similar model given in Ref. [63], with the modification that the minimum of the potential was now moved with an arbitrary time-dependent manner, Jiménez-Aquino et al. [65] computed the statistics of total work done on a Brownian particle by the harmonic force, and the corresponding transient fluctuation theorem for it was analyzed. Moreover, results were compared with the Ref. [63]. Furthermore, the statistics of work done on a Brownian particle and total entropy production for a model system of a Brownian particle confined in a two-dimensional trap driven by electromagnetic field were studied by Jiménez-Aquino et al. [66, 64]. Lahiri and Jayannavar [80] considered a Brownian particle in a double well potential, driven by a periodic force, and computed numerically the integral and detailed fluctuation theorems for the total entropy production in the non-equilibrium time periodic state. In another work, Saha et al. [112] used a model system of a harmonically confined Brownian particle in a fluid at a constant temperature. Two driving protocols in the theory were used: the particle was driven by an external time-dependent force, and the minimum of the potential was dragged with an arbitrary time-dependent protocol. They have argued that the total entropy production satisfies the detailed fluctuation theorem even in the transient regime when the initial distribution of the system is a canonical one. For a harmonic chain connected to two heat baths of distinct temperatures, Kundu et al. [76] studied the statistics of heat flow across the harmonic chain. Sahoo et al. [113] computed the probability density functions for classical work, thermodynamic work, total entropy production, and dissipated heat, and showed that the most probable values of thermodynamic work and total entropy production occurred in atypical regime (the regime which is absent for macroscopic systems) while for the other two observables, peaks were found in the typical regime. Using Darrida-Brunet approach, the heat fluctuation for a harmonically bound Brownian particle connected to two heat baths was observed by Fogedby and Imparato [37], and it was shown that the large deviation function is insensitive to the strength of the confining potential. Later, authors of Ref. [38] computed the statistics of heat flow through the harmonic chain connected to two heat baths of distinct temperatures. Saito and Dhar [115] computed the cumulant generating function for heat flow

through a three-dimensional cubic crystal whose ends were coupled with heat reservoirs of different temperatures and showed that the cumulant generating function satisfies Gallavotti-Cohen symmetry. Sabhapandit [110, 109] obtained exact probability density function and large deviation function in the non-equilibrium steady state for heat flow across the harmonic oscillator driven by a thermal gradient, and for work done on the harmonic oscillator driven by an external stochastic force, coupled to a heat bath. Pal and Sabhapandit computed the exact expression for the large deviation function and probability density function for work done on a harmonically coupled Brownian particle whose minimum was modulated by Ornstein-Uhlenbeck (OU) process in the overdamped regime [94], and for a free Brownian particle driven by OU process in the underdamped regime [93]. Consequently, for both cases, validity of work fluctuation theorem was shown in the parameter space. In contrast to deterministic driving protocol, two models where a two-level system is coupled to another two-level system, and an OU process coupled to another OU process, were studied by Verley et al. [140] to understand work statistics. Recently, a transient exchange fluctuation theorem for heat was proven by Pal et al. [95] within the framework of Hamiltonian dynamics in both classical and quantum regimes.

1.8 Experimental investigations on probability density function and fluctuation relations

Wang et al. [144] tested the integrated transient fluctuation theorem by dragging a optically trapped micron-sized transparent particle in a solvent of constant temperature. They observed appreciable violations of the second law of thermodynamics for a small system and for short time. Theoretical studies based on this model are given in Refs. [150, 151, 149]. Hatano-Sasa relation which deals with the transition between different steady states was tested by Trepagnier et al. [138] by moving a microscopic bead which was optically trapped in a harmonic confinement, in the water. van Zon et. al [148] made an analog of the experiment done by Wang et al. [144] onto an electrical circuit, and tested the transient and stationary state fluctuation theorems for heat and work done. A setup similar to Ref. [144] was used by Carberry et al. [16] to test the transient fluctuation theorem in which strength

of the stationary optical trap was changed discontinuously, and entropy production was observed from the relaxation of a colloidal particle by changing the strength of the trap. Wang et al. [145] used similar setup of an optically trapped particle [144], the minimum of the trap was now translated linearly and circularly, and the fluctuation theorem in the stationary state was observed. Using an experimental setup consisting of a resistor and capacitor connected in parallel, and driven away from equilibrium by supplying electrical current, Garnier and Ciliberto [41] observed the fluctuations of injected power in the circuit and the dissipated power in the resistor. The fluctuation theorem for these quantities was also studied by them. Douarche et al. [30, 28] considered a mechanical torsional pendulum made of a brass wire with a mirror glued in the middle of it. The whole setup was immersed in a cell filled with a fluid having definite viscosity. A small electric coil was fixed with the brass wire in the back of a mirror, and two magnets facing each other with the opposite poles in front of each other were placed. The system was set out of equilibrium by varying the electric current through the coil. In this setup, they verified the Jarzynski equality and Crooks fluctuation theorem, and showed that these results were found to be independent of the amplitude of the driving, dissipation, and the rate of the driving protocol. Subsequently, the same setup was utilized to understand the transient and steady state fluctuation theorem for work done [29] on the torsional pendulum. Blickle et al. [8] tested experimentally the stochastic formulation of the first law, Jarzynski equality and work fluctuation theorem for a colloidal particle in a time-dependent non-harmonic trap. Speck et al. [129] studied the distribution and fluctuation theorem of total entropy production in the non-equilibrium steady state in an experiment consisting of a colloidal particle in a periodic potential trapped in a toroidal geometry and driven by a constant external force. Imperato et al. [59] used a model where a Brownian particle (overdamped regime) was in a heat bath driven by a time-dependent potential, and computed the probability density function for work and heat flow analytically and verified these results in the experiment. Joubaud et al. [67] used the setup given in Ref. [30] to compute the probability distribution of work done and the heat in both stationary and transient regimes, and tested the corresponding fluctuation theorems. Using the experimental setups given in Refs. [41, 30], authors [68] studied the fluctuation theorem for total entropy production in

the non-equilibrium stationary state. Ciliberto et al. [21] measured the fluctuations of heat flux and the entropy production in a coupled electric circuit in the presence of thermal gradient. Bérut et al. [14] used two hydrodynamically coupled Brownian particles in two separate optical quadratic confinements. The hydrodynamic coupling between particles was due to the motion of the surrounding fluid. One of the traps was driven using stochastic driving which yielded a temperature gradient among the particles. The energy flow and correlation of positions were studied in this experiment, and compared with the analytical results. Subsequently, the same experimental setup was used to understand the stationary and transient fluctuation theorem for heat flux by Bérut et al. [6]. Gieseler et al. [44] used a vacuum trapped nanoparticle to analyze the validity of the fluctuation theorem for relative entropy change occurring during the relaxation from the non-equilibrium steady state. In Ref. [146], authors experimentally showed that entropy production in the case of strongly coupled plasmas, satisfies the fluctuation theorem. Some brief reviews on fluctuation theorems with theoretical and experimental investigations are given in Ref. [20, 19, 18, 108, 13].

1.9 Outline of the thesis

In this thesis, we have focused on small systems immersed in a heat bath at constant temperature. Since the length scale of the system is small, fluctuations play a significant role in the dynamics of these small systems. The evolution of the configuration of a system is governed by the Langevin equation. In the absence of external driving, the system remains in the equilibrium state as it does not produce entropy. These systems can be maintained out of equilibrium by driving them using external sources such as time-dependent fields, stochastic driving, deterministic driving, shear flow, periodic driving, etc. Similarly, a system can also be driven by connecting its ends to a temperature or chemical potential gradient. Here, we have considered those systems which are either driven by stochastic driving or by thermal gradient into the non-equilibrium steady state (except Chapter 7).

In non-equilibrium statistical mechanics, fluctuation theorems are the symmetry

relations obeyed by the probability density function of the certain stochastic observables such as total entropy production, entropy change in the medium, heat flow, work done, etc. When these relations hold, the symmetry properties or the fluctuation theorems are independent of the system and the choice of driving protocol considered. In contrast to this, the probability density functions of these observables do not have universal behavior, i.e. these are system specific and also depend upon the choice of external driving. In past two decades, several attempts have been made to estimate the probability density functions and the large deviation functions of certain observables in different systems along with different choices of external forces (see Secs. 1.7 and 1.8). The aim of this thesis is to extend our theoretical understanding of the distribution of stochastic observables and their fluctuation relations.

Consider a system consisting of many interacting degrees of freedom in a heat bath of constant temperature. The relaxation time of the bath molecule is much smaller than that of the individual degrees of freedom of the system. We refer to the system and the bath degrees of freedom as *slow* and *fast* variables, respectively. In the presence of external driving, the system produces entropy. Evidently, the total entropy production of the system in the steady state satisfies the fluctuation theorem [see Eq. (1.13)]. In some experiment, there may arise a situation where the full knowledge of the system is not available (see Chapter 2). The cause of this partial information may be due to hidden variables present in the system. Due to interaction between the observed and the hidden degrees of freedom, the entropy produced from observed degrees of freedom is not the same as that for complete system (observed plus hidden variables). Therefore, one may expect that the fluctuation theorem for such entropy production in the steady state would not hold. In the opposite limit, when the interaction between the observed and the hidden degrees of freedom is sufficiently weak, one might guess that the entropy produced from the partial system may satisfy the fluctuation theorem in the steady state. In this thesis (Chapters 2–5), we have given some model systems where one may see deviations from the fluctuation theorem of entropy production of a partial system even in the weak coupling limit. We have shown the mechanism and the possible cause of deviation from the fluctuation theorem for entropy production of a partial system in the weak coupling limit. In addition to that, we have also shown a recipe with which

the effect of the weak coupling can be diminished. It is worth mentioning that such a technique is quite useful while observing certain quantities in an experiment when the source of the weak coupling is not known.

In Chapter 2 [52, 53], we consider two Brownian particles in the heat bath, coupled via harmonic interaction. The system is driven into the non-equilibrium steady state using the stochastic driving on each particle. In the weak coupling limit, we observed the deviation from the fluctuation theorem for total entropy production by one of the particle in the coupled system in the steady state. In Chapter 3 [54], we study a coupled Brownian particle system (A and B) in which one of the particles (say A) is connected to a thermal gradient and the other one (say B) is connected to a single heat bath. The interaction between these two particles is harmonic. In the steady state, fluctuation of total entropy production due to particle A in the coupled system is computed and the deviation from the fluctuation theorem corresponding to it is observed. In contrast to Chapters 2 and 3 where the entropy production of the partial system may not satisfy the fluctuation theorem even in the weak coupling limit, we give a model system of two harmonically interacting Brownian particles in a harmonic confinement in Chapter 4 [52, 53, 51]. The whole system is in contact with a heat bath at constant temperature. Both of these particles are driven by external stochastic Gaussian forces. In the weak coupling limit, total entropy production of one of the particles in the coupled system is studied, and we show that the fluctuation theorem in the steady state in this case is satisfied. In all of the previous chapters, we consider the system consisting of slow degrees of freedom and the fluctuation theorem for the total entropy production of part of the system observed in the steady state in the weak coupling limit. However, in Chapter 5 [54], we consider a single Brownian particle connected to three heat baths (B_1 , B_2 , and B_3) of distinct temperatures. The coupling between one of the baths (say B_3) to the given Brownian particle is considered to be weak. Therefore, a slow degree of freedom is weakly coupled to a box of fast degrees of freedom. In this case, we observe the deviation of fluctuation theorem for total entropy production of the Brownian particle due to heat baths B_1 and B_2 . In the weak coupling limit, the fluctuation theorem holds for this case.

In macroscopic thermodynamics, a heat engine performs in a cyclic manner by

consuming the heat from a higher temperature reservoir and dumping a certain amount of heat in a cold reservoir. During this cycle, the amount of work extracted is the difference between the absorbed heat and the dumped heat. When this engine performs in the quasi-static regime as well as reversibly, the efficiency is given by Carnot's efficiency which is the maximum efficiency a reversible engine can achieve. However, in the microscopic regime where fluctuations are predominant, the output work and the heat absorbed by an engine become stochastic quantities. Consequently, the efficiency has a distribution function.

In Chapter 6 [55], we investigate the stochastic efficiency of an isothermal work-to-work converter machine composed of a Brownian particle, immersed in a heat bath of constant temperature. This Brownian particle acts as the working substance of the engine. Two external forces are applied on the engine called load and drive forces. The probability density function and the large deviation function of stochastic efficiency (output work/input work) of this engine are studied. In Chapter 7, we consider a one-dimensional isothermal machine composed of two Brownian particles where one of the particles is confined in a harmonic trap. We attach a constant load to the free particle and drag the harmonic trap with a constant velocity to lift the load. For a given duration of time, we compute the efficiency of this machine and its probability density function in the transient regime.

Chapter 2

Fluctuation theorem for partial entropy production in a coupled Brownian particle system

The total entropy production in the non-equilibrium steady state follows a remarkable symmetry relation called fluctuation theorem for all time. When a certain part of the system is masked or hidden, it is difficult to infer the exact estimate of the total entropy production. Entropy produced from the observed part of the system shows significant deviation from the steady state fluctuation theorem. This deviation may occur due to an interaction between the observed and the masked part of the system. A naive guess would be that the deviation from steady state fluctuation theorem may disappear in the limit of small interaction between both parts of the system. In contrast, we investigate the entropy production due to particle A in a harmonically coupled Brownian particle system (say, particle A and B) in a heat reservoir at a constant temperature. The system is maintained in the non-equilibrium steady state using stochastic driving. When the coupling between particle A (observed) and B (unobserved) is considered to be infinitesimally weak, the fluctuation theorem for total entropy production of particle A in the coupled system is studied. Numerical simulations are performed to support the analytical results.

2.1 Introduction

Small systems in the contact of a heat bath evolve according to stochastic dynamics [70, 152]. When such systems are driven out of equilibrium by some external forces, the value of the observables such as heat, work done, entropy production, etc. vary from one measurement to the other [123, 125, 3]. Consequently, the histogram of observable contains much information than their ensemble average value. Since these observables are functional of the state of a system, the complete knowledge of the system is desirable.

For a complex stochastic system where a number of coupled degrees of freedom (DOFs) are present, it is difficult to track all of them. In such a scenario, we might have partial information which is utilized to estimate the observables. In this direction, several efforts have been made to understand the fluctuations of the observables when complete information is not available. For example, Shiraishi and Sagawa [126] generalized the fluctuation theorem for a partially masked system. They defined partial entropy production for a subset of all transitions and showed that it satisfies the integral fluctuation theorem. In Ref. [71], the authors introduced the definition of hidden entropy production which is the difference between irreversible entropy production between the original and reduced dynamics and proved that such hidden entropy production satisfies the integral fluctuation theorem. Rahav *et al.* [105] considered a Markov jump process on a set of a finite number of states. The jump from a given state to another state is described by a transition rate. Assuming certain transition rates higher than other ones, the whole network of states is then mapped to a group of clusters. This type of coarse-graining modifies the entropy production, and they showed that the *coarse-grained entropy* satisfies the fluctuation theorem provided the transition rates of the system to jump within clusters are sufficiently high. Similar results found in Ref. [85] where authors have discussed the projection of Markov process with constant transition rates to a smaller number of observable aggregated states, and the resulting entropy production on the set of all aggregated state satisfied both detailed and integral fluctuation theorems. Puglisi *et al.* [104] showed an example where decimation of certain fast states with respect to a given threshold time does not affect the entropy production, provided

it does not entirely remove the loops carrying net probability current. In all of these references, it is shown that coarse-graining based on time-scale separation did not alter the underlying physics of the problem. There are some other studies which differ from the above-mentioned ones where the relaxation time of all relevant DOFs is much larger than that of bath DOFs. For example, in Ref. [89], two paramagnetic colloidal particles of the same size were trapped in separate non-overlapping toroidal traps. The whole system was in contact with the heat bath. Tangential forces were applied on each particle using laser field. Consequently, both particles reached in the non-equilibrium stationary state. A static magnetic field perpendicular to the plane of toroidal traps was used to set an interaction among these particles. The total entropy production due to one of the particles (i.e., partial entropy production as defined in this thesis) in the coupled system was measured, and the deviation from fluctuation theorem with the coupling strength was observed. In a theoretical model [11], fluctuation theorem for the entropy production of a single electron box is studied in a coupled electron box system. In another example [79], the authors studied molecular motors which are modeled by flashing ratchet and found that Gallavotti-Cohen symmetry [82] is preserved only when both chemical and mechanical DOFs are considered in theory. There are also some examples where partial information is utilized to get full system properties. For example, in Ref. [106], Ribezzi-Crivellari and Ritort have shown a method to infer full work distribution from the partial work measurement using Crooks fluctuation theorem. Amann *et al.* [2] have derived a criterion to describe a non-equilibrium steady state of a Markov system of three states using the data from sufficiently long two states trajectories. Some other studies related to the area of partial observation of a complete system can also be seen in Refs. [17, 97, 131, 99, 7, 139, 31, 98, 69]. The main conclusion of these studies is, when a system consists of DOFs having relaxation time much larger than that of bath DOFs, then the partial system or subsystem may not behave like a complete system for large coupling strength. In such case, when the total entropy production is computed or measured depending upon the available information, the probability density function of it may not satisfy fluctuation theorem. One naive guess is that the fluctuation theorem for total entropy production of the partial system may hold when the coupling between the observed and hidden part is infinitesimally small. In

contrast, we consider a model system of two Brownian particles (say A and B) interacting harmonically with a coupling parameter δ (dimensionless) in the heat bath at a temperature T [52, 53]. Both of these particles are driven using external stochastic Gaussian forces. The given system generates entropy. We consider two definitions of total entropy production of one of the particles in the coupled system: partial and apparent entropy production as defined in Sec. 2.2.1. Here, we show a mechanism under which the steady state fluctuation theorem for partial and apparent entropy production is not satisfied even in the weak coupling limit.

This chapter is organized as follows. In Sec. 2.2, we define a model system consists of two Brownian particles connected by a harmonic spring. The definitions of partial and apparent entropy production are given in Sec. 2.2.1. The steady state for the joint distribution $P_{ss}(U)$ of system variable $U^T = (y, v_A, v_B)$ is given in Sec. 2.3. Section 2.4 contains the Fokker-Planck equation for restricted moment generating function of stochastic quantity W given in Eq. (2.28) and its general solution in the large time limit. Further, we compute the moment generating function for total entropy production of one of the particles in the coupled system $Z(\lambda) = \langle e^{-\lambda \Delta S_{tot}^A} \rangle \approx g(\lambda) e^{(\tau/\tau_\gamma)\mu(\lambda)}$ using the method developed in Ref. [76] (Sec. 2.5). In Sec. 2.6, we invert the moment generating function $Z(\lambda)$ to obtain probability density function $P(\Delta S_{tot}^A)$. The results for a single Brownian particle in a heat bath driven by external Gaussian white noise are given in Sec. 2.7. In Sec. 2.8, we show the computation of $\mu(\lambda)$ in the limit $\delta \rightarrow 0$. The large deviation function $I(s)$, asymmetry function $f(s)$, and fluctuation theorem are discussed in Sec. 2.9. In Sec. 2.10, we show the comparison of numerical simulations with the analytical predictions. We summarize this chapter in Sec. 2.11.

2.2 Model

Consider two Brownian particles (say A and B) in an aqueous medium at a constant temperature T . For simplicity; we consider the motion of the system along one-dimension. Both of these particles are interacting with each other with a harmonic spring of stiffness k . The Hamiltonian $\mathcal{H}(y, v_A, v_B)$ of the coupled Brownian particle

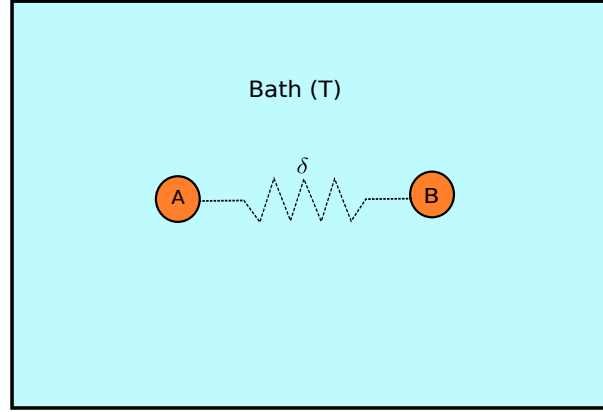


FIGURE 2.1: Two Brownian particles (A and B) of mass m are coupled to each other with the coupling parameter $\delta = 2km/\gamma^2$ (dimensionless). The whole setup is immersed in the heat bath of a constant temperature T .

system is

$$\mathcal{H}(y, v_A, v_B) = \frac{1}{2}mv_A^2 + \frac{1}{2}mv_B^2 + \frac{1}{2}ky^2, \quad (2.1)$$

where $y = x_A - x_B$ is the relative position of particle A with respect to particle B. The schematic diagram of the coupled system is shown in Fig. 2.1.

The given system is maintained in the non-equilibrium steady state using external stochastic Gaussian forces. Let $f_A(t)$ and $f_B(t)$ be the external forces acting on particle A and B, respectively. Therefore, the dynamics of coupled Brownian particle system is described by the following underdamped Langevin equations [152]

$$\dot{y} = v_A(t) - v_B(t), \quad (2.2)$$

$$m\dot{v}_A = -\gamma v_A(t) + \eta_A(t) - ky(t) + f_A(t), \quad (2.3)$$

$$m\dot{v}_B = -\gamma v_B(t) + \eta_B(t) + ky(t) + f_B(t), \quad (2.4)$$

where γ is the dissipation constant, v_A and v_B are the velocities of particle A and B, respectively. The thermal Gaussian noises $\eta_A(t)$ and $\eta_B(t)$ are acting on particle A and B, respectively, from the heat bath. These thermal Gaussian noises have mean zero and correlation $\langle \eta_i(t)\eta_j(t') \rangle = 2D\delta_{ij}\delta(t-t')$ where $D=\gamma T$. Similarly, the external forces $f_A(t)$ and $f_B(t)$ have mean zero and correlation $\langle f_A(t)f_A(t') \rangle = 2D\theta\delta(t-t')$, $\langle f_B(t)f_B(t') \rangle = 2D\theta\alpha^2\delta(t-t')$. In this chapter, we consider two different choices of external forces: (1) Both of the external forces are independent of each

other, and (2) the force on particle B is correlated with the force on particle A, i.e. $f_B(t) = \alpha f_A(t)$. Moreover, both external forces [$f_A(t)$ and $f_B(t)$] are uncorrelated with the thermal Gaussian noises [$\eta_A(t)$ and $\eta_B(t)$]. Here, we consider three dimensionless parameters: (1) strength of the force θ acting on particle A relative to that of bath, (2) strength of the force α^2 acting on particle B relative to that on particle A, and (3) coupling parameter $\delta = 2km/\gamma^2$. Throughout the calculation, we set Boltzmann's constant $k_B = 1$.

2.2.1 Total entropy production from particle A: partial and apparent entropy production

Incomplete information can be of two types: (1) the observer knows the full system, but intentionally observes the part of the system, and (2) the observer is not aware of hidden part of the system [52, 53]. In both scenarios, the actual information of the system is lost. In our case, we have a model system of a stochastically driven coupled Brownian particle system (particle A and B) in a heat bath. The observable in this chapter is the total entropy production of particle A in the coupled Brownian particle system in the steady state.

The total entropy production due to particle A of the coupled Brownian particle system [incomplete information of type (1)] is given by [121, 120]

$$\Delta \bar{S}_{tot}^A = -\frac{Q^A}{T} - \ln \frac{P_{ss}^A[v_A(\tau)]}{P_{ss}^A[v_A(0)]}, \quad (2.5)$$

The above definition of entropy production we call as *partial entropy production* where $Q^A = \int_0^\tau dt [\eta_A(t) - \gamma v_A(t)]v_A(t)$ is the heat absorbed by the Brownian particle A of the coupled system from the heat bath, and $P_{ss}^A(v_A)$ is the steady state probability distribution of the velocity of particle A obtained after integrating the joint steady state distribution $P_{ss}(y, v_A, v_B)$ obtained from Eqs. (2.2)–(2.4) over the relative separation y and the velocity of particle B. Thus,

$$P_{ss}^A[v_A(\tau)] = \frac{1}{\sqrt{2\pi H_P}} \exp \left[-\frac{v_A^2(\tau)}{2H_P} \right], \quad (2.6)$$

where H_P is given by

$$H_P = \lim_{\tau \rightarrow \infty} \langle [v_A(\tau) - \langle v_A(\tau) \rangle]^2 \rangle = \frac{D[(2 + \theta + \alpha^2 \theta)mk + 2(1 + \theta)\gamma^2]}{2m\gamma(\gamma^2 + mk)}, \quad (2.7)$$

for both choices of external forces. In Eq. (2.5), first and second terms on right hand side are the entropy change in the bath and system entropy production due to particle A in the coupled system shown in Fig. 2.1, respectively.

Using Eq. (2.3) and (2.6), we rewrite the partial entropy production $\Delta \bar{S}_{tot}^A$ as

$$\Delta \bar{S}_{tot}^A = \frac{1}{T} \int_0^\tau dt [f_A(t) - ky(t)]v_A(t) - \frac{1}{2} \left[\frac{m}{T} - \frac{1}{H_P} \right] [v_A^2(\tau) - v_A^2(0)]. \quad (2.8)$$

Total entropy production based on incomplete information of type (2) is called *apparent entropy production*. In this case, the observer is not aware of particle B. Therefore, he/she constructs the total entropy production for particle A as follows. Since particle A is only present in the heat bath, the velocity of it evolves according to the following underdamped Langevin equation [152]

$$m\dot{v}_A = -\gamma v_A(t) + \eta_A(t) + f_A(t), \quad (2.9)$$

where γ is the dissipation constant, and $v_A(t)$ is the velocity of particle A. The external Gaussian force $f_A(t)$ and the Gaussian noise from the medium $\eta_A(t)$ are acting on particle A. Both of them have mean zero and correlation $\langle f_A(t)f_A(t') \rangle = 2D\theta\delta(t-t')$, $\langle \eta_A(t)\eta_A(t') \rangle = 2D\delta(t-t')$, and $\langle f_A(t)\eta_A(t') \rangle = 0$ for all time.

Thus, the apparent entropy production for particle A is given by Eq. (2.8) with $k = 0$:

$$\Delta \tilde{S}_{tot}^A = \frac{1}{T} \int_0^\tau dt f_A(t)v_A(t) - \frac{1}{2} \left[\frac{m}{T} - \frac{1}{H_A} \right] [v_A^2(\tau) - v_A^2(0)]. \quad (2.10)$$

In the above equation,

$$H_A = H_P|_{k=0} = \frac{D(1 + \theta)}{m\gamma}. \quad (2.11)$$

One can combine both definitions of entropy production given in Eqs. (2.8) and (2.10), using a parameter Π defined as

$$\Pi = \begin{cases} 1 & \text{Partial entropy production,} \\ 0 & \text{Apparent entropy production.} \end{cases} \quad (2.12)$$

Therefore,

$$\Delta S_{tot}^A = \frac{1}{T} \int_0^\tau dt f_A(t) v_A(t) - \frac{\Pi k}{T} \int_0^\tau dt y(t) v_A(t) - \frac{1}{2} \left[\frac{m}{T} - \frac{1}{H} \right] [v_A^2(\tau) - v_A^2(0)], \quad (2.13)$$

where $H = \Pi H_p + (1 - \Pi) H_A$.

It is important to note that in both types of incomplete informations, the underlying dynamics of the coupled system is given by Eqs. (2.2)–(2.4). Therefore, we compute the distribution of ΔS_{tot}^A subject to the actual dynamics given in Eqs. (2.2)–(2.4).

2.3 Steady state distribution $P_{ss}(U)$

The underdamped Langevin equations given in Eqs. (2.2)–(2.4) describe the system shown in Fig. 2.1. It is convenient to write these equations in the matrix form as

$$\dot{y} = A^T V(t), \quad (2.14)$$

$$m \dot{V} = -\gamma V(t) - k A y(t) + F(t) + \xi(t), \quad (2.15)$$

where $V = (v_A, v_B)^T$, $A = (1, -1)^T$, $F = (f_A, f_B)^T$, and $\xi = (\eta_A, \eta_B)^T$.

Finite time Fourier transform and its inverse for any time dependent quantity $Q(t)$ are defined as

$$\tilde{Q}(\omega_n) = \frac{1}{\tau} \int_0^\tau dt Q(t) \exp(-i\omega_n t), \quad (2.16)$$

$$Q(t) = \sum_{n=-\infty}^{\infty} \tilde{Q}(\omega_n) \exp(i\omega_n t), \quad (2.17)$$

with $\omega_n = 2\pi n/\tau$.

Using Eq. (2.16), we write Eqs. (2.14) and (2.15) as

$$\tilde{y}(\omega_n) = A^T G(\omega_n) [\tilde{F}(\omega_n) + \tilde{\xi}(\omega_n)] - \frac{A^T G(\omega_n)}{2\tau} [(\gamma + im\omega_n)A\Delta y + 2m\Delta V], \quad (2.18)$$

$$\tilde{V}(\omega_n) = i\omega_n G(\omega_n) [\tilde{F}(\omega_n) + \tilde{\xi}(\omega_n)] + \frac{G(\omega_n)}{\tau} [kA\Delta y - i\omega_n m\Delta V], \quad (2.19)$$

where $\Delta y = y(\tau) - y(0)$, $\Delta V = V(\tau) - V(0)$, $\Phi = kAA^T$, and $G(\omega_n) = [i\gamma\omega_n - m\omega_n^2 + \Phi]^{-1}$. Therefore, we write $\tilde{y}(\omega_n)$ and $\tilde{v}_A(\omega_n)$ as

$$\tilde{y}(\omega_n) = (G_{11} - G_{12})(\tilde{\eta}_A + \tilde{f}_A - \tilde{\eta}_B - \tilde{f}_B) - \frac{q_1^T \Delta U}{\tau}, \quad (2.20)$$

$$\tilde{v}_A(\omega_n) = i\omega_n [G_{11}(\tilde{\eta}_A + \tilde{f}_A) + G_{12}(\tilde{\eta}_B + \tilde{f}_B)] + \frac{q_2^T \Delta U}{\tau}, \quad (2.21)$$

where

$$q_1^T = \left[\frac{\gamma + im\omega_n}{2} A^T G A, m(G_{11} - G_{12}), m(G_{12} - G_{11}) \right],$$

$$q_2^T = [k(G_{11} - G_{12}), -im\omega_n G_{11}, -im\omega_n G_{12}].$$

The Green's function matrix elements are $G_{11}(\omega_n) = G_{22}(\omega_n) = (i\gamma\omega_n - m\omega_n^2 + k)[i\omega_n(\gamma + im\omega_n)(2k - m\omega_n^2 + i\gamma\omega_n)]^{-1}$ and $G_{12}(\omega_n) = G_{21}(\omega_n) = k[i\omega_n(\gamma + im\omega_n)(2k - m\omega_n^2 + i\gamma\omega_n)]^{-1}$. For convenience, we write $G_{ij} = G_{ij}(\omega_n)$, $G_{ij}^* = G_{ij}(-\omega_n)$, $\tilde{f}_i = \tilde{f}_i(\omega_n)$, $\tilde{f}_i^* = \tilde{f}_i(-\omega_n)$, $\tilde{\eta}_i = \tilde{\eta}_i(\omega_n)$, and $\tilde{\eta}_i^* = \tilde{\eta}_i(-\omega_n)$.

The row vector $U^T(\tau) = [y(\tau), V^T(\tau)]$ is

$$U^T(\tau) = \lim_{\epsilon \rightarrow 0} \sum_{n=-\infty}^{\infty} e^{-i\omega_n \epsilon} \tilde{U}^T(\omega_n) = \lim_{\epsilon \rightarrow 0} \sum_{n=-\infty}^{\infty} e^{-i\omega_n \epsilon} [\tilde{y}(\omega_n), \tilde{V}^T(\omega_n)]. \quad (2.22)$$

Using Eqs. (2.18) and (2.19), we see that the terms

$$\sum_{n=-\infty}^{\infty} e^{-i\omega_n \epsilon} \frac{A^T G}{2\tau} [(\gamma + im\omega_n)A\Delta y + 2m\Delta V],$$

$$\sum_{n=-\infty}^{\infty} e^{-i\omega_n \epsilon} \frac{1}{\tau} [kA^T \Delta y - i\omega_n m\Delta V^T] G^T,$$

go to zero as $\tau \rightarrow \infty$. This is because in the large- τ limit, the summations can be

converted into integrals. As all the poles lie in the upper half of the complex ω -plane, the contribution to the integrals is zero. Therefore, Eq. (2.22) reduces to

$$\begin{aligned} U^T(\tau) &= \lim_{\epsilon \rightarrow 0} \sum_{n=-\infty}^{\infty} e^{-i\omega_n \epsilon} [(\tilde{F}^T + \tilde{\xi}^T)G^T A, i\omega_n (\tilde{F}^T + \tilde{\xi}^T)G^T] \\ &= \lim_{\epsilon \rightarrow 0} \sum_{n=-\infty}^{\infty} e^{-i\omega_n \epsilon} [(1-C)\{q_3^T(\tilde{\eta}_A + \tilde{f}_A) + q_4^T(\tilde{\eta}_B + \tilde{f}_B)\} + C(\tilde{\eta}_A l_1^T + \tilde{\eta}_B l_2^T + \tilde{f}_A l_3^T)], \end{aligned} \quad (2.23)$$

where

$$\begin{aligned} q_3^T &= l_1^T = (G_{11} - G_{12}, i\omega_n G_{11}, i\omega_n G_{12}), \\ q_4^T &= l_2^T = (G_{12} - G_{11}, i\omega_n G_{12}, i\omega_n G_{11}), \\ l_3^T &= [(1-\alpha)(G_{11} - G_{12}), i\omega_n(G_{11} + \alpha G_{12}), i\omega_n(G_{12} + \alpha G_{11})], \end{aligned}$$

and parameter C is defined as

$$C = \begin{cases} 0 & \text{for } \langle f_A(t)f_B(t') \rangle = 0 \forall t, t', \\ 1 & \text{for } f_B(t) = \alpha f_A(t). \end{cases} \quad (2.24)$$

Therefore, the mean and variance of U are given by

$$\langle U(\tau) \rangle = 0, \quad (2.25)$$

$$\begin{aligned} \langle U(\tau)U^T(\tau) \rangle &= \frac{D}{\pi} \int_{-\infty}^{\infty} d\omega [(1-C)\{(1+\theta)q_3 q_3^\dagger + (1+\alpha^2\theta)q_4 q_4^\dagger\} \\ &\quad + C(l_1 l_1^\dagger + l_2 l_2^\dagger + \theta l_3 l_3^\dagger)]. \end{aligned} \quad (2.26)$$

Since U is linear in the thermal Gaussian noises and the external Gaussian forces, the steady state distribution of the coupled system can be written using the mean and correlation of it [see Eqs. (2.25) and (2.26)]

$$P_{ss}(U) = \frac{e^{-\frac{1}{2}U^T M^{-1}U}}{\sqrt{(2\pi)^3 \det M}} \quad \text{where} \quad M_{ij} = \langle U(\tau)U^T(\tau) \rangle_{ij}. \quad (2.27)$$

In contrast to U , ΔS_{tot}^A given in Eq. (2.13), depends upon the thermal Gaussian noises and external forces quadratically. Therefore, the mean $\langle \Delta S_{tot}^A \rangle$ and variance $\langle [\Delta S_{tot}^A -$

$\langle \Delta S_{tot}^A \rangle^2$ are not sufficient to write the probability density of it.

We define

$$W = \frac{1}{T} \int_0^\tau dt f_A(t) v_A(t) - \frac{\Pi k}{T} \int_0^\tau dt y(t) v_A(t), \quad (2.28)$$

where both of the integrals follow Stratonovich rule of integration [124]. While the first term on the right hand side is the work done by the stochastic external force $f_A(t)$ on the Brownian particle A, the second term on the right hand side is the interaction energy. Both of these terms are measured with respect to the temperature T of the heat bath.

2.4 Fokker-Planck equation and its general solution

In this section, we compute the moment generating function for entropy production ΔS_{tot}^A . The quantity ΔS_{tot}^A given in Eq. (2.13), can be written as

$$\Delta S_{tot}^A = W - \frac{1}{2} \left[\frac{m}{T} - \frac{1}{H} \right] [v_A^2(\tau) - v_A^2(0)], \quad (2.29)$$

where the quantity W is the functional of all trajectories and the second term on the right hand side depends upon the initial $v_A(0)$ and final velocity $v_A(\tau)$ of the Brownian particle A. Therefore, the conditional moment generating function for ΔS_{tot}^A is

$$\begin{aligned} Z(\lambda, U, \tau | U_0) &= \langle e^{-\lambda \Delta S_{tot}^A} \delta[U - U(\tau)] \rangle_{U, U_0} \\ &= Z_W(\lambda, U, \tau | U_0) e^{\lambda/2(mT^{-1} - H^{-1})(U^T \Sigma U - U_0^T \Sigma U_0)}, \end{aligned} \quad (2.30)$$

where the angular brackets represent the average over all set of trajectories from fixed initial variable U_0 to final variable $U(\tau)$, $Z_W(\lambda, U, \tau | U_0) = \langle e^{-\lambda W} \delta[U - U(\tau)] \rangle_{U, U_0}$, and $\Sigma_{ij} = \delta_{i2} \delta_{ij}$ with $\{i, j\} = \{1, 2, 3\}$.

The evolution of the restricted moment generating function $Z_W(\lambda, U, \tau | U_0)$ is governed by the following Fokker-Planck equation [70, 107]

$$\frac{\partial Z_W(\lambda, U, \tau | U_0)}{\partial \tau} = \mathcal{L}_\lambda Z_W(\lambda, U, \tau | U_0) \quad (2.31)$$

with the initial condition $Z_W(\lambda, U, \tau|U_0) = \delta(U - U_0)$, and the Fokker-Planck operator \mathcal{L}_λ is

$$\begin{aligned} \mathcal{L}_\lambda = & \frac{1}{m} \sum_{i=A,B} \left[\frac{\partial \mathcal{H}}{\partial x_i} \frac{\partial}{\partial v_i} - \frac{\partial \mathcal{H}}{\partial v_i} \frac{\partial}{\partial x_i} \right] + \frac{D(1+\theta)}{m^2} \frac{\partial^2}{\partial v_A^2} + \frac{\gamma v_A}{m} (1+2\lambda\theta) \frac{\partial}{\partial v_A} \\ & + \frac{\gamma}{m} (v_B + 2C\lambda\alpha\theta v_A) \frac{\partial}{\partial v_B} + \gamma \left[\frac{2}{m} + \frac{\lambda}{D} \left(\Pi k y v_A + \frac{D\theta}{m} \right) \right] + \frac{\lambda^2 \gamma^2 v_A^2 \theta}{D} \\ & + \frac{D(1+\theta\alpha^2)}{m^2} \frac{\partial^2}{\partial v_B^2} + \frac{2CD\theta\alpha}{m^2} \frac{\partial^2}{\partial v_A \partial v_B}. \end{aligned} \quad (2.32)$$

In the above equation, C is the correlation parameter given in Eq. (2.24).

We are not aware of the analytical solution of the Fokker-Planck equation given in Eq. (2.31). Nevertheless, we can write the general solution in the large time limit ($\tau \rightarrow \infty$) as

$$Z_W(\lambda, U, \tau|U_0) = \chi(U_0, \lambda) \Psi(U, \lambda) e^{(\tau/\tau_\gamma)\mu(\lambda)} + \dots, \quad (2.33)$$

where τ_γ is the viscous relaxation time yet to be determined, $\mu(\lambda)$ is the largest eigenvalue of the Fokker-Planck operator \mathcal{L}_λ , and the corresponding right eigenfunction is $\Psi(U, \lambda)$, i.e. $\mathcal{L}_\lambda \Psi(U, \lambda) = \mu(\lambda) \Psi(U, \lambda)$. In Eq. (2.33), $\chi(U_0, \lambda)$ is the projection of initial state onto the left eigenvector of Fokker-Planck operator \mathcal{L}_λ corresponding to largest eigenvalue $\mu(\lambda)$. These left and right eigenfunctions satisfy normalization condition $\int dU \chi(U, \lambda) \Psi(U, \lambda) = 1$.

The moment generating function $Z(\lambda)$ for ΔS_{tot}^A is obtained by integrating the restricted moment generating function $Z(\lambda, U, \tau|U_0)$ given in Eq. (2.30), over the initial state U_0 with respect to the steady state distribution $P_{ss}(U_0)$ and the final state U :

$$Z(\lambda) = \int dU \int dU_0 P_{ss}(U_0) Z(\lambda, U, \tau|U_0) = g(\lambda) e^{(\tau/\tau_\gamma)\mu(\lambda)} + \dots, \quad (2.34)$$

where $g(\lambda)$ is the prefactor, and $\mu(\lambda)$ is the cumulant generating function.

2.5 Calculation for moment generating function

In this section, we show the complete calculation for moment generating function for ΔS_{tot}^A , i.e. $Z(\lambda) \sim g(\lambda) e^{(\tau/\tau_\gamma)\mu(\lambda)}$, using a method developed in Ref. [76]. Therefore,

we write the functional W given in Eq. (2.28) as

$$W = W_1 - W_2, \quad \text{where} \quad (2.35)$$

$$W_1 = \frac{1}{T} \int_0^\tau dt f_A(t) v_A(t), \quad (2.36)$$

$$W_2 = \frac{\Pi k}{T} \int_0^\tau dt y(t) v_A(t). \quad (2.37)$$

Using (2.17), we write W_1 as

$$W_1 = \frac{\tau}{2T} \sum_{n=-\infty}^{\infty} [\tilde{f}_A(\omega_n) \tilde{v}_A(-\omega_n) + \tilde{f}_A(-\omega_n) \tilde{v}_A(\omega_n)]. \quad (2.38)$$

Substituting $\tilde{v}_A(\omega_n)$ from Eq. (2.21) in the above equation yields

$$W_1 = \frac{\tau}{2T} \sum_{n=-\infty}^{\infty} \left[i\omega_n \{ G_{11} \tilde{f}_A^*(\tilde{\eta}_A + \tilde{f}_A) + G_{12} \tilde{f}_A^*(\tilde{\eta}_B + \tilde{f}_B) - G_{11}^* \tilde{f}_A(\tilde{\eta}_A^* + \tilde{f}_A^*) \right. \\ \left. - G_{12}^* \tilde{f}_A(\tilde{\eta}_B^* + \tilde{f}_B^*) \} + \frac{f_A q_2^\dagger \Delta U}{\tau} + \frac{f_A^* \Delta U^T q_2}{\tau} \right]. \quad (2.39)$$

Similarly, using (2.17), we write W_2 as

$$W_2 = \frac{\Pi k \tau}{2T} \sum_{n=-\infty}^{\infty} [\tilde{y}(\omega_n) \tilde{v}_A(-\omega_n) + \tilde{y}(-\omega_n) \tilde{v}_A(\omega_n)]. \quad (2.40)$$

Substituting $\tilde{y}(\omega_n)$ and $\tilde{v}_A(\omega_n)$ from Eqs. (2.20) and (2.21), respectively, in the above equation, we get

$$W_2 = \frac{\Pi k \tau}{2T} \sum_{n=-\infty}^{\infty} \left[i\omega_n \{ \{ G_{11}(\tilde{\eta}_A + \tilde{f}_A) + G_{12}(\tilde{\eta}_B + \tilde{f}_B) \} (G_{11}^* - G_{12}^*) (\tilde{\eta}_A^* + \tilde{f}_A^* - \tilde{\eta}_B^* - \tilde{f}_B^*) \right. \\ - \{ G_{11}^*(\tilde{\eta}_A^* + \tilde{f}_A^*) + G_{12}^*(\tilde{\eta}_B^* + \tilde{f}_B^*) \} (G_{11} - G_{12})(\tilde{\eta}_A + \tilde{f}_A - \tilde{\eta}_B - \tilde{f}_B) \\ + \frac{q_2^\dagger \Delta U}{\tau} (G_{11} - G_{12})(\tilde{\eta}_A + \tilde{f}_A - \tilde{\eta}_B - \tilde{f}_B) - \frac{i\omega_n}{\tau} q_1^\dagger \Delta U [G_{11}(\tilde{\eta}_A + \tilde{f}_A) + G_{12}(\tilde{\eta}_B + \tilde{f}_B)] \\ + \frac{i\omega_n}{\tau} \Delta U^T q_1 [G_{11}^*(\tilde{\eta}_A^* + \tilde{f}_A^*) + G_{12}^*(\tilde{\eta}_B^* + \tilde{f}_B^*)] + \frac{\Delta U^T q_2}{\tau} (G_{11}^* - G_{12}^*)(\tilde{\eta}_A^* + \tilde{f}_A^* - \tilde{\eta}_B^* - \tilde{f}_B^*) \\ \left. - \frac{\Delta U^T (q_1 q_2^\dagger + q_2 q_1^\dagger) \Delta U}{\tau^2} \right]. \quad (2.41)$$

Therefore, the restricted moment generating function $Z_W(\lambda, U, \tau|U_0)$ for functional W is

$$Z_W(\lambda, U, \tau|U_0) = \left\langle e^{-\lambda W} \delta[U - U(\tau)] \right\rangle_{U, U_0} = \int \frac{d^3\sigma}{(2\pi)^3} e^{i\sigma^T U} \left\langle e^{E(\tau)} \right\rangle_{U, U_0}, \quad (2.42)$$

where the angular brackets represent the average over set of all trajectories for fixed initial U_0 and final configuration U . In the above equation, we have used the integral representation of Dirac delta function and $E(\tau) = -\lambda W - i\sigma^T U(\tau)$. Substituting W and $U(\tau)$ from Eqs. (2.35) and (2.23), respectively, in $E(\tau)$ yields

$$E(\tau) = \sum_{n=1}^{\infty} \left[-\frac{\lambda\tau}{T} \zeta_n^T C_n \zeta_n^* + \zeta_n^T \alpha_n + \alpha_{-n}^T \zeta_n^* - \frac{\lambda\Pi k}{T\tau} |q_n|^2 \right] - \frac{\lambda\tau}{2T} \zeta_0^T C_0 \zeta_0 + \zeta_0^T \alpha_0 - \frac{\lambda\Pi k}{2T\tau} q_0^2, \quad (2.43)$$

where $C_n = C_n^I - \Pi k C_n^{II}$ and $|q_n|^2 = \Delta U^T (q_1 q_2^\dagger + q_2 q_1^\dagger) \Delta U$.

When the correlation parameter C is zero, the row vector containing thermal Gaussian noises and the external forces in the frequency domain is $\zeta^T = (\tilde{\eta}_A, \tilde{\eta}_B, \tilde{f}_A, \tilde{f}_B)$, and the matrices C_n^I and C_n^{II} are

$$C_n^I = \begin{bmatrix} 0 & 0 & i\omega_n G_{11} & 0 \\ 0 & 0 & i\omega_n G_{12} & 0 \\ -i\omega_n G_{11}^* & -i\omega_n G_{12}^* & i\omega_n [G_{11} & -i\omega_n G_{12}^* \\ & & -G_{11}^*] & \\ 0 & 0 & i\omega_n G_{12} & 0 \end{bmatrix}, \quad C_n^{II} = \begin{bmatrix} C_{11} & C_{12} & C_{13} & C_{14} \\ C_{12}^* & C_{22} & C_{23} & C_{24} \\ C_{13}^* & C_{23}^* & C_{33} & C_{34} \\ C_{14}^* & C_{24}^* & C_{34}^* & C_{44} \end{bmatrix}.$$

The matrix elements of C_n^{II} are given as

$$C_{11} = i\omega_n [G_{11}^* G_{12} - G_{11} G_{12}^*],$$

$$C_{12} = i\omega_n [|G_{12}|^2 - |G_{11}|^2],$$

$$C_{11} = C_{13} = C_{33} = -C_{22}, \quad C_{12} = C_{14} = C_{34}, \quad C_{12}^* = C_{23}, \quad C_{22} = C_{24} = C_{44}, \quad C_{ij}^* = C_{ij}(-\omega_n).$$

The column vector α_n is

$$\alpha_n = -\frac{\lambda}{T} \begin{pmatrix} a_{11}^T \Delta U \\ a_{21}^T \Delta U \\ a_{31}^T \Delta U \\ a_{41}^T \Delta U \end{pmatrix} - ie^{-i\omega\epsilon} \begin{pmatrix} q_3^T \sigma \\ q_4^T \sigma \\ q_3^T \sigma \\ q_4^T \sigma \end{pmatrix}, \quad \text{in which}$$

$$a_{11}^T = \Pi k [i\omega_n G_{11} q_1^\dagger - (G_{11} - G_{12}) q_2^\dagger],$$

$$a_{21}^T = \Pi k [i\omega_n G_{12} q_1^\dagger - (G_{12} - G_{11}) q_2^\dagger],$$

$$a_{31}^T = \Pi k [i\omega_n G_{11} q_1^\dagger - (G_{11} - G_{12}) q_2^\dagger] + q_2^\dagger,$$

$$a_{41}^T = \Pi k [i\omega_n G_{12} q_1^\dagger - (G_{12} - G_{11}) q_2^\dagger].$$

When the correlation parameter C is equal to one, the row vector containing thermal Gaussian noises and external force in frequency domain is $\zeta_n^T = (\tilde{\eta}_A, \tilde{\eta}_B, \tilde{f}_A)$, and the matrices C_n^I and C_n^{II} are

$$C_n^I = \begin{bmatrix} 0 & 0 & i\omega_n G_{11} \\ 0 & 0 & i\omega_n G_{12} \\ -i\omega_n G_{11}^* & -i\omega_n G_{12}^* & i\omega_n [\{G_{11} - G_{11}^*\} + \alpha \{G_{12} - G_{12}^*\}] \end{bmatrix}, \quad C_n^{II} = \begin{bmatrix} C_{11} & C_{12} & C_{13} \\ C_{12}^* & C_{22} & C_{23} \\ C_{13}^* & C_{23}^* & C_{33} \end{bmatrix},$$

where the matrix elements of C_n^{II} are

$$C_{11} = i\omega_n [G_{11}^* G_{12} - G_{11} G_{12}^*],$$

$$C_{12} = i\omega_n [|G_{12}|^2 - |G_{11}|^2],$$

$$C_{13} = i\omega_n [G_{12} (G_{11}^* + \alpha G_{12}^*) - G_{11} (G_{12}^* + \alpha G_{11}^*)],$$

$$C_{22} = -i\omega_n [G_{11}^* G_{12} - G_{11} G_{12}^*],$$

$$C_{23} = i\omega_n [|G_{11}|^2 - |G_{12}|^2 + \alpha (G_{11} G_{12}^* - G_{12} G_{11}^*)],$$

$$C_{33} = i\omega_n (1 - \alpha^2) [G_{11}^* G_{12} - G_{11} G_{12}^*].$$

The column vector α_n is

$$\alpha_n = -\frac{\lambda}{T} \begin{pmatrix} b_{11}^T \Delta U \\ b_{21}^T \Delta U \\ b_{31}^T \Delta U \end{pmatrix} - ie^{-i\omega\epsilon} \begin{pmatrix} l_1^T \sigma \\ l_2^T \sigma \\ l_3^T \sigma \end{pmatrix}, \quad \text{in which}$$

$$b_{11}^T = \Pi k [i\omega_n G_{11} q_1^\dagger - (G_{11} - G_{12}) q_2^\dagger],$$

$$b_{21}^T = \Pi k [i\omega_n G_{12} q_1^\dagger - (G_{12} - G_{11}) q_2^\dagger],$$

$$b_{31}^T = \Pi k [i\omega_n (G_{11} + \alpha G_{12}) q_1^\dagger - (1 - \alpha)(G_{11} - G_{12}) q_2^\dagger] + q_2^\dagger.$$

Therefore, we get

$$\begin{aligned} \langle e^{E(\tau)} \rangle_{U, U_0} &= \left\langle \exp \left[-\frac{\lambda\tau}{2T} \zeta_0^T C_0 \zeta_0 + \zeta_0^T \alpha_0 - \frac{\lambda \Pi k}{2T\tau} q_0^2 \right] \right\rangle \\ &\times \prod_{n=1}^{\infty} \left\langle \exp \left[-\frac{\lambda\tau}{T} \zeta_n^T C_n \zeta_n^* + \zeta_n^T \alpha_n + \alpha_{-n}^T \zeta_n^* - \frac{\lambda \Pi k}{T\tau} |q_n|^2 \right] \right\rangle. \end{aligned} \quad (2.44)$$

Here, the angular brackets show the average for each $n \geq 1$ term with respect to distribution given by

$$P(\zeta_n) = \begin{cases} \frac{\exp[-\zeta_n^T \Lambda^{-1} \zeta_n^*]}{\pi^4 \det \Lambda} & \text{for } C = 0, \\ \frac{\exp[-\zeta_n^T \Lambda^{-1} \zeta_n^*]}{\pi^3 \det \Lambda} & \text{for } C = 1, \end{cases} \quad (2.45)$$

whereas for $n = 0$ term, the average is computed with respect to the following distribution

$$P(\zeta_0) = \begin{cases} \frac{\exp[-\frac{1}{2} \zeta_0^T \Lambda^{-1} \zeta_0]}{\sqrt{(2\pi)^4 \det \Lambda}} & \text{for } C = 0, \\ \frac{\exp[-\frac{1}{2} \zeta_0^T \Lambda^{-1} \zeta_0]}{\sqrt{(2\pi)^3 \det \Lambda}} & \text{for } C = 1. \end{cases} \quad (2.46)$$

Vectors	C = 0	C = 1
ρ^T	$(q_3^*, q_4^*, q_3^*, q_4^*)$	(l_1^*, l_2^*, l_3^*)
a_1^T	$-\lambda/T(c_{11}, c_{12}, c_{13}, c_{14})$	$-\lambda/T(d_{11}, d_{12}, d_{13})$
ϕ	$\begin{pmatrix} q_3^T \\ q_4^T \\ q_3^T \\ q_4^T \end{pmatrix}$	$\begin{pmatrix} l_1^T \\ l_2^T \\ l_3^T \end{pmatrix}$
a_2	$-\frac{\lambda}{T} \begin{pmatrix} a_{11}^T \\ a_{21}^T \\ a_{31}^T \\ a_{41}^T \end{pmatrix}$	$-\frac{\lambda}{T} \begin{pmatrix} b_{11}^T \\ b_{21}^T \\ b_{31}^T \end{pmatrix}$

TABLE 2.1: Vectors ρ^T , a_1^T , ϕ , and a_2 are shown.

The diagonal matrix Λ given above is

$$\Lambda = \begin{cases} 2D/\tau \text{ diag}(1, 1, \theta, \alpha^2\theta) & \text{for } C = 0, \\ 2D/\tau \text{ diag}(1, 1, \theta) & \text{for } C = 1. \end{cases}$$

After computing the averages over the thermal Gaussian noises and external Gaussian forces, we get

$$\langle e^{E(\tau)} \rangle_{U, U_0} = e^{(\tau/\tau_\gamma)\mu(\lambda)} e^{\frac{1}{2} \sum_{n=-\infty}^{\infty} [\alpha_n^T \Omega_n^{-1} \alpha_n - \frac{\lambda \Pi k}{T\tau} |q_n|^2]}, \quad \text{where } \Omega_n = [\Lambda^{-1} + \lambda\tau/T C_n]. \quad (2.47)$$

In the large time limit ($\tau \rightarrow \infty$), we convert the summation into integration. Therefore,

$$\langle e^{E(\tau)} \rangle_{U, U_0} \approx e^{(\tau/\tau_\gamma)\mu(\lambda)} e^{-\frac{1}{2}\sigma^T H_1 \sigma + i\Delta U^T H_2 \sigma + \frac{1}{2}\Delta U^T H_3 \Delta U}, \quad \text{where} \quad (2.48)$$

$$\mu(\lambda) = -\frac{\tau_\gamma}{4\pi} \int_{-\infty}^{\infty} d\omega \ln[\det(\Lambda\Omega)], \quad (2.49)$$

$$H_1 = \frac{\tau}{2\pi} \int_{-\infty}^{\infty} d\omega \rho^T \Omega^{-1} \phi, \quad (2.50)$$

$$H_2 = -\frac{\tau}{2\pi} \int_{-\infty}^{\infty} d\omega e^{-i\omega\epsilon} a_1^T \Omega^{-1} \phi, \quad (2.51)$$

$$H_3 = \frac{\tau}{2\pi} \int_{-\infty}^{\infty} d\omega \left[a_1^T \Omega^{-1} a_2 - \frac{\lambda \Pi k}{T\tau} (q_1 q_2^\dagger + q_2 q_1^\dagger) \right]. \quad (2.52)$$

Here, the viscous relaxation time $\tau_\gamma = m/\gamma$, and the vectors ρ^T , a_1^T , ϕ , and a_2 are

given in TABLE 2.1 in which

$$\begin{aligned}
c_{11} &= -\text{Pk}[i\omega G_{11}^* q_1 + (G_{11}^* - G_{12}^*) q_2], \\
c_{12} &= -\text{Pk}[i\omega G_{12}^* q_1 + (G_{12}^* - G_{11}^*) q_2], \\
c_{13} &= -\text{Pk}[i\omega G_{11}^* q_1 + (G_{11}^* - G_{12}^*) q_2] + q_2, \\
c_{14} &= -\text{Pk}[i\omega G_{12}^* q_1 + (G_{12}^* - G_{11}^*) q_2], \\
d_{11} &= -\text{Pk}[i\omega G_{11}^* q_1 + (G_{11}^* - G_{12}^*) q_2], \\
d_{12} &= -\text{Pk}[i\omega G_{12}^* q_1 + (G_{12}^* - G_{11}^*) q_2], \\
d_{13} &= -\text{Pk}[i\omega (G_{11}^* + \alpha G_{12}^*) q_1 + (G_{11}^* - G_{12}^*) (1 - \alpha) q_2] + q_2.
\end{aligned}$$

Therefore, we write the restricted moment generating function for W using Eq. (2.42)

as

$$Z_W(\lambda, U, \tau | U_0) \approx e^{(\tau/\tau_\gamma)\mu(\lambda)} e^{\frac{1}{2}\Delta U^T H_3 \Delta U} \int \frac{d^3\sigma}{(2\pi)^3} e^{i\sigma^T U} e^{-\frac{1}{2}\sigma^T H_1 \sigma} e^{i\sigma^T H_2^T \Delta U}. \quad (2.53)$$

The integration over σ yields

$$Z_W(\lambda, U, \tau | U_0) \approx \frac{e^{(\tau/\tau_\gamma)\mu(\lambda)}}{\sqrt{(2\pi)^3 \det H_1(\lambda)}} e^{\frac{1}{2}\Delta U^T H_3 \Delta U} e^{-\frac{1}{2}(U^T + \Delta U^T H_2) H_1^{-1} (U + H_2^T \Delta U)}. \quad (2.54)$$

Factorizing the above equation in terms of the initial U_0 and final variable U [see Eq. (2.33)] gives the condition $(H_3 - H_2 H_1^{-1} H_2^T - H_1^{-1} H_2^T) + (H_3 - H_2 H_1^{-1} H_2^T - H_2 H_1^{-1})^T = 0$, therefore,

$$Z_W(\lambda, U, \tau | U_0) \approx \frac{e^{(\tau/\tau_\gamma)\mu(\lambda)} e^{-\frac{1}{2}U^T L_1(\lambda) U} e^{-\frac{1}{2}U_0^T L_2(\lambda) U_0}}{\sqrt{(2\pi)^3 \det H_1(\lambda)}}, \quad \text{where} \quad (2.55)$$

$$L_1(\lambda) = H_1^{-1} + H_1^{-1} H_2^T, \quad \text{and} \quad L_2(\lambda) = -H_1^{-1} H_2^T.$$

The steady state distribution for the coupled system is obtained by substituting $\lambda = 0$ and taking large time limit ($\tau \rightarrow \infty$) in the above equation:

$$Z_W(0, U, \tau \rightarrow \infty | U_0) = P_{ss}(U) = \frac{e^{-\frac{1}{2}U^T H_1^{-1}(0) U}}{\sqrt{(2\pi)^3 \det H_1(0)}}. \quad (2.56)$$

Moreover, one can verify from Eq. (2.26) that $\langle U(\tau)U^T(\tau) \rangle = H_1(0)$.

Using Eq. (2.30), the restricted moment generating function for total entropy production for particle A in the coupled system is

$$Z(\lambda, U, \tau|U_0) = \frac{e^{(\tau/\tau_\gamma)\mu(\lambda)} e^{-\frac{1}{2}U^T \tilde{L}_1(\lambda)U} e^{-\frac{1}{2}U_0^T \tilde{L}_2(\lambda)U_0}}{\sqrt{(2\pi)^3 \det H_1(\lambda)}}, \quad (2.57)$$

where the matrices $L_1(\lambda)$ and $L_2(\lambda)$ modify to

$$\tilde{L}_1(\lambda) = L_1(\lambda) - \lambda \Sigma \left[\frac{m}{T} - \frac{1}{H} \right], \quad \text{and} \quad \tilde{L}_2(\lambda) = L_2(\lambda) + \lambda \Sigma \left[\frac{m}{T} - \frac{1}{H} \right].$$

The moment generating function $Z(\lambda)$ is obtained by integrating $Z(\lambda, U, \tau|U_0)$ over the initial variable U_0 with respect to the steady state distribution $P_{ss}(U_0)$ and final variables U ,

$$Z(\lambda) = \int dU \int dU_0 P_{ss}(U_0) Z(\lambda, U, \tau|U_0) = g(\lambda) e^{(\tau/\tau_\gamma)\mu(\lambda)} + \dots, \quad (2.58)$$

where the cumulant generating function $\mu(\lambda)$ is given in Eq. (2.49), can be written as

$$\mu(\lambda) = -\frac{1}{4\pi} \int_{-\infty}^{\infty} du \ln \left[1 + \frac{h(u, \lambda)}{q(u)} \right]. \quad (2.59)$$

The function $h(u, \lambda)$ for first choice of forces ($C = 0$) is

$$\begin{aligned} h(u, \lambda) = & 4\theta\lambda(1-\lambda)[u^4 + (1-\delta)u^2 + \delta^2(2-\Pi)/4] - \lambda\delta^2\{\lambda\alpha^2\theta^2(\Pi-1)^2 + \lambda\Pi^2 \\ & - \Pi\theta[\alpha^2 + \lambda\{1 - \Pi(1 + \alpha^2)\}]\} \end{aligned} \quad (2.60)$$

whereas for second choice of forces ($C = 1$)

$$\begin{aligned} h(u, \lambda) = & 4\theta\lambda(1-\lambda)[u^4 + (1-\delta)u^2 + \delta^2/2] - 4\theta\lambda(1-\lambda\Pi)\delta\alpha u^2 \\ & - \lambda\delta^2[\lambda\Pi^2 + \theta\{\Pi - \Pi\lambda(2-\Pi) + \alpha(\lambda\Pi-1)(2+\alpha\Pi)\}]. \end{aligned} \quad (2.61)$$

The function $q(u)$ is same for both choices of external forces and also for both definitions of entropy production

$$q(u) = (1+u^2)[u^2 + (u^2 - \delta)^2]. \quad (2.62)$$

The prefactor $g(\lambda)$ in Eq. (2.58) is

$$g(\lambda) = \left[\det[H_1(\lambda)H_1(0)\tilde{L}_1(\lambda)] \det[H_1^{-1}(0) + \tilde{L}_2(\lambda)] \right]^{-1/2}. \quad (2.63)$$

2.6 Probability distribution function and the fluctuation theorem

In this chapter, our aim is to find the probability distribution function for ΔS_{tot}^A . To obtain that, we invert the moment generating function $Z(\lambda)$ using inverse transformation

$$P(\Delta S_{tot}^A = s\tau/\tau_\gamma) = \frac{1}{2\pi i} \int_{-i\infty}^{+i\infty} d\lambda Z(\lambda) e^{\lambda s\tau/\tau_\gamma}, \quad (2.64)$$

where the contour of integration is taken along the direction of imaginary axis passing through the origin of complex λ -plane, and $s = \Delta S_{tot}^A \tau_\gamma / \tau$ is the scaled variable. In the large- τ limit ($\tau \gg \tau_\gamma$), we rewrite the above given integral as

$$P(\Delta S_{tot}^A = s\tau/\tau_\gamma) \approx \frac{1}{2\pi i} \int_{-i\infty}^{+i\infty} d\lambda g(\lambda) e^{(\tau/\tau_\gamma)h_s(\lambda)}, \quad (2.65)$$

where $h_s(\lambda) = \mu(\lambda) + \lambda s$.

The above integral can be approximated using saddle-point method provided both $\mu(\lambda)$ and $g(\lambda)$ are analytic function of λ [136]. Thus,

$$P(\Delta S_{tot}^A = s\tau/\tau_\gamma) \approx \frac{g(\lambda^*) e^{(\tau/\tau_\gamma)h_s(\lambda^*)}}{\sqrt{2\pi\tau/\tau_\gamma |h_s''(\lambda^*)|}}, \quad (2.66)$$

where $\lambda^*(s)$ is the saddle point solution of the following equation

$$\left. \frac{\partial \mu(\lambda)}{\partial \lambda} \right|_{\lambda=\lambda^*} = -s, \quad (2.67)$$

and

$$h_s''(\lambda^*) = \left. \frac{\partial^2 h_s(\lambda)}{\partial \lambda^2} \right|_{\lambda=\lambda^*}. \quad (2.68)$$

The fluctuation theorem estimates the ratio of probability of positive total entropy production and that of negative total entropy production where the latter one can be

written as

$$P(\Delta S_{tot}^A = -s\tau/\tau_\gamma) \approx \frac{1}{2\pi i} \int_{-i\infty}^{+i\infty} d\lambda g(\lambda) e^{(\tau/\tau_\gamma)[\mu(\lambda)-\lambda s]}. \quad (2.69)$$

If both functions $\mu(\lambda)$ and $g(\lambda)$ satisfy Gallavotti-Cohen (GC) symmetry [82], i.e. $\mu(\lambda) = \mu(1 - \lambda)$ and $g(\lambda) = g(1 - \lambda)$, we can write

$$P(\Delta S_{tot}^A = -s\tau/\tau_\gamma) \approx \frac{e^{-s\tau/\tau_\gamma}}{2\pi i} \int_{1-i\infty}^{1+i\infty} d\lambda g(\lambda) e^{(\tau/\tau_\gamma)[\mu(\lambda)+\lambda s]},$$

where the contour of integration is along the imaginary axis at $\lambda = 1$ of complex λ -plane. In the absence of singularity in $\mu(\lambda)$ and $g(\lambda)$ between $(1 - i\infty, 1 + i\infty)$ to $(-i\infty, +i\infty)$, the contour of integration can be shifted from $\lambda = 1$ to the origin of complex λ -plane. Therefore,

$$P(\Delta S_{tot}^A = -s\tau/\tau_\gamma) \approx \frac{e^{-s\tau/\tau_\gamma}}{2\pi i} \int_{-i\infty}^{+i\infty} d\lambda g(\lambda) e^{(\tau/\tau_\gamma)[\mu(\lambda)+\lambda s]}. \quad (2.70)$$

From Eq. (2.65) and (2.70), we obtain the relation

$$\frac{P(\Delta S_{tot}^A = s\tau/\tau_\gamma)}{P(\Delta S_{tot}^A = -s\tau/\tau_\gamma)} \approx e^{s\tau/\tau_\gamma}. \quad (2.71)$$

The above relation is called fluctuation theorem for total entropy production in the steady state. Notice that the sign \approx indicates that the above given result is true for large but finite time τ . Therefore, the criteria for any observable to satisfy the fluctuation theorem in the steady state are: (1) the corresponding cumulant generating function $\mu(\lambda)$ and prefactor $g(\lambda)$ should be analytic function of $\lambda \in [0, 1]$, and (2) both functions must follow GC symmetry.

2.7 Single Brownian particle

We consider a single Brownian particle (see Fig. 2.1 with $\delta=0$) in the heat bath at a temperature T . Let the particle is driven by external Gaussian white noise. In this section, we show that the moment generating function corresponding to the total entropy production follows both conditions (1) and (2). When coupling is absent

($\delta = 0$), the cumulant generating function given in Eq. (2.59) reduces to

$$\mu_0(\lambda) = -\frac{1}{4\pi} \int_{-\infty}^{\infty} du \ln \left[1 + \frac{4\theta\lambda(1-\lambda)}{u^2 + 1} \right], \quad (2.72)$$

which can be solved exactly, and it is given by

$$\mu_0(\lambda) = 1/2[1 - \nu(\lambda)], \quad \text{where} \quad (2.73)$$

$$\nu(\lambda) = \sqrt{4\theta(\lambda_+ - \lambda)(\lambda - \lambda_-)} \quad \text{with} \quad \lambda_{\pm} = 1/2[1 \pm \sqrt{1 + \theta^{-1}}]. \quad (2.74)$$

In the above equation, the branch points $\lambda_+ > 0$ and $\lambda_- < 0$. Moreover, $\lambda_- + \lambda_+ = 1$. In this case, one can also compute the prefactor term exactly, and it is given by

$$g_0(\lambda) = \frac{2\sqrt{\nu(\lambda)}}{1 + \nu(\lambda)}, \quad (2.75)$$

This means that both $\mu_0(\lambda)$ and $g_0(\lambda)$ are analytic function of λ where $\lambda \in (\lambda_-, \lambda_+)$. Moreover, both of them follow GC symmetry, i.e. $\mu_0(\lambda) = \mu_0(1 - \lambda)$ and $g_0(\lambda) = g_0(1 - \lambda)$. Hence, steady state fluctuation theorem is satisfied in this case.

2.8 Analysis for cumulant generating function $\mu(\lambda)$

In the following, we show how to compute the integral given in Eq. (2.59). We rewrite the integral using integration by parts

$$\mu(\lambda) = \frac{1}{4\pi} \int_{-\infty}^{+\infty} du \frac{u[h'(u, \lambda)q(u) - h(u, \lambda)q'(u)]}{q(u)[q(u) + h(u, \lambda)]}, \quad (2.76)$$

where $'$ represents a derivative with respect to u . In the above integrand, the factors in the denominator are polynomials in the variable u^2 . Therefore, the denominator can be factored in terms of the roots of the polynomials:

$$q(u) + h(u, \lambda) = \prod_j (u^2 - u_j^2),$$

$$\text{and } q(u) = \prod_k (u^2 - w_k^2).$$

This gives a set of simple poles in the complex u -plane. Consequently, evaluating the integral by using the residue theorem, and using $q(u_j) + h(u_j, \lambda) = 0$ and $q(w_k) = 0$, gives

$$\mu(\lambda) = \frac{i}{2} \left[\sum_j u_j - \sum_k w_k \right], \quad (2.77)$$

where $\{u_j\}$ and $\{w_k\}$ are the zeros of the polynomials $[q(u) + h(u, \lambda)]$ and $q(u)$, respectively, that lies on the positive half of the complex u -plane. Clearly, $\{u_j\}$ are functions of λ while $\{w_k\}$ are independent of λ . The computation of $\mu(\lambda)$ using these residues is quite cumbersome. Nevertheless, one can compute $\mu(\lambda)$ numerically provided the range of λ is known within which the cumulant generating function remains real function. The range of λ is dependent upon the choice of θ and α for given δ . One can see that the domain is restricted between the branch point singularities of the cumulant generating function $\mu(\lambda)$. To obtain these singularities for $\delta > 0$, we analyze the argument of the logarithm in the integrand in Eq. (2.59), i.e. the terms $q(u)$ and $q(u) + h(u, \lambda)$. In all four cases, we find that the function $q(u)$ given in Eq. (2.62), is always positive for any real $u \in (-\infty, \infty)$. We also find that,

$$h(u, \lambda) = b(u)\lambda - p(u)\lambda^2, \quad (2.78)$$

where the functions $b(u)$ and $p(u)$ are different for all four cases [see Eqs. (2.60) and (2.61)]. In all the cases, $p(u)$ is always positive for any real $u \in (-\infty, \infty)$. The two roots

$$\lambda_{\pm}(u) = \frac{b(u) \pm \sqrt{b^2(u) + 4p(u)q(u)}}{2p(u)}, \quad (2.79)$$

of the quadratic polynomial $q(u) + h(u, \lambda)$, are always real for any real $u \in (-\infty, \infty)$. Moreover, $\lambda_+(u)$ is positive and $\lambda_-(u)$ is negative. For a given u , the integrand in Eq. (2.59) is real only within the range $\lambda \in (\lambda_-(u), \lambda_+(u))$. Therefore, $\mu(\lambda)$ is real only within the range $\lambda \in (\lambda_-^{(\delta)}, \lambda_+^{(\delta)})$, where

$$\lambda_-^{(\delta)} = \max_u \lambda_-(u) \quad \text{and} \quad \lambda_+^{(\delta)} = \min_u \lambda_+(u).$$

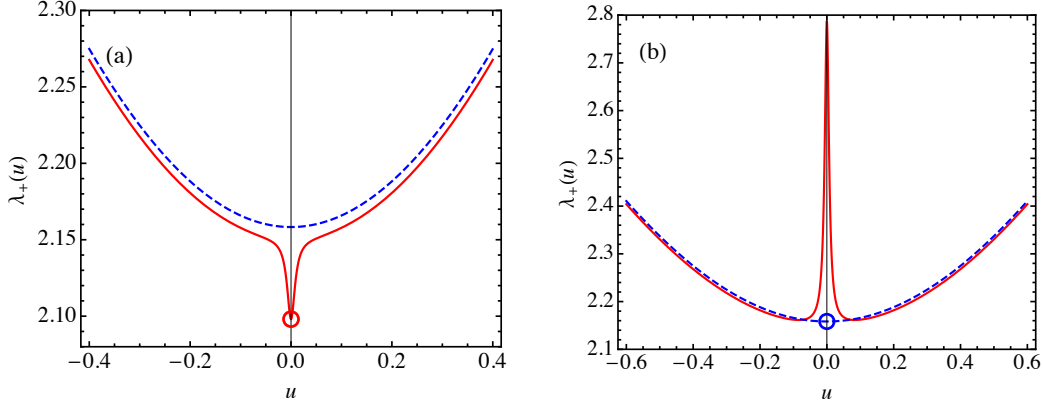


FIGURE 2.2: (a) The red solid line plots $\lambda_+(u)$ for $0 < \delta < 1$, which has one minimum (marked by the red circle) at $u = 0$. The blue dashed line plots $\lambda_+(u)$ for the $\delta = 0$ case, whose minimum stays above that of the red line. (b) The red solid line plots $\lambda_+(u)$ for $0 < \delta < 1$, which has two minima closer to $u = 0$ and a maximum at $u = 0$. The blue dashed line plots $\lambda_+(u)$ for the $\delta = 0$ case, which has a minimum. (marked by the red circle) at $u = 0$. In the limit $\delta \rightarrow 0$, the minima of the red line converges to the blue circle.

The equation for extremum is given by

$$\left. \frac{\partial \lambda_{\pm}(u)}{\partial u} \right|_{u=u_{\pm}^*} = 0. \quad (2.80)$$

Consequently, we write the equation which gives u_{\pm}^*

$$\begin{aligned} & [\sqrt{b^2(u_{\pm}^*) + 4p(u_{\pm}^*)q(u_{\pm}^*)} \pm b(u_{\pm}^*)] [p(u_{\pm}^*)b'(u_{\pm}^*) - p'(u_{\pm}^*)b(u_{\pm}^*)] \\ & \pm 2p(u_{\pm}^*) [p(u_{\pm}^*)q'(u_{\pm}^*) - p'(u_{\pm}^*)q(u_{\pm}^*)] = 0. \end{aligned} \quad (2.81)$$

Note that the above equation is true for all δ . In weak coupling limit ($\delta \rightarrow 0$), we can find u_{\pm}^* using Eq. (2.81). This gives $\lambda_{\pm}(u) \rightarrow \lambda_{\pm}^{(\delta)}$ as $u \rightarrow u_{\pm}^*$.

In Figs. 2.2 and 2.3, we plot $\lambda_{\pm}(u)$ given in Eq. (2.79), against u for different values of θ and α . For $0 < \delta < 1$, we find that $\lambda_+(u)$ has either one minimum located at $u = 0$ [see Fig. 2.2(a)] or two minima located at $u = \pm u_+^*$ [see Fig. 2.2(b)] (where $u_+^* \rightarrow 0$ as $\delta \rightarrow 0$) depending on the parameters θ and α . This is determined by whether

$$\left. \frac{\partial^2 \lambda_+(u)}{\partial u^2} \right|_{u=0} > 0 \quad \text{or} \quad \left. \frac{\partial^2 \lambda_+(u)}{\partial u^2} \right|_{u=0} < 0. \quad (2.82)$$

In the first case, we get $\lambda_+^{(\delta)} \rightarrow \tilde{\lambda}_+ < \lambda_+$ as $\delta \rightarrow 0$, whereas in the latter case $\lambda_+^{(\delta)}$ converges to λ_+ as $\delta \rightarrow 0$. Similarly, we get $\lambda_-^{(\delta)} \rightarrow \tilde{\lambda}_- > \lambda_-$ [see Fig. 2.3(a)] or λ_-

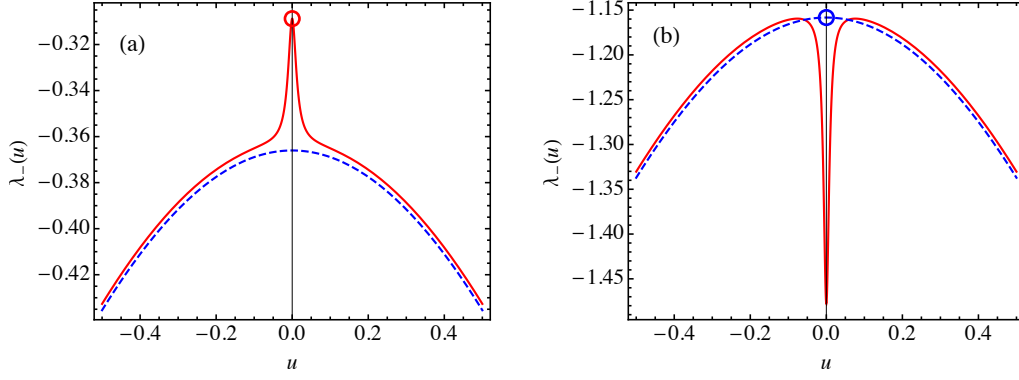


FIGURE 2.3: (a) The red solid line plots $\lambda_-(u)$ for $0 < \delta < 1$, which has one maximum (marked by the red circle) at $u = 0$. The blue dashed line plots $\lambda_-(u)$ for the $\delta = 0$ case, whose maximum stays below that of the red line. (b) The red solid line plots $\lambda_-(u)$ for $0 < \delta < 1$, which has two maxima closer to $u = 0$ and a minimum at $u = 0$. The blue dashed line plots $\lambda_-(u)$ for the $\delta = 0$ case, which has a maximum (marked by the red circle) at $u = 0$. In the limit $\delta \rightarrow 0$, the maxima of the red line converges to the blue circle.

[see Fig. 2.3(b)] depending on whether

$$\left. \frac{\partial^2 \lambda_-(u)}{\partial u^2} \right|_{u=0} < 0 \quad \text{or} \quad \left. \frac{\partial^2 \lambda_-(u)}{\partial u^2} \right|_{u=0} > 0. \quad (2.83)$$

It turns out that the sign of $\lambda''_{\pm}(0)$ gives the contour separating different possibilities of pair of branch point singularities $(\lambda_-^{\delta}, \lambda_+^{\delta})$, where $'$ represents a derivative with respect to u .

For parameters $\Pi = 1$, $C = 0$, and $0 < \delta < 1$, we see that $\lambda''_+(0) > 0$ and sign of $\lambda''_-(0)$ is determined by a function $r_1(\theta, \alpha, \delta)$. Therefore, the equation of contour in this case is given by

$$r_1(\theta, \alpha, \delta) = 0, \quad \text{where} \quad (2.84)$$

$$r_1(\theta, \alpha, \delta) = -1 - \theta(\alpha^2 - 3)(2 + \theta + \theta\alpha^2) + \delta[1 + \theta(1 + \alpha^2)]^2.$$

Therefore, we plot the phase diagram in (α, θ) plane using Eq. (2.84) in the limit $\delta \rightarrow 0$ as shown in Fig. 2.4(a). In this case, the pair of branch point singularities in the limit $\delta \rightarrow 0$ are $(\lambda_-, \tilde{\lambda}_+)$ and $(\tilde{\lambda}_-, \tilde{\lambda}_+)$ in region I and II, respectively, of Fig. 2.4(a), where

$$\tilde{\lambda}_+ = 1, \quad (2.85)$$

$$\tilde{\lambda}_- = -(1 + \theta + \theta\alpha^2)^{-1}. \quad (2.86)$$

For parameters $\Pi = 0$, $C = 0$, and $0 < \delta < 1$, the sign of $\lambda_+''(0)$ and $\lambda_-''(0)$ is determined by functions $r_2(\theta, \alpha, \delta)$, and $r_3(\theta, \alpha, \delta)$, respectively. Therefore, the equations of contours in this case are given by

$$r_2(\theta, \alpha, \delta) = 0, \quad (2.87)$$

$$r_3(\theta, \alpha, \delta) = 0, \quad (2.88)$$

where

$$\begin{aligned} r_2(\theta, \alpha, \delta) &= -4 + \alpha^4\theta^2 + 4\alpha^2\theta[\theta + \sqrt{\theta(2 + \theta + \theta\alpha^2)}] - \delta(2 + \theta\alpha^2)^2, \\ r_3(\theta, \alpha, \delta) &= 4 - \alpha^4\theta^2 - 4\alpha^2\theta[\theta - \sqrt{\theta(2 + \theta + \theta\alpha^2)}] + \delta(2 + \theta\alpha^2)^2. \end{aligned}$$

Therefore, using Eqs. (2.87) and (2.88), we plot the phase diagram in (α, θ) plane as shown in Fig. 2.4(b) in the limit $\delta \rightarrow 0$. In this case, the pair of branch point singularities in the limit $\delta \rightarrow 0$ are (λ_-, λ_+) , $(\lambda_-, \tilde{\lambda}_+)$, and $(\tilde{\lambda}_-, \tilde{\lambda}_+)$ in region I, II and III, respectively, of Fig. 2.4(b), where

$$\tilde{\lambda}_\pm = \frac{\theta \pm \sqrt{\theta(2 + \theta + \theta\alpha^2)}}{2\theta + \theta^2\alpha^2}. \quad (2.89)$$

For parameters $\Pi = 1$, $C = 1$, and $0 < \delta < 1$, we see that $\lambda_+''(0) > 0$ and sign of $\lambda_-''(0)$ is determined by a function $r_4(\theta, \alpha, \delta)$. Therefore, the equation of contour in this case is given by

$$r_4(\theta, \alpha, \delta) = 0, \quad \text{where} \quad (2.90)$$

$$\begin{aligned} r_4(\theta, \alpha, \delta) &= -1 - \theta(\alpha - 1)(3 + \alpha)[2 + (1 + \alpha)^2\theta] + 2\delta[1 - \theta(1 - \alpha^2)\{2 + (1 + \alpha)^2\theta\}] \\ &\quad - \delta^2[1 + \theta(1 + \alpha)^2]^2. \end{aligned}$$

Therefore, we use Eq. (2.90) to plot the phase diagram in (α, θ) plane in the limit $\delta \rightarrow 0$ as shown in Fig. 2.4(c). In this case, the pair of branch point singularities in the limit $\delta \rightarrow 0$ are $(\lambda_-, \tilde{\lambda}_+)$ and $(\tilde{\lambda}_-, \tilde{\lambda}_+)$ in region I and II, respectively, of Fig. 2.4(c),

where

$$\tilde{\lambda}_+ = 1, \quad (2.91)$$

$$\tilde{\lambda}_- = -[1 + \theta(1 + \alpha)^2]^{-1}. \quad (2.92)$$

Finally, for parameters $\Pi = 0$, $C = 1$, and $0 < \delta < 1$, we see that $\lambda_+''(0) < 0$ and sign of $\lambda_-''(0)$ is determined by a function $r_5(\theta, \alpha, \delta)$. Therefore, the equation of contour in this case is given by

$$r_5(\theta, \alpha, \delta) = 0, \quad \text{where} \quad (2.93)$$

$$r_5(\theta, \alpha, \delta) = 1 + 2\alpha\theta(1 + \alpha) - 2\alpha\sqrt{\theta[2 + \theta(1 + \alpha)^2]} - \delta^2.$$

In the limit $\delta \rightarrow 0$, the phase diagram in this case is plotted using Eq. (2.93) in (α, θ) plane as shown in Fig. 2.4(d), and the pair of branch point singularities in the limit $\delta \rightarrow 0$ are (λ_-, λ_+) and $(\tilde{\lambda}_-, \lambda_+)$ in region I and II, respectively, of Fig. 2.4(d), where

$$\tilde{\lambda}_- = \frac{\theta(1 + \alpha) - \sqrt{\theta[2 + \theta(1 + \alpha)^2]}}{2\theta}. \quad (2.94)$$

In all above cases, λ_{\pm} are given by Eq. (2.74). Notice that the axis (not shown) corresponds to δ is perpendicular to the plane of paper in all phase diagrams (see Fig. 2.4).

Near the branch point we write $\mu(\lambda) = \mu_a(\lambda) + \mu_s(\lambda)$, where $\mu_a(\lambda)$ and $\mu_s(\lambda)$ are the analytic and the singular part of $\mu(\lambda)$, respectively. We now analyze the roots of $q(u) + h(u, \lambda)$ with respect to the variable u , near a branch point. Let us consider the case $\lambda_+^{(\delta)} \rightarrow \tilde{\lambda}_+$. Using Eq. (2.78) and writing $\tilde{\lambda}_+ - \lambda = \epsilon$ near the branch point (where $\epsilon > 0$), we get

$$A(u) - \epsilon B(u) - O(\epsilon^2) = 0, \quad (2.95)$$

where

$$A(u) = q(u) + b(u)\tilde{\lambda}_+ - p(u)\tilde{\lambda}_+^2,$$

$$B(u) = b(u) - 2p(u)\tilde{\lambda}_+.$$

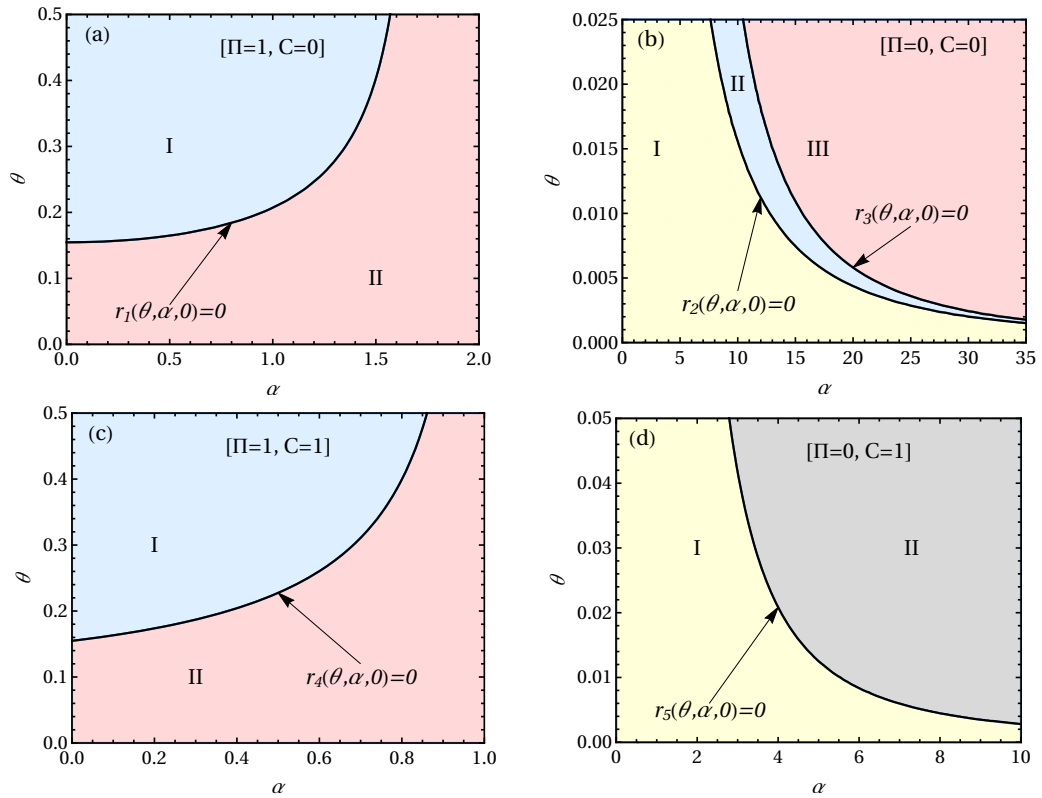


FIGURE 2.4: The phase diagrams corresponding to different choices of Π [see Eq. (2.12)] and C [see Eq. (2.24)] in the limit $\delta \rightarrow 0$, are shown. The axis (not shown) corresponds to δ is perpendicular to the plane of the paper. The contours (black solid lines) given in Eqs. (2.84), (2.87), (2.88), (2.90), and (2.93) separate the different possibilities of the singularities (in the limit $\delta \rightarrow 0$) in the cumulant generating function $\mu(\lambda)$ in the respective regions of the phase diagrams.

The left side of Eq. (2.95) is a polynomial in u^2 . Since the minimum is located at $u = 0$, the branch point $\tilde{\lambda}_+$ satisfies the equation $A(0) = 0$. Therefore, two of the roots $u_{1\pm}^2$ of Eq. (2.95) are of $O(\epsilon)$ for small ϵ , which are given by

$$u_{1\pm}^2 = \frac{2B(0)}{A''(0)} \epsilon + O(\epsilon^2).$$

On the other hand, by differentiating the equation

$$q(u) + b(u)\lambda_+(u) - p(u)\lambda_+^2(u) = 0,$$

and using the condition $\lambda'_+(0) = 0$, we get $B(0)/A''(0) = -1/\lambda''_+(0)$. Since, $\lambda''_+(0) > 0$, we finally get

$$u_{1\pm} = \pm i \frac{\sqrt{2\epsilon}}{\sqrt{\lambda''_+(0)}} + O(\epsilon). \quad (2.96)$$

The other roots are of $O(1)$, which at the leading order, satisfy the reduced equation $u^{-2}A(u) = 0$. Similarly, we can find the behavior near $\tilde{\lambda}_-$. Thus, from Eq. (2.77), we find the nature of the singularities near a branch point as:

$$\mu_s(\lambda) = \begin{cases} -\frac{1}{\sqrt{2\lambda''_+(0)}} \sqrt{\tilde{\lambda}_+ - \lambda} & \text{as } \lambda \rightarrow \tilde{\lambda}_+, \\ -\frac{1}{\sqrt{-2\lambda''_-(0)}} \sqrt{\lambda - \tilde{\lambda}_-} & \text{as } \lambda \rightarrow \tilde{\lambda}_-. \end{cases} \quad (2.97)$$

Note that $\pm\lambda''_{\pm}(0)$ diverges as $\delta \rightarrow 0$. Therefore, $\mu_s(\lambda)$ goes to zero as $\delta \rightarrow 0$.

In the other two cases where $\lambda_{\pm}^{(\delta)} \rightarrow \lambda_{\pm}$, the singular behaviors of $\mu(\lambda)$ near the singularities in the limit $\delta \rightarrow 0$ are same as that of $\mu_0(\lambda)$. In all cases, away from the singularities, $\mu(\lambda) \rightarrow \mu_0(\lambda)$ as $\delta \rightarrow 0$.

2.9 Large deviation function and asymmetry function

2.9.1 Large deviation function

The large deviation function (LDF) is defined by [136]

$$I(s) = \lim_{(\tau/\tau_\gamma) \rightarrow \infty} \frac{1}{(\tau/\tau_\gamma)} \ln P(\Delta S_{tot}^A = s\tau/\tau_\gamma). \quad (2.98)$$

Therefore, from Eq. (2.66) we get $I(s) = h_s(\lambda^*)$.

First consider the case when particles A is isolated from particle B ($\delta = 0$) (see Sec. 2.7). In this case, $\mu_0(\lambda)$ is analytic only within a finite region bounded by a pair of branch point singularities at λ_{\pm} . Here $\lambda_- < 0$ and $\lambda_+ > 1$ with $\lambda_+ + \lambda_- = 1$, where λ_{\pm} are given in Eq. (2.74). In this case, $g_0(\lambda)$ is also analytic within this region $\lambda \in (\lambda_-, \lambda_+)$.

The solution of following equation

$$\mu'_0(\lambda_0^*) = -s, \quad (2.99)$$

gives the saddle-point

$$\lambda_0^*(s) = \frac{1}{2} \left[1 - \frac{s}{\sqrt{s^2 + \theta}} \sqrt{1 + \frac{1}{\theta}} \right]. \quad (2.100)$$

It follows that

$$\lambda_0^*(s) = \begin{cases} \lambda_- + O(1/s^2) & \text{as } s \rightarrow +\infty, \\ \lambda_+ - O(1/s^2) & \text{as } s \rightarrow -\infty. \end{cases} \quad (2.101)$$

Therefore, as s decreases from ∞ to $-\infty$ the saddle point $\lambda_0^*(s)$ moves from λ_- to λ_+ on the real λ line.

Thus, LDF $I_0(s)$ is given by

$$I_0(s) = \mu_0(\lambda_0^*(s)) + \lambda_0^*(s)s = \begin{cases} \mu_0(\lambda_-) + \lambda_-s + O(1/s) & \text{as } s \rightarrow +\infty, \\ \mu_0(\lambda_+) + \lambda_+s - O(1/s) & \text{as } s \rightarrow -\infty. \end{cases} \quad (2.102)$$

In the presence of a nonzero coupling ($\delta > 0$), $\mu(\lambda)$ has branch points at $\lambda_{\pm}^{(\delta)}$. In this case, the LDF $I(s)$ is related to $\mu(\lambda)$ by

$$I(s) = \mu(\lambda^*) + \lambda^*s \quad \text{with } \mu'(\lambda^*) = -s,$$

where we have assumed that $g(\lambda)$ is analytic in the region $\lambda \in (\lambda_-^{(\delta)}, \lambda_+^{(\delta)})$. In case $g(\lambda)$ has a singularity within this range, it can change the above LDF. However, finally we are interested in the $\delta \rightarrow 0$ limit and in this limit we can write $g(\lambda) = g_0(\lambda) + \delta^c g_1(\lambda)$, with $c > 0$, where the function $g_1(\lambda)$ may have singularities. It

is clear that, the singularities of $g_1(\lambda)$ are not going to contribute to the probability density function in the $\delta \rightarrow 0$ limit.

Now, we see from the Sec. 2.8 in the limit $\delta \rightarrow 0$, $\lambda_+^{(\delta)} \rightarrow \tilde{\lambda}_+$ [see Fig. 2.2(a)] or λ_+ [see Fig. 2.2(b)] and $\lambda_-^{(\delta)} \rightarrow \tilde{\lambda}_-$ [see Fig. 2.3(a)] or λ_- [see Fig. 2.3(b)]. In general, we can write the $\mu(\lambda)$ around these singularities. Consider a case when $\lambda_-^{(\delta)} \rightarrow \tilde{\lambda}_-$ and $\lambda_+^{(\delta)} \rightarrow \lambda_+$, near $\tilde{\lambda}_-$, we can write $\mu(\lambda) = \mu_a(\lambda) + \mu_s(\lambda)$ where $\mu_a(\lambda)$ and $\mu_s(\lambda)$ are respectively the analytic and singular part of $\mu(\lambda)$. Evidently, $\mu_a(\lambda) \rightarrow \mu_0(\lambda)$ as $\delta \rightarrow 0$. On the other hand, for the singular part near $\tilde{\lambda}_-$, for small δ , $\mu_s(\lambda) \propto -\delta\sqrt{\lambda - \tilde{\lambda}_-}$ [see Eq. (2.97)]. Note that, for $\delta \rightarrow 0$, if $\lambda_-^{(\delta)} \rightarrow \tilde{\lambda}_-$ instead of λ_- , then it is necessary that $\lambda_- < \tilde{\lambda}_- < 0$. In the limit $\delta \rightarrow 0$, when s increases from $-\infty$ to ∞ , the saddle point $\lambda^*(s)$ moves from λ_+ to $\tilde{\lambda}_-$ on the real λ line. For $[\lambda^*(s) - \tilde{\lambda}_-] \gg \delta^2$, the saddle point is dominated by the equation $\mu'_a(\lambda^*) = -s$, which in the limit $\delta \rightarrow 0$ reduces to Eq. (2.99). Therefore, the LDF is the same $I_0(s)$, that has been obtained for the uncoupled case. On the other hand, for $[\lambda^*(s) - \tilde{\lambda}_-] \ll \delta^2$, the saddle point is dominated by the singular part of the saddle point equation, which results $\lambda^*(s) = \tilde{\lambda}_- + O(\delta^2/s^2)$. This gives $I(s) = \mu_a[\tilde{\lambda}_- + O(\delta^2/s^2)] + \tilde{\lambda}_-s + O(\delta^2/s)$. Thus, in the limit $\delta \rightarrow 0$, we get

$$I(s) = \begin{cases} I_0(s) & \text{for } s < s_1^*, \\ \mu_0(\tilde{\lambda}_-) + \tilde{\lambda}_-s & \text{for } s > s_1^*, \end{cases} \quad (2.103)$$

where s_1^* is given by

$$\lambda_0^*(s_1^*) = \tilde{\lambda}_-. \quad (2.104)$$

with $\lambda_0^*(s)$ is the saddle point given in Eq. (2.100) for uncoupled case ($\delta = 0$).

A similar calculation can be done for the case when $\lambda_-^{(\delta)} \rightarrow \lambda_-$ and $\lambda_+^{(\delta)} \rightarrow \tilde{\lambda}_+$, in the limit $\delta \rightarrow 0$

$$I(s) = \begin{cases} \mu_0(\tilde{\lambda}_+) + \tilde{\lambda}_+s & \text{for } s < s_2^*, \\ I_0(s) & \text{for } s > s_2^*, \end{cases} \quad (2.105)$$

where s_2^* is given by

$$\lambda_0^*(s_2^*) = \tilde{\lambda}_+, \quad (2.106)$$

with $\lambda_0^*(s)$ is the solution of Eq. (2.99).

Since $\lambda_0^*(s)$ is a monotonically decreasing function of s and $\tilde{\lambda}_+ > \tilde{\lambda}_-$, we have $s_2^* < s_1^*$, and for the case when $\lambda_-^{(\delta)} \rightarrow \tilde{\lambda}_-$ and $\lambda_+^{(\delta)} \rightarrow \tilde{\lambda}_+$, in the limit $\delta \rightarrow 0$

$$I(s) = \begin{cases} \mu_0(\tilde{\lambda}_+) + \tilde{\lambda}_+ s & \text{for } s < s_2^*, \\ I_0(s) & \text{for } s_2^* < s < s_1^*, \\ \mu_0(\tilde{\lambda}_-) + \tilde{\lambda}_- s & \text{for } s > s_1^*. \end{cases} \quad (2.107)$$

Finally, when $\lambda_-^{(\delta)} \rightarrow \lambda_-$ and $\lambda_+^{(\delta)} \rightarrow \lambda_+$, in the limit $\delta \rightarrow 0$, we get

$$I(s) = I_0(s) \quad \text{for all } s \quad (2.108)$$

2.9.2 Second order discontinuity of the large deviation function

Consider a case where the LDF given by Eq. (2.103) has following form

$$I(s) = \begin{cases} \mu_0(\lambda_0^*) + \lambda_0^* s & \text{for } s < s_1^*, \\ \mu_0(\tilde{\lambda}_-) + \tilde{\lambda}_- s & \text{for } s > s_1^*, \end{cases}$$

where $\lambda_0^*(s)$ is the solution of Eq. (2.99) and s_1^* is given by (2.104). Evidently, $I(s_{1-}^*) = I(s_{1+}^*)$, where $s_{1\pm}^* = \lim_{\epsilon \rightarrow 0} (s_1^* \pm \epsilon)$.

Taking a derivative with respect to s , for $s > s_1^*$ we have $I'(s) = \tilde{\lambda}_-$. On the other hand for $s < s_1^*$ we get

$$I'(s) = \lambda_0^*(s) + \frac{d\lambda_0^*}{ds} [\mu_0'(\lambda_0^*) + s].$$

Note that the prime ' represents the derivative with respect to s (λ_0^*) on left (right) hand side of above equation. Now using Eqs. (2.99) and (2.104), we have $I'(s_{1-}^*) = I'(s_{1+}^*)$.

For the second derivatives, for $s > s_1^*$ we have $I''(s) = 0$. On the other hand, for $s < s_1^*$, we get

$$I''(s) = \frac{d\lambda_0^*}{ds} = -\frac{1}{\mu_0''(\lambda_0^*)}.$$

Therefore, $I''(s_{1-}^*) = -1/\mu_0''(\tilde{\lambda}_-)$ whereas $I''(s_{1+}^*) = 0$ — the second derivative is discontinuous across $s = s_1^*$.

Similarly, one can show that LDF has second order discontinuities across s_1^* and s_2^* for other cases also.

2.9.3 The asymmetry function and its discontinuity

When the probability density function $p(s)$ obeys fluctuation theorem, it satisfies

$$\lim_{\tau/\tau_\gamma \rightarrow \infty} \frac{\tau_\gamma}{\tau} \ln \frac{p(s)}{p(-s)} = s, \quad (2.109)$$

where the probability density function $p(s)$ can be written as

$$p(s) = P(\Delta S_{tot}^A = s\tau/\tau_\gamma) \tau/\tau_\gamma. \quad (2.110)$$

One can define an asymmetry function $f(s)$ as

$$f(s) = \frac{\tau_\gamma}{\tau} \ln \frac{p(s)}{p(-s)}. \quad (2.111)$$

In the large time limit ($\tau \rightarrow \infty$),

$$f(s) = I(s) - I(-s). \quad (2.112)$$

We analyze below $f(s)$ only for $s > 0$, as for $s < 0$, it can be obtained from the relation $f(-s) = -f(s)$.

When $\lambda_-^{(\delta)} \rightarrow \lambda_-$ and $\lambda_+^{(\delta)} \rightarrow \lambda_+$, in the limit $\delta \rightarrow 0$, evidently $f(s) = s$ for all s . Now for the situation when $\lambda_-^{(\delta)} \rightarrow \tilde{\lambda}_-$ and $\lambda_+^{(\delta)} \rightarrow \lambda_+$ in the limit $\delta \rightarrow 0$, we analyze the asymmetry function using the expression of the LDF given by Eq. (2.103). Here, for brevity, we denote

$$I_1(s) = \mu_0(\tilde{\lambda}_-) + \tilde{\lambda}_- s.$$

From Eq. (2.100), $\lambda_0^*(s) + \lambda_0^*(-s) = 1$, and $\lambda_0^*(0) = 1/2$. Since $\lambda_0^*(s)$ is a monotonically decreasing function of s , we have $\lambda_0^* > 1/2$ for $s < 0$ and $\lambda_0^* < 1/2$ for $s > 0$.

Therefore, s_1^* is always positive as $\tilde{\lambda}_- < 0$. Now, for $s_1^* > 0$, we get

$$f(s) = \begin{cases} I_0(s) - I_0(-s) = s & \text{for } 0 \leq s < s_1^*, \\ I_1(s) - I_0(-s) & \text{for } s > s_1^*. \end{cases}$$

Since the LDF has a second order discontinuity at s_1^* , it is evident that $f(s)$ also has a second order discontinuity at s_1^* . The asymptotic expression of $f(s)$, as $s \rightarrow \infty$, is given by

$$f(s) = [\mu_0(\tilde{\lambda}_-) - \mu_0(\lambda_+)] + [\tilde{\lambda}_- + \lambda_+]s + \dots$$

When $\lambda_-^{(\delta)} \rightarrow \lambda_-$ and $\lambda_+^{(\delta)} \rightarrow \tilde{\lambda}_+$ in the limit $\delta \rightarrow 0$, we again for brevity, denote

$$I_2(s) = [\mu(\tilde{\lambda}_+) + \tilde{\lambda}_+s]$$

in Eq. (2.105). Since $\tilde{\lambda}_+ > 0$, we get $s_2^* < 0$ for $\tilde{\lambda}_+ > 1/2$ and $s_2^* > 0$ for $0 < \tilde{\lambda}_+ < 1/2$. Now when $s_2^* < 0$ we get

$$f(s) = \begin{cases} I_0(s) - I_0(-s) = s & \text{for } 0 \leq s < -s_2^*, \\ I_0(s) - I_2(-s) & \text{for } s > -s_2^*. \end{cases}$$

On the other hand, when $s_2^* > 0$, we get

$$f(s) = \begin{cases} I_2(s) - I_2(-s) = 2\tilde{\lambda}_+s & \text{for } 0 \leq s < s_2^*, \\ I_0(s) - I_2(-s) & \text{for } s > s_2^*. \end{cases}$$

Again, from the second order discontinuity of the LDF, it is evident that $f(s)$ also exhibits a second order discontinuity at $|s_2^*|$. The asymptotic expression of $f(s)$, as $s \rightarrow \infty$, is given by

$$f(s) = [\mu_0(\lambda_-) - \mu_0(\tilde{\lambda}_+)] + [\tilde{\lambda}_+ + \lambda_-]s + \dots$$

When $\lambda_-^{(\delta)} \rightarrow \tilde{\lambda}_-$ and $\lambda_+^{(\delta)} \rightarrow \tilde{\lambda}_+$ in the limit $\delta \rightarrow 0$, for the case $s_2^* > 0$, we get

$$f(s) = \begin{cases} I_2(s) - I_2(-s) = 2\tilde{\lambda}_+s & \text{for } 0 \leq s < s_2^*, \\ I_0(s) - I_2(-s) & \text{for } s_2^* < s < s_1^*, \\ I_1(s) - I_2(-s) & \text{for } s > s_1^*. \end{cases}$$

On the other hand, for $s_2^* < 0$, there may be two cases: (1) $-s_2^* < s_1^*$ and (2) $-s_2^* > s_1^*$.

In the first case, we have

$$f(s) = \begin{cases} I_0(s) - I_0(-s) = s & \text{for } 0 \leq s < -s_2^*, \\ I_0(s) - I_2(-s) & \text{for } -s_2^* < s < s_1^*, \\ I_1(s) - I_2(-s) & \text{for } s > s_1^*, \end{cases}$$

whereas for the second case, we get

$$f(s) = \begin{cases} I_0(s) - I_0(-s) = s & \text{for } 0 \leq s < s_1^*, \\ I_1(s) - I_0(-s) & \text{for } s_1^* < s < -s_2^*, \\ I_1(s) - I_2(-s) & \text{for } s > -s_2^*. \end{cases}$$

From, the second order discontinuities of the LDF at the points s_1^* and s_2^* , it is evident that $f(s)$ also exhibits second order discontinuity at the points s_1^* and $|s_2^*|$. Moreover, in all cases, for $s > \max(s_1^*, |s_2^*|)$, we have

$$f(s) = [\mu_0(\tilde{\lambda}_-) - \mu_0(\tilde{\lambda}_+)] + [\tilde{\lambda}_+ + \tilde{\lambda}_-]s.$$

We plotted the asymmetry functions $f(s)$ given in Eq. (2.112), against the scaled variable $s = \Delta S_{tot}^A \tau_\gamma / \tau$ for partial entropy production [Figs. 2.6(a) and 2.6(b)] and apparent entropy production [Figs. 2.6(c)–2.6(e)] for first choice of external forces ($C = 0$). Similarly, for second choice of external forces ($C = 1$), we plotted the the asymmetry functions $f(s)$ given in Eq. (2.112) against the scaled variable $s = \Delta S_{tot}^A \tau_\gamma / \tau$ for partial entropy production [Figs. 2.7(a) and 2.7(b)] and apparent entropy production [Figs. 2.7(c) and 2.6(d)]. These plots are shown for fixed $\delta = 0.1$ (magenta dashed line) and $\delta = 0.01$ (blue dotdashed line). In the limit $\delta \rightarrow 0$ (black

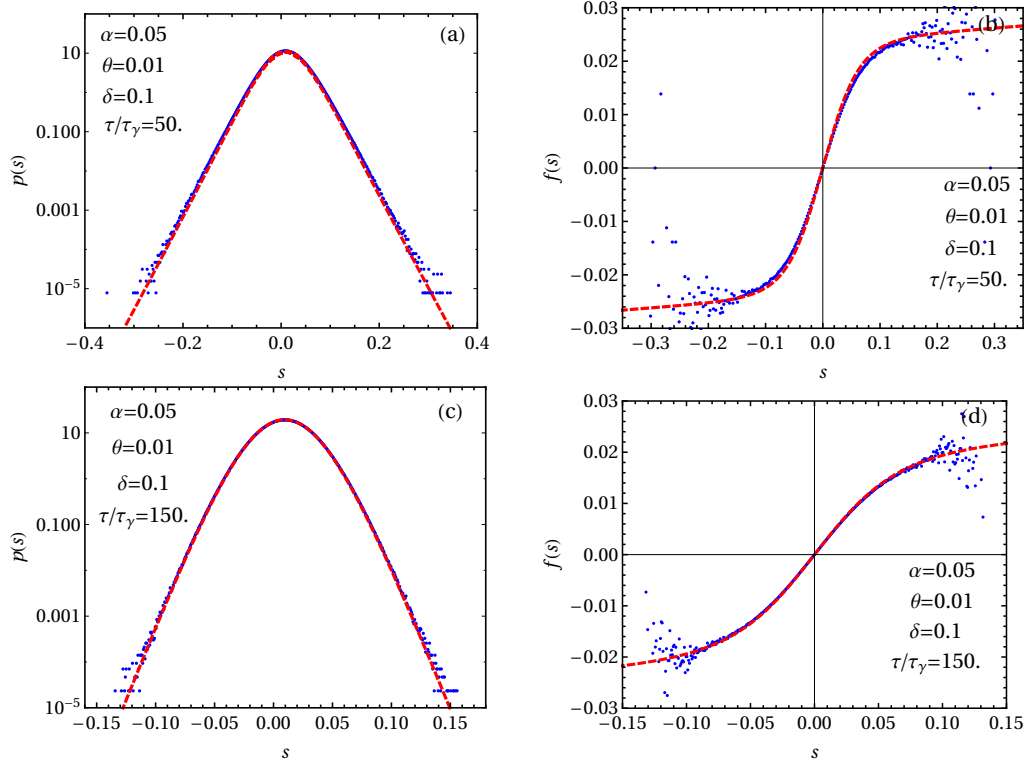


FIGURE 2.5: A comparison of the analytical probability density function $p(s)$ (red dashed lines) given by Eq. (2.110) and the asymmetry function $f(s)$ (red dashed line) given by Eq. (2.111) with the numerical simulations (blue dots) is shown for time $\tau/\tau_\gamma = 50$ [(a) and (b)] and $\tau/\tau_\gamma = 150$ [(c) and (d)]. The parameters θ and α are taken from Fig. 2.4(a) for the case of partial entropy production. The coupling parameter δ and temperature of the heat bath are fixed in all of the above figures and taken to be $\delta = 0.1$, and $T = 1$, respectively. This comparison indicates that as the observation time relative to viscous relaxation time gets longer, the agreement between theoretical prediction and the numerical simulation becomes better.

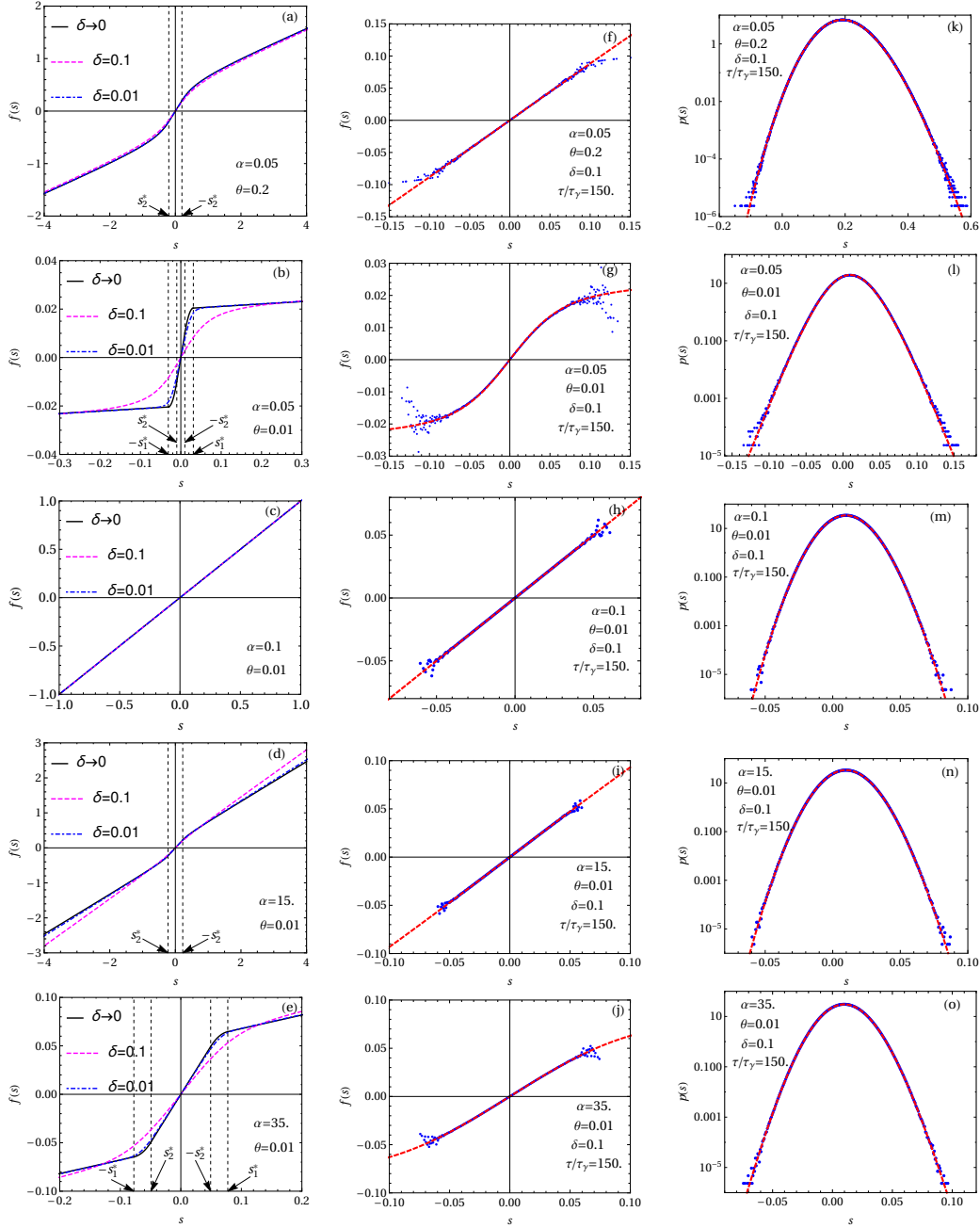


FIGURE 2.6: The above figures are plotted for first choice of external forces, i.e. $C = 0$. The analytical asymmetry function $f(s)$ given in Eq. (2.112), are plotted against the scaled variable $s = \Delta S_{tot}^A \tau_\gamma / \tau$ for: partial entropy production in (a) and (b), and apparent entropy production in (c)–(e), where s_1^* and s_2^* are given in Sec. 2.9. These plots are shown for coupling parameter $\delta = 0.1$ (magenta dashed line) and $\delta = 0.01$ (blue dotdashed line). The asymmetry functions in the limit $\delta \rightarrow 0$ (black solid line) are also shown for respective cases. The comparison of analytical asymmetry functions $f(s)$ (red dashed line) given in Eq. (2.111), with the numerical simulation results (blue dots) is shown for: partial entropy production in (f) and (g), and apparent entropy production in (h)–(j). The analytical probability density function $p(s)$ (red dashed line) given in Eq. (2.110) is compared with the numerical simulation result (blue dots) for: partial entropy production in (k) and (l), and apparent entropy production in (m)–(o). For comparison of analytical predictions with the numerical simulations, we choose $\delta = 0.1$ and the observation time with respect to viscous relaxation time $\tau/\tau_\gamma = 150$

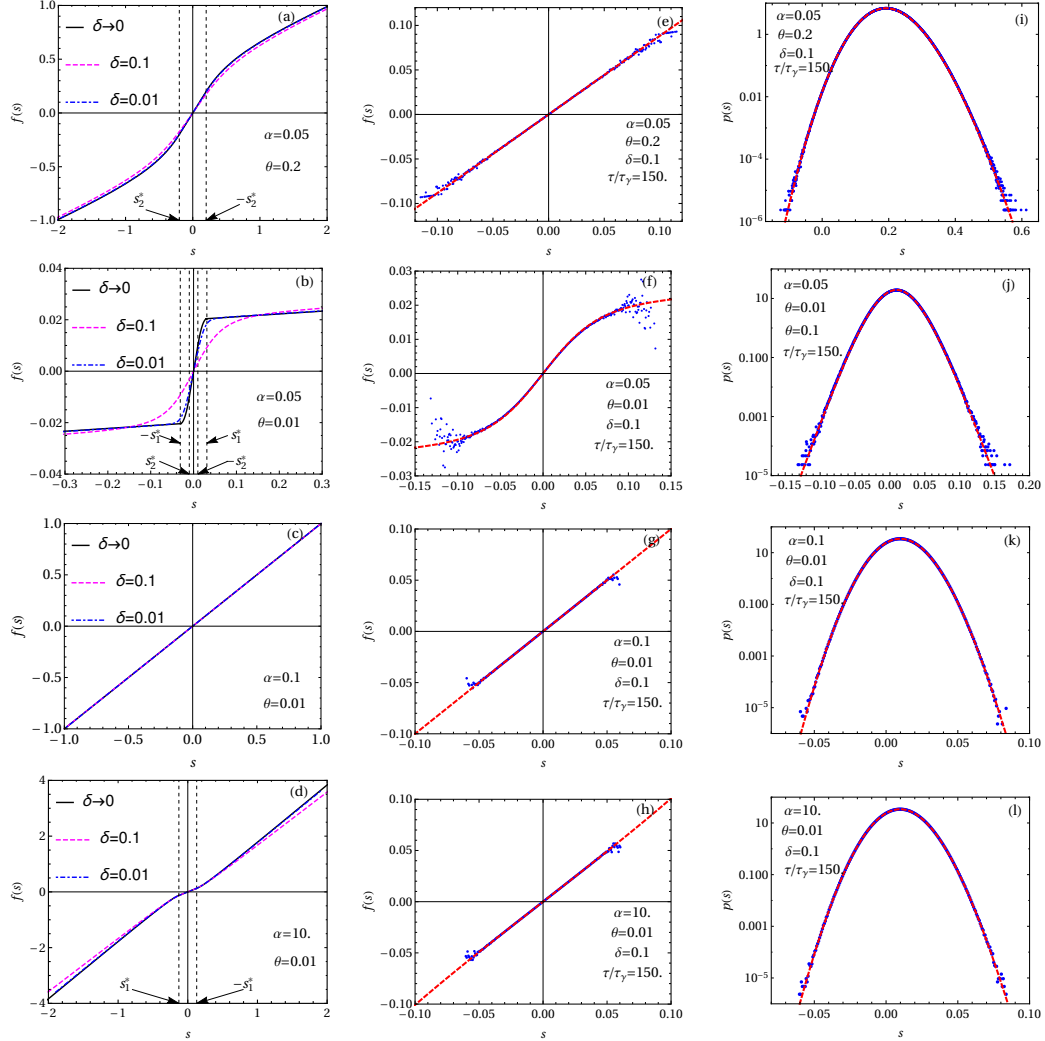


FIGURE 2.7: The above figures are plotted for second choice of external forces, i.e. $C = 1$. The analytical asymmetry functions $f(s)$ given in Eq. (2.112), are plotted against the scaled variable $s = \Delta S_{tot}^A \tau_\gamma / \tau$ for: partial entropy production in (a) and (b), and apparent entropy production in (c) and (d), where s_1^* and s_2^* are given in Sec. 2.9. These plots are shown for coupling parameter $\delta = 0.1$ (magenta dashed line) and $\delta = 0.01$ (blue dotdashed line). The asymmetry functions in the limit $\delta \rightarrow 0$ (black solid line) are also shown for respective cases. The comparison of analytical asymmetry functions $f(s)$ (red dashed line) given in Eq. (2.111), with the numerical simulation results (blue dots) is shown for: partial entropy production in (e) and (f), and apparent entropy production in (g) and (h). The analytical probability density function $p(s)$ (red dashed line) given in Eq. (2.110) is compared with the numerical simulation result (blue dots) for: partial entropy production in (i) and (j), and apparent entropy production in (k) and (l). For comparison of analytical predictions with the numerical simulations, we choose $\delta = 0.1$ and the observation time with respect to viscous relaxation time $\tau / \tau_\gamma = 150$.

solid line), the asymmetry functions $f(s)$ are also shown for each case. Therefore, one can see that as the coupling parameter δ decreases, the asymmetry function $f(s)$ converges to that of $\delta \rightarrow 0$ case.

The asymptotic expressions for the asymmetry function $f(s)$ in the limit $\delta \rightarrow 0$ and for large s ($s \rightarrow \infty$) are given as

$$f(s) = \begin{cases} [\mu_0(\lambda_-) - \mu_0(\tilde{\lambda}_+)] + [\lambda_- + \tilde{\lambda}_+]s & \text{for region I of Fig. 2.4(a),} \\ [\mu_0(\tilde{\lambda}_-) - \mu_0(\tilde{\lambda}_+)] + [\tilde{\lambda}_- + \tilde{\lambda}_+]s & \text{for region II of Fig. 2.4(a),} \\ [\mu_0(\lambda_-) - \mu_0(\lambda_+)] + [\lambda_- + \lambda_+]s & \text{for region I of Fig. 2.4(b),} \\ [\mu_0(\lambda_-) - \mu_0(\tilde{\lambda}_+)] + [\lambda_- + \tilde{\lambda}_+]s & \text{for region II of Fig. 2.4(b),} \\ [\mu_0(\tilde{\lambda}_-) - \mu_0(\tilde{\lambda}_+)] + [\tilde{\lambda}_- + \tilde{\lambda}_+]s & \text{for region III of Fig. 2.4(b),} \\ [\mu_0(\lambda_-) - \mu_0(\tilde{\lambda}_+)] + [\lambda_- + \tilde{\lambda}_+]s & \text{for region I of Fig. 2.4(c),} \\ [\mu_0(\tilde{\lambda}_-) - \mu_0(\tilde{\lambda}_+)] + [\tilde{\lambda}_- + \tilde{\lambda}_+]s & \text{for region II of Fig. 2.4(c),} \\ [\mu_0(\lambda_-) - \mu_0(\lambda_+)] + [\lambda_- + \lambda_+]s & \text{for region I of Fig. 2.4(d),} \\ [\mu_0(\tilde{\lambda}_-) - \mu_0(\lambda_+)] + [\tilde{\lambda}_- + \lambda_+]s & \text{for region II of Fig. 2.4(d),} \end{cases} \quad (2.113)$$

and $f(-s) = -f(s)$.

2.10 Numerical simulation

In Fig. 2.5, we show a comparison of theoretical predictions of probability density function $p(s)$ (red dashed line) given by Eq. (2.110) and the asymmetry function $f(s)$ (red dashed lines) given by Eq. (2.111) with the numerical simulations (blue dots) for time $\tau/\tau_\gamma = 50$ [(a) and (b)] and $\tau/\tau_\gamma = 150$ [(c) and (d)]. The parameters α and θ are taken from Fig. 2.4(a). For all these figures, we set the coupling parameter $\delta = 0.1$, and temperature of the heat bath $T = 1$. It is clear from these figures, as the observation time increases, the agreement between theoretical predictions and the numerical simulations gets better. The details of the numerical simulations are discussed in Appendix A.

For first choice of external forces, the comparison of analytical asymmetry function $f(s)$ (red dashed line) given by Eq. (2.111), with the numerical simulation (blue

dots) is shown for partial [Figs. 2.6(f) and 2.6(g)] and apparent entropy production [Figs. 2.6(h)–2.6(j)]. For second choice of external forces, we compare the analytical predictions of the asymmetry function $f(s)$ (red dashed lines) given in Eq. (2.111), with the numerical simulations (blue dots) for partial [Figs. 2.7(e) and 2.6(f)] and apparent entropy production [Figs. 2.7(g) and 2.7(h)]. We compare the probability density function $p(s)$ (red dashed lines) given in Eq. (2.110), with the numerical simulation result (blue dots) for first choice of external forces in Figs. 2.6(k) and 2.6(l), and Figs. 2.6(m)–2.6(o) for partial and apparent entropy production, respectively. For second choice of external forces, we compare the probability density function $p(s)$ (red dashed lines) given in Eq. (2.110), with the numerical simulation (blue dots) for partial [Figs. 2.7(i) and 2.7(j)] and apparent entropy production [Figs. 2.7(k) and 2.7(l)]. For all figures, we choose $\delta = 0.1$, $T = 1$, and the observation time $\tau/\tau_\gamma = 150$. These figures indicate that there is nice agreement between theoretical predictions and the numerical simulations.

2.11 Summary

We have considered a system of two Brownian particles, coupled by harmonic potential of stiffness k , immersed in a heat bath at a temperature T . Both of these particles are driven by external Gaussian white noises. Here, we have considered two different choices of forces: (1) both forces are uncorrelated with each other, and (2) both of them are correlated with each other. The strength of the force acting on particle A relative to strength of the noise from the bath is θ whereas the ratio of strength of the force acting on particle B to that on particle A is α^2 . A dimensionless coupling parameter $\delta = 2km/\gamma^2$ is also introduced. Because of driving forces, the given system reach in the non-equilibrium steady state and generates entropy. Evidently, the total entropy production from the combined system (A+B) satisfies fluctuation theorem. The central question we asked in this chapter is whether fluctuation theorem holds for partial system in weak coupling limit ($\delta \ll 1$)? To answer that we have focused on the total entropy production due to one of the particle (partial and apparent entropy production) in the coupled system. For each case, we have given

phase diagrams in (α, θ) plane in the limit $\delta \rightarrow 0$. Except for region I of phase diagrams shown in Figs. 2.4(b) and 2.4(d), the deviation from the fluctuation theorem for both definition of entropy production and also for both choices of external forces is observed even in the weak coupling limit ($\delta \rightarrow 0$). Numerical simulation are also done to verify the analytical results, and there is nice agreement between them.

Chapter 3

Partial entropy production in heat transport

In this chapter, we consider a system of two Brownian particles (say A and B), coupled to each other via harmonic potential of stiffness constant k . Particle A is connected to two heat baths of constant temperatures T_1 and T_2 , and particle B is connected to a single heat bath of a constant temperature T_3 . In the steady state, the total entropy production for both particles obeys the fluctuation theorem. We compute the total entropy production due to particle A in the coupled system (partial and apparent entropy production) in the steady state for a time segment τ . When both particles are weakly interacting with each other, the fluctuation theorem for partial and apparent entropy production is studied. We find a significant deviation from the fluctuation theorem. The analytical results are also verified using numerical simulations.

3.1 Introduction

When a potential difference is maintained across an electrical conductor, the electric current flows through it. Similarly, a thermal gradient causes a heat flow across a thermal conductor. These are examples of *Transport Phenomena*. For macroscopic systems, these phenomena are described by the Ohm's law for electric conduction, and the Fourier's law for heat transport. Microscopically, these involve the transfer of electric charges or lattice vibrations (phonons). Interestingly, there have been a lot of research carried out to understand these phenomena from the microscopic

point of view. For instance, heat transport studies include several questions such as heat transport in the low dimensions, the dependence of the transport coefficient on system size, etc. [27, 10, 84].

Small systems such as a Brownian particle, harmonic oscillator, harmonic or anharmonic chain, etc., having a finite number of degrees of freedom (DOFs) coupled to a thermal gradient, the heat flows from the hot reservoir at a temperature T_1 to the cold reservoir at a temperature T_2 . However, in this small system, due to thermal fluctuations, once in a while, the heat may flow in the reverse direction, although on an average, the heat current follows the sign of $(T_1 - T_2)$ in accordance with the second law of thermodynamics [15, 58, 147]. The entropy production in the baths is $\Delta S_{med} = -(Q_1/T_1 + Q_2/T_2)$ (see Sec. 3.6), where Q_i is the heat energy transferred by the i th bath to the system. This quantity may not always satisfy the steady state fluctuation theorem [see Eq. (1.13)] as shown in Sec. 3.6. However, once the system entropy production ΔS_{sys} is added to medium one, resulted total entropy production ΔS_{tot} in the steady state obeys the relation Eq. (1.13).

In the previous chapter, we discussed when the time-scale of relaxation of system DOFs is much larger than that of bath DOFs, and then one must include all relevant slow DOFs to compute the total entropy production. In the steady state, the total entropy production corresponding to them satisfies Eq. (1.13). However, when some of them are masked or hidden, the relation Eq. (1.13) may not be valid. In contrary to naive understanding where one assumes that the relation (1.13) might hold when the interaction between the observed and the hidden part of the system is vanishingly small, we tested the steady state fluctuation theorem for the total entropy production for a part of a coupled Brownian particle system in the weak coupling limit [52, 53]. The system was maintained in the non-equilibrium steady state by driving each particle with an external stochastic Gaussian force. We have shown that deviation from the fluctuation theorem can be seen even in this limit (see Chapter 2).

In this chapter [54], we consider a coupled Brownian particle system where one of the particles (say particle A) is connected to two heat baths at different temperatures while the other one (say particle B) is attached to a single heat bath. We take the interaction between these two particles to be harmonic. Here, we focus on the total entropy production in the steady state by one of the particles (say particle A) in the

coupled system (partial and apparent entropy production). In the limit of vanishing coupling, the deviation from the fluctuation theorem [see Eq. (1.13)] is studied. There are two important features of this chapter: (1) In contrast to the previous chapter, we have used a thermal gradient to drive the system into the nonequilibrium steady state, and (2) The asymmetry function given in Eq. (3.110), has a negative slope which was not observed in the earlier studies.

The remainder of this chapter is as follows. We describe the model system and give the definition of partial and apparent entropy production in Sec. 3.2. Section 3.3 contains the Fokker-Planck equation for the conditional moment generating function of functional W given in Eq. (3.21), and its general solution at the large time. We give the detailed calculation for the generating function $Z(\lambda) \sim g(\lambda)e^{(\tau/\tau_\gamma)\mu(\lambda)}$ in the large time limit ($\tau \rightarrow \infty$) for both definitions of entropy production in Sec. 3.4, and then, we invert $Z(\lambda)$ using saddle-point method which yields the probability density function for the partial and apparent entropy production (Sec. 3.5). In Sec. 3.6, we compute the medium entropy production by a single Brownian particle connected to a thermal gradient, and show that for the entropy production to satisfy the steady state fluctuation theorem for large but finite time, it is necessary to incorporate the system entropy production. Since we are interested in the steady state fluctuation theorem for the partial and apparent entropy production in the weak coupling limit, we discuss the assumption to approximate the prefactor term $g(\lambda) \approx g_0(\lambda)$ in Sec. 3.7. The cumulant generating function $\mu(\lambda)$ is analyzed in Sec. 3.8. In Sec. 3.8.1, we discuss the Gallavotti-Cohen symmetry [82] of the cumulant generating function $\mu(\lambda)$. The large deviation function, and the asymmetry function which measures the deviation from the steady state fluctuation theorem is discussed in Sec. 3.9. Section 3.10 contains the comparison of analytical predictions with numerical simulations. We summarize the chapter in Sec. 3.11.

3.2 Model

Consider a Brownian particle (say particle A) of mass m , in contact with two heat baths at temperatures T_1 and $T_2 < T_1$. Let γ_1 and γ_2 are the dissipation constants of baths with temperatures T_1 and T_2 , respectively. Suppose the Brownian particle A

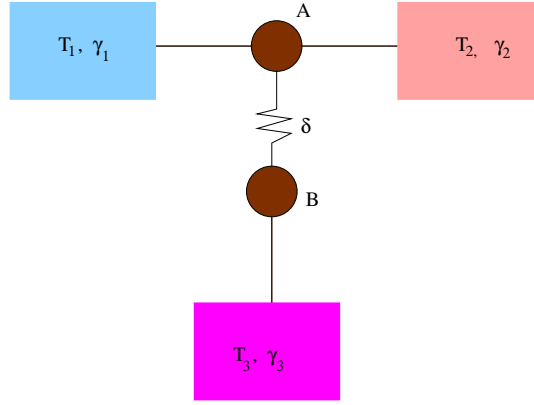


FIGURE 3.1: Brownian particle A is connected to two heat baths of temperatures (dissipation constants) T_1 (γ_1) and T_2 (γ_2) while particle B is connected to a bath of temperature (dissipation constant) T_3 (γ_3). Both particles are connected by a spring of coupling parameter $\delta = 2km/\gamma_1^2$ (dimensionless).

is coupled harmonically with another Brownian particle (say particle B) of mass m . The particle B is in contact with a single heat bath of a constant temperature T_3 and a dissipation constant γ_3 . The schematic diagram of the coupled Brownian particle system is shown in Fig. 3.1. The Hamiltonian of the system is given as

$$\mathcal{H}(y, v_A, v_B) = \frac{1}{2}mv_A^2 + \frac{1}{2}mv_B^2 + \frac{1}{2}ky^2, \quad (3.1)$$

where $y = x_A - x_B$ is the relative distance between particle A and B, k is the stiffness constant, v_A and v_B are the velocities of particle A and B, respectively. The evolution of the given system is described by the following Langevin equations

$$\dot{y} = v_A(t) - v_B(t), \quad (3.2)$$

$$m\dot{v}_A = -\gamma_A v_A(t) + \eta_A(t) - ky(t), \quad (3.3)$$

$$m\dot{v}_B = -\gamma_B v_B(t) + \eta_B(t) + ky(t), \quad (3.4)$$

where $\eta_A(t) = \eta_1(t) + \eta_2(t)$, $\eta_B(t) = \eta_3(t)$, $\gamma_A = \gamma_1 + \gamma_2$, and $\gamma_B = \gamma_3$. The thermal noises $\eta_1(t)$, $\eta_2(t)$, and $\eta_3(t)$ are from the heat baths with mean zero and correlation $\langle \eta_i(t)\eta_j(t') \rangle = 2T_i\gamma_i\delta_{ij}\delta(t-t')$, where $\{i,j\}=\{1,2,3\}$. We set Boltzmann's constant $k_B = 1$ throughout the calculations.

The aim of this chapter is to understand the validity of the fluctuation theorem for the total entropy production of a subsystem or partial system of the complete

system in the steady state. In the following subsections, we give two definitions of entropy production.

3.2.1 Partial entropy production

Suppose we are interested in the total entropy production due to particle A in a coupled Brownian particle system as shown in Fig. 3.1. The dynamics of particle A is given by Eq. (3.3). Multiplying Eq. (3.3) by $v_A(t)$ on both sides and integrating over time t from 0 to τ yields

$$\frac{1}{2}m[v_A^2(\tau) - v_A^2(0)] = Q_1(t) + Q_2(t) - k \int_0^\tau dt y(t)v_A(t), \quad (3.5)$$

where $Q_i = \int_0^\tau [\eta_i(t) - \gamma_i v_A(t)]v_A(t)dt$, is the heat absorbed by Brownian particle A from the i th heat bath. The term on the left hand side is the change in the kinetic energy of the Brownian particle A from time $t = 0$ to $t = \tau$. The third term on the right hand side is the energy change due to an interaction among the particles. Notice that the integrals on the right hand side of the above equation follow Stratonovich rule of integration [124]. All of the baths are of infinite size and have infinite heat capacity. Therefore, these are assumed to be always in thermal equilibrium. Using standard thermodynamics, the entropy production in the baths due to Brownian particle A can be written as

$$\Delta \bar{S}_{med}^A = -\left(\frac{Q_1}{T_1} + \frac{Q_2}{T_2}\right) = \Delta\beta Q_1 - \frac{k}{T_2} \int_0^\tau dt y(t)v_A(t) - \frac{m}{2T_2}[v_A^2(\tau) - v_A^2(0)], \quad (3.6)$$

where $\Delta\beta = \frac{1}{T_2} - \frac{1}{T_1}$ is the difference of inverse temperatures.

Total entropy production $\Delta \bar{S}_{tot}^A$ of Brownian particle A is the sum of the medium entropy production $\Delta \bar{S}_{med}^A$ and the system entropy production $\Delta \bar{S}_{sys}^A$ of the particle A. In the steady state, the system entropy production of the particle A from time $t = 0$ to $t = \tau$ is [121, 120]

$$\Delta \bar{S}_{sys}^A = -\ln P_{ss}(v_A(\tau)) + \ln P_{ss}(v_A(0)), \quad (3.7)$$

where $P_{ss}(v_A)$ is the steady state distribution obtained after integrating the joint steady state distribution $P_{ss}^{full}(y, v_A, v_B)$ over y and v_B :

$$P_{ss}(v_A) = \frac{1}{\sqrt{2\pi H_P}} \exp\left[-\frac{v_A^2}{2H_P}\right]. \quad (3.8)$$

In the above equation, H_P is given by

$$\begin{aligned} H_P &= \lim_{\tau \rightarrow \infty} \langle [v_A(\tau) - \langle v_A(\tau) \rangle]^2 \rangle \\ &= \frac{\gamma_3(\gamma_1 + \gamma_2 + \gamma_3)(\gamma_1 T_1 + \gamma_2 T_2) + mk(\gamma_1 T_1 + \gamma_2 T_2 + \gamma_3 T_3)}{m(\gamma_1 + \gamma_2 + \gamma_3)(mk + \gamma_1 \gamma_3 + \gamma_2 \gamma_3)}. \end{aligned} \quad (3.9)$$

Therefore, the total entropy production due to particle-A in the coupled system (i.e. partial entropy production) is given as

$$\Delta \tilde{S}_{tot}^A = \Delta \beta Q_1 - \frac{k}{T_2} \int_0^\tau dt y(t) v_A(t) - \frac{1}{2} \left[\frac{m}{T_2} - \frac{1}{H_P} \right] [v_A^2(\tau) - v_A^2(0)]. \quad (3.10)$$

3.2.2 Apparent entropy production

Consider an experiment where we want to find the entropy production for a single Brownian particle (say particle A) in contact with two heat baths of temperatures (dissipation constants) T_1 (γ_1) and T_2 (γ_2) (see Fig. 3.1 with $\delta = 0$). The Langevin equation for Brownian particle A is

$$m\dot{v}_A = -(\gamma_1 + \gamma_2)v_A(t) + \eta_1(t) + \eta_2(t). \quad (3.11)$$

Multiplying above equation by v_A on both sides and integrating over time t from 0 to τ gives Eq. (3.5) with $k = 0$. Therefore, one can write the entropy production in the baths due to Brownian particle A as

$$\Delta \tilde{S}_{med}^A = -\left(\frac{Q_1}{T_1} + \frac{Q_2}{T_2}\right) = \Delta \beta Q_1 - \frac{m}{2T_2} [v_A^2(\tau) - v_A^2(0)]. \quad (3.12)$$

The system entropy production of the Brownian particle A in steady state is given as

$$\Delta \tilde{S}_{sys}^A = -\ln \tilde{P}_{ss}(v_A(\tau)) + \ln \tilde{P}_{ss}(v_A(0)). \quad (3.13)$$

In the above equation, $\tilde{P}_{ss}(v_A)$ is the steady state distribution obtained from Eq. (3.11)

$$\tilde{P}_{ss}(v_A) = \frac{1}{\sqrt{2\pi H_A}} \exp\left(-\frac{v_A^2}{2H_A}\right), \quad (3.14)$$

where

$$H_A = \lim_{\tau \rightarrow \infty} \langle [v_A(\tau) - \langle v_A(\tau) \rangle]^2 \rangle = \frac{\gamma_1 T_1 + \gamma_2 T_2}{m(\gamma_1 + \gamma_2)}.$$

Therefore, the total entropy production of particle A can be written as

$$\Delta \tilde{S}_{tot}^A = \Delta \beta Q_1 - \frac{1}{2} \left[\frac{m}{T_2} - \frac{1}{H_A} \right] [v_A^2(\tau) - v_A^2(0)]. \quad (3.15)$$

It is important to note that Eq. (3.15) is written by assuming that there is no other particle is coupled to the given particle A. Therefore, an experimentalist naively uses Eq. (3.15) to compute the entropy production due to a single Brownian particle A coupled to two heat baths of distinct temperatures. If there is one more particle (say particle B) coupled to a heat bath, is present and interacting harmonically with given particle A, then the actual dynamics of particle A will be given by Eqs. (3.2)–(3.4). To understand what an experimentalist observes without the prior knowledge of particle B, we use Eq. (3.15) for entropy production with the actual dynamics given in Eqs. (3.2)–(3.4), and then we compute the distribution of total entropy production of particle A. This definition of entropy production we call *apparent entropy production*.

In fact, we can combine both definitions of entropy production [i.e. Eqs. (3.10) and (3.15)] using a parameter Π given in Eq. (2.12). Therefore, the generalize partial entropy production of particle A reads

$$\Delta S_{tot}^A = \Delta \beta Q_1 - \frac{\Pi k}{T_2} \int_0^\tau dt y(t) v_A(t) - \frac{1}{2} \left[\frac{m}{T_2} - \frac{1}{H} \right] [v_A^2(\tau) - v_A^2(0)], \quad (3.16)$$

where $H = \Pi H_P + (1 - \Pi) H_A$.

Our goal is to compute the distribution of the generalize partial entropy production for particle A in the coupled system, i.e. $P(\Delta S_{tot}^A)$, in the non-equilibrium steady state. From Eq. (3.16), we see that ΔS_{tot}^A depends on thermal noises quadratically. Therefore, the distribution of generalize partial entropy production will be non-Gaussian.

The quantity ΔS_{tot}^A given in Eq. (3.16), is a stochastic quantity whose value depends on both initial state of the system and thermal Gaussian noises. Therefore, the probability density function of it is obtained by inverting the moment generating function defined as

$$Z(\lambda) = \langle \exp(-\lambda \Delta S_{tot}^A) \rangle, \quad (3.17)$$

where the angular brackets indicate the average over both initial configuration of the system and set of all paths. Instead of computing $Z(\lambda)$ directly, it is useful to first compute the restricted moment generating function for ΔS_{tot}^A :

$$Z(\lambda, U, \tau | U_0) = \langle \exp(-\lambda \Delta S_{tot}^A) \delta[U - U(\tau)] \rangle_{U, U_0}, \quad (3.18)$$

where the angular brackets represent the average over trajectories starting from initial variable $U_0 = [y(0), v_A(0), v_B(0)]^T$ to final variable $U(\tau) = [y(\tau), v_A(\tau), v_B(\tau)]^T$. Substituting ΔS_{tot}^A from Eq. (3.16) in Eq. (3.18), we get

$$Z(\lambda, U, \tau | U_0) = Z_W(\lambda, U, \tau | U_0) e^{\lambda/2(mT_2^{-1} - H^{-1})(U^T \Sigma U - U_0^T \Sigma U_0)}, \quad (3.19)$$

where $\Sigma_{ij} = \delta_{i,j} \delta_{2,j}$ with $\{i,j\} = \{1,2,3\}$,

$$Z_W(\lambda, U, \tau | U_0) = \langle e^{-\lambda W} \delta[U - U(\tau)] \rangle_{U, U_0}, \quad (3.20)$$

and W is

$$W = \Delta\beta Q_1 - \frac{\Pi k}{T_2} \int_0^\tau dt y(t) v_A(t). \quad (3.21)$$

Since the boundary terms do not contribute in the averaging process in Eq. (3.19), we have taken them outside from the angular brackets. In the following, we write the evolution equation satisfied by $Z_W(\lambda, U, \tau | U_0)$.

3.3 Fokker-Planck equation

The restricted moment generating function $Z_W(\lambda, U, \tau | U_0)$ follows the Fokker-Planck equation [70, 107]

$$\frac{\partial Z_W(\lambda, U, \tau | U_0)}{\partial \tau} = \mathcal{L}_\lambda Z_W(\lambda, U, \tau | U_0), \quad (3.22)$$

where the differential operator \mathcal{L}_λ has the following form

$$\begin{aligned} \mathcal{L}_\lambda = & \frac{1}{m} \sum_{i=A,B} \left[\frac{\partial \mathcal{H}}{\partial x_i} \frac{\partial}{\partial v_i} - \frac{\partial \mathcal{H}}{\partial v_i} \frac{\partial}{\partial x_i} \right] + \frac{\gamma_B v_B}{m} \frac{\partial}{\partial v_B} + \frac{\gamma_1 T_1 + \gamma_2 T_2}{m^2} \frac{\partial^2}{\partial v_A^2} + \frac{\gamma_3 T_3}{m^2} \frac{\partial^2}{\partial v_B^2} + \sum_{i=1}^3 \frac{\gamma_i}{m} \\ & + \lambda \left[\gamma_1 \Delta \beta \left(v_A^2 + \frac{T_1}{m} \right) + \frac{\Pi k y v_A}{T_2} \right] + \lambda^2 \Delta \beta^2 v_A^2 \gamma_1 T_1 + \frac{v_A}{m} (\gamma_A + 2\lambda \gamma_1 T_1 \Delta \beta) \frac{\partial}{\partial v_A}. \end{aligned} \quad (3.23)$$

The differential Eq. (3.22) is subjected to the initial condition $Z_W(\lambda, U, 0|U_0) =$

$$Z(\lambda, U, 0|U_0) = \delta(U - U_0).$$

General solution of the differential Eq. (3.22) is

$$Z_W(\lambda, U, \tau|U_0) = \sum_n e^{\tau \tilde{\mu}_n(\lambda)} \chi_n(U_0, \lambda) \Psi_n(U, \lambda). \quad (3.24)$$

In the above equation, $\chi_n(U_0, \lambda)$ and $\Psi_n(U, \lambda)$ are the n th left and right eigenfunctions, respectively, corresponding to eigenvalue $\tilde{\mu}_n(\lambda)$ of the differential operator \mathcal{L}_λ . These eigenfunctions satisfy orthonormality condition:

$$\int \chi_n(U, \lambda) \Psi_m(U, \lambda) dU = \delta_{nm}. \quad (3.25)$$

Computation of these eigenvalues and eigenfunctions is quite involved and not illuminating to us. In most of the physical situations, one is interested in the large time solution of the differential equation. In such cases, the solution of differential Eq. (3.22), is dominated by the largest eigenvalue of the full spectrum, i.e. $\tilde{\mu}(\lambda) = \max\{\tilde{\mu}_n(\lambda)\}$. Thus, for large time

$$Z_W(\lambda, U, \tau|U_0) = e^{\tau \tilde{\mu}(\lambda)} \chi(U_0, \lambda) \Psi(U, \lambda) + \dots, \quad (3.26)$$

where $\tilde{\mu}(\lambda)$ is the largest eigenvalue of the differential operator \mathcal{L}_λ and the corresponding left and right eigenfunctions are $\chi(U_0, \lambda)$ and $\Psi(U, \lambda)$, respectively. Substituting $\lambda = 0$ in the restricted moment generating function, and identifying $\tilde{\mu}(0) = 0$ and $\chi(U_0, 0) = 1$ yields the steady state of the system: $P_{ss}^{full}(U) = Z_W(0, U, \tau \rightarrow \infty|U_0) = \Psi(U, 0)$. Therefore, integrating $Z(\lambda, U, \tau|U_0)$ given in Eq. (3.19), over the

initial steady state distribution $P_{ss}^{full}(U_0)$ and the final state U yields

$$Z(\lambda) = \int dU \int dU_0 P_{ss}^{full}(U_0) Z(\lambda, U, \tau | U_0) = g(\lambda) e^{\tau \tilde{\mu}(\lambda)} + \dots, \quad (3.27)$$

where $g(\lambda)$ is the prefactor given as

$$g(\lambda) = \int dU_0 \int dU P_{ss}^{full}(U_0) \chi(U_0, \lambda) \Psi(U, \lambda) e^{\lambda/2(mT_2^{-1} - H^{-1})(U^T \Sigma U - U_0^T \Sigma U_0)}. \quad (3.28)$$

The largest eigenvalues $\tilde{\mu}(\lambda)$ and the corresponding left eigenfunction $\chi(U_0, \lambda)$, and right eigenfunction $\Psi(U, \lambda)$ can be found using a technique developed in Ref. [76].

Therefore, the cumulant generating function $\mu(\lambda)$ obtained as

$$\mu(\lambda) = -\frac{1}{4\pi} \int_{-\infty}^{\infty} du \ln \left[1 + \frac{h(u, \lambda)}{q(u)} \right], \quad (3.29)$$

where $\mu(\lambda) = \tau_\gamma \tilde{\mu}(\lambda)$,

$$\begin{aligned} h(u, \lambda) = & 4\lambda(1 - \lambda)\beta_{12} [\alpha_{12}(1 - \beta_{12})^2 \{u^4 + u^2(\alpha_{13}^2 - \delta) + \delta^2/4\} + \delta^2 \alpha_{13} \beta_{13} (\beta_{12} + \Pi - 1)/4] \\ & - \lambda \delta^2 \alpha_{13} [(\beta_{12} + \beta_{13} \lambda \Pi - \beta_{13} \lambda)(\beta_{12} + \Pi - 1) + \alpha_{12} \beta_{12} \Pi (\beta_{12} - \beta_{13} + \beta_{13} \lambda \Pi)], \end{aligned} \quad (3.30)$$

$$\begin{aligned} q(u) = & \beta_{12}^2 [u^6 + u^4 \{(1 + \alpha_{12})^2 + \alpha_{13}^2 - 2\delta\} + u^2 \{(1 + \alpha_{12})^2 - \delta\} (\alpha_{13}^2 - \delta) \\ & + \delta^2 (1 + \alpha_{12} + \alpha_{13})^2 / 4]. \end{aligned} \quad (3.31)$$

Here, $\beta_{1j} = \frac{T_j}{T_1}$ and $\alpha_{1j} = \frac{\gamma_j}{\gamma_1}$ with $j = 2, 3$, the coupling parameter $\delta = \frac{2km}{\gamma_1^2}$, and $\tau_\gamma = \frac{m}{\gamma_1}$ is the viscous relaxation time.

3.4 Calculation for moment generating function $Z(\lambda)$

In this section, we compute the moment generating function $Z(\lambda) \sim g(\lambda) e^{(\tau/\tau_\gamma)\mu(\lambda)}$ in the large time limit using the method developed in [76]. Therefore, we write the Langevin equations given in Eqs. (3.2)–(3.4), for the coupled system shown in Fig. 3.1

in the matrix form as

$$\dot{y} = A^T V(t), \quad (3.32)$$

$$m\dot{V} = -\Gamma V(t) - kAy(t) + \xi(t), \quad (3.33)$$

where $A = (1, -1)^T$, $V = (v_A, v_B)^T$, $\xi = (\eta_A, \eta_B)^T$, and $\Gamma_{ij} = \delta_{ij}(\delta_{1j}\gamma_A + \delta_{2j}\gamma_B)$ with $\{i,j\}=\{1,2\}$. Using finite time Fourier transform [see Eq. (2.16)], we rewrite Eqs. (3.32) and (3.33) in the frequency domain as

$$\tilde{y}(\omega_n) = A^T G(\omega_n) \tilde{\xi}(\omega_n) - \frac{1}{\tau} \left[(\gamma_3 + im\omega_n)(G_{22} - G_{12})\Delta y + mA^T G(\omega_n)\Delta V \right], \quad (3.34)$$

$$\tilde{V}(\omega_n) = i\omega_n G(\omega_n) \tilde{\xi}(\omega_n) + \frac{G(\omega_n)}{\tau} [kA\Delta y - im\omega_n\Delta V]. \quad (3.35)$$

In the above equations, $\Delta y = y(\tau) - y(0)$, $\Delta V = V(\tau) - V(0)$, and the Green's function matrix $G(\omega_n) = [-m\omega_n^2 + i\omega_n\Gamma + \Phi]^{-1}$, where $\Phi_{rl} = k(2\delta_{lr} - 1)$ with $\{l,r\} = \{1,2\}$, and the matrix elements $G_{ij} = [G(\omega_n)]_{ij}$ are

$$G_{11} = \frac{-m\omega_n^2 + i\omega_n\gamma_B + k}{i\omega_n[(\gamma_A + \gamma_B)(k - m\omega_n^2) + i\omega_n(2km + \gamma_A\gamma_B) - im^2\omega_n^3]},$$

$$G_{22} = \frac{-m\omega_n^2 + i\omega_n\gamma_A + k}{i\omega_n[(\gamma_A + \gamma_B)(k - m\omega_n^2) + i\omega_n(2km + \gamma_A\gamma_B) - im^2\omega_n^3]},$$

$$G_{12} = G_{21} = \frac{k}{i\omega_n[(\gamma_A + \gamma_B)(k - m\omega_n^2) + i\omega_n(2km + \gamma_A\gamma_B) - im^2\omega_n^3]}.$$

Therefore, we can write $\tilde{y}(\omega_n)$ and $\tilde{v}_A(\omega_n)$ as

$$\tilde{y}(\omega_n) = (G_{11} - G_{12})[\tilde{\eta}_1(\omega_n) + \tilde{\eta}_2(\omega_n)] + (G_{12} - G_{22})\tilde{\eta}_3 - \frac{1}{\tau}\Delta U^T q_1, \quad (3.36)$$

$$\tilde{v}_A(\omega_n) = i\omega_n[G_{11}\{\tilde{\eta}_1(\omega_n) + \tilde{\eta}_2(\omega_n)\} + G_{12}\tilde{\eta}_3(\omega_n)] + \frac{1}{\tau}\Delta U^T q_2, \quad (3.37)$$

where

$$q_1^T = [(\gamma_3 + i\omega_n m)(G_{22} - G_{12}), m(G_{11} - G_{12}), m(G_{12} - G_{22})], \quad (3.38)$$

$$q_2^T = [k(G_{11} - G_{12}), -im\omega_n G_{11}, -im\omega_n G_{12}]. \quad (3.39)$$

The row vector $U^T(\tau) = [y(\tau), V^T(\tau)]$ is given as

$$U^T(\tau) = \lim_{\epsilon \rightarrow 0} \sum_{n=-\infty}^{\infty} e^{-i\epsilon\omega_n} [\tilde{y}(\omega_n), \tilde{V}^T(\omega_n)]. \quad (3.40)$$

Substituting Eqs. (3.34) and (3.35) in the above equation, we find that the terms

$$\begin{aligned} & \lim_{\epsilon \rightarrow 0} \sum_{n=-\infty}^{\infty} \frac{e^{-i\epsilon\omega_n}}{\tau} [(\gamma_3 + i\omega_n m)(G_{22} - G_{12})\Delta y + mA^T G(\omega_n)\Delta V], \\ & \lim_{\epsilon \rightarrow 0} \sum_{n=-\infty}^{\infty} \frac{e^{-i\epsilon\omega_n}}{\tau} [kA^T \Delta y - im\omega_n \Delta V^T] G^T(\omega_n), \end{aligned}$$

go to zero. This is because in the limit of large τ , we convert summations into integrations, and these terms have poles in the upper half of the complex ω -plane. Therefore, using the calculus of residue, one can find that the contributions from these terms vanishes. This implies

$$U^T(\tau) = \lim_{\epsilon \rightarrow 0} \sum_{n=-\infty}^{\infty} e^{-i\epsilon\omega_n} [\{\tilde{\eta}_1(\omega_n) + \tilde{\eta}_2(\omega_n)\}q_3^T + \tilde{\eta}_3(\omega_n)q_4^T], \quad \text{where} \quad (3.41)$$

$$q_3^T = (G_{11} - G_{12}, i\omega_n G_{11}, i\omega_n G_{12}), \quad (3.42)$$

$$q_4^T = (G_{12} - G_{22}, i\omega_n G_{12}, i\omega_n G_{22}). \quad (3.43)$$

The mean and variance of $U(\tau)$ are

$$\langle U(\tau) \rangle = 0, \quad (3.44)$$

$$\langle U(\tau)U^T(\tau) \rangle = \frac{1}{\pi} \int_{-\infty}^{\infty} d\omega [(T_1\gamma_1 + T_2\gamma_2)q_3q_3^\dagger + T_3\gamma_3q_4q_4^\dagger], \quad (3.45)$$

respectively. In Eq. (3.45), we have used the definition of correlation function of noises in the frequency domain as given by

$$\langle \tilde{\eta}_i(\omega)\tilde{\eta}_j(\omega') \rangle = \frac{2T_i\gamma_i}{\tau} \delta(\omega + \omega')\delta_{ij}. \quad (3.46)$$

From Eq. (3.41), it is clear that the steady state distribution of $U = (y, v_A, v_B)^T$ is Gaussian distribution whose mean and variance are given in Eqs. (3.44) and (3.45),

respectively:

$$P_{ss}^{full}(U) = \frac{1}{\sqrt{(2\pi)^3 \det M}} \exp \left[-\frac{1}{2} U^T M^{-1} U \right], \quad \text{where } M_{ij} = \langle U(\tau) U^T(\tau) \rangle_{ij}. \quad (3.47)$$

The quantity W is non-linear in thermal noises [see Eq. (3.21)]. Therefore, we write it in the frequency domain using Eq. (2.17) as

$$W = \frac{\tau}{2} \sum_{n=-\infty}^{\infty} \left[\Delta\beta I_{1n} - \frac{\Pi k}{T_2} I_{2n} \right], \quad \text{where} \quad (3.48)$$

$$I_{1n} = \tilde{\eta}_1(\omega_n) \tilde{v}_A(-\omega_n) + \tilde{\eta}_1(-\omega_n) \tilde{v}_A(\omega_n) - 2\gamma_1 \tilde{v}_A(\omega_n) \tilde{v}_A(-\omega_n), \quad (3.49)$$

$$I_{2n} = \tilde{y}(\omega_n) \tilde{v}_A(-\omega_n) + \tilde{y}(-\omega_n) \tilde{v}_A(\omega_n). \quad (3.50)$$

Substituting $\tilde{y}(\omega_n)$ and $\tilde{v}_A(\omega_n)$ from Eqs. (3.36) and (3.37) in Eqs. (3.49) and (3.50) yields

$$\begin{aligned} I_{1n} = & i\omega_n [G_{11}(\tilde{\eta}_1 + \tilde{\eta}_2)\tilde{\eta}_1^* + G_{12}\tilde{\eta}_3\tilde{\eta}_1^* - G_{11}^*\tilde{\eta}_1(\tilde{\eta}_1^* + \tilde{\eta}_2^*) - G_{12}^*\tilde{\eta}_1\tilde{\eta}_3^*] + \frac{\Delta U^T q_2}{\tau} \tilde{\eta}_1^* \\ & - 2\gamma_1 \omega_n^2 [|G_{11}|^2(\tilde{\eta}_1 + \tilde{\eta}_2)(\tilde{\eta}_1^* + \tilde{\eta}_2^*) + |G_{12}|^2\tilde{\eta}_3\tilde{\eta}_3^* + G_{11}G_{12}^*(\tilde{\eta}_1 + \tilde{\eta}_2)\tilde{\eta}_3^* \\ & + G_{12}G_{11}^*\tilde{\eta}_3(\tilde{\eta}_1^* + \tilde{\eta}_2^*)] - \frac{2\gamma_1}{\tau^2} \Delta U^T q_2 q_2^T \Delta U - 2i\gamma_1 \omega_n \frac{q_2^\dagger \Delta U}{\tau} [G_{11}(\tilde{\eta}_1 + \tilde{\eta}_2) + G_{12}\tilde{\eta}_3] \\ & + \frac{q_2^\dagger \Delta U}{\tau} \tilde{\eta}_1 + 2i\gamma_1 \omega_n \frac{\Delta U^T q_2}{\tau} [G_{11}^*(\tilde{\eta}_1^* + \tilde{\eta}_2^*) + G_{12}^*\tilde{\eta}_3^*], \end{aligned} \quad (3.51)$$

and

$$\begin{aligned} I_{2n} = & i\omega_n (\tilde{\eta}_1 + \tilde{\eta}_2)(\tilde{\eta}_1^* + \tilde{\eta}_2^*)(G_{12}G_{11}^* - G_{11}G_{12}^*) + i\omega_n (\tilde{\eta}_1 + \tilde{\eta}_2)\tilde{\eta}_3^* [G_{11}(G_{12}^* - G_{22}^*) \\ & - G_{12}^*(G_{11} - G_{12})] + i\omega_n \tilde{\eta}_3(\tilde{\eta}_1^* + \tilde{\eta}_2^*) [G_{12}(G_{11}^* - G_{12}^*) - G_{11}^*(G_{12} - G_{22})] \\ & + i\omega_n \tilde{\eta}_3\tilde{\eta}_3^* (G_{22}G_{12}^* - G_{12}G_{22}^*) + \frac{q_2^\dagger \Delta U}{\tau} [(G_{11} - G_{12})(\tilde{\eta}_1 + \tilde{\eta}_2) + (G_{12} - G_{22})\tilde{\eta}_3] \\ & + \frac{\Delta U^T q_2}{\tau} [(G_{11}^* - G_{12}^*)(\tilde{\eta}_1^* + \tilde{\eta}_2^*) + (G_{12}^* - G_{22}^*)\tilde{\eta}_3^*] - i\omega_n \frac{q_1^\dagger \Delta U}{\tau} [G_{11}(\tilde{\eta}_1 + \tilde{\eta}_2) + G_{12}\tilde{\eta}_3] \\ & + i\omega_n \frac{\Delta U^T q_1}{\tau} [G_{11}^*(\tilde{\eta}_1^* + \tilde{\eta}_2^*) + G_{12}^*\tilde{\eta}_3^*] - \frac{\Delta U^T (q_1 q_2^\dagger + q_2 q_1^\dagger) \Delta U}{\tau^2}. \end{aligned} \quad (3.52)$$

For convenience, in the above equations, we have written $G_{ij}^* = [G(-\omega_n)]_{ij}$, and $\tilde{\eta}_r^* = \tilde{\eta}_r(-\omega_n)$.

Now, the restricted moment generating function for W is given by

$$Z_W(\lambda, U, \tau | U_0) = \langle e^{-\lambda W} \delta[U - U(\tau)] \rangle_{U, U_0} = \int \frac{d^3 \sigma}{(2\pi)^3} e^{i\sigma^T U} \langle e^{E(\tau)} \rangle_{U, U_0}, \quad (3.53)$$

where we have used the integral representation of Dirac delta function, and $E(\tau)$ is given by

$$E(\tau) = -\lambda W - i\sigma^T U(\tau). \quad (3.54)$$

Using Eqs. (3.41) and (3.48), we write $E(\tau)$ as

$$E(\tau) = \sum_{n=1}^{\infty} \left[-\lambda \tau \zeta_n^T C_n \zeta_n^* + \zeta_n^T \bar{\alpha}_n + \bar{\alpha}_{-n}^T \zeta_n^* + \frac{\lambda}{\tau} |f_n|^2 \right] - \frac{\lambda \tau}{2} \zeta_0^T C_0 \zeta_0 + \zeta_0^T \bar{\alpha}_0 + \frac{\lambda}{2\tau} f_0^2, \quad (3.55)$$

where $C_n = \Delta \beta C_n^I - \frac{\Pi k}{T_2} C_n^{\text{II}}$, and the row vector containing thermal noises in the frequency domain is $\zeta_n^T = (\tilde{\eta}_1, \tilde{\eta}_2, \tilde{\eta}_3)$. Here the matrices C_n^I and C_n^{II} are

$$C_n^I = \begin{bmatrix} C_{11}^I & C_{12}^I & C_{13}^I \\ C_{12}^{I*} & C_{22}^I & C_{23}^I \\ C_{13}^{I*} & C_{23}^{I*} & C_{33}^I \end{bmatrix} \quad \text{and} \quad C_n^{\text{II}} = \begin{bmatrix} C_{11}^{\text{II}} & C_{12}^{\text{II}} & C_{13}^{\text{II}} \\ C_{21}^{\text{II}} & C_{22}^{\text{II}} & C_{23}^{\text{II}} \\ C_{13}^{\text{II}*} & C_{23}^{\text{II}*} & C_{33}^{\text{II}} \end{bmatrix},$$

whose matrix elements are

$$\begin{aligned} C_{11}^I &= i\omega_n (G_{11} - G_{11}^*) - 2\gamma_1 \omega_n^2 |G_{11}|^2, \\ C_{12}^I &= -i\omega_n G_{11}^* - 2\gamma_1 \omega_n^2 |G_{11}|^2, \\ C_{13}^I &= -i\omega_n G_{12}^* - 2\gamma_1 \omega_n^2 G_{11} G_{12}^*, \\ C_{22}^I &= -2\gamma_1 \omega_n^2 |G_{11}|^2, \\ C_{23}^I &= -2\gamma_1 \omega_n^2 G_{11} G_{12}^*, \\ C_{33}^I &= -2\gamma_1 \omega_n^2 |G_{12}|^2, \\ C_{11}^{\text{II}} &= C_{12}^{\text{II}} = C_{21}^{\text{II}} = C_{22}^{\text{II}} = i\omega_n [G_{12} G_{11}^* - G_{11} G_{12}^*], \\ C_{13}^{\text{II}} &= C_{23}^{\text{II}} = i\omega [G_{11} (G_{12}^* - G_{22}^*) - G_{12}^* (G_{11} - G_{12})], \\ C_{33}^{\text{II}} &= i\omega_n [G_{22} G_{12}^* - G_{12} G_{22}^*], \\ C_{ij}^{I, \text{II}*} &= C_{ij}^{I, \text{II}}(-\omega_n). \end{aligned}$$

The column vector $\bar{\alpha}_n$ is

$$\bar{\alpha}_n = -\lambda \begin{bmatrix} a_{11}^T \Delta U \\ a_{21}^T \Delta U \\ a_{31}^T \Delta U \end{bmatrix} - ie^{-i\epsilon\omega_n} \begin{bmatrix} q_3^T \sigma \\ q_3^T \sigma \\ q_4^T \sigma \end{bmatrix}, \quad (3.56)$$

in which

$$\begin{aligned} a_{11}^T &= \left[\Delta\beta(1 - 2i\gamma_1\omega_n G_{11}) - \frac{\Pi k}{T_2}(G_{11} - G_{12}) \right] q_2^\dagger + \frac{i\omega_n \Pi k}{T_2} G_{11} q_1^\dagger, \\ a_{21}^T &= \left[-2i\gamma_1\omega_n \Delta\beta G_{11} - \frac{\Pi k}{T_2}(G_{11} - G_{12}) \right] q_2^\dagger + \frac{i\omega_n \Pi k}{T_2} G_{11} q_1^\dagger, \\ a_{31}^T &= \left[-2i\gamma_1\omega_n \Delta\beta G_{12} - \frac{\Pi k}{T_2}(G_{12} - G_{22}) \right] q_2^\dagger + \frac{i\omega_n \Pi k}{T_2} G_{12} q_1^\dagger. \end{aligned}$$

In Eq. (3.55), $|f_n|^2$ is given by

$$|f_n|^2 = \Delta U^T \left[2\Delta\beta\gamma_1 q_2 q_2^\dagger - \frac{\Pi k}{T_2}(q_1 q_2^\dagger + q_2 q_1^\dagger) \right] \Delta U.$$

Therefore,

$$\begin{aligned} \langle e^{E(\tau)} \rangle_{U, U_0} &= \prod_{n=1}^{\infty} \left\langle \exp \left[-\lambda\tau\zeta_n^T C_n \zeta_n^* + \zeta_n^T \bar{\alpha}_n + \bar{\alpha}_{-n}^T \zeta_n^* + \frac{\lambda}{\tau} |f_n|^2 \right] \right\rangle \\ &\quad \times \left\langle \exp \left[-\frac{\lambda\tau}{2} \zeta_0^T C_0 \zeta_0 + \zeta_0^T \bar{\alpha}_0 + \frac{\lambda}{2\tau} f_0^2 \right] \right\rangle, \quad (3.57) \end{aligned}$$

where the angular brackets represent the average over the noise distribution. For $n = 0$, average is over the distribution $P(\zeta_0) = (2\pi)^{-3/2} (\det \Lambda)^{-1/2} \exp[-\frac{1}{2} \zeta_0^T \Lambda^{-1} \zeta_0]$ in which $\Lambda = \text{diag}\left(\frac{2T_1\gamma_1}{\tau}, \frac{2T_2\gamma_2}{\tau}, \frac{2T_3\gamma_3}{\tau}\right)$ whereas for each $n \geq 1$, average is over distribution $P(\zeta_n) = \pi^{-3} (\det \Lambda)^{-1} \exp[-\zeta_n^T \Lambda^{-1} \zeta_n^*]$. After some simplification, Eq. (3.57) becomes

$$\langle e^{E(\tau)} \rangle_{U, U_0} = e^{\tau\bar{\mu}(\lambda)} \exp \left[\frac{1}{2} \sum_{n=-\infty}^{\infty} \left(\alpha_{-n}^T \Omega_n^{-1} \alpha_n + \frac{\lambda |f_n|^2}{\tau} \right) \right], \quad (3.58)$$

where $\Omega_n = \Lambda^{-1} + \lambda\tau C_n$.

In the large time limit ($\tau \rightarrow \infty$), we convert the summation in the above equation into integration. Therefore, we get

$$\langle e^{E(\tau)} \rangle_{U, U_0} \approx e^{\tau \tilde{\mu}(\lambda)} e^{-\frac{1}{2} \sigma^T H_1(\lambda) \sigma + i \Delta U^T H_2(\lambda) \sigma + \frac{1}{2} \Delta U^T H_3(\lambda) \Delta U}, \quad (3.59)$$

where one can identify $\tilde{\mu}(\lambda)$, $H_1(\lambda)$, $H_2(\lambda)$, and $H_3(\lambda)$ as

$$\tilde{\mu}(\lambda) = -\frac{1}{4\pi} \int_{-\infty}^{\infty} d\omega \ln[\det(\Lambda\Omega)], \quad (3.60)$$

$$H_1(\lambda) = \frac{\tau}{2\pi} \int_{-\infty}^{\infty} d\omega \rho^T \Omega^{-1} \phi, \quad (3.61)$$

$$H_2(\lambda) = -\frac{\tau}{2\pi} \lim_{\epsilon \rightarrow 0} \int_{-\infty}^{\infty} d\omega e^{-i\epsilon\omega} b_1^T \Omega^{-1} \phi, \quad (3.62)$$

$$H_3(\lambda) = \frac{\tau}{2\pi} \int_{-\infty}^{\infty} d\omega \left[b_1^T \Omega^{-1} b_2 + \frac{\lambda}{\tau} \left\{ 2\Delta\beta\gamma_1 q_2 q_2^\dagger - \frac{\Pi k}{T_2} (q_1 q_2^\dagger + q_2 q_1^\dagger) \right\} \right], \quad (3.63)$$

with $\rho^T = (q_3^*, q_3^*, q_4^*)$, $b_1^T = -\lambda(b_{11}, b_{12}, b_{13})$, $b_2 = -\lambda(a_{11}^T, a_{21}^T, a_{31}^T)^T$, and $\phi = (q_3, q_3, q_4)^T$. The column vectors b_{1j} are given as

$$\begin{aligned} b_{11} &= q_2 \left[\Delta\beta(1 + 2i\gamma_1\omega G_{11}^*) - \frac{\Pi k}{T_2} (G_{11}^* - G_{12}^*) \right] - \frac{i\omega\Pi k}{T_2} q_1 G_{11}^*, \\ b_{12} &= q_2 \left[2i\gamma_1\omega\Delta\beta G_{11}^* - \frac{\Pi k}{T_2} (G_{11}^* - G_{12}^*) \right] - \frac{i\omega\Pi k}{T_2} q_1 G_{11}^*, \\ b_{13} &= q_2 \left[2i\gamma_1\omega\Delta\beta G_{12}^* - \frac{\Pi k}{T_2} (G_{12}^* - G_{22}^*) \right] - \frac{i\omega\Pi k}{T_2} q_1 G_{12}^*. \end{aligned}$$

Therefore, the moment generating function $Z_W(\lambda, U, \tau|U_0)$ can be rewritten as

$$\begin{aligned} Z_W(\lambda, U, \tau|U_0) &= \int \frac{d^3\sigma}{(2\pi)^3} e^{i\sigma^T U} \langle e^{E(\tau)} \rangle_{U, U_0} \\ &\approx \frac{e^{\tau \tilde{\mu}(\lambda)} e^{\frac{1}{2} \Delta U^T H_3 \Delta U} e^{-\frac{1}{2} (U^T + \Delta U^T H_2) H_1^{-1} (U + H_2^T \Delta U)}}{\sqrt{(2\pi)^3 \det H_1(\lambda)}}. \end{aligned} \quad (3.64)$$

We can factorize the restricted moment generating function $Z_W(\lambda, U, \tau|U_0)$ as Eq. (3.26) into left and right eigenfunctions. Consequently, the matrices $H_1(\lambda)$, $H_2(\lambda)$, $H_3(\lambda)$ satisfy the condition $H_3 - H_2 H_1^{-1} H_2^T - H_1^{-1} H_2^T = 0$. Therefore, we write

$$Z_W(\lambda, U, \tau|U_0) \approx \frac{e^{\tau \tilde{\mu}(\lambda)} e^{-\frac{1}{2} U^T L_1(\lambda) U} e^{-\frac{1}{2} U_0^T L_2(\lambda) U_0}}{\sqrt{(2\pi)^3 \det H_1(\lambda)}}, \quad (3.65)$$

where the matrices $L_1(\lambda) = H_1^{-1} + H_1^{-1} H_2^T$ and $L_2 = -H_1^{-1} H_2^T$.

Using Eq. (3.19), we can write the moment generating function for the total entropy production for particle A in the coupled system

$$Z(\lambda, U, \tau | U_0) \approx \frac{e^{\tau \tilde{\mu}(\lambda)} e^{-\frac{1}{2} U^T \tilde{L}_1(\lambda) U} e^{-\frac{1}{2} U_0^T \tilde{L}_2(\lambda) U_0}}{\sqrt{(2\pi)^3 \det H_1(\lambda)}}, \quad (3.66)$$

where the matrices $L_1(\lambda)$ and $L_2(\lambda)$ modify as

$$\begin{aligned} \tilde{L}_1(\lambda) &= L_1(\lambda) - \lambda(mT_2^{-1} - H^{-1})\Sigma, \\ \tilde{L}_2(\lambda) &= L_2(\lambda) + \lambda(mT_2^{-1} - H^{-1})\Sigma. \end{aligned}$$

The moment generating function $Z(\lambda)$ as given in Eq. (3.27), for the generalize partial entropy production ΔS_{tot}^A can be obtained by integrating the restricted moment generating function $Z(\lambda, U, \tau | U_0)$ over U_0 with respect to the initial steady state distribution $P_{ss}^{full}(U_0)$ and the final variable U . Therefore, the prefactor given in Eq. (3.28) reduces to

$$g(\lambda) = [\det H_1(0) \det H_1(\lambda) \det \tilde{L}_1(\lambda) \det[\tilde{L}_2(\lambda) + H_1^{-1}(0)]]^{-1/2}. \quad (3.67)$$

3.5 Probability distribution function

The probability distribution function for ΔS_{tot}^A whose moment generating function $Z(\lambda)$ is given in Eq. (3.27), is obtained by inverting it using inverse transformation

$$P(\Delta S_{tot}^A = s\tau/\tau_\gamma) = \int_{-i\infty}^{+i\infty} \frac{d\lambda}{2\pi i} Z(\lambda) e^{\lambda s\tau/\tau_\gamma} \approx \int_{-i\infty}^{+i\infty} \frac{d\lambda}{2\pi i} g(\lambda) e^{(\tau/\tau_\gamma)[\mu(\lambda) + \lambda s]}, \quad (3.68)$$

where $\mu(\lambda) = \tau_\gamma \tilde{\mu}(\lambda)$ is the cumulant generating function, and the contour of integration is taken along the direction of imaginary axis passing through the origin of the complex λ -plane. If both $\mu(\lambda)$ and $g(\lambda)$ are analytic functions of λ , in large time limit ($\tau \gg \tau_\gamma$), we can approximate the above integral using saddle-point method [136, 94, 93, 110, 109]. Therefore, we get

$$P(\Delta S_{tot}^A = s\tau/\tau_\gamma) \approx \frac{g(\lambda^*) e^{(\tau/\tau_\gamma)K(\lambda^*)}}{\sqrt{2\pi(\tau/\tau_\gamma)|K''(\lambda^*)|}}, \quad (3.69)$$

where the saddle point $\lambda^*(s)$ is the solution of the following equation

$$\left. \frac{\partial \mu(\lambda)}{\partial \lambda} \right|_{\lambda=\lambda^*(s)} = -s, \quad (3.70)$$

and the function $K(\lambda^*) = \mu(\lambda^*) + \lambda^*s$. In Eq. (3.69),

$$K''(\lambda^*) = \left. \frac{\partial^2}{\partial \lambda^2} [\mu(\lambda) + \lambda s] \right|_{\lambda=\lambda^*(s)}. \quad (3.71)$$

Now, assume that both $g(\lambda)$ and $\mu(\lambda)$ satisfy Gallavotti-Cohen symmetry (condition I) [82], i.e. $g(\lambda) = g(1 - \lambda)$ and $\mu(\lambda) = \mu(1 - \lambda)$. Therefore, we write the probability distribution function for negative entropy production as

$$\begin{aligned} P(\Delta S_{tot}^A = -s\tau/\tau_\gamma) &\approx \int_{-i\infty}^{+i\infty} \frac{d\lambda}{2\pi i} g(1 - \lambda) e^{(\tau/\tau_\gamma)[\mu(1-\lambda) + (1-\lambda)s - s]} \\ &\approx e^{-s\tau/\tau_\gamma} \int_{1-i\infty}^{1+i\infty} \frac{d\lambda}{2\pi i} g(\lambda) e^{(\tau/\tau_\gamma)[\mu(\lambda) + \lambda s]}. \end{aligned} \quad (3.72)$$

If both $g(\lambda)$ and $\mu(\lambda)$ do not have singularities between $\lambda \in [0, 1]$ (condition II), we can easily shift the contour of integration from $(1 - i\infty, 1 + i\infty)$ to $(-i\infty, +i\infty)$. Therefore, from Eqs. (3.68) and (3.72), we get

$$\frac{P(\Delta S_{tot}^A = s\tau/\tau_\gamma)}{P(\Delta S_{tot}^A = -s\tau/\tau_\gamma)} \approx e^{s\tau/\tau_\gamma}. \quad (3.73)$$

Equation (3.73) is the fluctuation theorem for ΔS_{tot}^A in steady state. If $g(\lambda)$ and $\mu(\lambda)$ satisfy both conditions I and II, then the corresponding observable (for instance, in our case, the observable is ΔS_{tot}^A) will satisfy fluctuation theorem. In the following section, we discuss the result for the entropy production for a single Brownian particle connected to a thermal gradient.

3.6 Single Brownian particle in contact with two heat baths ($\delta = 0$)

In this section, we consider only one Brownian particle (say particle A) in contact with two heat baths at temperatures T_1 and $T_2 < T_1$ (see Fig. 3.1 with $\delta = 0$). Note that this case is different from the case $\delta \rightarrow 0$. Here, we raise two important points

for this model: (1) the medium entropy production will not obey fluctuation theorem in the steady state, and (2) when the system entropy production is added to the medium entropy production, the total entropy production satisfies the fluctuation theorem in the steady state.

In this case, the underdamped Langevin equation for Brownian particle A coupled to two heat baths is

$$m\dot{v}_A = -(\gamma_1 + \gamma_2)v_A(t) + \eta_1(t) + \eta_2(t). \quad (3.74)$$

Entropy production in both baths due to particle A is given as

$$\Delta S_{med} = -\left[\frac{Q_1}{T_1} + \frac{Q_2}{T_2}\right] = \Delta\beta Q_1 - \frac{m}{2T_2}[v_A^2(\tau) - v_A^2(0)], \quad (3.75)$$

where $Q_1 = \int_0^\tau dt [\eta_1 - \gamma_1 v_A]v_A(t)$, is the heat energy given by the bath of a temperature T_1 and a dissipation constant γ_1 , to the Brownian particle A. Therefore, the restricted moment generating function for medium entropy production is given as

$$\begin{aligned} Z(\lambda, v_A, \tau | v_A(0)) &= \exp\left[\frac{\lambda m}{2T_2}\{v_A^2 - v_A^2(0)\}\right] \langle e^{-\lambda \Delta\beta Q_1} \delta[v_A - v_A(\tau)] \rangle_{v_A, v_A(0)} \\ &= \exp\left[\frac{\lambda m}{2T_2}\{v_A^2 - v_A^2(0)\}\right] \tilde{Z}(\lambda, v_A, \tau | v_A(0)), \end{aligned} \quad (3.76)$$

where $\tilde{Z}(\lambda, v_A, \tau | v_A(0))$ satisfies the following differential equation [70, 107]

$$\frac{\partial \tilde{Z}(\lambda, v_A, \tau | v_A(0))}{\partial \tau} = \mathcal{L}_\lambda^A \tilde{Z}(\lambda, v_A, \tau | v_A(0)). \quad (3.77)$$

In the above equation, the differential operator \mathcal{L}_λ^A is given as

$$\begin{aligned} \mathcal{L}_\lambda^A &= \frac{\gamma_1 T_1 + \gamma_2 T_2}{m^2} \frac{\partial^2}{\partial v_A^2} + \frac{v_A}{m} (\gamma_1 + \gamma_2 + 2\lambda \Delta\beta \gamma_1 T_1) \frac{\partial}{\partial v_A} + \left[\frac{\gamma_1 + \gamma_2}{m} \right. \\ &\quad \left. + \lambda \Delta\beta \left(\gamma_1 v_A^2 + \frac{\gamma_1 T_1}{m} \right) + \lambda^2 \Delta\beta^2 v_A^2 \gamma_1 T_1 \right]. \end{aligned} \quad (3.78)$$

The differential Eq. (3.77) is subjected to initial condition $\tilde{Z}(\lambda, v_A, \tau | v_A(0)) = \delta[v_A - v_A(0)]$. One can solve this differential equation exactly [143, 107]. In the limit of

large τ , we get

$$\begin{aligned}
Z(\lambda, v_A, \tau | v_A(0)) &\approx e^{(\tau/t_\gamma)\mu_0(\lambda)} \sqrt{\frac{m(\gamma_1 + \gamma_2)v(\lambda)}{2\pi(\gamma_1 T_1 + \gamma_2 T_2)}} \\
&\times \exp \left[-\frac{m(\gamma_1 + \gamma_2)v_A^2}{4(\gamma_1 T_1 + \gamma_2 T_2)} \{v(\lambda) - 2\lambda + 1\} \right] \\
&\times \exp \left[-\frac{m(\gamma_1 + \gamma_2)v_A^2(0)}{4(\gamma_1 T_1 + \gamma_2 T_2)} \{v(\lambda) + 2\lambda - 1\} \right], \quad (3.79)
\end{aligned}$$

where $t_\gamma = 2m/(\gamma_1 + \gamma_2)$. Integrating the above equation over the initial steady state distribution $Z(0, v_A, \tau \rightarrow \infty | v_A(0)) = \tilde{P}_{ss}(v_A(0))$ given in Eq. (3.14), and final variables v_A , we get

$$Z(\lambda) \approx e^{(\tau/t_\gamma)\mu_0(\lambda)} g_0(\lambda), \quad \text{where} \quad (3.80)$$

$$\mu_0(\lambda) = 1 - v(\lambda), \quad (3.81)$$

$$g_0(\lambda) = \frac{2\sqrt{v(\lambda)}}{\sqrt{1+v(\lambda)} - 2\lambda\sqrt{1+v(\lambda)} + 2\lambda'}, \quad (3.82)$$

with

$$v(\lambda) = \sqrt{1 + 4\alpha\lambda(1 - \lambda)} = \sqrt{4\alpha(\lambda_+ - \lambda)(\lambda - \lambda_-)}. \quad (3.83)$$

In the above equation, $\lambda_\pm = 1/2[1 \pm \sqrt{1 + 1/\alpha}]$ in which $\alpha = \gamma_1\gamma_2 T_1 T_2 \Delta\beta^2 / (\gamma_1 + \gamma_2)^2$. In Eq. (3.82), the first factor in the denominator comes from the integration over final variable v_A while the second one comes from the integration over the initial state $v_A(0)$ with respect to the distribution $\tilde{P}_{ss}(v_A(0))$. Here, $\mu_0(\lambda)$ is analytic function when $\lambda \in (\lambda_-, \lambda_+)$. First denominator in $g_0(\lambda)$ has one branch point at $\lambda = \lambda_a = 1$ for all $\alpha \in (0, \infty)$ where $\lambda_a \in (\lambda_-, \lambda_+)$ when $1 - 2\lambda_+ < 0$ while second denominator has a branch point at $\lambda = \lambda_b = (\alpha - 1)/(\alpha + 1)$ for $\alpha \leq 1/3$ where $\lambda_- \leq \lambda_b < \lambda_+$ when $1 + 2\lambda_- \leq 0$.

The probability distribution function of the medium entropy production ΔS_{med} can be obtained by inverting $Z(\lambda)$ given in Eq. (3.80) (see Sec. 3.5). Here, the saddle point $\lambda_0^*(s)$ is given by solving the following equation

$$\left. \frac{\partial \mu_0(\lambda)}{\partial \lambda} \right|_{\lambda=\lambda_0^*(s)} = -s. \quad (3.84)$$

When $\alpha > 1/3$, $g_0(\lambda)$ has only one singularity, i.e. at $\lambda = \lambda_a$. Therefore, the saddle point $\lambda_0^*(s)$ moves from λ_- to λ_a as s decreases from $s = +\infty$ to s_a , and gets stuck at $\lambda = \lambda_a$, where s_a is the solution of $\lambda_0^*(s_a) = \lambda_a$. Therefore, $P(\Delta S_{med} = s\tau/t_\gamma) \sim e^{(\tau/t_\gamma)[\mu_0(\lambda_-) + \lambda_- s]}$ as $s \rightarrow +\infty$. Around $s = s_a$, i.e. $\lambda_0^* = \lambda_a - \epsilon_a$, where $0 < \epsilon_a \ll 1$, $P(\Delta S_{med} = s\tau/t_\gamma) \sim e^{(\tau/t_\gamma)[\mu_0(\lambda_a) + \lambda_a s]}$. This implies for large s , we find [110, 109, 94, 93, 143, 52, 51]

$$\lim_{(\tau/t_\gamma) \rightarrow \infty} \frac{t_\gamma}{\tau} \ln \frac{P(\Delta S_{med} = s\tau/t_\gamma)}{P(\Delta S_{med} = -s\tau/t_\gamma)} = \mu_0(\lambda_-) - \mu_0(\lambda_a) + [\lambda_- + \lambda_a]s. \quad (3.85)$$

Similarly, for $\alpha \leq 1/3$, $g_0(\lambda)$ has both singularities, i.e. λ_a and λ_b . In this case, Eq. (3.85) modifies as

$$\lim_{(\tau/t_\gamma) \rightarrow \infty} \frac{t_\gamma}{\tau} \ln \frac{P(\Delta S_{med} = s\tau/t_\gamma)}{P(\Delta S_{med} = -s\tau/t_\gamma)} = \mu_0(\lambda_b) - \mu_0(\lambda_a) + [\lambda_b + \lambda_a]s. \quad (3.86)$$

Therefore, we find that entropy production in the medium will not satisfy fluctuation theorem for large scaled parameter s for any $\alpha \in (0, \infty)$. It is interesting to note that once we incorporate the entropy production of the system into entropy production in the medium, i.e. $\Delta S_{tot} = \Delta S_{med} + \Delta S_{sys}$, where $\Delta S_{sys} = -\ln \tilde{P}(v_A(\tau)) + \ln \tilde{P}(v_A(0))$, in which $\tilde{P}_{ss}(v_A(\tau))$ is given in Eq. (3.14), the prefactor term $g_0(\lambda)$ corresponding to ΔS_{tot} modifies to

$$g_0(\lambda) = \frac{2\sqrt{v(\lambda)}}{1 + v(\lambda)}, \quad (3.87)$$

and it is analytic function within the same domain as that of $\mu_0(\lambda)$. Moreover, both $\mu_0(\lambda)$ and $g_0(\lambda)$ satisfy condition I and II. Consequently, in this case, total entropy production satisfies fluctuation theorem for all α .

3.7 Analysis for prefactor $g(\lambda)$ for $\delta \neq 0$

In our problem, it is difficult to obtain the analytical expression for the prefactor term $g(\lambda)$ given in Eq. (3.67), as it requires the computation of matrices $H_1(\lambda)$, $H_2(\lambda)$ and $H_3(\lambda)$ [see Eqs. (3.61)–(3.63)]. Since we are interested in the weak coupling limit

($\delta \rightarrow 0$), we can write

$$g(\lambda) \approx g_0(\lambda) + \delta^a g_1(\lambda), \quad \text{where } a > 0. \quad (3.88)$$

The term $g_0(\lambda)$ is the same prefactor term as given in Eq. (3.87). The term $g_1(\lambda)$ may have singularities, but in the limit $\delta \rightarrow 0$, we can approximate the correction term as [52, 53]

$$g(\lambda) \approx g_0(\lambda). \quad (3.89)$$

3.8 Analysis for cumulant generating function $\mu(\lambda)$ for $\delta \neq 0$

In this section, we show how to compute the cumulant generating function. For simplicity, we assume $\alpha_{12} = \alpha_{13} = 1$, i.e. $\gamma_1 = \gamma_2 = \gamma_3 = \gamma$. Therefore, $h(u, \lambda)$ and $q(u)$ in Eq. (3.29) become

$$\begin{aligned} h(u, \lambda) = & 4\lambda(1 - \lambda)\beta_{12}[(1 - \beta_{12})^2\{u^4 + u^2(1 - \delta) + \delta^2/4\} + \delta^2\beta_{13}(\beta_{12} + \Pi - 1)/4] \\ & - \lambda\delta^2[(\beta_{12} + \beta_{13}\lambda\Pi - \beta_{13}\lambda)(\beta_{12} + \Pi - 1) + \beta_{12}\Pi\{\beta_{12} - \beta_{13} + \beta_{13}\lambda\Pi\}], \end{aligned} \quad (3.90)$$

$$q(u) = \beta_{12}^2[u^6 + u^4(5 - 2\delta) + u^2(4 - \delta)(1 - \delta) + 9\delta^2/4]. \quad (3.91)$$

The analytical computation of the integral given in Eq. (3.29), is quite involved and not very illuminating to us. Therefore, we compute $\mu(\lambda)$ numerically for fixed parameters δ , β_{12} , and β_{13} as a function of λ . The range of λ is not arbitrary. It is restricted by the saddle point $\lambda^*(s)$ which is the solution of Eq. (3.70). As one varies the scaled parameter s , the saddle point $\lambda^*(s)$ moves on the real line between two end points λ_{\pm}^{δ} , i.e. $\lambda^*(s \rightarrow \mp\infty) \rightarrow \lambda_{\pm}^{\delta}$. In the following, we identify these branch points singularities λ_{\pm}^{δ} present in $\mu(\lambda)$. We see that arguments of the logarithm in the integrand in Eq. (3.29) are $q(u)$ and $[h(u, \lambda) + q(u)]$. Clearly, the function

$$q(u) = \beta_{12}^2[u^2(u^2 + 1 - \delta)^2 + 3\{(u^2 - \delta/2)^2 + u^2 + \delta^2/2\}] \quad (3.92)$$

is positive for all real $u \in (-\infty, \infty)$. We write $[h(u, \lambda) + q(u)]$ as

$$\begin{aligned} h(u, \lambda) + q(u) &= 0 \\ -p_1(u)\lambda^2 + p_2(u)\lambda + q(u) &= 0, \end{aligned} \quad (3.93)$$

where

$$\begin{aligned} p_1(u) &= 4\beta_{12}[(1 - \beta_{12})^2\{u^4 + u^2(1 - \delta) + \delta^2/4\} + \delta^2\beta_{13}(\beta_{12} + \Pi - 1)/4] \\ &\quad + \delta^2\beta_{13}[(\Pi - 1)(\beta_{12} + \Pi - 1) + \beta_{12}\Pi^2], \end{aligned} \quad (3.94)$$

and

$$\begin{aligned} p_2(u) &= 4\beta_{12}[(1 - \beta_{12})^2\{u^4 + u^2(1 - \delta) + \delta^2/4\} + \delta^2\beta_{13}(\beta_{12} + \Pi - 1)/4] \\ &\quad - \delta^2\beta_{12}[\beta_{12} + \Pi - 1 + \Pi(\beta_{12} - \beta_{13})]. \end{aligned} \quad (3.95)$$

The roots of the quadratic Eq. (3.93) are given as

$$\lambda_{\pm}^{\delta}(u) = \frac{p_2(u) \pm \sqrt{p_2(u)^2 + 4p_1(u)q(u)}}{2p_1(u)}. \quad (3.96)$$

Figure 3.2 shows the variation of $\lambda_{\pm}^{\delta}(u)$ with respect to u for different values of β_{12} , β_{13} , and Π , in which red solid and blue dashed lines correspond to $0 < \delta < 1$ and $\delta = 0$ case, respectively. It is clear from Fig. 3.2, both $\lambda_{\pm}^{\delta}(u)$ have either one extremum or two extrema depending upon the choice of parameters β_{12} and β_{13} for given Π and δ . We see that the curvature of the functions $\lambda_{\pm}^{\delta}(u)$ changes around $u = 0$. Therefore, the equation

$$\lambda_{\pm}^{\delta\prime\prime}(0) = \left. \frac{\partial^2 \lambda_{\pm}^{\delta}(u)}{\partial u^2} \right|_{u=0} \quad (3.97)$$

decides the extrema of the function $\lambda_{\pm}^{\delta}(u)$ for given Π and δ .

In the case of partial entropy production ($\Pi = 1$), we see that

$$\left. \frac{\partial^2 \lambda_{\pm}^{\delta}(u)}{\partial u^2} \right|_{u=0} = \frac{2\beta_{12}(1 - \delta)r_p^{\pm}(\beta_{12}, \beta_{13}, \delta)}{\delta^2 x_1 [(1 - \beta_{12})^2 + \beta_{13}(1 + \beta_{12})]^2}, \quad (3.98)$$

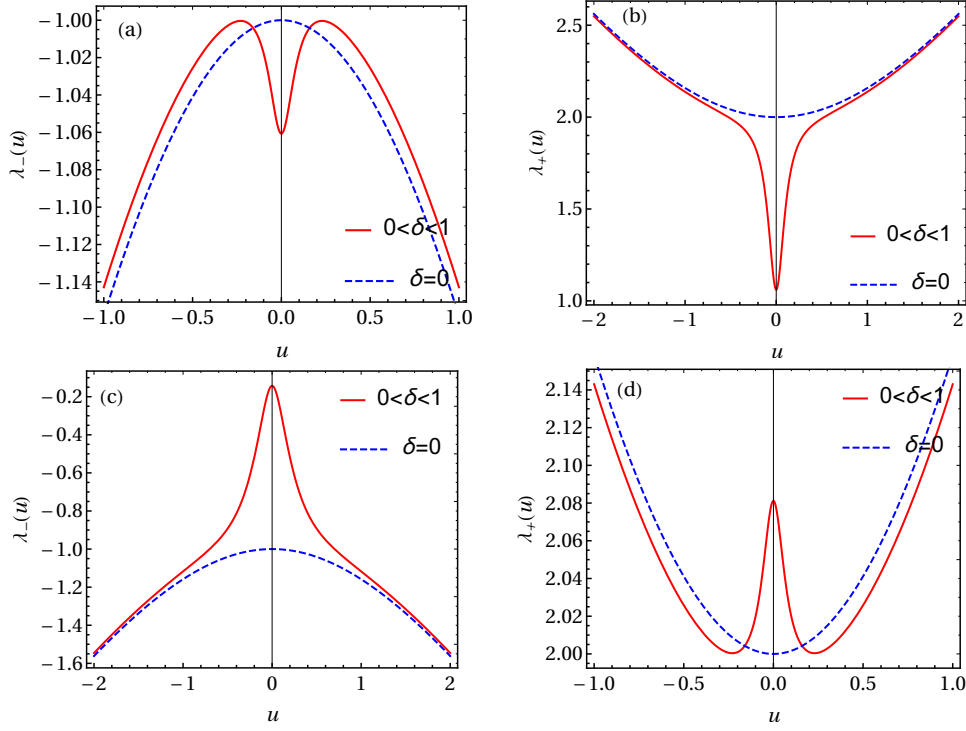


FIGURE 3.2: The figures show the variations of $\lambda_{\pm}^{\delta}(u)$ given in Eq. (3.96), with respect to u for different values of β_{12} , β_{13} , and Π , in which blue dashed lines correspond to $\delta = 0$ (coupling is absent) whereas red solid lines correspond to $0 < \delta < 1$ case.

where

$$r_p^{\pm}(\beta_{12}, \beta_{13}, \delta) = (1 - \beta_{12})^2 [4x_1 \mp (1 + 6\beta_{12} + \beta_{12}^2)] \pm \beta_{13}(1 + \beta_{12}) [3(1 - \beta_{12})^2 + 4\beta_{13}(1 + \beta_{12})] \mp [(1 - \beta_{12})^2 + \beta_{13}(1 + \beta_{12})]^2 \delta.$$

In Eq. (3.98), we take $0 < \delta < 1$, and function x_1 is given by

$$x_1 = \sqrt{(1 + \beta_{12})(1 + \beta_{12} + \beta_{13})[(\beta_{12} - 1/2)^2 + \beta_{13}(1 + \beta_{12}) + 3/4]},$$

where x_1 is a positive functions of β_{12} and β_{13} .

While the function $r_p^+(\beta_{12}, \beta_{13}, \delta) > 0$ for all β_{12}, β_{13} at $0 < \delta < 1$ which indicates that function $\lambda_+^{\delta}(u)$ has similar behavior as shown in Fig. 3.2(b), the function $r_p^-(\beta_{12}, \beta_{13}, \delta)$ changes sign depending upon the choice of parameters β_{12}, β_{13} at $0 < \delta < 1$. Therefore, the contour separating these two regions is given by

$$r_p^-(\beta_{12}, \beta_{13}, \delta) = 0. \quad (3.99)$$

We plot the phase diagram as shown in Fig. 3.3(a) in the limit $\delta \rightarrow 0$, in which red dashed contour corresponds to above equation. Thus, $\lambda_{\pm}^{\delta}(u)$ has similar behaviours as shown in Figs. 3.2(a) and 3.2(c) for region I and II, respectively, of Fig. 3.3(a).

In the case of apparent entropy production ($\Pi = 0$), we find that

$$\left. \frac{\partial^2 \lambda_{\pm}^{\delta}(u)}{\partial u^2} \right|_{u=0} = \frac{2\beta_{12}(1-\delta)r_A^{\pm}(\beta_{12}, \beta_{13}, \delta)}{\delta^2 x_2 (1-\beta_{12})(\beta_{12} + \beta_{13})^2}, \quad (3.100)$$

where

$$r_A^{\pm}(\beta_{12}, \beta_{13}, \delta) = \mp [(\beta_{12} - \beta_{13})(4 \pm 2x_2) + \beta_{12}\beta_{13}(1 + 2\delta) + \beta_{12}^2(3 + \delta) - \beta_{13}^2(2 - \delta)],$$

In Eq. (3.100), we take $0 < \delta < 1$, and function x_2 is given by

$$x_2 = \sqrt{(1 + \beta_{12} + \beta_{13})(4 + \beta_{12} + \beta_{13})}, \quad (3.101)$$

where x_2 is positive function of β_{12} and β_{13} .

The function $r_A^{-}(\beta_{12}, \beta_{13}, \delta) > 0$ for all β_{12} , β_{13} and $0 < \delta < 1$ which suggests that the function $\lambda_{-}^{\delta}(u)$ has variation with respect to u as shown in Fig. 3.2(a). The function $r_A^{+}(\beta_{12}, \beta_{13}, \delta)$ can be either positive or negative depending upon the choice of β_{12} , β_{13} at $0 < \delta < 1$. Therefore, the equation of contour separating these two regions is given as

$$r_A^{+}(\beta_{12}, \beta_{13}, \delta) = 0. \quad (3.102)$$

In the limit $\delta \rightarrow 0$, the phase diagram is shown in Fig. 3.3(b) where red dashed contour is given by above equation. Thus, the root $\lambda_{+}^{\delta}(u)$ has the variations as shown in Figs. 3.2(d) and 3.2(b) in region I and II, respectively, of Fig. 3.3(b). Note that in both phase diagram, the axis (not shown) corresponds to δ is perpendicular to the plane of the paper.

The extrema of $\lambda_{\pm}^{\delta}(u)$ shown in Fig. 3.2, give the cut-off on the real line of the complex λ -plane within which the cumulant generating function $\mu(\lambda)$ is a real function. Notice that the saddle point $\lambda^*(s)$ also lies within this domain. The equation for extremum is given by

$$\left. \frac{\partial \lambda_{\pm}^{\delta}(u)}{\partial u} \right|_{u=u_{\pm}^*} = 0, \quad (3.103)$$

where u_{\pm}^* is the solution of the following equation

$$\begin{aligned} & [\sqrt{p_2^2(u_{\pm}^*) + 4p_1(u_{\pm}^*)q(u_{\pm}^*) \pm p_2(u_{\pm}^*)}][p_1(u_{\pm}^*)p_2'(u_{\pm}^*) - p_2(u_{\pm}^*)p_1'(u_{\pm}^*)] \\ & \pm 2p_1(u_{\pm}^*)[p_1(u_{\pm}^*)q'(u_{\pm}^*) - q(u_{\pm}^*)p_1'(u_{\pm}^*)] = 0. \end{aligned} \quad (3.104)$$

In the above equation, $'$ represents the derivative with respect to u . In the weak coupling limit ($\delta \rightarrow 0$), we compute u_{\pm}^* (upto leading order in δ) using perturbation theory for both definitions of entropy production. In the case of partial entropy production ($\Pi = 1$),

$$u_{-}^* = \begin{cases} \pm \sqrt{\delta} \frac{[5 - 3\beta_{12}^2 - 4\beta_{13} - 2\beta_{12}(1 + 2\beta_{13})]^{1/4}}{\sqrt{2(1 - \beta_{12})}} + o(\sqrt{\delta}) & \text{for region I of Fig. 3.3(a),} \\ 0 & \text{for region II of Fig. 3.3(a),} \end{cases}$$

and $u_{+}^* = 0$ for region I and II of Fig. 3.3(a). Thus, $\lambda_{-}^{\delta}(u_{-}^*) \rightarrow \lambda_{-}$ in the region I whereas $\lambda_{-}^{\delta}(u_{-}^*) \rightarrow \tilde{\lambda}_{-}$ in the region II of Fig. 3.3(a) in the limit of $\delta \rightarrow 0$. Similarly, $\lambda_{+}^{\delta}(u_{+}^*) \rightarrow \tilde{\lambda}_{+}$ for both regions I and II of Fig. 3.3(a) in the limit $\delta \rightarrow 0$.

In the case of apparent entropy production ($\Pi = 0$),

$$u_{+}^* = \begin{cases} \pm \sqrt{\delta} \frac{[5\beta_{12}^2 + 4\beta_{12}(1 - \beta_{13}) - 4\beta_{13}]^{1/4}}{\sqrt{2\beta_{12}}} + o(\sqrt{\delta}) & \text{for region I of Fig. 3.3(b),} \\ 0 & \text{for region II of Fig. 3.3(b),} \end{cases}$$

whereas $u_{-}^* = \sqrt{\delta/2} + o(\sqrt{\delta})$ for region I and II of Fig. 3.3(b). In the weak coupling limit, $\lambda_{+}^{\delta}(u_{+}^*) \rightarrow \lambda_{+}$ in the region-I and $\lambda_{+}^{\delta}(u_{+}^*) \rightarrow \tilde{\lambda}_{+}$ in the region II of Fig. 3.3(b). Similarly, $\lambda_{-}^{\delta}(u_{-}^*) \rightarrow \lambda_{-}$ for both regions I and II of Fig. 3.3(b) in the limit $\delta \rightarrow 0$.

For $\Pi = 1$, $\tilde{\lambda}_{\pm}$ are given by

$$\tilde{\lambda}_{\pm} = \frac{1 + \beta_{13} + \beta_{12}(-4 + \beta_{12} + \beta_{13}) \pm x_1}{2[1 + \beta_{13} + \beta_{12}(-2 + \beta_{12} + \beta_{13})]}, \quad (3.105)$$

whereas $\tilde{\lambda}_{+}$ for $\Pi = 0$ is

$$\tilde{\lambda}_{+} = \frac{\beta_{12}(2 - \beta_{12} - \beta_{13} + x_2)}{2(1 - \beta_{12})(\beta_{12} + \beta_{13})}. \quad (3.106)$$

One can find λ_{\pm} in Sec. 3.6.

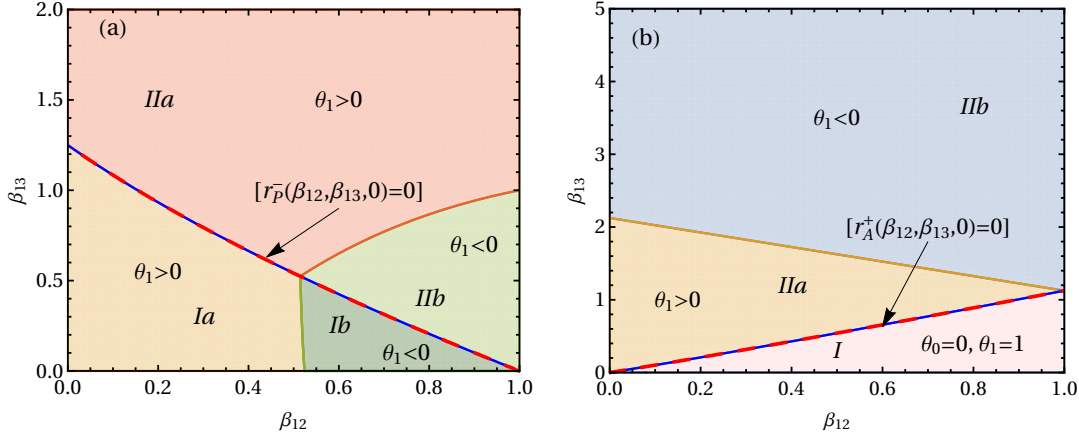


FIGURE 3.3: Phase diagrams for partial (a) and apparent (b) entropy production are shown. The red dashed contours correspond to Eqs. (3.99) and (3.102) in figures (a) and (b), respectively, in the limit $\delta \rightarrow 0$, separate the pairs of singularities present in the cumulant generating function $\mu(\lambda)$. The pairs of singularities are $(\lambda_-, \tilde{\lambda}_+)$ and $(\tilde{\lambda}_-, \tilde{\lambda}_+)$ in regions I and II of figure (a), respectively. For figure (b), the pairs of singularities are (λ_-, λ_+) and $(\lambda_-, \tilde{\lambda}_+)$ in regions I and II, respectively. Moreover, regions I and II of figure (a) and region II of figure (b) have two subregions depending upon the sign of the parameter θ_1 , where θ_1 is the slope of the asymmetry function $f(s) = \theta_0 + \theta_1 s$ as $s \rightarrow \infty$ [see Eqs. (3.111) and (3.112)].

3.8.1 Gallavotti-Cohen symmetry for cumulant generating function $\mu(\lambda)$

It can be seen from Eq. (3.29) that $\mu(\lambda)$ does not satisfy the Gallavotti-Cohen symmetry, i.e. $\mu(\lambda) \neq \mu(1 - \lambda)$ for large δ , which is also a signature of partial measurement. In Fig. 3.4, we have plotted the cumulant generating function $\mu(\lambda)$ (blue solid line) and $\mu(1 - \lambda)$ (red dashed line) against λ for: (a) region I of Fig. 3.3(a), (b) region II of Fig. 3.3(a), (c) region I of Fig. 3.3(b), and (d) region II of Fig. 3.3(b). All of these figures are plotted for fixed coupling parameter $\delta = 10^{-10}$. Except for region I of Fig. 3.3(b), the cumulant generating function does not satisfy the Gallavotti-Cohen symmetry for all λ . Therefore, we expect that the fluctuation theorem for apparent entropy production in the steady state, may hold in the region I of Fig. 3.3(b) in the limit $\delta \rightarrow 0$. It is interesting to note that range of λ over which $\mu(\lambda) = \mu(1 - \lambda)$ [see Figs. 3.4(a), 3.4(b), and 3.4(d)], there exists a corresponding range of scaled parameter s where the fluctuation theorem would hold in the weak coupling limit ($\delta \rightarrow 0$) [52, 53].

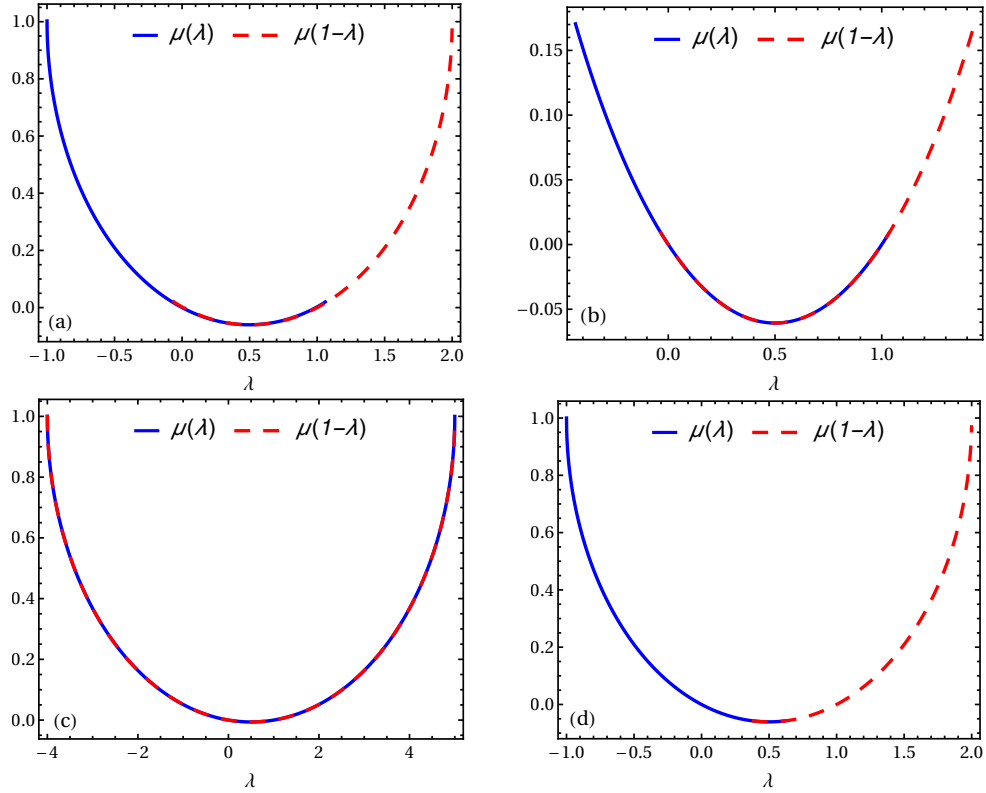


FIGURE 3.4: The cumulant generating function $\mu(\lambda)$ (blue solid line) and $\mu(1-\lambda)$ (red dashed line) are plotted against λ for: (a) region I of Fig. 3.3(a), (b) region II of Fig. 3.3(a), (c) region I of Fig. 3.3(b), and (d) region II of Fig. 3.3(b). All of the above figures are plotted for fixed coupling parameter $\delta = 10^{-10}$. Except for region I of Fig. 3.3(b), the cumulant generating function $\mu(\lambda)$ does not satisfy the Gallavotti-Cohen symmetry even in the limit $\delta \rightarrow 0$.

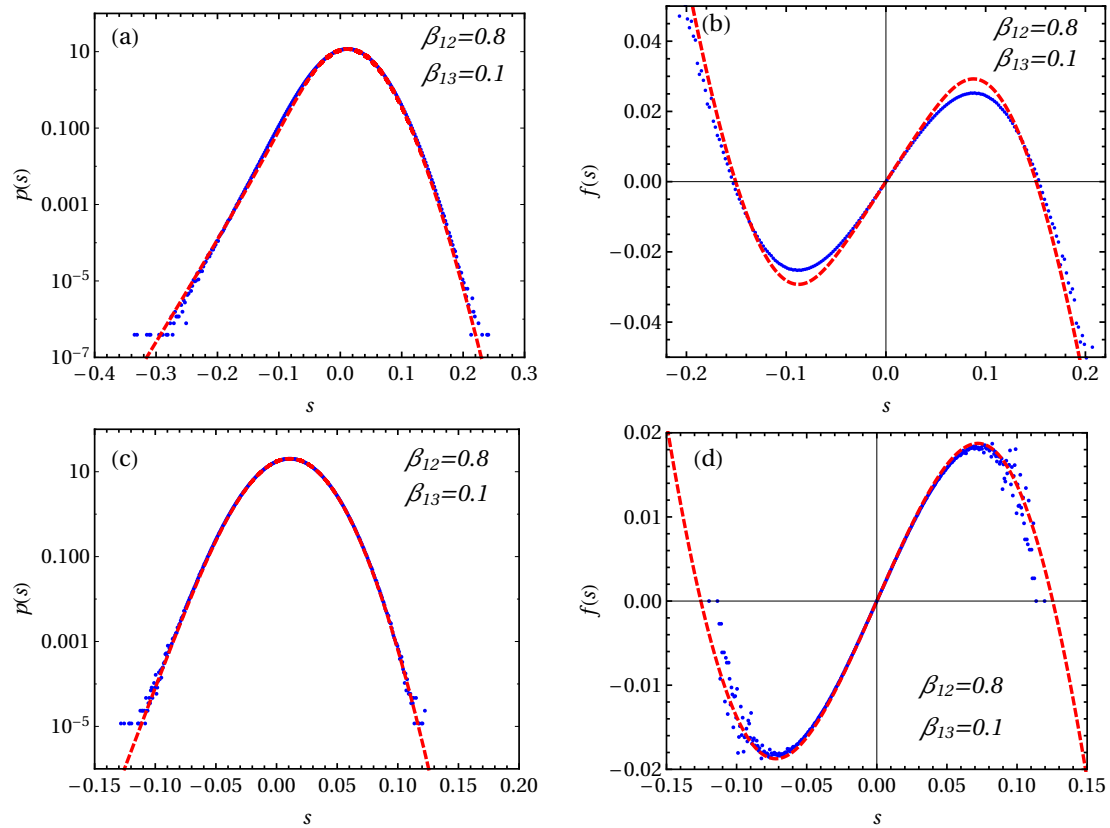


FIGURE 3.5: A comparison of analytically obtained results (red dashed lines) of probability density function $p(s)$ and asymmetry function $f(s)$ given in Eq. (3.108) and Eq. (3.109), respectively, with the numerical simulations (blue dots) is shown for partial entropy production with time $\tau/\tau_\gamma = 50.0$ [figures (a) and (b)] and $\tau/\tau_\gamma = 150.0$ [figures (c) and (d)]. All of the above figures are shown for coupling strength $\delta = 0.1$. This comparison indicates that as the time of the observation increases, the agreement between theory and numerical simulation gets better.

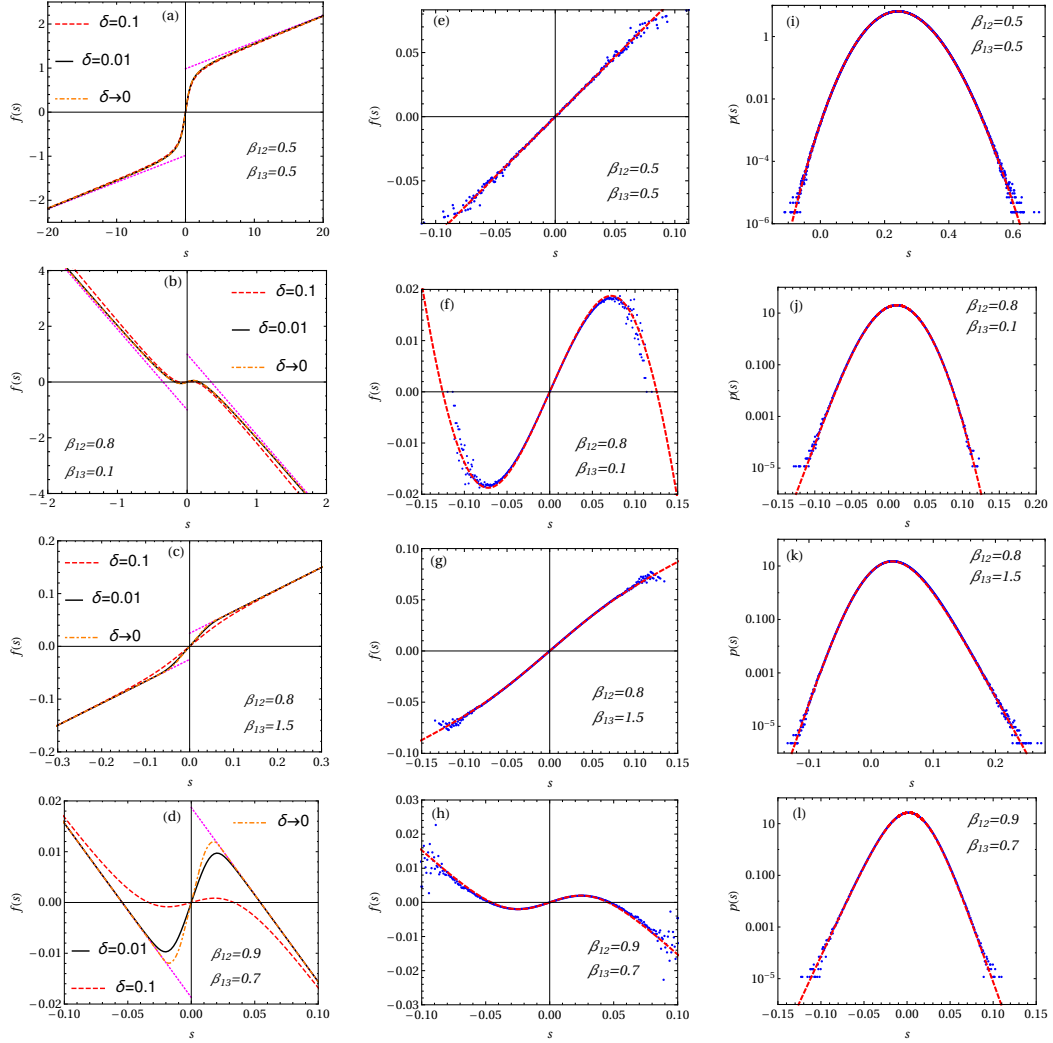


FIGURE 3.6: The analytically evaluated asymmetry function $f(s)$ given in Eq. (3.110) for partial entropy production is plotted against the scaled variable $s = \Delta \bar{S}_{tot}^A \tau_\gamma / \tau$ in figures (a)–(d) for respective β_{12} and β_{13} of phase diagram shown in Fig. 3.3(a). These plots are obtained for $\delta = 0.1$ (red dashed line) and $\delta = 0.01$ (black solid line). The asymmetry functions in the limit $\delta \rightarrow 0$ (orange dotdashed line) are also plotted for respective cases [52]. The asymptotic behaviours for asymmetry function $f(s)$ for partial entropy production given in (3.111) are shown by magenta tiny dashed lines. The comparison of analytical results (red dashed line) for asymmetry function $f(s)$ given by Eq. (3.109) and probability density function $p(s)$ given by Eq. (3.108) with the numerical simulations (blue dots) for partial entropy production is shown in figures (e)–(h) and figures (i)–(l), respectively. These comparisons are shown for fixed $\delta = 0.1$ and $\tau/\tau_\gamma = 150.0$.

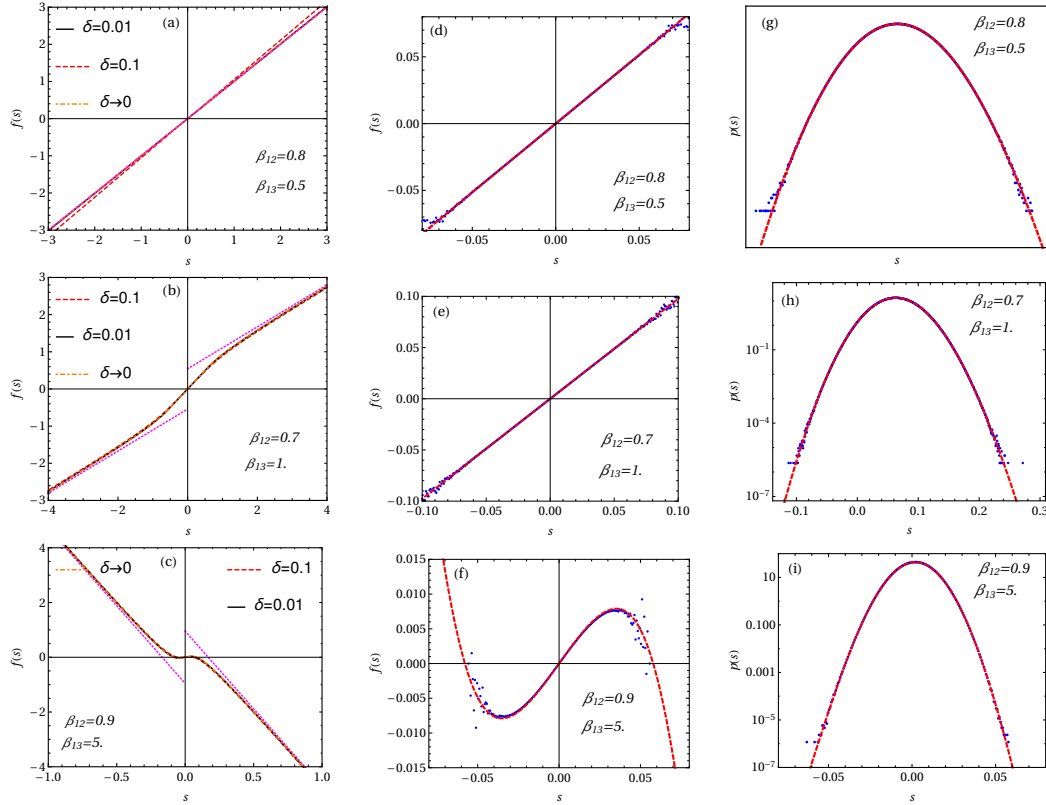


FIGURE 3.7: The analytical expression for $f(s)$ given in Eq. (3.110) of apparent entropy production is plotted against the scaled variable $s = \Delta \tilde{S}_{tot}^A \tau_\gamma / \tau$ in figures (a)–(c) for respective β_{12} and β_{13} of phase diagram shown in Fig. 3.3(b) for $\delta = 0.1$ (red dashed line) and $\delta = 0.01$ (black solid line). The asymmetry functions in the limit $\delta \rightarrow 0$ (orange dot-dashed line) are also plotted for respective cases [52]. Magenta tiny dashed lines represent the asymptotic expressions of $f(s)$ given in Eq. (3.112). In figures (d)–(f) and figures (g)–(i), we compared the asymmetry function $f(s)$ given in Eq. (3.109) and probability density function given in Eq. (3.108) with the numerical simulation results, respectively, for apparent entropy production for given $\delta = 0.1$ and $\tau/\tau_\gamma = 150$.

3.9 Large deviation function, fluctuation theorem and asymmetry function

Both $\mu(\lambda)$ and $g_0(\lambda)$ are real functions within any pair of singularities, i.e. $\lambda_-^\delta(u_-^*)$ and $\lambda_+^\delta(u_+^*)$ depending upon the choice of β_{12} and β_{13} in the weak coupling limit. The saddle point $\lambda^*(s)$ moves from $\lambda_-^\delta(u_-^*)$ to $\lambda_+^\delta(u_+^*)$ as s decreases from $+\infty$ to $-\infty$. Therefore, the probability density function $p(s)$ for large s has the following large deviation form

$$p(s) \sim e^{(\tau/\tau_\gamma)I(s)} \quad (3.107)$$

where the probability density function is obtained from Eq. (3.69)

$$p(s) = (\tau/\tau_\gamma)P(\Delta S_{tot}^A = s\tau/\tau_\gamma), \quad (3.108)$$

and $I(s) = K(\lambda^*(s))$ is the large deviation function [136]. We define an asymmetry function $f(s)$ as

$$f(s) = \frac{\tau_\gamma}{\tau} \ln \frac{p(s)}{p(-s)}. \quad (3.109)$$

Thus, in the large time limit ($\tau/\tau_\gamma \rightarrow \infty$), the asymmetry function is given by

$$f(s) = \lim_{\tau/\tau_\gamma \rightarrow \infty} \frac{\tau_\gamma}{\tau} \ln \frac{p(s)}{p(-s)} = I(s) - I(-s). \quad (3.110)$$

The quantity of interest is the variation of the asymmetry function $f(s)$ with the scaled parameter $s = \Delta S_{tot}^A \tau_\gamma / \tau$, and deviation from $f(s) = s$ will indicate the violation of steady state fluctuation theorem. In the limit $\delta \rightarrow 0$, the asymptotic behavior of $f(s)$ in the case of partial entropy production for $s \rightarrow \infty$ is given by [52]

$$f(s) = \begin{cases} \mu_0(\lambda_-) - \mu_0(\tilde{\lambda}_+) + (\lambda_- + \tilde{\lambda}_+)s, & \text{for region I of Fig. 3.3(a),} \\ \mu_0(\tilde{\lambda}_-) - \mu_0(\tilde{\lambda}_+) + (\tilde{\lambda}_- + \tilde{\lambda}_+)s, & \text{for region II of Fig. 3.3(a),} \end{cases} \quad (3.111)$$

whereas for apparent entropy production

$$f(s) = \begin{cases} s, & \text{for region I of Fig. 3.3(b),} \\ \mu_0(\lambda_-) - \mu_0(\tilde{\lambda}_+) + (\lambda_- + \tilde{\lambda}_+)s, & \text{for region II of Fig. 3.3(b),} \end{cases} \quad (3.112)$$

and $f(-s) = -f(s)$. In Eqs. (3.111) and (3.112), the cumulant generating function $\mu_0(\lambda)$ corresponds to the case $\delta = 0$, is given in Eq. (3.81).

We plot the analytical asymmetry function $f(s)$ given in Eq. (3.110) against s in Figs. 3.6(a)–3.6(d) and Figs. 3.7(a)–3.7(c) for partial and apparent entropy production, respectively, for $\delta = 0.1$ (red dashed line) and $\delta = 0.01$ (black solid line). The asymmetry function $f(s)$ in the limit $\delta \rightarrow 0$ (orange dotdashed line) is also plotted for each case [52]. In these figures, magenta tiny dashed lines correspond to the asymptotic expression of asymmetry function $f(s)$ given by Eqs. (3.111) and (3.112) for partial and apparent entropy production, respectively. One can see, as the coupling parameter δ reduces, the asymmetry function $f(s)$ converges to that of $\delta \rightarrow 0$ case.

3.10 Numerical simulation

In Figs. 3.5(a)–3.5(d), we show the comparison of theoretical predictions (red dashed line) of probability density function $p(s)$ given by Eq. (3.108) and the asymmetry function $f(s)$ given by Eq. (3.109) for partial entropy production for coupling parameter $\delta = 0.1$ with the numerical simulation results (blue dots) with time $\tau = 50.0$ [Figs. 3.5(a) and 3.5(b)] and $\tau = 150.0$ [Figs. 3.5(c) and 3.5(d)]. This comparison indicates that as the observation time τ/τ_γ increases, the agreement between theoretical predictions and numerical simulation results gets better. The details of the numerical simulations are given in Appendix A.

We compare the analytical asymmetry functions $f(s)$ given in Eq. (3.109) (red dashed line) with the numerical simulation results (blue dots) for $\delta = 0.1$ in Figs. 3.6(e)–3.6(h) and Figs. 3.7(d)–3.7(f) for partial and apparent entropy production, respectively. The probability density function $p(s)$ (red dashed line) given in Eq. (3.108) is

also compared with numerical simulation results (blue dots) for $\delta = 0.1$ in Figs. 3.6(i)–3.6(l) and Figs. 3.7(g)–3.7(i) for partial and apparent entropy production, respectively. All of these results are compared at time $\tau/\tau_\gamma = 150$, and show that there is nice agreement between theoretical prediction and numerical simulation.

3.11 Summary

We have considered a coupled Brownian particle system. Both particles are connected by a harmonic spring of stiffness k . One of the particles is connected to a thermal gradient and the other one is connected to a single bath of a constant temperature. The goal of this chapter is to understand the deviation of fluctuation theorem for total entropy production of one of the particles (say particle A) in the coupled system in the non-equilibrium steady state when the interaction between particles is weak. We have given two definitions of total entropy production of a partial system: partial and apparent entropy production. For convenience, we defined five dimensionless parameters: (1) coupling constant $\delta = 2km/\gamma_1^2$, (2) $\beta_{12} = T_2/T_1$, (3) $\beta_{13} = T_3/T_1$, (4) $\alpha_{12} = \gamma_2/\gamma_1$, and (5) $\alpha_{13} = \gamma_3/\gamma_1$. When $\alpha_{12} = \alpha_{13} = 1$, we plotted phase diagrams in (β_{12}, β_{13}) plane, for both definitions of entropy production, in the limit $\delta \rightarrow 0$. In the weak coupling limit ($\delta \rightarrow 0$), we have found that fluctuation theorem for apparent entropy production in the steady state is satisfied only in the region I of the phase diagram shown in Fig. 3.3(b). The results given above are also supported by the numerical simulations, and they have very nice agreement.

Chapter 4

Entropy production for partially observed system in a harmonic trap

We consider a harmonically coupled system of two Brownian particles (say A and B) in a harmonic confinement. The whole system is immersed in the heat bath at a constant temperature T . Each particle is driven by an external stochastic Gaussian white noise. This system generates entropy and that total entropy production satisfies the fluctuation theorem in the steady state. In the weak coupling limit, the partial system of the coupled system (i.e., particle A) also satisfies the steady state fluctuation theorem for the total entropy production (i.e., partial and apparent entropy production). Numerical simulations are done to verify analytical results and they have good agreements.

4.1. Introduction

Consider a system of n interacting degrees of freedom (DOFs). The time scale of relaxation of these DOFs is much larger than that of bath DOFs. The state of system at time $t \in [0, \tau]$ is represented by $x(t) := (x_1(t), x_2(t), \dots, x_n(t))$ in the phase space. These $\{x_i(t)\}$ can be either continuous or discrete DOFs. The evolution of the continuous variable $x(t)$ is described by the Langevin equation and its probability density function obeys the Fokker-Planck equation [107]. Similarly, the discrete variable $x(t)$ evolves according to the stochastic dynamics and the associated probability distribution follows the master equation [70]. In practice, there can be some technical difficulties due to which one cannot access the whole system. Suppose m -DOFs

of the system are experimentally observed which we call a subsystem or partial system of the complete system, i.e. $x_s(t) := (x_1(t), x_2(t), \dots, x_m(t))$ where $m < n$. In such case, observable statistics of the partial system might not be same as that of the complete system. In Chapters 2 and 3, we have considered systems which are either driven by external stochastic forces or by a thermal gradient into a non-equilibrium steady state. In those systems, we computed the total entropy production for a part of the system (partial and apparent entropy production). We showed that such a partial measurement leads to a new fluctuation theorem for partial and apparent entropy production when the interaction among the observed and hidden DOFs are considered to be infinitesimally small, i.e. *in the weak coupling limit*, which is quite remarkable result [52, 53]. In certain experiment, the above scenario is possible. In this chapter, we present a scheme where the effect of weak coupling of complement DOFs, i.e. $x_c(t) := (x_{m+1}(t), x_{m+2}(t), \dots, x_n(t))$ on $x_s(t)$ can be nullified. This can be feasible once we trap the whole system $x(t)$ in a harmonic confinement and do the measurement on the system. In such case, the observed DOFs will behave as if there are no weakly coupled hidden variables [52, 53, 51].

In this chapter, we consider a coupled Brownian particle system (say particle A and B) in a harmonic confinement of stiffness k_0 . Both particles are interacting harmonically with a spring of stiffness k . The whole system is immersed in the heat bath at a constant temperature T . In the absence of driving, the system is in equilibrium as it does not produce entropy. When these particles are driven using some external forcing, the system generates entropy. In the steady state, total entropy production obeys the steady state fluctuation theorem [see Eq. (1.13)]. Here, we drive each particle using an stochastic Gaussian noise and compute the total entropy production due to one of the particles (say of particle A) in the coupled system. We show that the steady state fluctuation theorem for the total entropy production of particle A in the coupled system holds in the weak coupling limit ($k \ll k_0$). It is interesting to mention that one can use this technique in an experiment to nullify the effect of weak coupling of hidden DOFs on the observed ones. Note that when $k = 0$, this system is similar to an experimentally studied model where work fluctuations by the external stochastic force on the free-end of the cantilever were measured by Gomez-Solano et al. [49]. Thus, it may be feasible to study systems similar to our model.

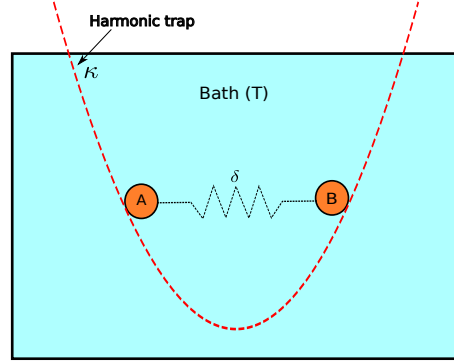


FIGURE 4.1: Two Brownian particles (A and B) of mass m are coupled to each other with the coupling parameter $\delta = 2km/\gamma^2$ (dimensionless), and are trapped in a harmonic confinement of strength $\kappa = k_0m/\gamma^2$. The whole setup is immersed in the heat bath of a constant temperature T .

The rest of the chapter is organized as follows. We define the model system in Sec. 4.2. In Secs. 4.2.1 and 4.2.2, we give the definitions for partial and apparent entropy production. The Fokker-Planck equation for the restricted moment generating function for W [see Eq. (4.23)] and its general solution in large- τ limit are given in Sec. 4.3. In Sec. 4.4, we give the complete calculation to obtain the moment generating function $Z(\lambda) = \langle e^{-\lambda \Delta S_{tot}^A} \rangle \sim g(\lambda) e^{(\tau/\tau_\gamma)\mu(\lambda)}$. The results for a special case of a single Brownian particle in a harmonic trap, driven by an external stochastic Gaussian force is given in Sec. 4.5. In Sec. 4.6, we invert the moment generating function $Z(\lambda)$ using saddle-point method to get the probability distribution for ΔS_{tot}^A . Section 4.7 contains large deviation function and fluctuation theorem for partial and apparent entropy production. In Sec. 4.8, we show the comparison of analytical results with the numerical simulations. We summarize the chapter in Sec. 4.9.

4.2. Model

Consider a system of two Brownian particles (say particle A and B) of mass m coupled by a harmonic spring of stiffness k , in a harmonic trap of stiffness k_0 . The whole system is immersed in the heat bath of a constant temperature T . The Hamiltonian of this coupled system is given as

$$\mathcal{H}(x_A, x_B, v_A, v_B) = \frac{1}{2}mv_A^2 + \frac{1}{2}mv_B^2 + \frac{1}{2}k_0x_A^2 + \frac{1}{2}k_0x_B^2 + \frac{1}{2}k(x_A - x_B)^2, \quad (4.1)$$

where $x_A(x_B)$ and $v_A(v_B)$ are the position and velocity of particle A (particle B), respectively. The schematic diagram is shown in Fig. 4.1.

The Langevin equations for the above coupled system in the presence of external forces are

$$\dot{x}_A = v_A(t), \quad (4.2)$$

$$\dot{x}_B = v_B(t), \quad (4.3)$$

$$m\dot{v}_A = -\gamma v_A(t) - (k + k_0)x_A(t) + kx_B(t) + f_A(t) + \eta_A(t), \quad (4.4)$$

$$m\dot{v}_B = -\gamma v_B(t) + kx_A(t) - (k + k_0)x_B(t) + f_B(t) + \eta_B(t), \quad (4.5)$$

where γ is the dissipation constant, $\eta_A(t)$ and $\eta_B(t)$ are the thermal noises from the heat bath with mean zero and correlation $\langle \eta_i(t)\eta_j(t') \rangle = 2\gamma T\delta_{ij}\delta(t - t')$, acting on particle A and B, respectively. The external forces $f_A(t)$ and $f_B(t)$ are acting on particle A and particle B, respectively, with mean zero and correlation $\langle f_A(t)f_A(t') \rangle = 2\gamma T\theta\delta(t - t')$, $\langle f_B(t)f_B(t') \rangle = 2\gamma T\theta\alpha^2\delta(t - t')$. Moreover, the thermal noises $\eta_i(t)$ and external forces $f_j(t)$ are uncorrelated with each other for all time: $\langle f_i(t)\eta_j(t') \rangle = 0$ for all t, t', i, j . Here, we consider two choices of external forces. For first choice, both $f_A(t)$ and $f_B(t)$ are uncorrelated for all time while in the another choice $f_B(t) = \alpha f_A(t)$. We define four dimensionless parameters α , θ , trap strength $\kappa = mk_0/\gamma^2$, and coupling parameter $\delta = 2km/\gamma^2$. For simplicity, the Boltzmann's constant k_B is set to 1. In the following subsections, we give the definitions of total entropy production for particle A in the coupled system.

4.2.1. Partial entropy production

It is well known that the total entropy production obeys the fluctuation theorem in the steady state for all time [121, 120]. The main concern of this chapter is to verify this result for a part of a harmonically confined system. To do so, we write down the total entropy production for one of the particles (say particle A) in the coupled system. Total entropy production consists of two terms. First term comes from change in the entropy of the bath while the second one is due to change in the configuration of the particle A between initial and final time. Both of these terms are computed in the steady state of the coupled system. Since the bath is infinitely large,

it always remains in the thermal equilibrium with the temperature T . Therefore, using the standard thermodynamics, we write the entropy production in the bath due to particle A as

$$\Delta \bar{S}_{med}^A = -\frac{Q^A}{T}, \quad (4.6)$$

where Q^A is the amount of heat energy transferred to particle A from the heat bath for time duration τ

$$Q^A = \int_0^\tau dt [\eta_A(t) - \gamma v_A(t)] v_A(t). \quad (4.7)$$

In the above equation, the integral follows the Stratonovich rule of integration [124]. The system entropy production of particle A in the coupled system for a time duration τ is [121, 120]

$$\Delta \bar{S}_{sys}^A = -\ln P_{ss}[\tilde{U}(\tau)] + \ln P_{ss}[\tilde{U}(0)], \quad (4.8)$$

where $\tilde{U} = (x_A, v_A)^T$, and $P_{ss}[\tilde{U}(\tau)]$ is the steady state distribution of particle A at time τ , obtained after integrating the full joint steady state distribution $P_{ss}^{full}(x_A, x_B, v_A, v_B)$ over x_B and v_B :

$$P_{ss}[\tilde{U}(\tau)] = \int_{-\infty}^{+\infty} dx_B \int_{-\infty}^{+\infty} dv_B P_{ss}^{full}(x_A, x_B, v_A, v_B). \quad (4.9)$$

Therefore, we get

$$P_{ss}[\tilde{U}(\tau)] = \frac{\exp[-\frac{1}{2} \tilde{U}^T \tilde{H}_P^{-1} \tilde{U}]}{\sqrt{(2\pi)^2 \det \tilde{H}_P}}. \quad (4.10)$$

In the above equation, the matrix \tilde{H}_P is given by

$$\tilde{H}_P = \begin{pmatrix} H_P^{11} & 0 \\ 0 & H_P^{33} \end{pmatrix}. \quad (4.11)$$

The matrix element H_P^{11} for first choice of external forces is given by

$$H_P^{11} = \frac{\bar{D}m[\delta^3(2 + \theta + \alpha^2\theta) + 16\kappa(1 + \theta)(\delta + \kappa) + 2\delta^2(2 + \theta + \alpha^2\theta)(1 + \kappa)]}{4\gamma^3\kappa(\delta + \kappa)(2\delta + \delta^2 + 4\kappa)},$$

whereas for second choice of external forces

$$H_P^{11} = \frac{\bar{D}m[\delta^3\{2 + \theta(1 + \alpha)^2\} + 16\kappa(1 + \theta)(\delta + \kappa) + 2\delta^2(2 + \theta + \alpha^2\theta)(1 + \kappa) + 4\delta\kappa\theta(\delta + 2\kappa)]}{4\gamma^3\kappa(\delta + \kappa)(2\delta + \delta^2 + 4\kappa)},$$

with $\bar{D} = \gamma T$.

On the other hand, H_p^{33} is same for both choices of external forces

$$H_p^{33} = \frac{\bar{D}[4(1+\theta)(\delta+2\kappa) + \delta^2(2+\theta+\alpha^2\theta)]}{2m\gamma(2\delta+\delta^2+4\kappa)}.$$

Using Eqs. (4.4), (4.6), and (4.8), the total entropy production by particle A in the coupled Brownian particle system can be written as

$$\begin{aligned} \Delta \bar{S}_{tot}^A = & \frac{1}{T} \int_0^\tau dt f_A(t) v_A(t) + \frac{k}{T} \int_0^\tau dt x_B(t) v_A(t) - \frac{1}{2} \tilde{U}^T (\tilde{\Sigma}_P - \tilde{H}_P^{-1}) \tilde{U} \\ & + \frac{1}{2} \tilde{U}_0^T (\tilde{\Sigma}_P - \tilde{H}_P^{-1}) \tilde{U}_0, \end{aligned} \quad (4.12)$$

where the diagonal matrix $\tilde{\Sigma}_P = \frac{1}{T} \text{diag}(k + k_0, m)$.

4.2.2. Apparent entropy production

When a number of DOFs are interacting with each other, then the precise distribution of entropy production rely on the exact number of relevant DOFs. In experiments, there may arise a situation where some of the DOFs are hidden. In such case, the distribution of total entropy production might vary from the case where the exact information of the system is known. Therefore, based on observed DOFs, one may use the definition of total entropy production (which might be different from the actual scenario), and compute it experimentally. This type of entropy production we call *apparent entropy production*. Note that this definition of total entropy production of a partial system is different from the definition given in the previous subsection (see Sec. 4.2.1). In that definition, we know the full system, and we were computing the total entropy production for a part of the system. But in this case, we are not aware of hidden variables.

For a simple model system, suppose we want to compute the total entropy production of a single Brownian particle (say particle A) of mass m confined in a harmonic trap of stiffness constant k_0 . The whole system is immersed in the heat bath of a constant temperature T . The given system is driven using an external Gaussian white noise $f_A(t)$ in the nonequilibrium steady state. The underdamped Langevin

equations for that Brownian particle are given as

$$\dot{x}_A = v_A(t), \quad (4.13)$$

$$m\dot{v}_A = -\gamma v_A(t) - k_0 x_A(t) + f_A(t) + \eta_A(t), \quad (4.14)$$

where γ is the dissipation constant, and $\eta_A(t)$ is the noise acting on the Brownian particle from the heat bath with mean zero and correlation $\langle \eta_A(t)\eta_A(t') \rangle = 2\gamma T\delta(t-t')$. The external Gaussian force $f_A(t)$ is acting on the particle with mean zero and correlation $\langle f_A(t)f_A(t') \rangle = 2\gamma T\theta\delta(t-t')$. The thermal noise $\eta_A(t)$ and external force $f_A(t)$ are uncorrelated with each other for all time: $\langle f_A(t)\eta_A(t') \rangle = 0$ for all t, t' .

The total entropy production of particle A can be written as

$$\Delta\tilde{S}_{tot}^A = \Delta\tilde{S}_{med}^A + \Delta\tilde{S}_{sys}^A, \quad (4.15)$$

where medium and system entropy production are

$$\Delta\tilde{S}_{med}^A = \frac{1}{T} \int_0^\tau dt f_A(t)v_A(t) - \Delta E_A, \quad (4.16)$$

$$\Delta\tilde{S}_{sys}^A = -\ln \tilde{P}_{ss}[\tilde{U}(\tau)] + \ln \tilde{P}_{ss}[\tilde{U}(0)], \quad (4.17)$$

respectively. In Eq. (4.17), the column vector $\tilde{U} = (x_A, v_A)^T$. On the right hand side of Eq. (4.16), the first term is the work done by the stochastic force $f_A(t)$ on the Brownian particle A, and the second term is the change in the internal energy ΔE_A of particle A where

$$\Delta E_A = \frac{k_0}{2T} [x_A^2(\tau) - x_A^2(0)] + \frac{m}{2T} [v_A^2(\tau) - v_A^2(0)]. \quad (4.18)$$

Both of these terms are measured with respect to the temperature T of the heat bath.

In Eq. (4.17), $\tilde{P}_{ss}[\tilde{U}(\tau)]$ is the steady state probability distribution computed from Eqs. (4.13) and (4.14), and its form is

$$\tilde{P}_{ss}[\tilde{U}(\tau)] = \frac{\exp[-\frac{1}{2}\tilde{U}^T \tilde{H}_A^{-1} \tilde{U}]}{\sqrt{(2\pi)^2 \det \tilde{H}_A}}. \quad (4.19)$$

In the above equation, the matrix \tilde{H}_A is given by

$$\tilde{H}_A = \begin{pmatrix} H_A^{11} & 0 \\ 0 & H_A^{33} \end{pmatrix}, \quad (4.20)$$

where the matrix elements H_A^{11} and H_A^{33} are given as

$$H_A^{11} = \frac{\bar{D}m(1+\theta)}{\gamma^3\kappa}, \quad H_A^{33} = \frac{\bar{D}(1+\theta)}{m\gamma}.$$

Therefore, Eq. (4.15) becomes

$$\Delta\tilde{S}_{tot}^A = \frac{1}{T} \int_0^\tau dt f_A(t)v_A(t) - \frac{1}{2}\tilde{U}^T(\tilde{\Sigma}_A - \tilde{H}_A^{-1})\tilde{U} + \frac{1}{2}\tilde{U}_0^T(\tilde{\Sigma}_A - \tilde{H}_A^{-1})\tilde{U}_0, \quad (4.21)$$

where the diagonal matrix $\tilde{\Sigma}_A = \frac{1}{T}\text{diag}(k_0, m)$.

Equation (4.21) is written with the assumption that there is only one particle present in the harmonic trap [see Eqs. (4.13) and (4.14)]. Suppose, there is one more particle present in the harmonic trap in addition to the given particle A, which we are not aware of. Let us assume that these particles are interacting harmonically with spring constant k . Then, the actual dynamics of particle A is given by Eqs. (4.2)–(4.5). In such case, the total entropy production given by Eq. (4.21) is called apparent entropy production. Therefore, we compute this apparent entropy production given in Eq. (4.21) using actual dynamics [see Eqs. (4.2)–(4.5)] as an experimentalist who is not aware of a hidden particle in the same trap.

We can combine both definitions of entropy production [see Eqs. (4.12) and (4.21)] using a parameter Π defined in Eq. (2.12). Therefore, we get

$$\Delta S_{tot}^A = W - \frac{1}{2}U^T H^{-1}U + \frac{1}{2}U_0^T H^{-1}U_0, \quad (4.22)$$

where

$$W = \frac{1}{T} \int_0^\tau dt f_A(t)v_A(t) + \frac{\Pi k}{T} \int_0^\tau dt x_B(t)v_A(t). \quad (4.23)$$

In Eq. (4.22),

$$H^{-1} = \Pi(\Sigma_P - H_P^{-1}) + (1 - \Pi)(\Sigma_A - H_A^{-1})$$

in which

$$\begin{aligned}
H_P^{-1} &= \text{diag}(1/H_P^{11}, 0, 1/H_P^{33}, 0), \\
H_A^{-1} &= \text{diag}(1/H_A^{11}, 0, 1/H_A^{33}, 0), \\
\Sigma_P &= \text{diag}((k+k_0)/T, 0, m/T, 0), \\
\Sigma_A &= \text{diag}(k_0/T, 0, m/T, 0), \\
U^T &= (x_A, x_B, v_A, v_B).
\end{aligned}$$

Since Eqs. (4.2)–(4.5) show that the column vector $U = (x_A, x_B, v_A, v_B)^T$ depends linearly on the thermal Gaussian noises and external stochastic Gaussian forces, the probability distribution function of it is a Gaussian distribution. On the other hand, the entropy production given in Eq. (4.22) is not linear with the thermal Gaussian noises and external stochastic Gaussian forces. Thus, the expected distribution of it will not be Gaussian in nature. Nevertheless, we will show the recipe to obtain the distribution for ΔS_{tot}^A in next sections.

4.3. Fokker-Planck equation and its general solution

The stochastic observable ΔS_{tot}^A depends on Gaussian noises quadratically. Therefore, mean and variance of it are not sufficient to obtain the probability density function. Our goal is to find the probability density function for ΔS_{tot}^A , i.e. $P(\Delta S_{tot}^A)$, which is given as

$$P(\Delta S_{tot}^A) = \int dU \int dU_0 P(\Delta S_{tot}^A, U, \tau | U_0) P_{ss}^{full}(U_0), \quad (4.24)$$

where $P(\Delta S_{tot}^A, U, \tau | U_0)$ is the joint distribution of ΔS_{tot}^A and U at time τ starting from $\Delta S_{tot}^A = 0$ and $U = U_0$ at time $t = 0$.

Multiplying both sides by $e^{-\lambda \Delta S_{tot}^A}$ and integrating over ΔS_{tot}^A , we get

$$Z(\lambda) = \int dU \int dU_0 Z(\lambda, U, \tau | U_0) P_{ss}^{full}(U_0), \quad (4.25)$$

where $Z(\lambda, U, \tau|U_0)$ is the restricted moment generating function:

$$Z(\lambda, U, \tau|U_0) = \langle e^{-\lambda \Delta S_{tot}^A} \delta[U - U(\tau)] \rangle_{U, U_0}. \quad (4.26)$$

In the above equation, the angular brackets show the average over set of all trajectories starting from initial variable U_0 to final variable $U(\tau)$. Using Eq. (4.22), one can write the restricted moment generating function for ΔS_{tot}^A

$$Z(\lambda, U, \tau|U_0) = e^{\frac{\lambda}{2} U^T H^{-1} U - \frac{\lambda}{2} U_0^T H^{-1} U_0} Z_W(\lambda, U, \tau|U_0), \quad (4.27)$$

where

$$Z_W(\lambda, U, \tau|U_0) = \langle e^{-\lambda W} \delta[U - U(\tau)] \rangle_{U, U_0}. \quad (4.28)$$

In Eq. (4.22), the second and third terms on right hand side are boundary terms, and do not contribute in the averaging process as shown in Eq. (4.27).

In order to compute the moment generating function $Z(\lambda) = \langle e^{-\lambda \Delta S_{tot}^A} \rangle$, we first find $Z_W(\lambda, U, \tau|U_0)$ whose evolution is given by the following Fokker-Planck equation [107, 70]

$$\frac{\partial Z_W(\lambda, U, \tau|U_0)}{\partial \tau} = \mathcal{L}_\lambda Z_W(\lambda, U, \tau|U_0) \quad (4.29)$$

with the initial condition $Z_W(\lambda, U, 0|U_0) = \delta(U - U_0)$. In the above equation, \mathcal{L}_λ is the Fokker-Planck operator given as

$$\begin{aligned} \mathcal{L}_\lambda = & \frac{1}{m} \sum_{i=A,B} \left[\frac{\partial \mathcal{H}}{\partial x_i} \frac{\partial}{\partial v_i} - \frac{\partial \mathcal{H}}{\partial v_i} \frac{\partial}{\partial x_i} \right] + \frac{\gamma T(1+\theta)}{m^2} \frac{\partial^2}{\partial v_A^2} + \frac{\gamma v_A}{m} (1+2\lambda\theta) \frac{\partial}{\partial v_A} \\ & + \frac{\gamma}{m} (v_B + 2C\lambda\alpha\theta v_A) \frac{\partial}{\partial v_B} + \gamma \left[\frac{2}{m} - \frac{\lambda}{\gamma T} \left(\Pi k x_B v_A - \frac{\gamma T \theta}{m} \right) \right] + \frac{\lambda^2 v_A^2 \gamma \theta}{T} \\ & + \frac{\gamma T(1+\theta\alpha^2)}{m^2} \frac{\partial^2}{\partial v_B^2} + \frac{2C\gamma T \theta \alpha}{m^2} \frac{\partial^2}{\partial v_A \partial v_B}. \end{aligned} \quad (4.30)$$

In the above equation, \mathcal{H} is the Hamiltonian of the coupled system [see Eq. (4.1)], and C is the correlation parameter defined in Eq. (2.24)

As described in previous chapters, the general solution of differential equation (4.29) can be written as

$$Z_W(\lambda, U, \tau|U_0) = \sum_n e^{\tau \mathcal{E}_n(\lambda)} \Psi_n(U, \lambda) \chi_n(U_0, \lambda), \quad (4.31)$$

where $\mathcal{E}_n(\lambda)$ is the eigenvalue of the Fokker-Planck operator \mathcal{L}_λ and corresponding left and right eigenfunctions are $\chi_n(U_0, \lambda)$ and $\Psi_n(U, \lambda)$. These left and right eigenfunctions satisfy the orthonormality condition $\int dU \Psi_n(U, \lambda) \chi_m(U, \lambda) = \delta_{n,m}$. Thus, the restricted moment generating function for long time ($\tau \rightarrow \infty$) is given by

$$Z_W(\lambda, U, \tau|U_0) = e^{(\tau/\tau_\gamma)\mu(\lambda)} \Psi(U, \lambda) \chi(U_0, \lambda) + \dots, \quad (4.32)$$

where $\mu(\lambda)\tau_\gamma^{-1} := \max\{\mathcal{E}_n(\lambda)\}$ is the largest eigenvalue of the Fokker-Planck operator \mathcal{L}_λ and corresponding left and right eigenfunctions are $\chi(U_0, \lambda)$ and $\Psi(U, \lambda)$. In the above equation, $\tau_\gamma = m/\gamma$ is the viscous relaxation time. Here $Z(0, U, \tau|U_0) = Z_W(0, U, \tau|U_0) = P(U, \tau|U_0)$ [see Eq. (4.27)] is the joint distribution of U at time τ starting from initial variable U_0 at time $t = 0$. Therefore, in the large time limit, the steady state distribution can be computed from $Z_W(0, U, \tau \rightarrow \infty|U_0) = P_{ss}^{full}(U) = \Psi(U, 0)$. It directly implies $\mu(0) = 0$ and $\chi(U_0, 0) = 1$.

The Fokker-Planck equation (4.29) is difficult to solve to obtain the largest eigenvalue $\mu(\lambda)\tau_\gamma^{-1}$ and corresponding eigenfunctions. Nevertheless, there is a technique developed in Ref. [76] and used in previous chapters which we use to compute these functions. Detailed calculations for evaluating these functions are given in Sec. 4.4. Using Eq. (4.27) and the restricted moment generating function for W given in Eq. (4.32), we write the restricted moment generating function $Z(\lambda, U, \tau|U_0)$ for both definitions of entropy production ΔS_{tot}^A and for both choices of external forces. Further, we integrate $Z(\lambda, U, \tau|U_0)$ over the initial steady state ensemble $P_{ss}^{full}(U_0)$ and final variable U [see Eq. (4.25)], and get the moment generating function for ΔS_{tot}^A :

$$Z(\lambda) = g(\lambda) e^{(\tau/\tau_\gamma)\mu(\lambda)} + \dots, \quad (4.33)$$

where $g(\lambda)$ is the prefactor given by

$$\begin{aligned} g(\lambda) &= \int dU \int dU_0 P_{ss}^{full}(U_0) \Psi(U, \lambda) \chi(U_0, \lambda) e^{\frac{\lambda}{2} U^T H^{-1} U - \frac{\lambda}{2} U_0^T H^{-1} U_0} \\ &= \int dU \int dU_0 \Psi(U_0, 0) \Psi(U, \lambda) \chi(U_0, \lambda) e^{\frac{\lambda}{2} U^T H^{-1} U - \frac{\lambda}{2} U_0^T H^{-1} U_0}. \end{aligned} \quad (4.34)$$

In Eq. (4.33), $\mu(\lambda)$ is the cumulant generating function.

4.4. Calculation of moment generating function

In this section, we give the complete calculation of the moment generating function for ΔS_{tot}^A . The Langevin equations given in Eqs. (4.2)–(4.5) for the system shown in Fig. 4.1 can be expressed in the matrix form as

$$\dot{X} = V(t), \quad (4.35)$$

$$m\dot{V} = -\gamma V(t) - \Phi X(t) + \zeta(t) + F(t), \quad (4.36)$$

where $X(t) = (x_A(t), x_B(t))^T$, $V(t) = (v_A(t), v_B(t))^T$, $\zeta(t) = (\eta_A(t), \eta_B(t))^T$, $F(t) = (f_A(t), f_B(t))^T$, and the matrix Φ is given by

$$\Phi = \begin{pmatrix} k_0 + k & -k \\ -k & k_0 + k \end{pmatrix}.$$

Using Eq. (2.16), one can write Eqs. (4.35) and (4.36) in frequency domain as

$$\tilde{X}(\omega_n) = G(\omega_n)[\tilde{F}(\omega_n) + \tilde{\zeta}(\omega_n)] - \frac{G(\omega_n)}{\tau}[(im\omega_n + \gamma)\Delta X + m\Delta V], \quad (4.37)$$

$$\tilde{V}(\omega_n) = i\omega_n G(\omega_n)[\tilde{F}(\omega_n) + \tilde{\zeta}(\omega_n)] + \frac{G(\omega_n)}{\tau}[\Phi\Delta X - im\omega_n\Delta V], \quad (4.38)$$

where $\Delta X = X(\tau) - X(0)$, $\Delta V = V(\tau) - V(0)$, and $G(\omega_n) = [-m\omega_n^2 + i\gamma\omega_n + \Phi]^{-1}$ is the Green's function symmetric matrix.

We write $U^T(\tau) = [X^T(\tau), V^T(\tau)]$ as

$$U^T(\tau) = \lim_{\epsilon \rightarrow 0} \sum_{n=-\infty}^{\infty} e^{-i\omega_n\epsilon} [\tilde{X}^T(\omega_n), \tilde{V}^T(\omega_n)]. \quad (4.39)$$

In the large time limit ($\tau \rightarrow \infty$), we can convert the above given summation into integration over ω . Using Eqs. (4.37) and (4.38) in the above equation, we see the following terms

$$\begin{aligned} \lim_{\epsilon \rightarrow 0} \frac{1}{2\pi} \int_{-\infty}^{\infty} d\omega e^{-i\omega\epsilon} [(im\omega + \gamma)\Delta X^T + m\Delta V^T] G^T &\rightarrow 0, \\ \lim_{\epsilon \rightarrow 0} \frac{1}{2\pi} \int_{-\infty}^{\infty} d\omega e^{-i\omega\epsilon} [\Delta X^T \Phi^T - im\omega\Delta V^T] G^T &\rightarrow 0. \end{aligned}$$

This is because the contour of integration (clockwise) is a semicircle in the lower half

of the complex ω -plane with center at the origin, and all of the poles lie in the upper half of complex ω -plane. Therefore, $U^T(\tau)$ becomes

$$U^T(\tau) = \lim_{\epsilon \rightarrow 0} \sum_{n=-\infty}^{\infty} e^{-i\epsilon\omega_n} [(1-C)\{(\tilde{\eta}_A + \tilde{f}_A)q_1^T + (\tilde{\eta}_B + \tilde{f}_B)q_2^T\} + C(\tilde{\eta}_A l_1^T + \tilde{\eta}_B l_2^T + \tilde{f}_A l_3^T)], \quad \text{where} \quad (4.40)$$

$$q_1^T = l_1^T = (G_{11}, G_{12}, i\omega_n G_{11}, i\omega_n G_{12}),$$

$$q_2^T = l_2^T = (G_{12}, G_{11}, i\omega_n G_{12}, i\omega_n G_{11}),$$

$$l_3^T = [G_{11} + \alpha G_{12}, G_{12} + \alpha G_{11}, i\omega_n(G_{11} + \alpha G_{12}), i\omega_n(G_{12} + \alpha G_{11})].$$

For convenience, we write $\tilde{\eta}_i = \tilde{\eta}_i(\omega_n)$, $\tilde{\eta}_i^* = \tilde{\eta}_i(-\omega_n)$, $\tilde{f}_i = \tilde{f}_i(\omega_n)$, $\tilde{f}_i^* = \tilde{f}_i(-\omega_n)$, $G_{ij} = [G(\omega_n)]_{ij}$, and $G_{ij}^* = [G(-\omega_n)]_{ij}$.

From Eq. (4.40), the mean and correlation of $U(\tau)$ are obtained as

$$\langle U(\tau) \rangle = 0, \quad (4.41)$$

$$\langle U(\tau)U^T(\tau) \rangle = \frac{T\gamma}{\pi} \int_{-\infty}^{\infty} d\omega [(1-C)\{(1+\theta)q_1 q_1^\dagger + (1+\theta\alpha^2)q_2 q_2^\dagger\} + C\{l_1 l_1^\dagger + l_2 l_2^\dagger + \theta l_3 l_3^\dagger\}]. \quad (4.42)$$

Since U is linear with Gaussian noises, the steady state distribution of it can be written using mean and correlation given by Eqs. (4.41) and (4.42), respectively, which gives

$$P_{ss}^{full}(U) = \frac{e^{-\frac{1}{2}U^T M^{-1}U}}{\sqrt{(2\pi)^4 \det M}}, \quad \text{where } M_{ij} = \langle U(\tau)U^T(\tau) \rangle_{ij}. \quad (4.43)$$

Using Eqs. (4.37) and (4.38), we write $\tilde{x}_B(\omega_n)$ and $\tilde{v}_A(\omega_n)$ as

$$\tilde{x}_B(\omega_n) = G_{12}(\tilde{\eta}_A + \tilde{f}_A) + G_{11}(\tilde{\eta}_B + \tilde{f}_B) - \frac{1}{\tau} q_3^T \Delta U, \quad (4.44)$$

$$\tilde{v}_A(\omega_n) = i\omega [G_{11}(\tilde{\eta}_A + \tilde{f}_A) + G_{12}(\tilde{\eta}_B + \tilde{f}_B)] + \frac{1}{\tau} q_4^T \Delta U, \quad (4.45)$$

where

$$q_3^T = [(\gamma + i\omega_n m)G_{12}, (\gamma + i\omega_n m)G_{11}, mG_{12}, mG_{11}],$$

$$q_4^T = ([G\Phi]_{11}, [G\Phi]_{12}, -i\omega_n mG_{11}, -i\omega_n mG_{12}).$$

From Eq. (4.23), W can be written as a sum of W_1 and W_2 :

$$W = W_1 + W_2, \quad \text{where} \quad (4.46)$$

$$W_1 = \frac{1}{T} \int_0^\tau dt f_A(t) v_A(t), \quad (4.47)$$

$$W_2 = \frac{\Pi k}{T} \int_0^\tau dt x_B(t) v_A(t). \quad (4.48)$$

Using Eq. (2.17), we write W_1 as

$$W_1 = \frac{\tau}{2T} \sum_{n=-\infty}^{\infty} [\tilde{f}_A(\omega_n) v_A(-\omega_n) + \tilde{f}_A(-\omega_n) v_A(\omega_n)]. \quad (4.49)$$

Substituting $\tilde{v}_A(\omega_n)$ from Eq. (4.45) in the above equation, we get

$$W_1 = \frac{\tau}{2T} \sum_{n=-\infty}^{\infty} \left[i\omega_n \{ G_{11}(\tilde{\eta}_A + \tilde{f}_A) \tilde{f}_A^* + G_{12}(\tilde{\eta}_B + \tilde{f}_B) \tilde{f}_A^* - G_{11}^*(\tilde{\eta}_A^* + \tilde{f}_A^*) \tilde{f}_A \right. \\ \left. - G_{12}^*(\tilde{\eta}_B^* + \tilde{f}_B^*) \tilde{f}_A \} + \frac{\tilde{f}_A q_4^\dagger \Delta U}{\tau} + \frac{\tilde{f}_A^* \Delta U^T q_4}{\tau} \right]. \quad (4.50)$$

Similarly, we can write W_2 as

$$W_2 = \frac{\Pi k \tau}{2T} \sum_{n=-\infty}^{\infty} [\tilde{x}_B(\omega_n) v_A(-\omega_n) + \tilde{x}_B(-\omega_n) v_A(\omega_n)]. \quad (4.51)$$

Substituting $\tilde{x}_B(\omega_n)$ and $\tilde{v}_A(\omega_n)$ from Eqs. (4.44) and (4.45), respectively, in the above equation, we get

$$\begin{aligned}
W_2 = & \frac{\Pi k \tau}{2T} \sum_{n=-\infty}^{\infty} \left[i\omega_n \{ [G_{11}(\tilde{\eta}_A + \tilde{f}_A) + G_{12}(\tilde{\eta}_B + \tilde{f}_B)] [G_{12}^*(\tilde{\eta}_A^* + \tilde{f}_A^*) + G_{11}^*(\tilde{\eta}_B^* + \tilde{f}_B^*)] \right. \\
& - [G_{12}(\tilde{\eta}_A + \tilde{f}_A) + G_{11}(\tilde{\eta}_B + \tilde{f}_B)] [G_{11}^*(\tilde{\eta}_A^* + \tilde{f}_A^*) + G_{12}^*(\tilde{\eta}_B^* + \tilde{f}_B^*)] \} \\
& + \frac{q_4^\dagger \Delta U}{\tau} [G_{12}(\tilde{\eta}_A + \tilde{f}_A) + G_{11}(\tilde{\eta}_B + \tilde{f}_B)] + \frac{\Delta U^T q_4}{\tau} [G_{12}^*(\tilde{\eta}_A^* + \tilde{f}_A^*) + G_{11}^*(\tilde{\eta}_B^* + \tilde{f}_B^*)] \\
& + \frac{i\omega_n \Delta U^T q_3}{\tau} [G_{11}^*(\tilde{\eta}_A^* + \tilde{f}_A^*) + G_{12}^*(\tilde{\eta}_B^* + \tilde{f}_B^*)] - \frac{i\omega_n q_3^\dagger \Delta U}{\tau} [G_{11}(\tilde{\eta}_A + \tilde{f}_A) + G_{12}(\tilde{\eta}_B + \tilde{f}_B)] \\
& \left. - \frac{\Delta U^T (q_3 q_4^\dagger + q_4 q_3^\dagger) \Delta U}{\tau^2} \right]. \tag{4.52}
\end{aligned}$$

Restricted moment generating function for W is given as

$$Z_W(\lambda, U, \tau | U_0) = \langle e^{-\lambda W} \delta[U - U(\tau)] \rangle_{U, U_0} = \int \frac{d^4 \sigma}{(2\pi)^4} e^{i\sigma^T U} \langle e^{E(\tau)} \rangle_{U, U_0}, \tag{4.53}$$

where we have use the integral representation of Dirac delta function, and $E(\tau) = -\lambda W - i\sigma^T U(\tau)$. Using Eqs. (4.40) and (4.46), we write $E(\tau)$ as

$$E(\tau) = \sum_{n=1}^{\infty} \left[-\frac{\lambda \tau}{T} \zeta_n^T C_n \zeta_n^* + \zeta_n^T \alpha_n + \alpha_{-n}^T \zeta_n^* + \frac{\lambda \Pi k}{T \tau} |q_n|^2 \right] - \frac{\lambda \tau}{2T} \zeta_0^T C_0 \zeta_0 + \zeta_0^T \alpha_0 + \frac{\lambda \Pi k}{2T \tau} q_0^2, \tag{4.54}$$

where $C_n = C_n^I + \Pi k C_n^{II}$ and $|q_n|^2 = \Delta U^T (q_3 q_4^\dagger + q_4 q_3^\dagger) \Delta U$.

For *uncorrelated forces* ($C = 0$), the row vector $\zeta_n^T = (\tilde{\eta}_A, \tilde{\eta}_B, \tilde{f}_A, \tilde{f}_B)$, the matrix C_n^I is

$$C_n^I = \begin{pmatrix} 0 & 0 & i\omega_n G_{11} & 0 \\ 0 & 0 & i\omega_n G_{12} & 0 \\ -i\omega_n G_{11}^* & -i\omega_n G_{12}^* & i\omega_n [G_{11} - G_{11}^*] & -i\omega_n G_{12}^* \\ 0 & 0 & i\omega_n G_{12} & 0 \end{pmatrix},$$

and matrix C_n^{II} is

$$C_n^{II} = \begin{pmatrix} C_{11} & C_{12} & C_{13} & C_{14} \\ C_{12}^* & C_{22} & C_{23} & C_{24} \\ C_{13}^* & C_{23}^* & C_{33} & C_{34} \\ C_{14}^* & C_{24}^* & C_{34}^* & C_{44} \end{pmatrix}$$

whose matrix elements are

$$C_{11} = -C_{22} = C_{33} = -C_{44} = C_{13} = i\omega_n[G_{11}G_{12}^* - G_{12}G_{11}^*],$$

$$C_{12} = C_{14} = C_{34} = -C_{23} = i\omega_n[|G_{11}|^2 - |G_{12}|^2],$$

$$C_{24} = -C_{11},$$

$$C_{ij}^* = C_{ij}(-\omega_n).$$

The column vector α_n is given by

$$\alpha_n = -\frac{\lambda}{T} \begin{pmatrix} a_{11}^T \Delta U \\ a_{21}^T \Delta U \\ a_{31}^T \Delta U \\ a_{41}^T \Delta U \end{pmatrix} - ie^{-i\epsilon\omega_n} \begin{pmatrix} q_1^T \sigma \\ q_2^T \sigma \\ q_1^T \sigma \\ q_2^T \sigma \end{pmatrix}, \quad \text{in which}$$

$$a_{11}^T = -\Pi k(i\omega_n q_3^\dagger G_{11} - q_4^\dagger G_{12}),$$

$$a_{21}^T = a_{41}^T = -\Pi k(i\omega_n q_3^\dagger G_{12} - q_4^\dagger G_{11}),$$

$$a_{31}^T = -\Pi k(i\omega_n q_3^\dagger G_{11} - q_4^\dagger G_{12}) + q_4^\dagger.$$

For second choice of external forces ($C = 1$), the row vector $\zeta_n^T = (\tilde{\eta}_A, \tilde{\eta}_B, \tilde{f}_A)$, the matrix C_n^I and C_n^{II} are

$$C_n^I = \begin{pmatrix} 0 & 0 & i\omega_n G_{11} \\ 0 & 0 & i\omega_n G_{12} \\ -i\omega_n G_{11}^* & -i\omega_n G_{12}^* & i\omega_n [(G_{11} - G_{11}^*) + \alpha(G_{12} - G_{12}^*)] \end{pmatrix} \quad \text{and} \quad C_n^{II} = \begin{pmatrix} C_{11} & C_{12} & C_{13} \\ C_{12}^* & C_{22} & C_{23} \\ C_{13}^* & C_{23}^* & C_{33} \end{pmatrix}$$

where matrix elements of C_n^{Π} are

$$\begin{aligned} C_{11} &= -C_{22} = i\omega_n[G_{11}G_{12}^* - G_{11}^*G_{12}], \\ C_{12} &= i\omega_n[|G_{11}|^2 - |G_{12}|^2], \\ C_{13} &= -C_{23} = C_{11} + \alpha C_{12}, \\ C_{33} &= (1 - \alpha^2)C_{11}, \\ C_{ij}^* &= C_{ij}(-\omega_n). \end{aligned}$$

The column vector α_n in this case is given by

$$\alpha_n = -\frac{\lambda}{T} \begin{pmatrix} c_{11}^T \Delta U \\ c_{21}^T \Delta U \\ c_{31}^T \Delta U \end{pmatrix} - ie^{-i\epsilon\omega_n} \begin{pmatrix} l_1^T \sigma \\ l_2^T \sigma \\ l_3^T \sigma \end{pmatrix}, \quad \text{in which}$$

$$\begin{aligned} c_{11}^T &= -\Pi k(i\omega_n q_3^\dagger G_{11} - q_4^\dagger G_{12}), \\ c_{21}^T &= -\Pi k(i\omega_n q_3^\dagger G_{12} - q_4^\dagger G_{11}), \\ c_{31}^T &= -\Pi k[i\omega_n q_3^\dagger (G_{11} + \alpha G_{12}) - q_4^\dagger (G_{12} + \alpha G_{11})] + q_4^\dagger. \end{aligned}$$

Therefore, we get

$$\begin{aligned} \langle e^{E(\tau)} \rangle_{U, U_0} &= \left\langle \exp \left[-\frac{\lambda\tau}{2T} \zeta_0^T C_0 \zeta_0 + \zeta_0^T \alpha_0 + \frac{\lambda\Pi k}{2T\tau} q_0^2 \right] \right\rangle \\ &\times \prod_{n=1}^{\infty} \left\langle \exp \left[-\frac{\lambda\tau}{T} \zeta_n^T C_n \zeta_n^* + \zeta_n^T \alpha_n + \alpha_{-n}^T \zeta_n^* + \frac{\lambda\Pi k}{T\tau} |q_n|^2 \right] \right\rangle. \end{aligned} \quad (4.55)$$

In the above equation, the angular brackets represent the average over the joint Gaussian distribution of thermal and external noises ζ_n . For $n \geq 1$, the average is done independently on each term using the distribution given in Eq. (2.45) and the average for $n = 0$ term is done with respect to the distribution given in Eq. (2.46) After computation of averages, we get

$$\langle e^{E(\tau)} \rangle_{U, U_0} = e^{(\tau/\tau_\gamma)\mu(\lambda)} \exp \left[\frac{1}{2} \sum_{n=-\infty}^{\infty} \left(\alpha_{-n}^T \Omega_n^{-1} \alpha_n + \frac{\lambda\Pi k}{T\tau} |q_n|^2 \right) \right], \quad (4.56)$$

where $\Omega_n = [\Lambda^{-1} + \lambda\tau/T C_n]$.

In the large time limit ($\tau \rightarrow \infty$), we convert the summation into integration. Therefore, we get

$$\langle e^{E(\tau)} \rangle_{U, U_0} \approx e^{(\tau/\tau_\gamma)\mu(\lambda)} e^{-\frac{1}{2}\sigma^T H_1 \sigma + i\Delta U^T H_2 \sigma + \frac{1}{2}\Delta U^T H_3 \Delta U}, \quad \text{where} \quad (4.57)$$

$$\begin{aligned} \mu(\lambda) &= -\frac{\tau_\gamma}{4\pi} \int_{-\infty}^{\infty} d\omega \ln[\det(\Lambda\Omega)], \\ H_1 &= \frac{\tau}{2\pi} \int_{-\infty}^{\infty} d\omega \rho^T \Omega^{-1} \phi, \\ H_2 &= -\frac{\tau}{2\pi} \int_{-\infty}^{\infty} d\omega e^{-i\omega\epsilon} a_1^T \Omega^{-1} \phi, \\ H_3 &= \frac{\tau}{2\pi} \int_{-\infty}^{\infty} d\omega \left[a_1^T \Omega^{-1} a_2 + \frac{\lambda\Pi k}{T\tau} (q_3 q_4^\dagger + q_3^\dagger q_4) \right]. \end{aligned} \quad (4.58)$$

The vectors ρ^T , a_1^T , ϕ , and a_2 are given in TABLE 4.1 in which

$$\begin{aligned} b_{11} &= \Pi k [i\omega G_{11}^* q_3 + G_{12}^* q_4], \\ b_{12} &= \Pi k [i\omega G_{12}^* q_3 + G_{11}^* q_4] = b_{14}, \\ b_{13} &= \Pi k [i\omega G_{11}^* q_3 + G_{12}^* q_4] + q_4, \\ d_{11} &= \Pi k [i\omega G_{11}^* q_3 + G_{12}^* q_4], \\ d_{12} &= \Pi k [i\omega G_{12}^* q_3 + G_{11}^* q_4], \\ d_{13} &= \Pi k [i\omega (G_{11}^* + \alpha G_{12}^*) q_3 + (G_{12}^* + \alpha G_{11}^*) q_4] + q_4. \end{aligned}$$

The restricted moment generating function for W can be written as

$$Z_W(\lambda, U, \tau | U_0) \approx e^{(\tau/\tau_\gamma)\mu(\lambda)} e^{\frac{1}{2}\Delta U^T H_3 \Delta U} \int \frac{d^4\sigma}{(2\pi)^4} e^{i\sigma^T U} e^{-\frac{1}{2}\sigma^T H_1 \sigma} e^{i\sigma^T H_2^T \Delta U}. \quad (4.59)$$

Calculating integration over σ , we get

$$Z_W(\lambda, U, \tau | U_0) \approx \frac{e^{(\tau/\tau_\gamma)\mu(\lambda)}}{\sqrt{(2\pi)^4 \det H_1(\lambda)}} e^{\frac{1}{2}\Delta U^T H_3 \Delta U} e^{-\frac{1}{2}(U^T + \Delta U^T H_2) H_1^{-1} (U + H_2^T \Delta U)}. \quad (4.60)$$

We can factorize the above equation in terms of the initial and final variables [see Eq. (4.32)] which implies $(H_3 - H_2 H_1^{-1} H_2^T - H_1^{-1} H_2^T) + (H_3 - H_2 H_1^{-1} H_2^T - H_2 H_1^{-1})^T =$

Vectors	Uncorrelated forces	Correlated forces
ρ^T	$(q_1^*, q_2^*, q_1^*, q_2^*)$	(l_1^*, l_2^*, l_3^*)
a_1^T	$-\lambda/T(b_{11}, b_{12}, b_{13}, b_{14})$	$-\lambda/T(d_{11}, d_{12}, d_{13})$
ϕ	$\begin{pmatrix} q_1^T \\ q_2^T \\ q_1^T \\ q_2^T \end{pmatrix}$	$\begin{pmatrix} l_1^T \\ l_2^T \\ l_3^T \end{pmatrix}$
a_2	$-\frac{\lambda}{T} \begin{pmatrix} a_{11}^T \\ a_{21}^T \\ a_{31}^T \\ a_{41}^T \end{pmatrix}$	$-\frac{\lambda}{T} \begin{pmatrix} c_{11}^T \\ c_{21}^T \\ c_{31}^T \end{pmatrix}$

TABLE 4.1: The vectors ρ^T , a_1^T , ϕ , and a_2 are shown.

0. Therefore, we get

$$Z_W(\lambda, U, \tau | U_0) \approx \frac{e^{(\tau/\tau_\gamma)\mu(\lambda)} e^{-\frac{1}{2}U_0^T L_2(\lambda) U_0} e^{-\frac{1}{2}U^T L_1(\lambda) U}}{\sqrt{(2\pi)^4 \det H_1(\lambda)}}, \quad \text{where} \quad (4.61)$$

$$L_1(\lambda) = H_1^{-1} + H_1^{-1} H_2^T \quad \text{and} \quad L_2(\lambda) = -H_1^{-1} H_2^T.$$

Therefore, the restricted moment generating function for ΔS_{tot}^A is given as

$$Z(\lambda, U, \tau | U_0) \approx \frac{e^{(\tau/\tau_\gamma)\mu(\lambda)} e^{-\frac{1}{2}U_0^T \tilde{L}_2(\lambda) U_0} e^{-\frac{1}{2}U^T \tilde{L}_1(\lambda) U}}{\sqrt{(2\pi)^4 \det H_1(\lambda)}}, \quad \text{with} \quad (4.62)$$

$$\tilde{L}_1(\lambda) = L_1(\lambda) - \lambda H^{-1}, \quad \text{and} \quad \tilde{L}_2(\lambda) = L_2(\lambda) + \lambda H^{-1}.$$

The moment generating function is obtained by integrating over the initial steady state distribution $P_{ss}^{full}(U_0)$ and final variable U

$$Z(\lambda) = \int dU \int dU_0 P_{ss}^{full}(U_0) Z(\lambda, U, \tau | U_0) \approx g(\lambda) e^{(\tau/\tau_\gamma)\mu(\lambda)}. \quad (4.63)$$

In the above equation, the cumulant generating function $\mu(\lambda)$ is given by

$$\mu(\lambda) = -\frac{1}{4\pi} \int_{-\infty}^{\infty} du \ln \left[1 + \frac{h(u, \lambda)}{q(u)} \right], \quad (4.64)$$

where function $q(u)$ is

$$q(u) = [(\kappa - u^2)^2 + u^2][(\delta + \kappa - u^2)^2 + u^2]. \quad (4.65)$$

The form of $h(u, \lambda)$ for first choice of forces, i.e. for uncorrelated forces, is given as

$$\begin{aligned} h(u, \lambda) = & 4\theta\lambda(1 - \lambda)u^2[u^4 + (1 - 2\kappa - \delta)u^2 + \kappa^2 + \kappa\delta + (2 - \Pi)\delta^2/4] \\ & - \lambda\delta^2u^2[\lambda\alpha^2\theta^2(\Pi - 1)^2 + \lambda\Pi^2 + \theta\Pi\{\lambda(1 + \alpha^2)\Pi - \lambda - \alpha^2\}], \end{aligned} \quad (4.66)$$

whereas for second choice of forces, i.e. for $f_B(t) = \alpha f_A(t)$, is

$$\begin{aligned} h(u, \lambda) = & 4\theta\lambda(1 - \lambda)u^2[u^4 + (1 - 2\kappa - \delta)u^2 + \kappa^2 + \kappa\delta + (2 - \Pi)\delta^2/4] \\ & - \lambda u^2[\theta\delta\alpha(\lambda\Pi - 1)\{4(\kappa - u^2) + \delta(2 + \alpha\Pi)\} + \lambda\Pi\delta^2(\Pi - \theta(1 - \Pi))]. \end{aligned} \quad (4.67)$$

The prefactor $g(\lambda)$ in Eq. (4.63) is given as

$$g(\lambda) = \left[\det[H_1(\lambda)H_1(0)\tilde{L}_1(\lambda)] \det[H_1^{-1}(0) + \tilde{L}_2(\lambda)] \right]^{-1/2}. \quad (4.68)$$

The computation of $g(\lambda)$ is quite involved and not very illuminating as it requires the computation of matrices $H_1(\lambda)$, $\tilde{L}_1(\lambda)$, and $\tilde{L}_2(\lambda)$. In Sec. 4.6, we show how to solve $\mu(\lambda)$ and the assumption to approximate the prefactor $g(\lambda)$.

4.5. Single Brownian particle in a harmonic trap

Consider a single Brownian particle in a harmonic trap of stiffness k_0 , driven by an external stochastic Gaussian white noise $f_A(t)$. The given system is in contact with the heat bath at a constant temperature T . The Langevin equations for the stochastically driven Brownian particle in a harmonic trap are given by Eqs. (4.13) and (4.14). It is interesting to note that both definitions of entropy production and also for both choices of forces [see Eq. (4.22)] coincide at $\delta = 0$. In this case, the

cumulant generating function $\mu_0(\lambda)$ in the integral form is given as

$$\mu_0(\lambda) = -\frac{1}{4\pi} \int_{-\infty}^{\infty} du \ln \left[1 + \frac{h_0(u, \lambda)}{q_0(u)} \right], \quad (4.69)$$

where $h_0(u, \lambda) = 4\theta\lambda(1-\lambda)u^2$ and $q_0(u) = (u^2 - \kappa)^2 + u^2$. We can solve the integral given in Eq. (4.69) easily which gives

$$\mu_0(\lambda) = \frac{1}{2}[1 - v(\lambda)], \quad \text{where} \quad (4.70)$$

$$v(\lambda) = \sqrt{1 + 4\theta\lambda(1-\lambda)} = \sqrt{4\theta(\lambda_+ - \lambda)(\lambda - \lambda_-)}. \quad (4.71)$$

Here, λ_{\pm} are given by

$$\lambda_{\pm} = 1/2(1 \pm \sqrt{1 + \theta^{-1}}). \quad (4.72)$$

One can also obtain the prefactor $g_0(\lambda)$ as

$$g_0(\lambda) = \frac{4v(\lambda)}{[1 + v(\lambda)]^2}. \quad (4.73)$$

In the above equations, the subscript 0 corresponds to $\delta = 0$. From Eqs. (4.70) and (4.73), it is clear that both $\mu_0(\lambda)$ and $g_0(\lambda)$ are analytic functions for $\lambda \in (\lambda_-, \lambda_+)$ and satisfy the Gallavotti-Cohen symmetry [82].

4.6. Probability distribution function

The probability density function for ΔS_{tot}^A is computed by inverting the moment generating function $Z(\lambda)$ using the inverse transform

$$P(\Delta S_{tot}^A = s\tau/\tau_\gamma) = \frac{1}{2\pi i} \int_{-i\infty}^{+i\infty} d\lambda Z(\lambda) e^{\lambda \Delta S_{tot}^A}, \quad (4.74)$$

where the contour of integration is along the direction of imaginary axis passing through the origin of the complex λ -plane. Using large time solution ($\tau \gg \tau_\gamma$) of

moment generating function $Z(\lambda)$ given in Eq. (4.63), we obtain

$$P(\Delta S_{tot}^A = s\tau/\tau_\gamma) \approx \frac{1}{2\pi i} \int_{-i\infty}^{+i\infty} d\lambda g(\lambda) e^{(\tau/\tau_\gamma)I_s(\lambda)}, \quad (4.75)$$

where $s = \Delta S_{tot}^A \tau_\gamma / \tau$ is the scaled variable, and the function $I_s(\lambda) = \mu(\lambda) + \lambda s$.

If both $\mu(\lambda)$ and $g(\lambda)$ are analytic function of λ , then in the limit of large time ($\tau \gg \tau_\gamma$), one can use saddle-point method [136] to approximate the integral (4.75).

Therefore, we get

$$P(\Delta S_{tot}^A = s\tau/\tau_\gamma) \approx \frac{g(\lambda^*) e^{(\tau/\tau_\gamma)I_s(\lambda^*)}}{\sqrt{2\pi(\tau/\tau_\gamma) |I_s''(\lambda^*)|}}. \quad (4.76)$$

In the above equation

$$I_s''(\lambda^*) = \left. \frac{\partial^2 I_s(\lambda)}{\partial \lambda^2} \right|_{\lambda=\lambda^*(s)}, \quad (4.77)$$

and $\lambda^*(s)$ is the saddle point obtained from solving the following equation

$$\left. \frac{\partial I_s(\lambda)}{\partial \lambda} \right|_{\lambda=\lambda^*(s)} = 0. \quad (4.78)$$

At the saddle point, the function $I_s(\lambda^*)$ reads as

$$I_s(\lambda^*(s)) = \mu(\lambda^*(s)) + \lambda^*(s)s. \quad (4.79)$$

The probability density function $p(s)$ is

$$p(s) = P(\Delta S_{tot}^A = s\tau/\tau_\gamma) \left| \frac{d\Delta S_{tot}^A}{ds} \right| \approx \frac{g(\lambda^*) e^{(\tau/\tau_\gamma)I_s(\lambda^*)}}{\sqrt{2\pi(\tau_\gamma/\tau) |I_s''(\lambda^*)|}}. \quad (4.80)$$

If both $\mu(\lambda)$ and $g(\lambda)$ follow the Gallavotti-Cohen symmetry [82], i.e. $\mu(\lambda) = \mu(1 - \lambda)$ and $g(\lambda) = g(1 - \lambda)$, and there is no singularities in $\mu(\lambda)$ and $g(\lambda)$ within $\lambda \in [0, 1]$, then we can obtain the probability distribution of negative entropy production as

$$P(\Delta S_{tot}^A = -s\tau/\tau_\gamma) \approx \frac{e^{-s\tau/\tau_\gamma}}{2\pi i} \int_{-i\infty}^{+i\infty} d\lambda g(\lambda) e^{(\tau/\tau_\gamma)I_s(\lambda)}. \quad (4.81)$$

From Eqs. (4.75) and (4.81), we get

$$\frac{P(\Delta S_{tot}^A = s\tau/\tau_\gamma)}{P(\Delta S_{tot}^A = -s\tau/\tau_\gamma)} \approx e^{s\tau/\tau_\gamma}, \quad (4.82)$$

which is steady state fluctuation theorem for ΔS_{tot}^A .

In the case of single Brownian particle confined in a harmonic trap (see Sec. 4.5), the cumulant generating function $\mu(\lambda) \rightarrow \mu_0(\lambda)$ and the prefactor $g(\lambda) \rightarrow g_0(\lambda)$. Both of these functions are analytic when $\lambda \in (\lambda_-, \lambda_+)$. Moreover, they satisfy the Gallavotti-Cohen Symmetry. Therefore, the total entropy production in this case satisfies the steady state fluctuation theorem.

But in our problem, $\mu(\lambda)$ does not satisfy the Gallavotti-Cohen symmetry for large coupling δ . Thus, one may not expect that the total entropy production by the partial system (partial and apparent entropy production) must satisfy fluctuation theorem for large value of coupling parameter δ .

Computation of the prefactor $g(\lambda)$ is quite involved. Here, our aim is to understand the fluctuation theorem for partial system in the weak coupling limit (i.e. $\delta \rightarrow 0$). Therefore, we approximate $g(\lambda)$ to the prefactor of the moment generating function of a stochastically driven single Brownian particle in a harmonic trap: $g(\lambda) \approx g_0(\lambda)$ [see Eq. (4.73)][52, 53, 54].

On the other hand, one can, in general, compute the integral (4.64) to get $\mu(\lambda)$ as shown in Chapter 2. Alternatively, we can evaluate the integral given in Eq. (4.64) numerically using MATHEMATICA. To do so, we first analyze the domain within which the function $\mu(\lambda)$ is a real quantity. Notice that this domain is the same where saddle point $\lambda^*(s)$ stays for finite scaled variable s .

First consider the integral of cumulant generating function for a single Brownian particle in a harmonic trap, given in Eq. (4.69) (similar method we have used in Chapters 2 and 3). The arguments of logarithm in the integrand of $\mu_0(\lambda)$ are $q_0(u)$ and $[h_0(u, \lambda) + q_0(u)]$. While the function $q_0(u)$ is always positive for all real values of u , the function $[h_0(u, \lambda) + q_0(u)]$ can have any sign. To understand the sign, we

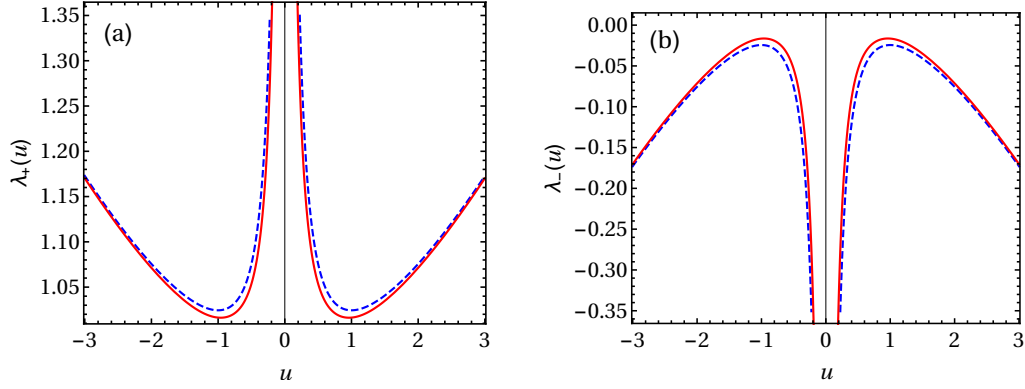


FIGURE 4.2: Variation of $\lambda_{\pm}^{\delta}(u)$ is plotted against u for $0 < \delta < 1$ (red solid) and $\delta=0$ (blue dashed lines) at fixed $\kappa = 1$.

solve the quadratic equation

$$\begin{aligned} h_0(u, \lambda) + q_0(u) &= 0 \\ a_0(u)\lambda^2 - b_0(u)\lambda - q_0(u) &= 0, \end{aligned} \quad (4.83)$$

in λ where $a_0(u) = b_0(u) = 4\theta u^2$ and $q_0(u) = (u^2 - \kappa)^2 + u^2$. The roots of above quadratic equation are

$$\lambda_{\pm}^0(u) = \frac{b_0(u) \pm \sqrt{b_0^2(u) + 4a_0(u)q_0(u)}}{2a_0(u)}. \quad (4.84)$$

In Figs. 4.2(a) and 4.2(b), we show the variation of $\lambda_{\pm}^0(u)$ (see blue dashed lines) against u at fixed $\kappa = 1$. In the complex λ -plane, we see that $\mu_0(\lambda)$ is a real function for $\lambda \in (\lambda_{max}, \lambda_{min})$ where $\lambda_{min} = \min\{\lambda_+^0(u)\}$ and $\lambda_{max} = \max\{\lambda_-^0(u)\}$. In this case, the extrema of functions $\lambda_{\pm}^0(u)$ occur at $u^* = \pm\sqrt{\kappa}$ (see Fig. 4.2). Therefore,

$$\lambda_{\pm}^0(u^* = \pm\sqrt{\kappa}) = \lambda_{\pm} = 1/2[1 \pm \sqrt{1 + \theta^{-1}}]. \quad (4.85)$$

This implies $\mu_0(\lambda)$ is a real function within (λ_-, λ_+) .

Similar recipe we will use to find the domain within which $\mu(\lambda)$ is a real quantity. For $\delta \neq 0$, the argument of logarithm of the integrand in Eq. (4.64) are $q(u)$ and $[h(u, \lambda) + q(u)]$, where $q(u)$ is clearly positive function for all real u . To see the

domain, we write the quadratic equation

$$\begin{aligned} h(u, \lambda) + q(u) &= 0 \\ a(u)\lambda^2 - b(u)\lambda - q(u) &= 0, \end{aligned} \quad (4.86)$$

in λ . The function $q(u)$ is given in Eq. (4.65), and one can find $a(u)$ and $b(u)$ from Eqs. (4.66) and (4.67) for both definitions of entropy production and for both choices of external forces. The roots of the quadratic equation (4.86) are

$$\lambda_{\pm}^{\delta}(u) = \frac{b(u) \pm \sqrt{b^2(u) + 4a(u)q(u)}}{2a(u)}. \quad (4.87)$$

Figs. 4.2(a) and 4.2(b) show the variation of $\lambda_{\pm}^{\delta}(u)$ (red solid line) against u for $0 < \delta < 1$ at fixed $\kappa = 1$. We have also compared the given curve with $\delta = 0$ case (blue dashed lines). It is clear from Fig. 4.2 that $\lambda_{\pm}^{\delta}(u)$ converge to $\lambda_{\pm}^0(u)$ in the limit of $\delta \rightarrow 0$. Therefore, one can use perturbation theory to evaluate u^* in the limit $\delta \rightarrow 0$. For first type of forces and both definitions of entropy production, we see that

$$u^* = \pm \left[\sqrt{\kappa} + \frac{\delta}{4\sqrt{\kappa}} + O(\delta^2) \right], \quad (4.88)$$

whereas for second type of forces

$$u^* = \begin{cases} \pm \left[\sqrt{\kappa} + \frac{\delta(1-\alpha)}{4\sqrt{\kappa}} + O(\delta^2) \right], & \text{Partial entropy production,} \\ \pm \left[\sqrt{\kappa} + \frac{\delta[1 + 2\alpha(\theta + \sqrt{\theta(1+\theta)})]}{4\sqrt{\kappa}} + O(\delta^2) \right], & \text{Apparent entropy production,} \end{cases} \quad (4.89)$$

For each case, we substitute u^* in Eq. (4.87). In the limit of $\delta \rightarrow 0$, we get $\lambda_{\pm}^{\delta}(u^*) \rightarrow \lambda_{\pm}$ where λ_{\pm} are given in Eq. (4.72). When $\lambda \in (\lambda_-, \lambda_+)$, $g_0(\lambda)$ is also analytic function. Therefore, one can directly use saddle-point approximation in Eq. (4.75) to get the probability distribution function for ΔS_{tot}^A .

4.7. Large deviation theorem and fluctuation theorem

The large deviation function $h(s) = I_s(\lambda^*(s))$ is defined as [136]

$$h(s) = \lim_{\tau/\tau_\gamma \rightarrow \infty} \frac{\tau_\gamma}{\tau} \ln P(\Delta S_{tot}^A = s\tau/\tau_\gamma). \quad (4.90)$$

Therefore, the large deviation form of the distribution is given by

$$P(\Delta S_{tot}^A = s\tau/\tau_\gamma) \sim e^{(\tau/\tau_\gamma)h(s)}. \quad (4.91)$$

The distribution which satisfies fluctuation theorem, we find that

$$\lim_{\tau/\tau_\gamma \rightarrow \infty} \frac{\tau_\gamma}{\tau} \ln \left[\frac{P(\Delta S_{tot}^A = +s\tau/\tau_\gamma)}{P(\Delta S_{tot}^A = -s\tau/\tau_\gamma)} \right] = s. \quad (4.92)$$

From the above equation, one can conclude that the large deviation function satisfies a symmetry properties given as

$$h(s) - h(-s) = s \quad \text{for all } s. \quad (4.93)$$

For convenience, we define an asymmetry function $f(s)$ as

$$f(s) = \frac{\tau_\gamma}{\tau} \ln \frac{P(\Delta S_{tot}^A = +s\tau/\tau_\gamma)}{P(\Delta S_{tot}^A = -s\tau/\tau_\gamma)}. \quad (4.94)$$

In the large time limit ($\tau \rightarrow \infty$), we find

$$f(s) = h(s) - h(-s). \quad (4.95)$$

In the example considered in Sec. 4.5, the slope of the associated asymmetry function $f(s)$ remains unity. Thus, for that system, total entropy production satisfies the steady state fluctuation theorem. In the following, we show the comparison of analytical results with the numerical simulation for both definitions of entropy production and for both choices of external forces.

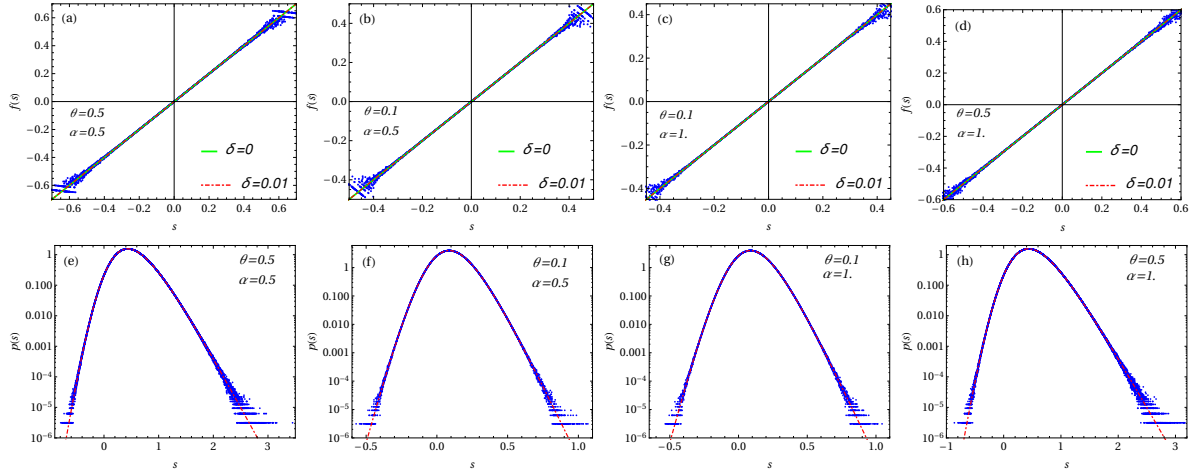


FIGURE 4.3: The asymmetry functions $f(s)$ are plotted against the scaled variable $s = \Delta S_{tot}^A \tau_\gamma / \tau$ for: (a) partial entropy production for first choice of external forces, (b) apparent entropy production for first choice of external forces, (c) partial entropy production for second choice of external forces, and (d) apparent entropy production for second choice of external forces. The probability density functions $p(s)$ are plotted against the scaled variable $s = \Delta S_{tot}^A \tau_\gamma / \tau$ for: (e) partial entropy production for first choice of external forces, (f) apparent entropy production for first choice of external forces, (g) partial entropy production for second choice of external forces, and (h) apparent entropy production for second choice of external forces. In all of the above figures, blue points represent the numerical simulation results whereas red dot-dashed lines correspond to asymmetry function $f(s)$ and probability density function $p(s)$ obtained from Eqs. (4.94) and (4.80), respectively. The green solid lines in figures (a)-(d), correspond to the case when there is no coupling between particle A and particle B ($\delta = 0$): $f(s) = s$. For all above figures, we choose the trap strength $\kappa = 2.0$, coupling parameter $\delta = 0.01$, temperature of the heat bath $T = 1$, and the observation time relative to viscous relaxation time $\tau / \tau_\gamma = 20$.

4.8. Numerical simulation

In Fig. 4.3, we compare the analytical results of asymmetry function $f(s)$ and probability density function $p(s)$ using Eqs. (4.94) and (4.80), respectively, with the numerical simulation results for: partial entropy production for first choice of external forces, apparent entropy production for first choice of external forces, partial entropy production for second choice of external forces, and apparent entropy production for second choice of external forces. All of these results are obtained for a fixed trap strength $\kappa = 2.0$, coupling parameter $\delta = 0.01$, temperature of the heat bath $T = 1$, and the observation time relative to relaxation time $\tau/\tau_\gamma = 20$. Figure 4.3 shows a very good agreement between theoretical predictions and numerical simulation. The details of the numerical simulations are discussed in Appendix A.

From Figs. 4.3 (a)–(d), it is clear that the slope of asymmetry function $f(s)$ is unity in the limit $\delta \rightarrow 0$ which indicates that both definitions of total entropy production of partial system satisfy the steady state fluctuation theorem.

4.9. Summary

We have considered two harmonically coupled Brownian particles with coupling strength $k = \delta\gamma^2/(2m)$, where δ is the dimensionless coupling parameter. The system is placed in a harmonic confinement of stiffness k_0 , and immersed in the heat bath of a constant temperature T . Both of these particles are externally driven to the nonequilibrium steady state by stochastic Gaussian forces: $f_A(t)$ and $f_B(t)$. While the strength of the force acting on particle A is θ with respect to the strength of the thermal noise of the bath, the relative strength of the force acting on particle B with respect to particle A is α^2 . Two different choices of forces are considered. In the first choice, both of these forces are independent of each other while in the second choice $f_B(t) = \alpha f_A(t)$. In the presence of external driving, system generates entropy and the total entropy production satisfies the steady state fluctuation theorem. In this chapter, we have concentrated on the total entropy production by one of the particles in the coupled system, and two different definitions of it are

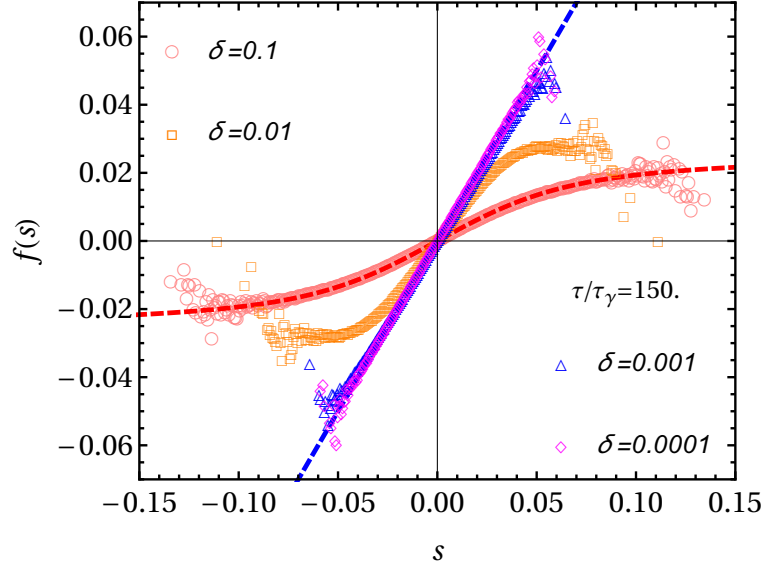


FIGURE 4.4: In the absence of harmonic confinement, the asymmetry function $f(s)$ obtained from numerical simulation is plotted against the scaled variable s for fixed observation time $\tau/\tau_\gamma = 150$ for four different values of coupling parameters: (1) $\delta = 0.1$ (red circles), (2) $\delta = 0.01$ (orange squares), (3) $\delta = 0.001$ (blue triangles), and (4) $\delta = 0.0001$ (magenta rhombuses). While the blue straight dashed line denotes $f(s) = s$, the red dashed curve represents the analytical result for the asymmetry function $f(s)$ for the coupling parameter $\delta = 0.1$ at the observation time $\tau/\tau_\gamma = 150$. The parameters $\theta = 0.01$ and $\alpha = 0.05$ are taken from the phase diagram Fig. 2.4(a). This figure indicates that as the coupling parameter δ decreases, the fluctuation theorem restores its form, i.e., $f(s) = s$, (e.g. see magenta rhombuses and blue straight dashed line) at time $\tau/\tau_\gamma = 150$ which is much smaller than the coupling time scale $t_y \sim O(\delta^{-2})$.

considered, i.e. partial and apparent entropy production. We have studied the fluctuation theorem for both definitions of entropy production and also for both choices of external forces, and showed that steady state fluctuation theorem would deviate from $f(s) = s$ with $O(\delta)$. Thus, in the weak coupling limit, the fluctuation theorem for partial and apparent entropy production is restored. Therefore, we have found a mechanism with which the effect of weak interactions is diminished when the whole system is trapped in a harmonic confinement.

To understand why trap helps to nullify the effect of weak coupling of the hidden DOFs on the observed ones, let us consider the overdamped case, where in the presence of trap, the relative spacing $y = (x_A - x_B)$, evolves according to overdamped

Langevin equation given as

$$\dot{y} = -\frac{\delta + \kappa}{\tau_\gamma} y + \frac{\eta(t) + f(t)}{\gamma}. \quad (4.96)$$

Here the thermal noise and external force in the relative frame are $\eta(t) = \eta_A(t) - \eta_B(t)$ and $f(t) = f_A(t) - f_B(t)$, respectively.

First consider the case when there is no harmonic confinement ($\kappa = 0$). In this case the force due to the coupling becomes important when $y \sim O(\tau_\gamma/\delta)$. The typical time-scale above which we can see the effect of coupling is given by the diffusive scale $t_y \sim y^2 \sim O(\tau_\gamma^2/\delta^2)$, as for $y \ll O(\tau_\gamma/\delta)$, the effect of the coupling is negligible. Therefore, when the observation time τ is much larger than t_y , we see finite contribution to the medium entropy production from the term δy as it becomes comparable to the external force f_A even in the weak coupling limit $\delta \rightarrow 0$ (see Chapters 2 and 3). In Fig. 4.4, we plot the numerically obtained asymmetry function $f(s)$ against s for four different values of the coupling parameters: (1) $\delta = 0.1$ (red circles), (2) $\delta = 0.01$ (orange squares), (3) $\delta = 0.001$ (blue triangles), and (4) $\delta = 0.0001$ (magenta rhombuses) at the observation time $\tau/\tau_\gamma = 150$. The red dashed line is the analytical result for the asymmetry function $f(s)$ at the coupling parameter $\delta = 0.1$ whereas the blue straight line correspond to $f(s) = s$ ($\delta = 0$ case). The parameters $\theta = 0.01$ and $\alpha = 0.05$ are taken from the phase diagram Fig. 2.4(a). This figure indicates that the fluctuation theorem restores its form once the observation time τ/τ_γ is taken to be small as compared to the coupling time scale $t_y \sim O(\delta^{-2})$ (e.g. see magenta rhombuses and blue straight dashed line).

On the other hand ($\kappa \neq 0$ and $\delta \ll \kappa$), typically y scales as $y \sim O(\tau_\gamma/\sqrt{\kappa})$ because it gets saturate due to harmonic confinement. Therefore, the force from the coupling term $\delta y \sim O(\delta\tau_\gamma/\sqrt{\kappa})$ which is much smaller than the external force $f_A(t)$. Thus, in this limit ($\delta \rightarrow 0$), the contribution in the medium entropy production from the term δy is vanishingly small. Therefore, the steady state fluctuation theorem holds for both definitions of entropy production.

Chapter 5

Effect of weakly coupled fast degrees of freedom on fluctuation theorem

We consider a single Brownian particle in contact with two heat baths of different temperatures (T_1 and T_2). The given particle is then connected to a third heat bath of a distinct temperature δT_3 . In the limit of weak coupling ($\delta \rightarrow 0$) between the Brownian particle and the third heat bath, we show analytically that the steady state fluctuation theorem for the total entropy production due to two heat baths with temperatures T_1 and T_2 will retain its form (1.13). Numerical simulations are also done to verify analytical results.

5.1. Introduction

In systems where a few slow degrees of freedom (DOFs) (for example, those of a colloidal particle in water) interact with a large number of fast DOFs (for example, those of the water molecules)—and there is a clear separation of time scales between the fast and slow DOFs—the effects of the fast DOFs on the slow DOFs can be replaced by an effective white noise (and dissipation) [152]. This leads to a stochastic dynamics for the slow DOFs where the fast DOFs act as a heat bath. In Chapters 2–4, we have considered a system of interacting slow DOFs. These DOFs are driven into a non-equilibrium steady state using an external source of driving. In the non-equilibrium stationary state, the probability density function of the total entropy

production from all slow DOFs satisfies the symmetry relation (1.13) (*steady state fluctuation theorem*) [121, 120, 122]. Evidently, the partial system will not obey such a symmetry relation due to interactions between the partial system and the unobserved part of the system. The central question we asked there, what is the nature of the fluctuation theorem when those interactions are considered to be infinitesimally weak? In Chapters 2 and 3, we show that the hidden slow DOFs indeed affect the fluctuation theorem for the total entropy production of a partial system even in the limit of coupling tending to zero [52, 53, 54]. In Chapter 4, we have given a technique with which the effect of the weak coupling of hidden variables can be diminished. Consequently, the fluctuation theorem for the total entropy production of a partial system was shown to be obeyed [53, 51]. In this chapter, we asked whether one can see the deviation from the steady state fluctuation theorem for the partial entropy production [see Eq. (5.10)] when one observes a slow DOF coupled to fast DOFs weakly [54]? Therefore, we consider a simple system where a single Brownian particle is coupled to a thermal gradient (T_1 and T_2). The given particle is also coupled to a third heat bath of temperature δT_3 . In the weak coupling limit (i.e., $\delta \rightarrow 0$), the deviation from the steady state fluctuation theorem for the total entropy production of the Brownian particle due to a thermal gradient (T_1 and T_2) is observed.

This chapter is organized as follow. We define the model and the definition of partial entropy production in Sec. 5.2. In Sec. 5.3, we give the Fokker-Planck equation for the conditional moment generating function for the partial medium entropy production, and then we obtain the moment generating function for the partial entropy production $Z(\lambda) \sim g(\lambda)e^{(\tau/\tau_\gamma)\mu(\lambda)}$. In Sec. 5.4, we invert the moment generating function $Z(\lambda)$ to obtain the probability density function for the partial entropy production. Section 5.5 discusses the large deviation function and fluctuation theorem for the partial entropy production. In Sec. 5.6, we summarize this chapter.

5.2. Model

Consider a single Brownian particle of mass m in contact with three heat reservoirs of temperatures T_1, T_2 and δT_3 and respective dissipation constants γ_1, γ_2 and $\delta\gamma_3$. The schematic diagram is shown in Fig. 5.1. The dynamics of the Brownian particle

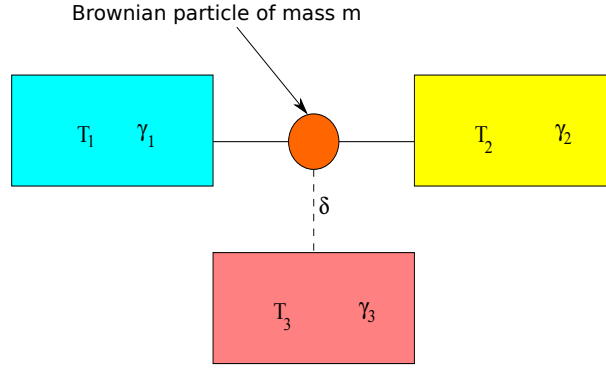


FIGURE 5.1: The schematic diagram for a single Brownian particle connected to three heat baths of temperatures T_1 , T_2 and T_3 and dissipation constants γ_1 , γ_2 and $\delta\gamma_3$.

is governed by underdamped Langevin equation

$$m\dot{v} = [-\gamma_1 v(t) + \eta_1(t)] + [-\gamma_2 v(t) + \eta_2(t)] + \delta[-\gamma_3 v(t) + \eta_3(t)], \quad (5.1)$$

where v is the velocity of the particle. The noises η_1 , η_2 and η_3 has mean $\langle \eta_i(t) \rangle = 0$ and correlations $\langle \eta_i(t) \eta_j(t') \rangle = 2D_i \delta_{ij} \delta(t - t')$, where $D_i = T_i \gamma_i$ with $\{i,j\} = \{1,2,3\}$. We set Boltzmann's constant $k_B = 1$ throughout the chapter.

The observable in this chapter is the total entropy production ΔS_{tot} in the steady state for a span of time τ . Total entropy production ΔS_{tot} is the sum of two contributions: first contribution arises from the energy transferred from heat baths to the Brownian particle, and the second one comes from the change in the configurations of that particle between time 0 and τ in the steady state [121, 120, 122]

Multiplying Eq. (5.1) by $v(t)$ on both sides, and integrating over time t from 0 to τ yields

$$\frac{m}{2}(v_\tau^2 - v_0^2) = Q_1 + Q_2 + Q_3 \quad (5.2)$$

where v_u is a velocity of the Brownian particle at time u , $Q_i = \int_0^\tau dt [(1 - \delta_{i3}) + \delta_{i3}\delta][\eta_i(t) - \gamma_i v(t)]v(t)$, is the heat energy given by i th bath to the particle, and the term on left hand side is the change in the kinetic energy of the Brownian particle.

It is clear from Eq. (5.1) that the velocity of the Brownian particle depends on

thermal Gaussian noises linearly. Therefore, it has a Gaussian distribution characterized by its mean and variance:

$$\langle v_\tau \rangle = v_0 e^{-\tau/t_\gamma}, \quad (5.3)$$

$$\langle [v_\tau - \langle v_\tau \rangle]^2 \rangle = \frac{D_1 + D_2 + \delta^2 D_3}{m(\gamma_1 + \gamma_2 + \delta\gamma_3)} (1 - e^{-2\tau/t_\gamma}), \quad (5.4)$$

where v_0 is the initial velocity, $t_\gamma = m/(\gamma_1 + \gamma_2 + \delta\gamma_3)$ is the time-scale of relaxation, and the angular brackets represent the average over thermal Gaussian noises. Thus, in the large time limit ($\tau \rightarrow \infty$), mean $\langle v_\tau \rangle_{ss} = 0$ and variance is

$$\sigma_v^2 = \langle [v_\tau - \langle v_\tau \rangle]^2 \rangle_{ss} = \frac{D_1 + D_2 + \delta^2 D_3}{m(\gamma_1 + \gamma_2 + \delta\gamma_3)}. \quad (5.5)$$

Thus, the steady state distribution for the velocity of the Brownian particle is

$$P_{ss}(v_\tau) = \frac{1}{\sqrt{2\pi\sigma_v^2}} \exp\left[-\frac{v_\tau^2}{2\sigma_v^2}\right]. \quad (5.6)$$

The system entropy production ΔS_{sys} reads

$$\Delta S_{sys} = -\ln P_{ss}(v_\tau) + \ln P_{ss}(v_0) = \frac{1}{2\sigma_v^2} [v_\tau^2 - v_0^2]. \quad (5.7)$$

Here, we are considering the total entropy production due to baths of temperatures T_1 and T_2 (i.e. *partial entropy production*). Therefore, change in the entropy in baths (see Chapters 2–4) of temperature T_1 and T_2 during the time τ is given by [58, 15, 147]

$$\Delta S_{med}^{1,2} = -\left(\frac{Q_1}{T_1} + \frac{Q_2}{T_2}\right). \quad (5.8)$$

We define

$$W = aQ_1 + bQ_2, \quad (5.9)$$

where $a = -1/T_1$, $b = -1/T_2$, and $W = \Delta S_{med}^{1,2}$. Therefore, the partial entropy production is

$$\Delta S_{tot}^{1,2} = \Delta S_{med}^{1,2} + \Delta S_{sys}. \quad (5.10)$$

Since Q_i depends on thermal noises quadratically, W will not have Gaussian distribution. In the following section, we solve the Fokker-Planck equation corresponding

to the restricted moment generating function for W .

5.3. Fokker-Planck equation

The Fokker-Planck equation for the joint probability density function for v and W starting from $v = v_0$ and $W = 0$ is [70, 107]

$$\begin{aligned} \frac{\partial P(W, v, \tau | v_0)}{\partial \tau} = & \left[\frac{\gamma_1 + \gamma_2 + \delta\gamma_3}{m} \frac{\partial}{\partial v} v + \frac{D_1 + D_2 + \delta^2 D_3}{m^2} \frac{\partial^2}{\partial v^2} + \left\{ (a\gamma_1 + b\gamma_2)v^2 \right. \right. \\ & \left. \left. - \frac{(aD_1 + bD_2)}{m} \right\} \frac{\partial}{\partial W} + (a^2 D_1 + b^2 D_2)v^2 \frac{\partial^2}{\partial W^2} + \frac{2(aD_1 + bD_2)}{m} \frac{\partial^2}{\partial W \partial v} \right] P(W, v, \tau | v_0). \end{aligned} \quad (5.11)$$

We use the Fourier transform $Z(\lambda, v, \tau | v_0) = \int_{-\infty}^{+\infty} dW e^{-\lambda W} P(W, v, \tau | v_0)$ in the above differential equation

$$\begin{aligned} \frac{\partial Z_W(\lambda, v, \tau | v_0)}{\partial \tau} = & \left[\frac{D_1 + D_2 + \delta^2 D_3}{m^2} \frac{\partial^2}{\partial v^2} + \left\{ \frac{\gamma_1 + \gamma_2 + \delta\gamma_3 + 2\lambda(aD_1 + bD_2)}{m} \right\} v \frac{\partial}{\partial v} \right. \\ & + \frac{\gamma_1 + \gamma_2 + \delta\gamma_3 + 2\lambda(aD_1 + bD_2)}{m} + \lambda[(a\gamma_1 + b\gamma_2)v^2 - (aD_1 + bD_2)/m] \\ & \left. + (a^2 D_1 + b^2 D_2)\lambda^2 v^2 \right] Z(\lambda, v, \tau | v_0), \end{aligned} \quad (5.12)$$

where $Z_W(\lambda, v, \tau | v_0)$ is the restricted moment generating function for W . The above differential equation is subjected to the initial condition $Z(\lambda, v, \tau = 0 | v_0) = \delta(v - v_0)$.

We choose $Z_W(\lambda, v, \tau | v_0) = \phi_\lambda(v | v_0) \Psi_\lambda(v, \tau | v_0)$, and substitute it in Eq. (5.12), we get

$$\begin{aligned} \frac{\partial \Psi}{\partial \tau} = & \frac{D}{m^2} \Psi'' + \left[\frac{2D}{m^2} \frac{\phi'}{\phi} + v \frac{\gamma_t - 2\lambda(\gamma_1 + \gamma_2)}{m} \right] \Psi' + \left[\frac{D}{m^2} \frac{\phi''}{\phi} + (a\gamma_1 + b\gamma_2)\lambda(1 - \lambda)v^2 \right. \\ & \left. + v \frac{\gamma_t - 2\lambda(\gamma_1 + \gamma_2)}{m} \frac{\phi'}{\phi} + \frac{\gamma_t - \lambda(\gamma_1 + \gamma_2)}{m} \right] \Psi, \end{aligned} \quad (5.13)$$

where $D = D_1 + D_2 + \delta^2 D_3$, $\gamma_t = \gamma_1 + \gamma_2 + \delta\gamma_3$, and $' \equiv \partial/\partial v$. For convenience, we write $\phi \equiv \phi_\lambda(v | v_0)$ and $\Psi \equiv \Psi_\lambda(v, \tau | v_0)$.

For a particular choice of $\phi = \exp \left[-\frac{m(v^2 - v_0^2)[\gamma_t - 2\lambda(\gamma_1 + \gamma_2)]}{4D} \right]$, the Fokker-Planck equation given in Eq. (5.13) reduces to

$$\frac{\partial \Psi}{\partial \tau} = \frac{D}{m^2} \Psi'' + v^2 \left[(a\gamma_1 + b\gamma_2)\lambda(1 - \lambda) - \frac{\{\gamma_t - 2\lambda(\gamma_1 + \gamma_2)\}^2}{4D} \right] \Psi + \frac{\gamma_t \Psi}{2m} \quad (5.14)$$

We map the above given differential equation (classical problem) to the Schrödinger's equation for the quantum harmonic oscillator (QHO)

$$i\hbar \frac{\partial \Psi}{\partial t} = -\frac{\hbar^2}{2m} \frac{\partial^2 \Psi}{\partial x^2} + U(x)\Psi. \quad (5.15)$$

Identifying the mapping $it/\hbar \rightarrow \tau$, $x \rightarrow v$, and $\hbar^2/2m \rightarrow D/m^2$, we find the harmonic potential in which the Brownian particle is confined (in the classical problem)

$$U(v) = \frac{1}{2}m\omega^2 v^2 = -v^2 \left[(a\gamma_1 + b\gamma_2)\lambda(1 - \lambda) - \frac{\{\gamma_t - 2\lambda(\gamma_1 + \gamma_2)\}^2}{4D} \right]. \quad (5.16)$$

Using $\hbar^2 = 2D/m$, we get

$$\hbar\omega = \frac{1}{m} \sqrt{[\gamma_t - 2\lambda(\gamma_1 + \gamma_2)]^2 - 4D(a\gamma_1 + b\gamma_2)\lambda(1 - \lambda)}. \quad (5.17)$$

Mapping of our classical problem onto the QHO gives the advantage to recognize energy eigenvalues and eigenstates of our problem. Thus, in the n th eigenstate, the energy eigenvalue reads

$$\epsilon_n = \left(n + \frac{1}{2} \right) \hbar\omega - \frac{\gamma_t}{2m}. \quad (5.18)$$

The eigenfunction $\Psi_\lambda(v, \tau|v_0)$ is written as

$$\Psi_\lambda(v, \tau|v_0) = \langle v|e^{-\tau\hat{H}}|v_0\rangle = \sum_{n=0}^{\infty} e^{-\epsilon_n\tau} \psi_n(v) \psi_n^*(v_0), \quad (5.19)$$

where the superscript * corresponds to the complex conjugation operation and \hat{H} is the quantum Hamiltonian

$$\hat{H} = -\frac{D}{m^2} \frac{\partial^2}{\partial v^2} - v^2 \left[(a\gamma_1 + b\gamma_2)\lambda(1 - \lambda) - \frac{\{\gamma_t - 2\lambda(\gamma_1 + \gamma_2)\}^2}{4D} \right] - \frac{\gamma_t}{2m}. \quad (5.20)$$

For simplicity, we choose $\gamma_1 = \gamma_2 = \gamma_3 = \gamma$. Using eigenfunctions of the harmonic

oscillator and the mapping defined above, we write the full solution of the Fokker-Planck equation. In the large time limit ($\tau \gg \tau_\gamma$, where $\tau_\gamma = m/\gamma$ is the viscous relaxation time), the dominating contribution to the solution is from $n = 0$ term,

$$Z_W(\lambda, v, \tau|v_0) = \sqrt{\frac{m\gamma v(\lambda)}{2\pi D}} e^{(\tau/\tau_\gamma)\mu(\lambda)} e^{-\frac{m\gamma v^2}{4D}[2+\delta-4\lambda+v(\lambda)]} e^{-\frac{m\gamma v_0^2}{4D}[-2-\delta+4\lambda+v(\lambda)]} + \dots, \quad (5.21)$$

where

$$\mu(\lambda) = \frac{1}{2}[2 + \delta - v(\lambda)], \quad \text{in which} \quad (5.22)$$

$$v(\lambda) = \sqrt{(2 + \delta - 4\lambda)^2 - 4\lambda(1 - \lambda)(T_1 + T_2 + \delta^2 T_3)(a + b)}. \quad (5.23)$$

Therefore, the restricted moment generating function for $\Delta S_{tot}^{1,2}$ is

$$\begin{aligned} Z(\lambda, v, \tau|v_0) &= e^{-\lambda \Delta S_{sys}} Z_W(\lambda, v, \tau|v_0) \\ &= \sqrt{\frac{m\gamma v(\lambda)}{2\pi D}} e^{(\tau/\tau_\gamma)\mu(\lambda)} e^{-\frac{m\gamma v^2}{4D}[2+\delta+2\lambda\delta+v(\lambda)]} e^{-\frac{m\gamma v_0^2}{4D}[-2-\delta-2\lambda\delta+v(\lambda)]} + \dots \end{aligned} \quad (5.24)$$

Notice that substituting $\lambda = 0$ in the above equation and identifying $\mu(0) = 0$ gives the steady state distribution $Z(0, v, \tau \rightarrow \infty|v_0) = P_{ss}(v)$ [see Eq. (5.6)].

The moment generating function for the partial entropy production is obtained from $Z(\lambda, v, \tau|v_0)$ by integrating over the final velocity variable v and the initial velocity v_0 with respect to initial steady state distribution $P_{ss}(v_0)$

$$Z(\lambda) = \int dv \int dv_0 P_{ss}(v_0) Z(\lambda, v, \tau|v_0) = e^{(\tau/\tau_\gamma)\mu(\lambda)} g(\lambda) + \dots, \quad (5.25)$$

where the prefactor is

$$g(\lambda) = \frac{2\sqrt{(2 + \delta)v(\lambda)}}{\sqrt{2 + \delta + 2\lambda\delta + v(\lambda)}\sqrt{2 + \delta - 2\lambda\delta + v(\lambda)}}. \quad (5.26)$$

Here, the first and second term in the denominator come from integrating the restricted moment generating function of the partial entropy production over the final variable v and the initial variable v_0 with respect to the steady state ensemble $P_{ss}(v_0)$,

respectively.

5.4. Probability distribution function

Our goal of this chapter is to compute the probability density function of the partial entropy production. Thus, we invert the moment generating function $Z(\lambda)$ using the inverse transformation

$$P(\Delta S_{tot}^{1,2} = s\tau/\tau_\gamma) = \int_{-i\infty}^{+i\infty} \frac{d\lambda}{2\pi i} Z(\lambda) e^{\Delta S_{tot}^{1,2}} = \int_{-i\infty}^{+i\infty} \frac{d\lambda}{2\pi i} g(\lambda) e^{(\tau/\tau_\gamma) I_s(\lambda)} + \dots \quad (5.27)$$

where $s = \Delta S_{tot}^{1,2} \tau_\gamma / \tau$ is the scaled variable. The contour of integration in the above equation is taken along the imaginary axis passing through the origin of the complex λ -plane. The function $I_s(\lambda)$ reads as

$$I_s(\lambda) = \mu(\lambda) + \lambda s. \quad (5.28)$$

The function $\nu(\lambda)$ is real and positive when $\lambda \in (\lambda_-^\delta, \lambda_+^\delta)$ where

$$\lambda_\pm^\delta = \frac{1}{2(\alpha - 16)} [\alpha - 8(2 + \delta) \pm \sqrt{\alpha} \sqrt{\alpha - 16 + 4\delta^2}], \quad (5.29)$$

where $\lambda_+^\delta > 0$, $\lambda_-^\delta < 0$, and $\alpha = 4(1 + 1/\beta_{12})(1 + \beta_{12} + \delta^2\beta_{13})$, and $\beta_{ij} = T_j/T_1$. Therefore, $I_s(\lambda)$ is also real function when $\lambda \in (\lambda_-^\delta, \lambda_+^\delta)$.

The long time result of the integral (5.27) can be calculated using saddle-point method [136]. The saddle point $\lambda^*(s)$ is the solution of the following equation

$$\left. \frac{\partial \mu(\lambda)}{\partial \lambda} \right|_{\lambda=\lambda^*(s)} = -s, \quad (5.30)$$

and given by

$$\lambda^*(s) = \frac{1}{2(\alpha - 16)} \left[\alpha - 8(2 + \delta) - 2s \sqrt{\frac{\alpha(\alpha - 16 + 4\delta^2)}{\alpha - 16 + 4s^2}} \right], \quad (5.31)$$

where $\alpha - 16 > 0$. Note that, in the limit of large s , we see that

$$\lambda^*(s) = \begin{cases} \lambda_-^\delta & s \rightarrow +\infty, \\ \lambda_+^\delta & s \rightarrow -\infty. \end{cases} \quad (5.32)$$

At the saddle point, we find that

$$\left. \frac{\partial^2 I_s(\lambda)}{\partial \lambda^2} \right|_{\lambda=\lambda^*(s)} = \frac{(4s^2 + \alpha - 16)^{3/2}}{\sqrt{\alpha(4\delta^2 + \alpha - 16)}}, \quad (5.33)$$

is positive function of s . Thus, the function $I_s(\lambda)$ is minimum at the saddle point $\lambda^*(s)$ along the $Re(\lambda)$ axis of the complex λ -plane. Therefore, we choose the contour of integration along the $Im(\lambda)$ axis of the complex λ -plane at the saddle point $\lambda^*(s)$.

The function $h(s) = I_s(\lambda^*(s))$ at the saddle point reads

$$h(s) = 1 + \frac{\delta}{2} + \frac{s[\alpha - 8(2 + \delta)]}{2(\alpha - 16)} - \frac{1}{4} \sqrt{\frac{\alpha(\alpha - 16 + 4\delta^2)}{\alpha - 16 + 4s^2}} \left(1 + \frac{4s^2}{\alpha - 16} \right). \quad (5.34)$$

In $g(\lambda)$, both of the denominators have one zero each for a particular choice of β_{12} , β_{13} and δ . Corresponding to first denominator, $\lambda = \lambda_a$ is the zero of $2 + \delta + 2\lambda\delta + \nu(\lambda)$, and $\lambda_a \in (\lambda_-^\delta, \lambda_+^\delta)$ when $[2 + \delta + 2\delta\lambda_-^\delta] \leq 0$ (condition-I). On the other hand, $\lambda = \lambda_b$ is the zero of second denominator having $2 + \delta - 2\lambda\delta + \nu(\lambda)$, and $\lambda_b \in (\lambda_-^\delta, \lambda_+^\delta)$ only when $[2 + \delta - 2\delta\lambda_+] \leq 0$ (condition-II). Condition-II is simply given by $\delta \geq 2$.

The branch point singularities $\lambda_{a,b}$ are

$$\lambda_a = \frac{(\alpha - 16 - 4\delta(\delta + 4))}{(\alpha - 16 + 4\delta^2)} \quad (5.35)$$

$$\lambda_b = 1. \quad (5.36)$$

Using condition-I, we plot the phase diagram shown in Fig. 5.2 in (β_{12}, β_{13}) plane for various values of δ . In the phase diagram, condition-I does not hold to the left side of contours at respective δ . From the Fig. 5.2, it is clear that there is no singularity present in the prefactor $g(\lambda)$ in the weak coupling limit, i.e. $\delta \rightarrow 0$. Hence, $g(\lambda)$ is analytic function of λ in the weak coupling limit. Therefore, we can compute the

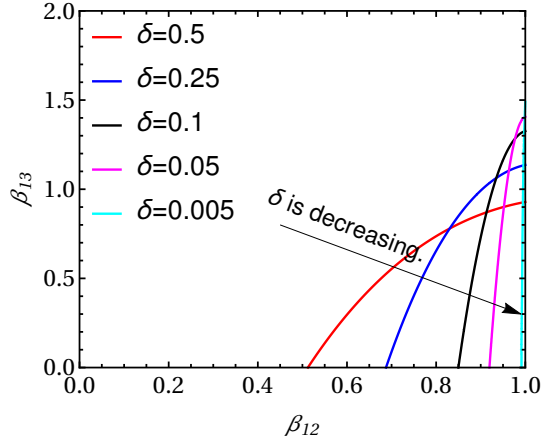


FIGURE 5.2: Phase diagram in (β_{12}, β_{13}) plane is shown for different values of the coupling parameter δ . Condition-I is not satisfied to the left side of the contours at respective coupling parameters.

integral given in Eq. (5.27) using saddle-point approximation:

$$p(s) = P(\Delta S_{tot}^{1,2} = s\tau/\tau_\gamma)\tau/\tau_\gamma \approx \frac{\tau/\tau_\gamma \tilde{g}(s) e^{(\tau/\tau_\gamma)h(s)}}{\sqrt{2\pi\tau/\tau_\gamma |I_s''(\lambda^*(s))|}}, \quad (5.37)$$

where $\tilde{g}(s) = g(\lambda^*(s))$. In Fig. 5.3(a), we have compared the analytical expression of the probability density function given in Eq. (5.37) with the numerical simulation for $\beta_{12} = 0.5$, $\beta_{13} = 0.5$, and $\delta = 0.2$ at time $\tau/\tau_\gamma = 100$.

5.5. Large deviation function and fluctuation theorem

In the large time limit, the probability density function of the partial entropy production $p(s)$ has the following form (ignoring the prefactor to the exponential)

$$p(s) \approx e^{(\tau/\tau_\gamma)h(s)}, \quad (5.38)$$

where the function $h(s)$ is called as large deviation function [136], and by definition

$$h(s) = \lim_{\tau/\tau_\gamma \rightarrow \infty} \frac{\tau_\gamma}{\tau} \ln p(s). \quad (5.39)$$

When the fluctuation theorem is satisfied, we see that

$$\lim_{\tau/\tau_\gamma \rightarrow \infty} \frac{\tau_\gamma}{\tau} \ln \frac{p(s)}{p(-s)} = s, \quad (5.40)$$

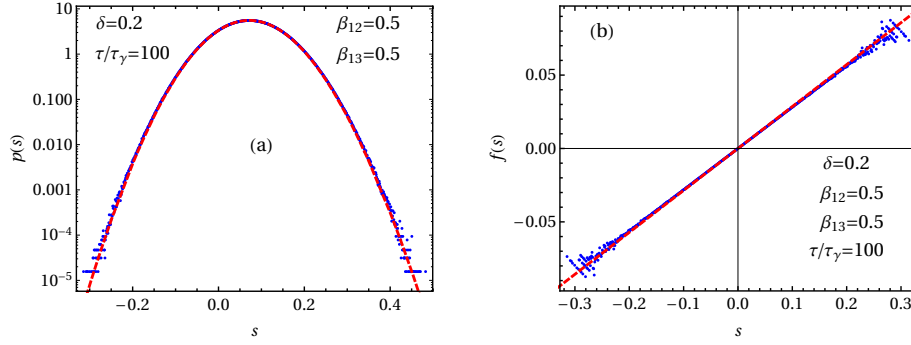


FIGURE 5.3: (a): Probability density function for the partial entropy production $p(s)$ is plotted against the scaled partial entropy production $s = \Delta S_{tot}^{1,2} \tau_\gamma / \tau$ for $\beta_{12} = 0.5$, $\beta_{13} = 0.5$, and $\delta = 0.2$ at time $\tau / \tau_\gamma = 100.0$. (b): The asymmetry function $f(s) := h(s) - h(-s)$ is plotted against the scaled partial entropy production $s = \Delta S_{tot}^{1,2} \tau_\gamma / \tau$ for $\beta_{12} = 0.5$, $\beta_{13} = 0.5$, and $\delta = 0.2$ at time $\tau / \tau_\gamma = 100$. In both figures, red solid lines are the analytical results [Eqs. (5.37) and (5.42) in (a) and (b), respectively] whereas blue points are obtained from numerical simulations.

which reflect a symmetry in the large deviation function as

$$h(s) - h(-s) = s. \quad (5.41)$$

In the present case, the symmetry of the large deviation modifies to

$$h(s) - h(-s) = \frac{s[\alpha - 16 - 8\delta]}{\alpha - 16}. \quad (5.42)$$

Clearly, in the weak coupling limit, i.e. $\delta \rightarrow 0$, the fluctuation theorem restores as given in Eq. (5.41). In Fig. 5.3(b), we plot $f(s) = h(s) - h(-s)$ against the scaled partial entropy production $s = \Delta S_{tot}^{1,2} \tau / \tau_\gamma$ for $\beta_{12} = 0.5$, $\beta_{13} = 0.5$, and $\delta = 0.2$ at time $\tau / \tau_\gamma = 100$.

5.6. Summary

We have considered a single Brownian particle in contact with three heat baths of temperatures (dissipation constants) T_1 (γ_1), T_2 (γ_2), and δT_3 ($\delta\gamma_3$), where δ is the dimensionless coupling parameter. We have computed the total entropy production of a single Brownian due two heat baths (T_1 , γ_1) and (T_2 , γ_2), i.e. *partial entropy production*. In the limit $\delta \rightarrow 0$, we have found that this partial entropy production in

the steady state satisfies the fluctuation theorem. The results shown in this chapter are contrary to what we have seen in Chapters 2 and 3 [54]. This is because in those chapters we have considered the system where slow DOFs are coupled, and computed the total entropy production for the part of the system. But, in this chapter, we considered the coupling of the slow DOF with the fast DOFs. Therefore, one can conclude that once the fast DOFs are weakly coupled to the slow DOFs, the total entropy production of the slow DOFs will obey the fluctuation theorem in the steady state.

Chapter 6

Stochastic efficiency of an isothermal work-to-work converter engine

In previous chapters, we computed the probability density function for the partial and apparent entropy production in the steady state. In this chapter, we investigate the efficiency of an isothermal work-to-work converter engine, composed of a Brownian particle in the heat bath at a constant temperature. This system is maintained out of equilibrium using two time dependent, uncorrelated stochastic Gaussian forces. These forces are called load and drive force. The function of drive force is to drive the Brownian particle against the load force. The work done by these forces are stochastic quantities. The efficiency of this engine which is the ratio of work done against the load force and the work done by the drive force, is also a stochastic quantity. We analytically obtained the probability density function as well as the large deviation function of stochastic efficiency, and compared with numerical simulations.

6.1. Introduction

Heat engine [15, 147] is a machine that operates between two temperatures in a cyclic process. It converts a part of the heat Q_H taken from the hot reservoir at a temperature T_H to useful work W , and the remaining part of the heat Q_C is dumped into the cold reservoir at a temperature $T_C < T_H$. At the end of the cyclic process,

the engine returns to its initial state. The efficiency of an engine is given by the ratio of work done by it and the heat consumed from the hot reservoir: $\eta = W/Q_H$. When such engines work in the quasi-static limit as well as in a reversible fashion, its efficiency is given by the Carnot efficiency $\eta_C = 1 - T_C/T_H$. The efficiency of any engine is bounded above by the Carnot efficiency: $\eta \leq \eta_C$. This bound is universal, and does not depend upon the nature of the composition of the engine. In the quasi-static regime, the power delivered by the engine is identically zero: $W/t \rightarrow 0$ in the limit $t \rightarrow \infty$. Therefore, the Carnot engine is not useful for doing work in a reasonable time in practice.

Modern technology helps in engineering machines on a microscopic scale. These small nanosized devices can be seen in many areas of biological science [1, 130, 81, 43, 72, 12]. The fluctuations present in the surrounding environment can disturb the deterministic nature of such small-scale devices. Nevertheless, the state of the system can be described in the probabilistic manner, whose evolution is governed by the master equation or Fokker-Planck equation [70]. Interestingly, nowadays various properties of these small systems can be understood by realizing them in controlled experiments [9, 87, 73, 114, 137, 21, 23, 48, 20].

When such small-scale machines are driven by external forces, like temperature or concentration gradient, shear flow, time-dependent external field, etc., observables such as work done, heat flow, power injection, entropy production, etc., become stochastic quantities [110, 109, 94, 93, 140, 144, 143, 76, 36, 52, 150, 151, 149]. The probability distributions of these quantities have richer information than their ensemble average values.

Over the past two decades, a lot of research has been devoted to refining the thermodynamic principle in the mesoscopic scale. While the first law of thermodynamics is also valid at the trajectory level, the second law of thermodynamics is replaced by the symmetry property of the probability distribution of total entropy production [123, 121, 120]. This symmetry property is referred to as the *fluctuation theorem* (FT) [32, 34, 118, 117, 39, 77, 82, 25, 24, 26], which accounts for the measure of the likelihood of trajectories violating the second law of thermodynamics.

For a small-scale heat engine connected to two heat reservoirs, the efficiency becomes a fluctuating quantity, whose value changes from one measurement to the

other. Hence, it is described by a probability distribution $P(\eta, t)$. In particular, one is interested in its large deviation form [136] $P(\eta, t) \sim e^{tJ(\eta)}$, where $J(\eta)$ is the large deviation function defined as $J(\eta) = \lim_{t \rightarrow \infty} \frac{1}{t} \ln P(\eta)$. It captures the large time statistics of the efficiency of the stochastic engine. In a recent study, Verley *et al.* [142] computed the large deviation function $J(\eta)$ using FT for microscopic heat engine using two set of examples: work-to-work converter engine and a photoelectric device. They have shown that the Carnot efficiency is least likely in the long time limit, which is a remarkable result. Moreover, the large deviation function has two extrema: a maximum corresponds to the most probable efficiency, and the minimum occurs at Carnot efficiency. In a similar context, Verley *et al.* [141], found an efficient way to compute the large deviation function of stochastic efficiency using the cumulant generating function of entropy productions for a small engine with finite state space. This method was verified by considering an example of a stochastic engine made up of a system of two states where each of these states is coupled to a heat reservoir at a distinct temperature. To drive this system in the nonequilibrium state, a time-dependent periodic field is applied. They have computed the large deviation function for stochastic efficiency which supported the prediction given in Ref. [142]. Gingrich *et al.* [46] computed the finite time probability density function for stochastic efficiency of a two-level heat engine using time-asymmetric driving in a cyclic process. Poletti *et al.* [99] derived the probability density function for stochastic efficiency where thermodynamic fluxes are distributed by a multivariate Gaussian distribution. Using FT for entropy production, it is shown that the probability of efficiency larger than the Carnot one, called *super-Carnot efficiency*, is favored by trajectories violating the second law of thermodynamics. Moreover, the distribution function has two maxima and one minimum: one maximum corresponds to the most probable efficiency, while the other is at efficiency larger than the Carnot efficiency. The location of the minimum is at the Carnot efficiency. It is observed that the other maximum does not appear in the large deviation function because in the long time limit that maximum occurs at infinity. Proesmans *et al.* [100] considered an effusion process using two compartments at different temperatures and chemical potentials, where particles flow from a compartment at a higher temperature and low chemical potential to the compartment at a low temperature and high chemical potential. In

the finite and long time limit, the distribution for the stochastic efficiency is computed for this effusion engine. Some of these models are briefly discussed in Ref. [101]. In the case of isothermal energy transformation [103], authors considered a Brownian particle in a harmonic potential driven by a duo of time-periodic forces. This setup is used as an engine which converted the Gaussian stochastic input work to Gaussian stochastic output work. They have reproduced the latest discovered connection between different operational regimes (maximum power, maximum efficiency, minimum dissipation) [5, 127, 102]. Moreover, the probability density function for stochastic efficiency is also computed, and all of these results were verified experimentally by them. Park *et al.* [96] modeled an engine which is driven by time-independent (time-symmetric) driving. In contrast to Refs. [142, 141], the phase space is found to be continuous with infinite microstates, and it has been shown that the large deviation function does not follow the universal nature as mentioned in Refs. [142, 141].

In this chapter, we mainly focus on an isothermal energy converter where a system consists of a Brownian particle coupled to a heat bath at a constant temperature. In the absence of external forces, total entropy production is identically zero as the system, described by the velocity variable, enjoys equilibrium. The given system is maintained in the nonequilibrium steady state using two time-dependent stochastic Gaussian external forces. This system functions as an engine which converts one form of the work (*input work*) into another form (*output work*). Note that this engine is different from the usual heat engines where the working substance undergoes the cyclic transformation between two temperatures. Such an isothermal engine can be seen in biological systems, for example, adenosine triphosphate functions as an energy converter in the cell [1, 130]. The work done by these forces is stochastic random variables. The efficiency of this isothermal engine is defined by the ratio of the work done against the load force and the work done by the drive force, which is also a stochastic quantity. We compute the distribution of stochastic efficiency from the joint distribution of work done against the load force (output work) and work done by the drive force (input work). There are three important features of this chapter: (1) In contrast to previous studies, we have applied stochastic forces to drive the system out of equilibrium, (2) FT for the joint probability distribution of input and

output work does not remain valid for all strength of stochastic forces, and (3) the phase space is continuous with infinite microstates. While the first two features were not introduced in this context earlier as reported in Refs. [103, 96], the third feature is similar to as mentioned in Ref. [96].

The remainder of the chapter is organized as follows. In Sec. 6.2, we give a model system of an engine which converts the input work to the output work. Section 6.3 contains the calculation of the joint characteristic function of the input and output work, $Z(\lambda_1, \lambda_2) \sim g(\lambda_1, \lambda_2)e^{(t/t_\gamma)\mu(\lambda_1, \lambda_2)}$ at large t . In Sec. 6.4, we discuss the method to invert the characteristic function $Z(\lambda_1, \lambda_2)$ to get the probability density function $P_t(W_1, W_2)$. In Sec. 6.4.1, we analyze the singularity present in $g(\lambda_1, \lambda_2)$. In Sec. 6.4.2, we write the asymptotic expression for the joint probability density $P_t(W_1, W_2)$ using a saddle point approximation in the absence of a singularity in the prefactor $g(\lambda_1, \lambda_2)$, and in Sec. 6.4.3, we discuss the joint probability density function $P_t(W_1, W_2)$ in the presence of a singularity in $g(\lambda_1, \lambda_2)$. FT for $P_t(W_1, W_2)$ is discussed in Sec. 6.4.4. In Sec. 6.5.1, we give the expression for the probability density function for stochastic efficiency $P(\eta, t)$ when $g(\lambda_1, \lambda_2)$ does not have singularities, and the result for this case is shown in Sec. 6.5.2. In the case, when $g(\lambda_1, \lambda_2)$ has singularities, we discuss the methodology to get the asymptotic expression for $P(\eta, t)$ in Sec. 6.5.3, and results in this case are shown in Secs. 6.5.5 and 6.5.6. We summarized the chapter in Sec. 6.6.

6.2. Model

Consider a Brownian particle of mass m diffusing in the heat bath at a temperature T . In the absence of external forces, velocity distribution of Brownian particle reaches a steady state as given by Gibbs's equilibrium distribution. For this particle to behave as an engine, we apply two different time dependent forces. One of the force is called load force and the other one is called drive force. The function of the drive force is to drive the particle against the load force. For simplicity, we have chosen external forces as Gaussian white noise, and both of them are uncorrelated with each other.

Therefore, the equation of motion of the Brownian particle is given by

$$m\dot{v} = -\gamma v + \xi(t) + f_1(t) + f_2(t) \quad (6.1)$$

where v is the velocity of the Brownian particle, γ is the dissipation constant, and $\xi(t)$ is the Gaussian white noise from the bath, with mean zero and variance $\langle \xi(t)\xi(t') \rangle = 2T\gamma\delta(t-t')$, according to the fluctuation-dissipation theorem. We set Boltzmann's constant to unity throughout the calculation. The load force $f_1(t)$ and the drive force $f_2(t)$ are external stochastic Gaussian forces with mean zero and variances $\langle f_i(t)f_j(t') \rangle = \delta_{i,j}\bar{f}_i^2\delta(t-t')$. They are uncorrelated with the thermal noise $\langle f_i(t)\xi(t') \rangle = 0$ for all t, t' . It turns out that only the relative strengths amongst the external forces and the thermal noise are important, not their absolute values. Therefore, we set $\bar{f}_1^2 = 2T\gamma\theta$ and $\bar{f}_2^2 = 2T\gamma\theta\alpha^2$, where θ and α are positive parameters.

Multiplying both sides of Eq. (6.1) by v , and integrating with respect to time from 0 to t , yields the conservation of energy relation (*first law of thermodynamics*)

$$\Delta E = Q + W_1 + W_2, \quad (6.2)$$

where

$$\Delta E = \frac{m}{2T}[v^2(t) - v^2(0)] \quad (6.3)$$

$$Q = \frac{1}{T} \int_0^t dt' [\xi(t') - \gamma v(t')]v(t') \quad (6.4)$$

$$W_1 = \frac{1}{T} \int_0^t dt' f_1(t')v(t') \quad (6.5)$$

$$W_2 = \frac{1}{T} \int_0^t dt' f_2(t')v(t'). \quad (6.6)$$

Here, we measure change in the internal energy ΔE , heat absorbed from the surrounding bath Q , work done by load and drive forces W_1 and W_2 respectively, in the scale of temperature of the heat bath. The integrals given in Eqs. (6.4)–(6.6) follow Stratonovich rule on integration [124].

It is clear from Eq. (6.1) that the velocity v depends linearly on both thermal noise $\xi(t)$ and external Gaussian forces $f_1(t)$ and $f_2(t)$. Therefore, the distribution of $v(t)$ is Gaussian, where the mean and the variance can be easily computed from Eq. (6.1).

In the limit $t \rightarrow \infty$, the mean velocity becomes zero, and the variance is given by

$$[\langle v^2(t) \rangle - \langle v(t) \rangle^2]_{t \rightarrow \infty} = \frac{T(1 + \theta + \theta\alpha^2)}{m}. \quad (6.7)$$

On the other hand, W_1 and W_2 given in Eqs. (6.5) and (6.6), respectively, depend on thermal noise $\zeta(t)$ and external Gaussian forces $f_1(t)$ and $f_2(t)$ quadratically. Thus, the joint distribution $P_t(W_1, W_2)$ is not expected to be Gaussian.

The quantity of interest is the the efficiency of a stochastic engine η which converts the input work W_2 to the output work $-W_1$,

$$\eta = -\frac{W_1}{W_2}. \quad (6.8)$$

The distribution of this stochastic efficiency $P(\eta, t)$ is computed from the joint distribution of input and output work $P_t(W_1, W_2)$ by integrating over W_1 while using Dirac delta function $\delta(\eta + W_1/W_2)$. Therefore,

$$P(\eta, t) = \int_{-\infty}^{\infty} dW_2 |W_2| P_t(-\eta W_2, W_2), \quad (6.9)$$

where $|W_2|$ is the Jacobian.

Note that, when the joint distribution $P_t(W_1, W_2)$ is Gaussian (that is not the case here), i.e.,

$$P_t(W_1 = w_1 t, W_2 = w_2 t) = \frac{1}{t \sqrt{(2\pi)^2 \det C}} e^{-\frac{1}{2} \bar{w}^T C^{-1} \bar{w}}, \quad (6.10)$$

using Eq. (6.9), the distribution of the stochastic efficiency $P(\eta, t)$ can be easily shown to be

$$P(\eta, t) = \frac{e^{j(\eta)t} [2e^{-\frac{t}{2} a(\eta) b(\eta)^2} + b(\eta) \sqrt{2\pi t a(\eta)} \operatorname{erf}(b(\eta) \sqrt{a(\eta) t/2})]}{\sqrt{(2\pi)^2 \det C} a(\eta)}, \quad (6.11)$$

where $\bar{w}^T = (w_1 - \mu_1, w_2 - \mu_2)$, $C_{ij} = (\langle W_i W_j \rangle - \langle W_i \rangle \langle W_j \rangle) / t$, $\mu_i = \langle W_i \rangle / t$, and

$$j(\eta) = -\frac{1}{2} \frac{(\eta \mu_2 + \mu_1)^2}{C_{22} \eta^2 + 2C_{12} \eta + C_{11}}, \quad (6.12)$$

$$a(\eta) = \frac{(\eta C_{22} + C_{12})^2 + \det C}{C_{22} \det C}, \quad (6.13)$$

$$b(\eta) = \frac{(C_{11} + C_{12} \eta) \mu_2 - (C_{12} + C_{22} \eta) \mu_1}{C_{22} \eta^2 + 2C_{12} \eta + C_{11}}. \quad (6.14)$$

In the Eq. (6.11), $\text{erf}(u)$ is the error function given by

$$\text{erf}(u) = \frac{2}{\sqrt{\pi}} \int_0^u e^{-x^2} dx. \quad (6.15)$$

6.2.1. Example

Consider a Brownian particle in the heat bath at a constant temperature T . Suppose the Brownian particle is diffusing in a plane with initial condition $\vec{x}(0) = (0, 0)$. Let two constant forces \vec{F}_1 and \vec{F}_2 applied on particle are the load and drive force, respectively. The evolution of the Brownian particle is given by overdamped Langevin equation [142],

$$\gamma \dot{\vec{x}} = \vec{\zeta}(t) + \vec{F}_1 + \vec{F}_2, \quad (6.16)$$

$\zeta^k(t)$ is the thermal noise in the k -direction, having mean zero and correlation $\langle \zeta^k(t) \zeta^l(t') \rangle = 2T\gamma \delta_{kl} \delta(t - t')$. Work done by i th forces is given by

$$W_i = \int_0^t dt' \vec{F}_i \cdot \dot{\vec{x}}(t') = \vec{F}_i \cdot \vec{x}(t), \quad (6.17)$$

where $i = 1, 2$. Note that in this example, we are not measuring the work done W_i with respect to the temperature T of the heat bath.

Stochastic efficiency η is given by Eq. (6.8). Since the distribution of $\vec{x}(t)$ is Gaussian, the distribution of each W_i is also Gaussian. In this case, both W_1 and W_2 are correlated with each other and their mean is non zero. The mean and correlation of W_1 and W_2 are given as

$$\begin{aligned} \langle W_i \rangle &= \vec{F}_i \cdot \vec{F} t / \gamma, \\ \langle W_i W_j \rangle - \langle W_i \rangle \langle W_j \rangle &= 2Tt \vec{F}_i \cdot \vec{F}_j / \gamma. \end{aligned} \quad (6.18)$$

where $\{i, j\} = 1, 2$, and $\vec{F} = \vec{F}_1 + \vec{F}_2$ is the total force acting on the Brownian particle. Scaled mean μ_i and correlations C_{ij} are given above. Using mean and correlations of W_1 and W_2 , we can write the probability distribution function for stochastic efficiency $P(\eta, t)$ [see Eq. (6.11)]. In Fig. 6.1, we plot the probability density function (left panel) and large deviation function (right panel) for the stochastic efficiency η . In Fig. 6.1(left panel), the blue points are obtained from numerical simulation while

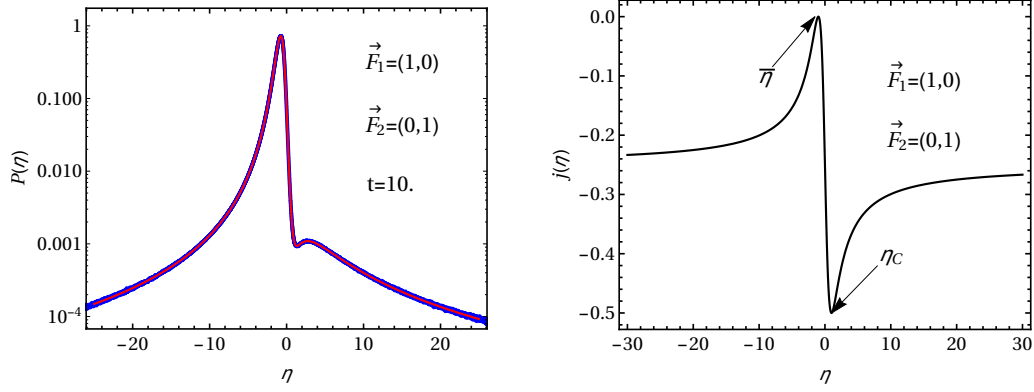


FIGURE 6.1: The distribution and large deviation function for the stochastic efficiency is plotted against η for $\gamma = 1$, $T = 1$, $\vec{F}_1 = (1, 0)$, and $\vec{F}_2 = (0, 1)$. Left panel: Blue dots represents the numerical simulation while the red solid line is for analytical expression of probability density function given in Eq. (6.11) for $t = 10.0$. Right panel: Black solid line shows the large deviation function given in Eq. (6.12).

the red solid line is the exact distribution given in Eq. (6.11). The large deviation function (black solid line) given in Eq. (6.12) is plotted in Fig. 6.1 (right panel).

In the present case, our aim is to understand the statistics of the efficiency fluctuation when $P_t(W_1, W_2)$ is non-Gaussian.

6.3. Fokker-Planck equation

To compute $P_t(W_1, W_2)$, it is convenient to first compute the characteristic function $Z(\lambda_1, \lambda_2) = \langle \exp(-\lambda_1 W_1 - \lambda_2 W_2) \rangle$. The conditional characteristic function $Z(\lambda_1, \lambda_2, v, t|v_0)$ for fixed initial and final conditions, $v(0) = v_0$ and $v(t) = v$, satisfies

$$\frac{\partial Z(\lambda_1, \lambda_2, v, t|v_0)}{\partial t} = \mathcal{L}_{\lambda_1, \lambda_2} Z(\lambda_1, \lambda_2, v, t|v_0), \quad (6.19)$$

where the differential operator $\mathcal{L}_{\lambda_1, \lambda_2}$ is given by

$$\mathcal{L}_{\lambda_1, \lambda_2} = \left[\frac{T\gamma(1 + \theta + \theta\alpha^2)}{m^2} \frac{\partial^2}{\partial v^2} + \frac{\gamma[1 + 2\theta(\lambda_1 + \alpha^2\lambda_2)]}{m} v \frac{\partial}{\partial v} + \frac{\gamma[1 + \theta(\lambda_1 + \alpha^2\lambda_2)]}{m} + \frac{\lambda_1^2 + \alpha^2\lambda_2^2}{T} \gamma\theta v^2 \right]. \quad (6.20)$$

The differential equation given in Eq. (6.19) is subject to initial condition $Z(\lambda_1, \lambda_2, v, 0|v_0) = \delta(v - v_0)$. Note that, putting $\lambda_1 = \lambda_2 = 0$ in $Z(\lambda_1, \lambda_2, v, t|v_0)$, gives the distribution

of velocity v at time t for given initial velocity v_0 , $P(v, t|v_0) = Z(0, 0, v, t|v_0)$. Consequently, the steady-state velocity distribution is given by $P_{ss}(v) = Z(0, 0, v, t \rightarrow \infty|v_0)$, independent of v_0 .

The characteristic function $Z(\lambda_1, \lambda_2)$ is obtained from $Z(\lambda_1, \lambda_2, v, t|v_0)$ by averaging over the initial velocity with respect to the steady-state distribution $P_{ss}(v_0)$ and integrating over the final velocity v :

$$Z(\lambda_1, \lambda_2) = \int_{-\infty}^{+\infty} dv \int_{-\infty}^{+\infty} dv_0 P_{ss}(v_0) Z(\lambda_1, \lambda_2, v, t|v_0). \quad (6.21)$$

To solve differential equation given in Eq. (6.19), we write

$$Z(\lambda_1, \lambda_2, v, t|v_0) = e^{-\frac{1}{2T}[U(v)-U(v_0)]} \psi_{\lambda_1, \lambda_2}(v, t|v_0). \quad (6.22)$$

It follows that, for the particular choice

$$U(v) = \frac{m[1 + 2\theta(\lambda_1 + \alpha^2\lambda_2)]}{2(1 + \theta + \theta\alpha^2)} v^2, \quad (6.23)$$

$\Psi_{\lambda_1, \lambda_2}(v, t|v_0)$ satisfies the Schrödinger equation in the imaginary time $-i\hbar t$ (and identifying $[T\gamma(1 + \theta + \theta\alpha^2)/m^2]$ with $[\hbar^2/(2m_q)]$ in the quantum problem),

$$\frac{\partial \psi_{\lambda_1, \lambda_2}(v, t|v_0)}{\partial t} = \left[\frac{T\gamma(1 + \theta + \theta\alpha^2)}{m^2} \frac{\partial^2}{\partial v^2} - V(v) \right] \psi_{\lambda_1, \lambda_2}(v, t|v_0), \quad (6.24)$$

for a quantum harmonic oscillator (QHO), where

$$V(v) = \frac{1}{2} m_q \omega_q^2 v^2 - \frac{\gamma}{2m}, \quad (6.25)$$

with the identification

$$m_q \omega_q^2 = \frac{\gamma}{T} \left[\frac{[1 + 2\theta(\lambda_1 + \alpha^2\lambda_2)]^2}{2(1 + \theta + \theta\alpha^2)} - 2\theta(\lambda_1^2 + \alpha^2\lambda_2^2) \right]. \quad (6.26)$$

Thus, $\psi_{\lambda_1, \lambda_2}(v, t|v_0) = \langle v|e^{-\hat{H}t}|v_0\rangle$ is recognized as the propagator of the QHO, which is known exactly. For our purpose, it is convenient to expand $\psi_{\lambda_1, \lambda_2}(v, t|v_0)$ in

the eigenbasis $\{\psi_n(v)\}$ of \hat{H} as

$$\psi_{\lambda_1, \lambda_2}(v, t|v_0) = \sum_{n=0}^{\infty} e^{-tE_n(\lambda_1, \lambda_2)} \psi_n(v) \psi_n^*(v_0), \quad (6.27)$$

where the eigenvalues are given by

$$E_n = \left(n + \frac{1}{2}\right) \hbar \omega_q - \frac{\gamma}{2m}, \quad n = 0, 1, 2, \dots \quad (6.28)$$

From the above identification between the quantum and the stochastic problem, we have

$$\hbar \omega_q = (\gamma/m) \nu(\lambda_1, \lambda_2) \quad (6.29)$$

with

$$\nu(\lambda_1, \lambda_2) = [1 + 4\theta\{\lambda_1(1 - \lambda_1) + \alpha^2\lambda_2(1 - \lambda_2) - \alpha^2\theta(\lambda_1 - \lambda_2)^2\}]^{1/2}. \quad (6.30)$$

In the long time limit, Eq. (6.27) is dominated by the $n = 0$ (ground state) term. Thus, for large t , Eq. (6.22) becomes

$$Z(\lambda_1, \lambda_2, v, t|v_0) = e^{(t/t_\gamma) \mu(\lambda_1, \lambda_2)} \Psi(v, \lambda_1, \lambda_2) \chi(v_0, \lambda_1, \lambda_2) + \dots, \quad (6.31)$$

where $t_\gamma = m/\gamma$ is the viscous relaxation time, and

$$\mu(\lambda_1, \lambda_2) = \frac{1}{2}[1 - \nu(\lambda_1, \lambda_2)], \quad (6.32)$$

$$\Psi(v, \lambda_1, \lambda_2) = A_0 e^{-\frac{\beta}{2}U(v)} \psi_0(v), \quad (6.33)$$

$$\chi(v_0, \lambda_1, \lambda_2) = A_0^{-1} e^{\frac{\beta}{2}U(v_0)} \psi_0^*(v_0), \quad (6.34)$$

where A_0 is an arbitrary function of λ_1 and λ_2 . Note that $\chi(v_0, \lambda_1, \lambda_2)$ and $\Psi(v, \lambda_1, \lambda_2)$, respectively are also the left and right eigenfunctions of the differential operator $\mathcal{L}_{\lambda_1, \lambda_2}$ corresponding to the largest eigenvalue $\mu(\lambda_1, \lambda_2)$. Using the ground state

eigenfunction of the QHO, with a particular choice of A_0 , it can easily be found that

$$\Psi(v, \lambda_1, \lambda_2) = \sqrt{\frac{m\gamma v(\lambda_1, \lambda_2)}{2\pi\Theta}} \exp\left(-\frac{m\gamma v^2}{4\Theta}[v(\lambda_1, \lambda_2) + 1 + 2\theta(\lambda_1 + \alpha^2\lambda_2)]\right), \quad (6.35)$$

$$\chi(v_0, \lambda_1, \lambda_2) = \exp\left(-\frac{m\gamma}{4\Theta}[v(\lambda_1, \lambda_2) - 1 - 2\theta(\lambda_1 + \alpha^2\lambda_2)]v_0^2\right), \quad (6.36)$$

with $\Theta = T\gamma(1 + \theta + \theta\alpha^2)$. The left and right eigenfunctions satisfy the normalization condition

$$\int_{-\infty}^{+\infty} \chi(v, \lambda_1, \lambda_2) \Psi(v, \lambda_1, \lambda_2) dv = 1. \quad (6.37)$$

From the above expressions, we find that $\mu(0, 0) = 0$ and $\chi(v_0, 0, 0) = 1$. Therefore, the steady state distribution $P_{ss}(v) = Z(0, 0, v, t \rightarrow \infty | v_0)$ of the velocity is given by

$$P_{ss}(v) = \Psi(v, 0, 0) = \sqrt{\frac{m\gamma}{2\pi\Theta}} \exp\left[-\frac{m\gamma v^2}{2\Theta}\right]. \quad (6.38)$$

The characteristic function $Z(\lambda_1, \lambda_2)$ is obtained after carrying out integrals given in Eq. (6.21),

$$Z(\lambda_1, \lambda_2) = g(\lambda_1, \lambda_2) \exp[(t/t_\gamma)\mu(\lambda_1, \lambda_2)] + \dots \quad (6.39)$$

Here, the prefactor

$$g(\lambda_1, \lambda_2) = \frac{2\sqrt{v(\lambda_1, \lambda_2)}}{\sqrt{f^+(\lambda_1, \lambda_2)}\sqrt{f^-(\lambda_1, \lambda_2)}}, \quad (6.40)$$

in which $f^\pm(\lambda_1, \lambda_2) = 1 \pm 2\theta(\lambda_1 + \alpha^2\lambda_2) + v(\lambda_1, \lambda_2)$. The first factor in the denominator of $g(\lambda_1, \lambda_2)$ is due to the integration over the final velocity v , and the second factor in the denominator of $g(\lambda_1, \lambda_2)$ comes from averaging over the initial velocity v_0 with respect to steady-state distribution $P_{ss}(v_0)$.

Note from Eqs. (6.32) and (6.40) that largest eigenvalue $\mu(\lambda_1, \lambda_2)$ satisfies the Gallavotti-Cohen symmetry whereas the prefactor $g(\lambda_1, \lambda_2)$ does not, i.e., $\mu(\lambda_1, \lambda_2) = \mu(1 - \lambda_1, 1 - \lambda_2)$ and $g(\lambda_1, \lambda_2) \neq g(1 - \lambda_1, 1 - \lambda_2)$.

6.4. Joint Probability density function $P_t(W_1, W_2)$

The joint distribution of input and output work $P_t(W_1, W_2)$ can be obtained by inverting the characteristic function $Z(\lambda_1, \lambda_2)$ given in Eq. (6.39):

$$P_t(W_1, W_2) = \int_{-i\infty}^{i\infty} \frac{d\lambda_1}{2\pi i} \int_{-i\infty}^{i\infty} \frac{d\lambda_2}{2\pi i} Z(\lambda_1, \lambda_2) e^{\lambda_1 W_1 + \lambda_2 W_2}. \quad (6.41)$$

Thus, for large t ,

$$P_t(W_1, W_2) = \int_{-i\infty}^{i\infty} \frac{d\lambda_1}{2\pi i} \int_{-i\infty}^{i\infty} \frac{d\lambda_2}{2\pi i} g(\lambda_1, \lambda_2) e^{(t/t_\gamma) I_{w_1, w_2}(\lambda_1, \lambda_2)} + \dots, \quad (6.42)$$

where $w_1 = W_1 t_\gamma / t$ and $w_2 = W_2 t_\gamma / t$ are scaled variables. Here, the contours of integration are taken along $\text{Im}(\lambda_1)$ and $\text{Im}(\lambda_2)$ axes passing through the origin of the complex (λ_1, λ_2) plane. The function $I_{w_1, w_2}(\lambda_1, \lambda_2)$ is given as

$$I_{w_1, w_2}(\lambda_1, \lambda_2) = \mu(\lambda_1, \lambda_2) + \lambda_1 w_1 + \lambda_2 w_2. \quad (6.43)$$

It can be seen $\nu(\lambda_1, \lambda_2)$ is a real and positive quantity when $(\lambda_1, \lambda_2) \in \mathbb{R}_1$ where \mathbb{R}_1 is the region shown in Fig. 6.2, bounded by $(\lambda_1(\phi), \lambda_2(\phi))$ in which

$$\lambda_1(\phi) = \frac{1}{2} \left[1 + \sqrt{\frac{\alpha^2 \theta}{1 + \alpha^2 \theta}} \sin \phi + \sqrt{\frac{1 + \theta + \theta \alpha^2}{\theta(1 + \alpha^2 \theta)}} \cos \phi \right], \quad (6.44)$$

$$\lambda_2(\phi) = \frac{1}{2} \left[1 + \sqrt{\frac{1 + \alpha^2 \theta}{\alpha^2 \theta}} \sin \phi \right], \quad \text{with } \phi \in [-\pi, \pi]. \quad (6.45)$$

Here, $(\lambda_1(\phi), \lambda_2(\phi))$ is the parametric representation of equation of ellipse [see Eq. (6.30)]

$$1 + 4\theta[\lambda_1(1 - \lambda_1) + \alpha^2 \lambda_2(1 - \lambda_2) - \alpha^2 \theta(\lambda_1 - \lambda_2)^2] = 0. \quad (6.46)$$

The maximum and minimum values of $\lambda_1(\phi)$ and $\lambda_2(\phi)$ (see black dashed lines in Fig. 6.2) are

$$\lambda_{10}^{\pm} = \frac{1}{2} \left[1 \pm \sqrt{1 + \frac{1}{\theta}} \right], \quad (6.47)$$

$$\lambda_{20}^{\pm} = \frac{1}{2} \left[1 \pm \sqrt{1 + \frac{1}{\alpha^2 \theta}} \right], \quad (6.48)$$

where $+$ and $-$ signs correspond to maximum and minimum value, respectively. Consequently, $I_{w_1, w_2}(\lambda_1, \lambda_2)$ is also a real quantity when $(\lambda_1, \lambda_2) \in \mathbb{R}_1$.

The long-time result of the integral given in Eq. (6.42) can be approximated using the saddle-point method [136]. The saddle point $(\lambda_1^*, \lambda_2^*)$ can be obtained by solving the following equations simultaneously:

$$\left. \frac{\partial I_{w_1, w_2}(\lambda_1, \lambda_2)}{\partial \lambda_1} \right|_{\lambda_{1,2}=\lambda_{1,2}^*} = 0, \quad (6.49)$$

$$\left. \frac{\partial I_{w_1, w_2}(\lambda_1, \lambda_2)}{\partial \lambda_2} \right|_{\lambda_{1,2}=\lambda_{1,2}^*} = 0. \quad (6.50)$$

This gives

$$\lambda_1^*(w_1, w_2) = \frac{1}{2} \left[1 - \frac{\alpha[w_1 + (w_1 + w_2)\theta]}{\Lambda} \right], \quad (6.51)$$

$$\lambda_2^*(w_1, w_2) = \frac{-w_2 - (w_1 + w_2)\alpha^2\theta + \alpha\Lambda}{2\alpha\Lambda}, \quad (6.52)$$

where

$\Lambda = \sqrt{\theta[w_1^2\alpha^2 + w_2^2 + (w_1 + w_2)^2\alpha^2\theta + \alpha^2\theta(1 + \theta + \theta\alpha^2)]}$. Clearly, one can see that $(\lambda_1^*, \lambda_2^*) \in \mathbb{R}_1$. Moreover, at the saddle point, the function $I(w_1, w_2) := I_{w_1, w_2}(\lambda_1^*, \lambda_2^*)$ reads as

$$I(w_1, w_2) = \frac{1}{2} \left[1 + w_1 + w_2 - \frac{\Lambda}{\alpha\theta} \right]. \quad (6.53)$$

Now, to solve the integral given in Eq. (6.42), we have to analyze whether $g(\lambda_1, \lambda_2)$ is analytic when $(\lambda_1, \lambda_2) \in \mathbb{R}_1$. If there is no singularity present in $g(\lambda_1, \lambda_2)$ between the origin of the (λ_1, λ_2) plane and saddle point $(\lambda_1^*, \lambda_2^*)$, one can deform the contours of integration through the saddle point $(\lambda_1^*, \lambda_2^*)$ and carry out saddle-point integration to approximate the integral given in Eq. (6.42) [94, 93, 136]. However, if $g(\lambda_1, \lambda_2)$ contains a singularity between the saddle point and the origin of (λ_1, λ_2) plane, then

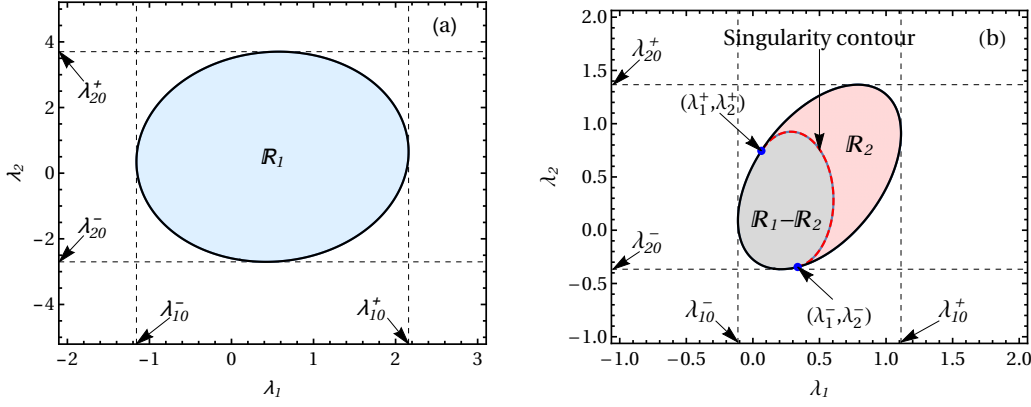


FIGURE 6.2: Two scenarios are shown here. (a) $g(\lambda_1, \lambda_2)$ is analytic for all $(\lambda_1, \lambda_2) \in \mathbb{R}_1$. (b) The light red region \mathbb{R}_2 represents the area where $g(\lambda_1, \lambda_2)$ is imaginary, whereas it is real in $\mathbb{R}_1 - \mathbb{R}_2$. The red contour (thick dashed) is the singularity line and corresponds to Eq. (6.54). End points $(\lambda_{1,2}^\pm)$ are given in the Eq. (6.72). In both cases, the black solid contour represents the region \mathbb{R}_1 bounded by $(\lambda_1(\phi), \lambda_2(\phi))$, $\phi \in [-\pi, \pi]$. Black dashed lines show the maximum and minimum values of $\lambda_1(\phi)$ and $\lambda_2(\phi)$ as given by Eqs. (6.47) and (6.48).

the saddle-point approximation will not be valid. In the following subsections, we consider both cases.

6.4.1. Analytic behavior of the correction term $g(\lambda_1, \lambda_2)$

In $g(\lambda_1, \lambda_2)$, $f^+(\lambda_1, \lambda_2) > 0$ for all $\theta \in (0, \infty)$ and $\alpha \in (0, \infty)$ whereas the function $f^-(\lambda_1, \lambda_2)$ can attain any sign depending on the values of θ and α . It turns out that there can be two scenarios, which are shown in Fig. 6.2. In both scenarios, \mathbb{R}_1 is the region bounded by contour $(\lambda_1(\phi), \lambda_2(\phi))$ where $\phi \in [-\pi, \pi]$ (see black solid contour in Fig. 6.2). In Fig. 6.2(a), $f^-(\lambda_1, \lambda_2) > 0$ for all $(\lambda_1, \lambda_2) \in \mathbb{R}_1$, and hence $g(\lambda_1, \lambda_2)$ does not have any singularity in the whole region \mathbb{R}_1 . On the other hand, in Fig. 6.2(b), $f^-(\lambda_1, \lambda_2) \leq 0$ in the region $(\lambda_1, \lambda_2) \in \mathbb{R}_2$ and positive in $(\lambda_1, \lambda_2) \in \mathbb{R}_1 - \mathbb{R}_2$. Hence $g(\lambda_1, \lambda_2)$ has singularities given by the curve

$$f^-(\lambda_1, \lambda_2) = 0. \quad (6.54)$$

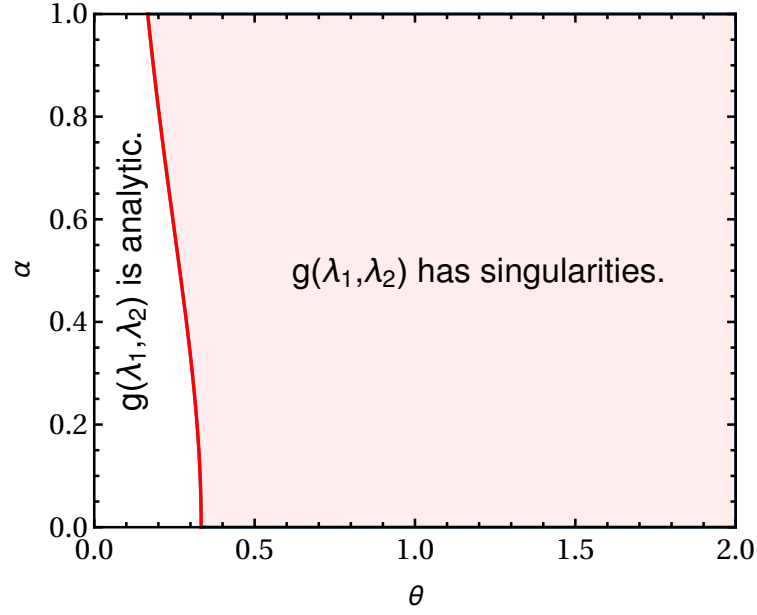


FIGURE 6.3: Contour (red solid line) separates two regions depending upon if $g(\lambda_1, \lambda_2)$ has singularities or not.

The singularity contour given by above equation can be written in parametric representation as

$$\lambda_1(\Phi) = \frac{1}{1 + \theta + \theta\alpha^2} \left(1 + \sqrt{1 + \alpha^2} \cos \Phi \right) \quad (6.55)$$

$$\lambda_2(\Phi) = \frac{1}{1 + \theta + \theta\alpha^2} \left(1 + \frac{\sqrt{1 + \alpha^2}}{\alpha} \sin \Phi \right) \quad (6.56)$$

where $\Phi \in (\Phi_-, \Phi_+)$.

When singularity contour given by Eq. (6.54), intersects the boundary of domain \mathbb{R}_1 , we get,

$$f^-(\lambda_1(\phi_{\pm}), \lambda_2(\phi_{\pm})) = 0, \quad (6.57)$$

$$\cos \phi_{\pm} + A \sin \phi_{\pm} - B = 0, \quad (6.58)$$

where

$$A = \alpha \sqrt{1 + \theta + \theta\alpha^2}, \quad (6.59)$$

$$B = \sqrt{(1 + \alpha^2\theta) / [\theta(1 + \theta + \theta\alpha^2)](1 - \theta - \theta\alpha^2)}. \quad (6.60)$$

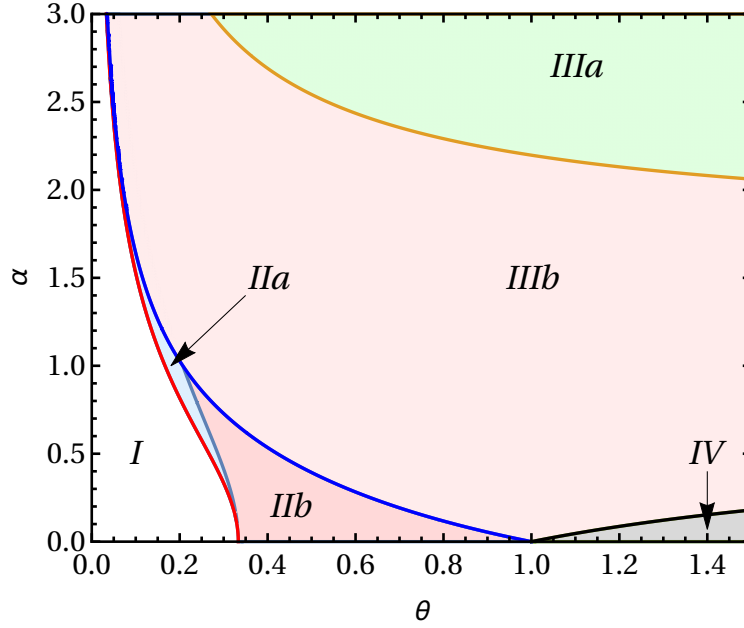


FIGURE 6.4: Phase diagram indicates the sign of $C_{1,2}^\pm$. Region-I: $g(\lambda_1, \lambda_2)$ is analytic. In subregions *IIa*: $C_{1,2}^\pm > 0$. In subregion *IIb*: $C_{1,2}^+ > 0$, $C_1^- < 0$ and $C_2^- > 0$. In subregion *IIIa*: $C_{1,2}^+ < 0$, $C_1^- < 0$ and $C_2^- > 0$. In subregion *IIIb*: $C_1^+ > 0$, $C_2^+ < 0$, $C_1^- < 0$ and $C_2^- > 0$. In region *IV*: $C_1^+ > 0$, $C_2^+ < 0$ and $C_{1,2}^- < 0$.

In the Eq. (6.58), we have used $v(\lambda_1(\phi_\pm), \lambda_2(\phi_\pm)) = 0$.

Consider $\sin \phi_\pm = y$, therefore Eq. (6.58) becomes

$$\pm \sqrt{1 - y^2} = -Ay + B. \quad (6.61)$$

Solution of Eq. (6.61) is given by

$$y_\pm = \frac{AB \pm \sqrt{1 + A^2 - B^2}}{A^2 + 1}. \quad (6.62)$$

Since y_\pm is a real number, therefore, $1 + A^2 - B^2 = -1 + 3(1 + \alpha^2)\theta \geq 0$. Thus,

$$-1 + 3(1 + \alpha^2)\theta \geq 0 \quad (6.63)$$

gives us the restriction on α and θ for which the singularity contours appears in the scenario as shown in Fig. 6.2(b). Using above inequality, we have plotted the phase diagram shown in Fig. 6.3. y_\pm is the solution of equation $\pm \sqrt{1 - y^2} = -Ay + B$

when

$$(1) \quad B \geq +A\sqrt{1+A^2-B^2} \quad \text{for} \quad y_+ \quad (6.64)$$

$$(2) \quad B \geq -A\sqrt{1+A^2-B^2} \quad \text{for} \quad y_- \quad (6.65)$$

Similarly, y_{\pm} is the solution of equation $-\sqrt{1-y^2} = -Ay + B$ when

$$(3) \quad B \leq +A\sqrt{1+A^2-B^2} \quad \text{for} \quad y_+ \quad (6.66)$$

$$(4) \quad B \leq -A\sqrt{1+A^2-B^2} \quad \text{for} \quad y_- \quad (6.67)$$

Therefore, using y_{\pm} and conditions (1) – (4), one can find the end points of the contour $\lambda_{1,2}(\phi_{\pm})$.

In the following, we give the range for Φ to draw the singularity contour as given by the parametric form in Eqs. (6.55) and (6.56) in (λ_1, λ_2) plane.

Comparing $\lambda_{1,2}(\Phi_{\pm}) = \lambda_{1,2}(\phi_{\pm})$, we get

$$\sin \Phi_{\pm} = C_1^{\pm} \quad \text{and} \quad \cos \Phi_{\pm} = C_2^{\pm}, \quad (6.68)$$

where

$$C_1^{\pm} = \frac{\alpha}{\sqrt{1+\alpha^2}} [(1+\theta+\theta\alpha^2)\lambda_2(\phi_{\pm}) - 1], \quad (6.69)$$

$$C_2^{\pm} = \frac{1}{\sqrt{1+\alpha^2}} [(1+\theta+\theta\alpha^2)\lambda_1(\phi_{\pm}) - 1], \quad (6.70)$$

with $(C_1^{\pm})^2 + (C_2^{\pm})^2 = 1$. Using Eq. (6.68), one can find the restriction on Φ which is given as follows

$$\Phi_{\pm} = -i \ln[C_2^{\pm} + iC_1^{\pm}]. \quad (6.71)$$

Sign of $C_{1,2}^{\pm}$ can be anything. Based on the sign, it is decided that in which quadrant Φ_{\pm} are. Depending upon the sign, we modified the phase diagram Fig. 6.3 as shown in Fig. 6.4.

Given Φ_{\pm} , one can use Eq. (6.56) to plot the singularity contour in (λ_1, λ_2) plane. It is important to note that the sense or direction is always taken from Φ_- to Φ_+ (anti-clockwise). Therefore, the end point of the singularity contour are given by

[see Eq. (6.63)]

$$\lambda_{1,2}^{\pm} = \lambda_{1,2}(\Phi_{\pm}). \quad (6.72)$$

We see two regions in the phase diagram in (α, θ) plane shown in Fig. 6.3, which distinguish these two scenarios, and the equation of contour which separates these two regions is given by

$$(1 + \alpha^2)\theta = 1/3. \quad (6.73)$$

6.4.2. Case 1: Singularity contour is absent

When there is no singularity contour present in the domain \mathbb{R}_1 [see Fig. 6.2(a)], we can approximate the integral given in Eq. (6.42) by the saddle-point method. Therefore, we get

$$P_t(W_1, W_2) \approx \frac{\tilde{g}(w_1, w_2) e^{(t/t_\gamma) I(w_1, w_2)}}{2\pi t/t_\gamma \sqrt{|\tilde{H}(w_1, w_2)|}}, \quad (6.74)$$

where $\tilde{g}(w_1, w_2) := g(\lambda_1^*, \lambda_2^*)$, and $\tilde{H}(w_1, w_2) := H(\lambda_1^*, \lambda_2^*)$ is the determinant of the Hessian matrix,

$$\begin{aligned} H(\lambda_1^*, \lambda_2^*) &= \left[\frac{\partial^2 I_{w_1, w_2}(\lambda_1, \lambda_2)}{\partial \lambda_1^2} \frac{\partial^2 I_{w_1, w_2}(\lambda_1, \lambda_2)}{\partial \lambda_2^2} - \left(\frac{\partial^2 I_{w_1, w_2}(\lambda_1, \lambda_2)}{\partial \lambda_1 \partial \lambda_2} \right)^2 \right] \Big|_{\lambda_{1,2} = \lambda_{1,2}^*} \\ &= \frac{4\Lambda^4}{\alpha^2 \theta^2 (1 + \theta + \theta \alpha^2)^2}. \end{aligned} \quad (6.75)$$

The function $I(w_1, w_2)$ is given by Eq. (7.45). Here, $\tilde{H}(w_1, w_2) > 0$ for all θ , α , w_1 , and w_2 which implies that along axes $\text{Re}(\lambda_1)$ and $\text{Re}(\lambda_2)$, function $I_{w_1, w_2}(\lambda_1, \lambda_2)$ given in Eq. (6.43), is minimum at the saddle point $(\lambda_1^*, \lambda_2^*)$. Therefore, contours of integration are taken along the direction perpendicular to both $\text{Re}(\lambda_1)$ and $\text{Re}(\lambda_2)$ axes of the complex (λ_1, λ_2) plane at the saddle point $(\lambda_1^*, \lambda_2^*)$ [94, 93].

6.4.3. Case 2: Singularity contour is present

When a singularity contour is present in the region $(\lambda_1, \lambda_2) \in \mathbb{R}_1$ [see red contour (thick dashed) in Fig. 6.2(b)], we have to compute the integral given in Eq. (6.42) carefully. In such a case, there will be two types of contributions, namely, saddle and branch point contributions. When the saddle point $(\lambda_1^*, \lambda_2^*)$ does not cross the branch point contour given by Eq. (6.54) [see red contour (thick dashed) in Fig. 6.2(b)] i.e.,

the saddle point does not enter the light red region \mathbb{R}_2 of Fig. 6.2(b), the contribution is the same as given in Eq. (6.74). As the saddle point crosses the branch point contour given by Eq. (6.54), then, the integral can not be approximated with the usual saddle-point solution, and one has to evaluate Eq. (6.42) carefully by taking into account of the singularities [94, 93, 83, 91].

Since the equation of the singularity contour is given by Eq. (6.54), in the (w_1, w_2) plane, the contour separating these two regions (saddle and branch points) becomes $h(w_1, w_2) := f^-(\lambda_1^*, \lambda_2^*) = 0$. The joint probability distribution of W_1 and W_2 is given as

$$P_t(W_1, W_2) = \begin{cases} P_S(W_1, W_2, t) & h(w_1, w_2) \gg 0, \\ P_B(W_1, W_2, t) & h(w_1, w_2) \ll 0, \end{cases} \quad (6.76)$$

where $P_S(W_1, W_2, t)$ and $P_B(W_1, W_2, t)$ are saddle and branch point contributions, respectively. Signs \ll and \gg show that both saddle and branch point contributions are valid away from the singularity contour [see the red contour (thick dashed) in Fig. 6.2(b)] [94, 93].

6.4.4. Large deviation function and FT for joint distribution $P_t(W_1, W_2)$

The large deviation function is defined as

$$I(w_1, w_2) = \lim_{t/t_\gamma \rightarrow \infty} \frac{t_\gamma}{t} \ln P_t(W_1, W_2), \quad (6.77)$$

and the large deviation form of joint distribution is usually written as

$$P_t(W_1, W_2) \sim e^{(t/t_\gamma)I(w_1, w_2)}. \quad (6.78)$$

For the distribution satisfying FT, it is seen that

$$\lim_{t/t_\gamma \rightarrow \infty} \frac{t_\gamma}{t} \ln \left[\frac{P(W_1 = +w_1 t/t_\gamma, W_2 = +w_2 t/t_\gamma)}{P(W_1 = -w_1 t/t_\gamma, W_2 = -w_2 t/t_\gamma)} \right] = w_1 + w_2. \quad (6.79)$$

When the above relation holds, the large deviation function satisfies a symmetry property given as

$$I(w_1, w_2) - I(-w_1, -w_2) = w_1 + w_2 \quad \text{for all } (w_1, w_2). \quad (6.80)$$

The phase diagram given in Fig. 6.3 characterizes regions of analyticity for the prefactor $g(\lambda_1, \lambda_2)$. If $g(\lambda_1, \lambda_2)$ does not have any singularity in the region $(\lambda_1, \lambda_2) \in \mathbb{R}_1$, the dominant contribution to the joint distribution $P_t(W_1, W_2)$ comes from the saddle-point approximation as given by Eq. (6.74). However, when the saddle point $(\lambda_1^*, \lambda_2^*)$ crosses the branch point contour shown in Fig. 6.2(b) [see light red region \mathbb{R}_2 of Fig. 6.2(b)], the contribution to $P_t(W_1, W_2)$ comes from both saddle and branch points as given by Eq. (6.76). Thus, for the region where $g(\lambda_1, \lambda_2)$ does not have any singularity (see Fig. 6.3), the large deviation function $I(w_1, w_2)$ is given by Eq. (7.45) and satisfies the relation given in Eq. (6.80), and hence, the fluctuation theorem is satisfied. On the other hand, when $g(\lambda_1, \lambda_2)$ has singularities, the fluctuation theorem would not be satisfied for large (w_1, w_2) .

6.5. Probability density function of Stochastic efficiency $P(\eta, t)$

After computing the asymptotic form of $P_t(W_1, W_2)$, we have to carry out one more integral given in Eq. (6.9) to get the probability density function of stochastic efficiency. There are two cases, which we will discuss in the next subsections.

6.5.1. Case 1: $g(\lambda_1, \lambda_2)$ does not have singularities

When the asymptotic form of $P_t(W_1, W_2)$ is given by only the saddle-point contribution [see Eq. (6.74)], then the integral given in Eq. (6.9) can also be computed using the saddle-point method. In that case, by solving the saddle-point equation

$$\left. \frac{\partial I(-\eta w_2, w_2)}{\partial w_2} \right|_{w_2=w_2^*} = 0, \quad (6.81)$$

we find the saddle point $w_2^*(\eta)$ as

$$w_2^*(\eta) = \frac{(1-\eta)\alpha^2\theta\sqrt{1+\theta+\theta\alpha^2}}{\sqrt{(1+\eta^2\alpha^2)[1+\eta^2\alpha^2+\alpha^2\theta(1-\eta)^2]}}. \quad (6.82)$$

Finally, the probability density function for stochastic efficiency is given by

$$P(\eta, t) \approx \frac{t\tilde{g}(-\eta w_2^*, w_2^*)\zeta(\eta, t)}{2\pi t_\gamma \sqrt{|\tilde{H}(-\eta w_2^*, w_2^*)|}} \exp[(t/t_\gamma) I(-\eta w_2^*, w_2^*)], \quad (6.83)$$

where

$$\zeta(\eta, t) = \frac{e^{-KY^2} + \sqrt{\pi KY} \operatorname{erf}(\sqrt{KY})}{K}, \quad (6.84)$$

with $Y = w_2^*(\eta)$, $K = t/(2t_\gamma) |\partial^2 I(-\eta w_2, w_2) / \partial w_2^2|_{w_2^*}$, and $\operatorname{erf}(u)$ is given by Eq. (6.15).

The large deviation function $J(\eta) := I(-\eta w_2^*, w_2^*)$ is given by

$$J(\eta) = \frac{1}{2} \left[1 - \sqrt{\frac{(1 + \alpha^2 \eta^2)(1 + \theta + \theta \alpha^2)}{1 + \alpha^2[\eta^2 + (1 - \eta)^2 \theta]}} \right] \quad (6.85)$$

The large deviation function $J(\eta)$ for stochastic efficiency has two extrema. The minimum occurs at $\eta^* = 1$ while the maximum is at $\bar{\eta} = -\alpha^{-2}$. The efficiency at which the large deviation function is minimum is called *an analog of the Carnot efficiency* [99] as this is essentially the maximum value that the efficiency of a reversible engine can achieve in macroscopic systems. At the efficiency $\bar{\eta}$, $J(\bar{\eta}) = J'(\eta = \bar{\eta}) = 0$, which are the properties of a large deviation function.

6.5.2. Numerical simulation

We compare the analytical form given in Eq. (6.83) with the numerical simulation (see Appendix A). We take parameter $\theta = 0.1$ and $\alpha = 0.5$ at three different times: $t/t_\gamma = 20$, $t/t_\gamma = 50$, and $t/t_\gamma = 100$. Figure 6.5 shows a very good agreement with simulation and theoretical prediction.

6.5.3. Case 2: $g(\lambda_1, \lambda_2)$ has singularities

When $g(\lambda_1, \lambda_2)$ has singularities in the region $(\lambda_1, \lambda_2) \in \mathbb{R}_1$ [see Fig. 6.2(b)], we need to be careful while computing the asymptotic form of $P_t(W_1, W_2)$, as given by Eq. (6.76).

It turns out that the saddle point $w_2^*(\eta)$ given in Eq. (6.82), from the saddle-point contribution of $P_t(-\eta W_2, W_2)$ stays either in saddle point region (possibility I) or in both saddle- and branch-point regions (possibility II) of $P_t(-\eta w_2, w_2)$ depending upon parameters θ and α as shown in Fig. 6.6. In Fig. 6.6 light blue (S.P. region) and light red (B.P. region) regions correspond to the saddle- and branch-point contributions of joint distribution $P_t(-\eta W_2, W_2)$, respectively.

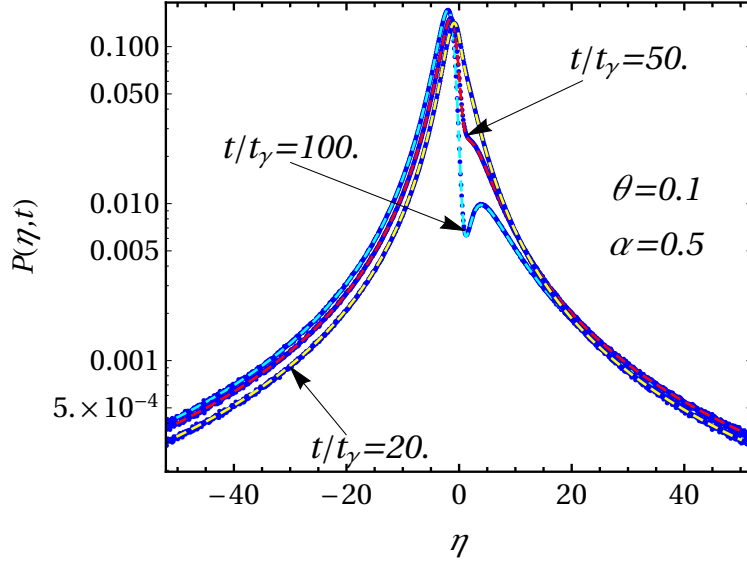


FIGURE 6.5: Distribution of stochastic efficiency $P(\eta, t)$ is plotted against the stochastic efficiency η for $\theta = 0.1$ and $\alpha = 0.5$ at three different times: $t/t_\gamma = 20, 50, 100$. Yellow ($t/t_\gamma = 20$), red ($t/t_\gamma = 50$), and cyan ($t/t_\gamma = 100$) dashed lines are plotted for analytical expression given in Eq. (6.83) while the blue dots are for the numerical simulations at the corresponding times t/t_γ .

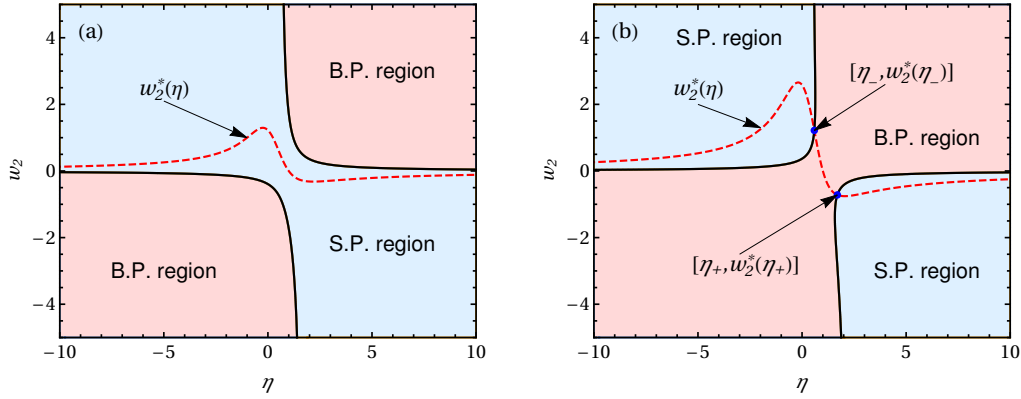


FIGURE 6.6: Two possibilities are shown. (a) Saddle point $w_2^*(\eta)$ stays in the saddle-point region of $P_t(-\eta W_2, W_2)$. (b) Saddle point $w_2^*(\eta)$ stays in both the saddle- and branch-point regions of $P_t(-\eta W_2, W_2)$. Light blue (S.P. region) [$h(-\eta w_2, w_2) > 0$] and light red (B.P. region) [$h(-\eta w_2, w_2) < 0$] shaded areas are for saddle- and branch-point contributions of $P_t(-\eta W_2, W_2)$, respectively. Black solid line corresponds to $h(-\eta w_2, w_2) = 0$. Blue points are given by $(\eta_-, w_2^*(\eta_-))$ and $(\eta_+, w_2^*(\eta_+))$.

As saddle point $w_2^*(\eta)$ intersects the contour $h(-\eta w_2, w_2) = 0$, it satisfies

$$h(-\eta_\pm w_2^*(\eta_\pm), w_2^*(\eta_\pm)) = 0, \quad (6.86)$$

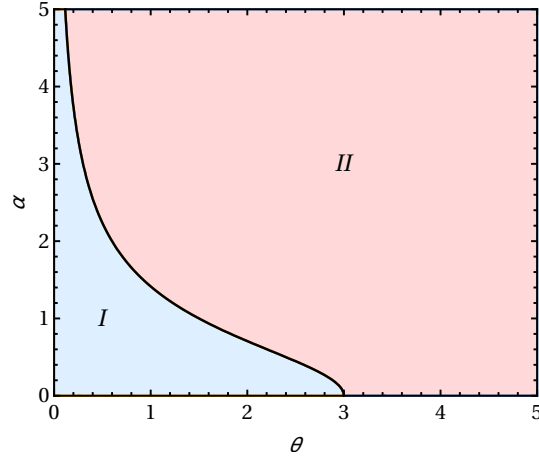


FIGURE 6.7: Possibility I: The distribution of efficiency $P(\eta, t)$ can be computed by only saddle point solution given by Eq. (6.74). Possibility II: The distribution of efficiency $P(\eta, t)$ requires the branch point contribution of $P_t(-\eta W_2, W_2)$.

in which

$$\eta_{\pm} = \frac{4\alpha\theta \pm \sqrt{3(1+\theta+\theta\alpha^2)}\sqrt{-3+\theta+\theta\alpha^2}}{\alpha[3(1+\theta)-\alpha^2\theta]}. \quad (6.87)$$

Therefore, points where saddle point $w^*(\eta)$ intersects the contour $h(-\eta w_2, w_2) = 0$ are given by $(\eta_-, w_2^*(\eta_-))$ and $(\eta_+, w_2^*(\eta_+))$. Note that in Fig. 6.6(b), we have shown possibility II when $\eta_- < \eta_+$. The contour, which separates possibility I from possibility II in the (θ, α) space, is given by the condition $\eta_+ = \eta_-$, which results in

$$-3 + \theta + \theta\alpha^2 = 0. \quad (6.88)$$

It also follows from the fact that the efficiency is a real quantity, and therefore, η_{\pm} must be real, which implies $(-3 + \theta + \theta\alpha^2) \geq 0$.

Using the above equation, we can draw a phase diagram in the (θ, α) plane as shown in Fig. 6.7. In possibility I, saddle point $w^*(\eta)$ does not intersect the contour given by $h(-\eta w_2, w_2) = 0$, and stays in the saddle point region of joint distribution $P_t(-\eta W_2, W_2)$. Therefore, only the saddle-point contribution of $P(-\eta W_2, W_2)$ is required to compute the asymptotic expression of $P(\eta, t)$. But, for possibility II, we actually need to compute the branch-point contribution to calculate the asymptotic

expression for $P(\eta, t)$. Therefore, the distribution of efficiency $P(\eta, t)$ is given as

$$P(\eta, t) \begin{cases} = \text{Eq. (6.83)} & h(-\eta w_2, w_2) > 0 \\ \neq \text{Eq. (6.83)} & h(-\eta w_2, w_2) < 0. \end{cases} \quad (6.89)$$

The analytical computation of the joint distribution for possibility II is not very illuminating. Nevertheless, we can perform numerical saddle-point integration to calculate $P(\eta, t)$. This method is described in the following subsection.

6.5.4. Numerical saddle-point integration

We write the integral given in Eq. (6.42) as

$$P_t(-\eta W_2, W_2) = \int_{-i\infty}^{i\infty} \frac{d\lambda_1}{2\pi i} \int_{-i\infty}^{i\infty} \frac{d\lambda_2}{2\pi i} g_0(\lambda_1, \lambda_2) e^{(t/t_\gamma) f(\lambda_1, \lambda_2, \eta, w_2, t)}, \quad (6.90)$$

with

$$f(\lambda_1, \lambda_2, \eta, w_2, t) = I_{-\eta w_2, w_2}(\lambda_1, \lambda_2) - \frac{t_\gamma}{2t} \ln f^-(\lambda_1, \lambda_2). \quad (6.91)$$

Here $g_0(\lambda_1, \lambda_2)$ is the analytic part of $g(\lambda_1, \lambda_2)$, given as

$$g_0(\lambda_1, \lambda_2) = \frac{2\sqrt{v(\lambda_1, \lambda_2)}}{\sqrt{f^+(\lambda_1, \lambda_2)}}. \quad (6.92)$$

Therefore, the saddle point $(\lambda_1^*(\eta, w_2, t), \lambda_2^*(\eta, w_2, t))$ is the solution of following equations simultaneously:

$$\left. \frac{\partial f(\lambda_1, \lambda_2, \eta, w_2, t)}{\partial \lambda_1} \right|_{\lambda_{1,2}=\lambda_{1,2}^*(\eta, w_2, t)} = 0, \quad (6.93)$$

$$\left. \frac{\partial f(\lambda_1, \lambda_2, \eta, w_2, t)}{\partial \lambda_2} \right|_{\lambda_{1,2}=\lambda_{1,2}^*(\eta, w_2, t)} = 0. \quad (6.94)$$

For a given value of η , we compute the saddle point $(\lambda_1^*(\eta, w_2, t), \lambda_2^*(\eta, w_2, t)) \in \mathbb{R}_1 - \mathbb{R}_2$ where $g(\lambda_1, \lambda_2)$ is analytic, at fixed θ , α , and t as a function of w_2 . Further, we compute the integral given in Eq. (6.90), numerically. Finally, the numerical expression for $P_t(-\eta W_2, W_2)$ is utilized to compute the distribution of efficiency for a given efficiency η .

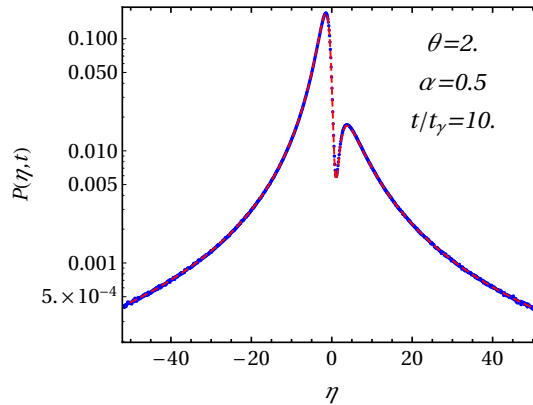


FIGURE 6.8: Distribution of stochastic efficiency $P(\eta, t)$ is plotted against the stochastic efficiency η for $\theta = 2$ and $\alpha = 0.5$ at time $t/t_\gamma = 10$. Red dashed lines plotted for analytical expression given in Eq. (6.83) while the blue dots are for the numerical simulation.

6.5.5. Numerical simulation: Possibility I

We compare the analytical results given by Eq. (6.83) with the numerical simulation (see Appendix A) for parameters $\theta = 2.0$ and $\alpha = 0.5$ at time $t/t_\gamma = 10$. Note that the point (θ, α) we have chosen lies in the region (see Figs. 6.3 and 6.7) where $g(\lambda_1, \lambda_2)$ has singularities. Figure 6.8 shows very good agreement between numerical simulation and theoretical prediction.

6.5.6. Numerical simulation: Possibility II

We compare the numerical simulation (see Appendix A) for the distribution of stochastic efficiency with the result obtained by the numerical saddle-point integration explained in Sec. 6.5.4, for $\theta = 3.0$ and $\alpha = 0.5$ at time $t/t_\gamma = 50$. Figure 6.9 shows that there is nice agreement between numerical simulation and theoretical prediction.

6.6. Summary

We have considered a microscopic engine in which a Brownian particle is coupled to a heat bath at a constant temperature, and two external time-dependent forces, called load force and drive force, are applied to the particle. Both forces are assumed to be uncorrelated and stochastic Gaussian noises. The function of the drive force is to drive the Brownian particle against the load force. Work done by the load force and the drive force, W_1 and W_2 , respectively, are stochastic quantities. Hence,

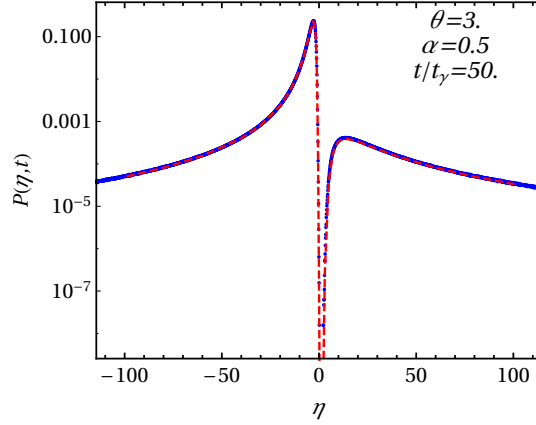


FIGURE 6.9: Distribution of stochastic efficiency $P(\eta, t)$ is plotted against the stochastic efficiency η for $\theta = 3$ and $\alpha = 0.5$ at time $t/t_\gamma = 50$. The red dashed line is plotted for the distribution $P(\eta, t)$ evaluated numerically as explained in Sec. 6.5.4 while the blue dots correspond to the numerical simulation.

the efficiency of the engine, which is the ratio of output work to the input work, $\eta = -W_1/W_2$, is also a stochastic quantity. In this chapter, we have computed the distribution of stochastic efficiency $P(\eta, t)$ for large t .

To compute $P(\eta, t)$, we have first computed the characteristic function $\langle e^{-\lambda_1 W_1 - \lambda_2 W_2} \rangle \sim g(\lambda_1, \lambda_2) e^{(t/t_\gamma)\mu(\lambda_1, \lambda_2)}$. The asymptotic form of the joint distribution $P_t(W_1, W_2)$ for large t is usually obtained by inverting the characteristic function using a saddle-point approximation. We have found that $g(\lambda_1, \lambda_2)$ can have singularities within the domain where the saddle point lies, and in that case we have computed the asymptotic distribution $P_t(W_1, W_2)$ by taking the singularities into account. Whether $g(\lambda_1, \lambda_2)$ has singularities or not depends on the choice of the parameters θ and α (see Fig. 6.3), which describe the strengths of the external forces relative to each other as well as to the strength of the thermal noise.

Using $P_t(W_1, W_2)$, we have finally computed $P(\eta, t)$, which have the large deviation form $P(\eta, t) \sim \exp[(t/t_\gamma)J(\eta)]$. The large deviation function $J(\eta)$ shows two extrema: a minimum η^* corresponds to *an analog of Carnot efficiency* while the maximum $\bar{\eta}$ is at the most probable efficiency.

As a final remark, since the random external forcing can be realized in an experimental setup [49], it would be interesting to compare the theoretical results obtained here with experiments.

Chapter 7

Exact distribution for work and stochastic efficiency of an isothermal machine

We consider an isothermal machine composed of two Brownian particles (say particle A and B) connected by a harmonic spring. A constant load is attached to particle A, and the particle B is trapped in a harmonic confinement whose minimum is dragged with a constant velocity. The distribution of work done on particle A, particle B, and on both particles together is obtained, and the corresponding transient fluctuation theorem is tested. Furthermore, we compute the stochastic efficiency which is the ratio of the work done against the load force on particle A and the work done on particle B of this machine. The probability density function for stochastic efficiency is computed for all time. Numerical simulations are also done to verify the analytical results.

7.1. Introduction

The function of an engine is to convert one form of energy into another form. For example, windmills convert wind energy to electrical energy as a wind turbine or to pump the water as a windpump, a turbine connected to an electric generator utilizes the energy from the flowing water to convert into electrical energy, a refrigerator pumps the heat from the cold environment to the hot environment, etc. The performance of an engine depends on the amount of output power it delivers at the

expense of the input power. For instance, a heat engine [15, 58, 147] extracts heat Q_h from the hot reservoir at a temperature T_h and dumps some amount of heat Q_c to the cold reservoir at a temperature $T_c < T_h$ in a cyclic manner, and it generates useful work $W = Q_h - Q_c$. The efficiency η of such an engine is given by $\eta = W/Q_h$, and it is bounded from above by the Carnot efficiency $\eta_c = 1 - T_c/T_h$, i.e. $\eta \leq \eta_c$, where η_c is the maximum possible efficiency achieved by an engine operating in a quasi-static limit and in a reversible fashion. Hence, an engine operating at Carnot efficiency has zero power (output work per unit time) and is practically useless to do a work in a reasonable amount of time.

For a microscopic machine or engine converting the input power into the output power, the efficiency which is the ratio of the output power and the input power is a stochastic quantity. In this area, a number of studies have been done to understand the statistics of it [142, 46, 100, 99, 101, 102, 5, 127, 96] (see Chapter 6). Moreover, several experiments have been performed to understand the efficiency of a microscopic engine [9, 73], and fluctuation of it [103, 87]. In the previous chapter [55], we generalized a model of an isothermal work-to-work converter engine given in [142] in the underdamped limit using the stochastic external load and stochastic drive force instead of constant external forces Sec. 6.2.1. We obtained the large deviation function and large but finite time probability density function for the stochastic efficiency of an isothermal engine in the non-equilibrium steady state.

In this chapter [50], we consider a one-dimensional isothermal engine composed of two Brownian particles (say A and B) interacting with each other with a harmonic potential where particle B is confined in a harmonic trap. When time $t \leq 0$, the minimum of the harmonic trap is stationary and is at the origin of the x -axis. Hence, the system has equilibrium Boltzmann's distribution at $t = 0$. The minimum of the harmonic confinement is dragged with a constant velocity and a load is attached to the Brownian particle A for a duration τ which is measured immediately after the motion of the harmonic trap. We study the work done on particle A (W_A) and particle B (W_B), and the stochastic efficiency η of this isothermal engine which is the ratio of the work done against the load on particle A to the work done on particle B by dragging the minimum of the harmonic potential with a constant velocity. The probability density function for W_A , W_B , and η are obtained for all time. Notice that

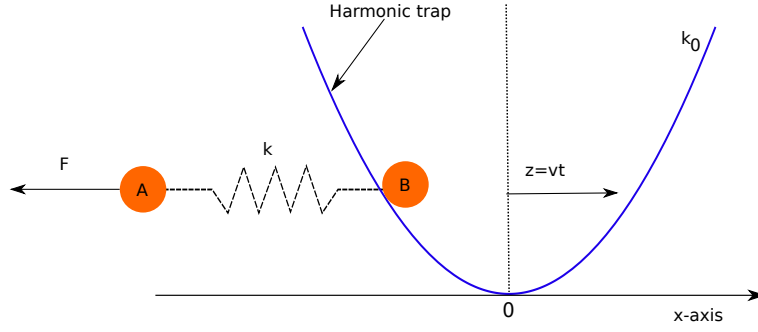


FIGURE 7.1: The schematic diagram for an isothermal work-to-work converter machine is shown. The particle B is confined in a harmonic trap of stiffness constant k_0 . The particle A is coupled harmonically with particle B with a spring of stiffness k . The whole setup is immersed in a heat bath (not shown) of constant temperature T . When $t \geq 0$, the minimum of the potential z is moved with a constant velocity v , i.e. $z = vt$ for $t \in [0, \tau]$, and a load F is attached to particle A. Sign of F is taken to be negative if the load is pulling the particle A and sign of v is taken to be positive if the minimum of the trap is moving towards positive direction of x -axis. The vertical dotted line indicates the location of the minimum of the harmonic trap at time t .

a model system similar to our machine can be realized in an experiment [14, 106].

The chapter is organized as follows. In Sec. 7.2, we give the model system and definitions of work done on particle A, particle B, and the stochastic efficiency. Section 7.3 contains the joint distribution of the work done on particle A and particle B. The transient fluctuation theorem [34] is studied for work done on particle A and B in Sec. 7.4. In Sec. 7.5, we discuss the transient fluctuation theorem for total work done on the system. The probability density function for the stochastic efficiency is computed in Sec. 7.6. We summarize this chapter in Sec. 7.7.

7.2. Model

Consider a model of a machine consists of two Brownian particles (say particle A and B) coupled by a harmonic spring of stiffness k . Suppose particle B is trapped in a harmonic confinement of stiffness k_0 . The whole setup is immersed in a heat bath of a constant temperature T . The potential energy of the system is given by

$$V(x_A, x_B, t) = \frac{k}{2}(x_A - x_B)^2 + \frac{k_0}{2}(x_B - z)^2, \quad (7.1)$$

where z is the minimum of the harmonic trap which is time-dependent, and x_A and x_B are the positions of particle A and B, respectively.

Suppose the minimum of the harmonic trap is moved with a constant finite velocity v and is at $z = vt$ at time t , and a constant finite load F is attached to particle A from time $t = 0$ to $t = \tau$, i.e. τ is the duration which is measured immediately after the trap is being set into the motion. The schematic diagram of the machine is shown in Fig. 7.1. Notice that a model for a single Brownian particle confined in a harmonic potential ($k = 0$) whose minimum is dragged with a given velocity is already studied both theoretically [88, 150, 151, 149] and experimentally [144, 145].

The dynamics of the given system is described by the following overdamped Langevin equations

$$\gamma \dot{x}_A = -k(x_A - x_B) + \zeta_A(t) + F, \quad (7.2)$$

$$\gamma \dot{x}_B = -k(x_B - x_A) + \zeta_B(t) - k_0(x_B - z), \quad (7.3)$$

where dot represents a derivative with respect to time, γ is the dissipation constant, $\zeta_A(t)$ and $\zeta_B(t)$ are the thermal noises acting on particle A and B, respectively, from the heat bath, having mean zero and correlation $\langle \zeta_i(t) \zeta_j(t') \rangle = 2\gamma T \delta_{ij} \delta(t - t')$. We set Boltzmann's constant $k_B = 1$ throughout the calculation.

Multiplying Eq. (7.2) by $\dot{x}_A(t)$ and Eq. (7.3) by $\dot{x}_B(t)$ on both sides, integrating over time from $t = 0$ to $t = \tau$, and adding them together, yields first law of thermodynamics

$$\Delta V = W_A + W_B + Q_A + Q_B, \quad (7.4)$$

in which

$$\Delta V = \frac{1}{T} [V(x_A(\tau), x_B(\tau), \tau) - V(x_A(0), x_B(0), 0)], \quad (7.5)$$

$$W_A = \frac{F}{T} \int_0^\tau dt \dot{x}_A(t) = \frac{F}{T} [x_A(\tau) - x_A(0)], \quad (7.6)$$

$$W_B = \frac{v\gamma}{T\tau_\gamma} \int_0^\tau dt [z - x_B(t)], \quad (7.7)$$

$$Q_A = \frac{1}{T} \int_0^\tau dt [\zeta_A(t) - \gamma \dot{x}_A(t)] \dot{x}_A(t), \quad (7.8)$$

$$Q_B = \frac{1}{T} \int_0^\tau dt [\zeta_B(t) - \gamma \dot{x}_B(t)] \dot{x}_B(t). \quad (7.9)$$

In Eq. (7.7), $\tau_\gamma = \gamma/k_0$ is the characteristic time scale. Notice that observables given in Eqs. (7.5)–(7.9) are scaled by temperature T of the thermal bath. Therefore, ΔV is the change in dimensionless potential energy, W_A and W_B are the dimensionless work done on particle A and B, respectively, and Q_A and Q_B are the dimensionless heat absorbed (i.e. negative of the entropy change in the heat bath) by particle A and B from the heat bath, respectively. For convenience, we drop the word dimensionless to address them in the rest of chapter. Moreover, the quantities W'_i s (Q'_i s) are taken to be positive if work is performed on (heat is absorbed by) i th particle. These quantities are measured with respect to the initial steady state distribution given in Eq. (7.12). In Eqs. (7.6) and (7.7), work done on particle A and B are due to purely non-conservative and conservative force, respectively. The integrals shown in Eqs. (7.8) and (7.9) follow the Stratonovich rule of integration [124].

The observable in this chapter is efficiency η of the machine which is the ratio of work done ($-W_A$) against the load force F on particle A to the work done (W_B) on particle B, i.e.

$$\eta = -\frac{W_A}{W_B}. \quad (7.10)$$

In the above expression, both W_A and W_B are stochastic quantities. Therefore, the efficiency is also a stochastic observable. The probability density function for the stochastic efficiency $p_\tau(\eta)$ is computed as follows:

$$\begin{aligned} p_\tau(\eta) &= \int_{-\infty}^{+\infty} dW_A \int_{-\infty}^{+\infty} dW_B P_\tau(W_A, W_B) \delta(\eta + W_A/W_B) \\ &= \int_{-\infty}^{+\infty} dW_B |W_B| P_\tau(-\eta W_B, W_B), \end{aligned} \quad (7.11)$$

where $|W_B|$ is the Jacobian of transformation obtained after performing the integration on the joint distribution $P_\tau(W_A, W_B)$ of W_A and W_B at time τ over W_A while using the Dirac delta function $\delta(\eta + W_A/W_B)$.

7.3. Joint distribution $P_\tau(W_A, W_B)$

In this chapter, our aim is to compute the efficiency of a machine which does work against the load F attached to particle A by dragging the harmonic trap which confines the particle B from time $t = 0$ to $t = \tau$. When time $t \leq 0$, there was no load

attached to particle A, and the minimum of the trap was at the origin of x -axis, i.e. $z = 0$. Thus, the system obeys the steady state distribution at time $t = 0$:

$$P(U_0) = \frac{1}{\sqrt{(2\pi)^2 \det \Sigma}} \exp \left[-\frac{1}{2} U_0^T \Sigma^{-1} U_0 \right], \quad (7.12)$$

where the row vector $U_0^T = [x_A(0), x_B(0)]$, and the correlation matrix

$$\Sigma = \frac{T\tau_\gamma}{\gamma} \begin{pmatrix} 1 + 1/\delta & 1 \\ 1 & 1 \end{pmatrix}, \quad (7.13)$$

in which $\delta = k/k_0$ is the dimensionless coupling parameter.

For $t \geq 0$, the dynamics of the system given in Eqs. (7.2) and (7.3), can be rewritten in a matrix form as

$$\frac{dU}{dt} = -\frac{1}{\tau_\gamma} AU + \frac{1}{\gamma} \zeta(t) + B(t), \quad (7.14)$$

where column vectors $\zeta(t) = [\zeta_A(t), \zeta_B(t)]^T$, $B(t) = (F/\gamma, z/\tau_\gamma)^T$, and the matrix A is

$$A = \begin{pmatrix} \delta & -\delta \\ -\delta & 1 + \delta \end{pmatrix}.$$

The solution of above equation at time t is given by

$$U(t) = G(t)U_0 + \frac{1}{\gamma} \int_0^t dt' G(t-t') [\gamma B(t') + \zeta(t')], \quad (7.15)$$

where the symmetric matrix $G(t) = e^{-(t/\tau_\gamma)A}$ is given by

$$G(u_t) = \begin{pmatrix} G_{11}(u_t) & G_{12}(u_t) \\ G_{12}(u_t) & G_{22}(u_t) \end{pmatrix}, \quad (7.16)$$

in which

$$\begin{aligned} G_{11}(u_t) &= -\frac{1}{4r_2}[1 - 2r_2 - (1 + 2r_2)e^{2r_2u_t}]e^{-\lambda_1u_t}, \\ G_{12}(u_t) &= -\frac{1}{2r_2}\delta(1 - e^{2r_2u_t})e^{-\lambda_1u_t}, \\ G_{22}(u_t) &= \frac{1}{4r_2}[1 + 2r_2 - (1 - 2r_2)e^{2r_2u_t}]e^{-\lambda_1u_t}. \end{aligned}$$

In the above matrix elements, $u_t = t/\tau_\gamma$, $r_1 = \frac{1+2\delta}{2}$, $r_2 = \frac{\sqrt{1+4\delta^2}}{2}$, $\lambda_1 = r_1 + r_2$, and $\lambda_2 = r_1 - r_2$. Clearly, $\lambda_1 > \lambda_2 > 0$ for all $\delta > 0$.

Therefore, the mean and correlation of $U(t)$ are

$$\overline{\langle U(t) \rangle} = \int_0^t dt' G(t-t')B(t'), \quad (7.17)$$

$$\overline{\langle M(t)M^T(t) \rangle} = \Sigma, \quad (7.18)$$

where superscript T refers the transpose of a matrix, Σ is given in Eq. (7.13), and $M(t) = U(t) - \overline{\langle U(t) \rangle}$. In the above equations, the angular brackets and overhead bar represent the averaging over thermal noises and the initial state U_0 with respect to the steady state distribution $P(U_0)$ [see Eq. (7.12)], respectively. After some computation, the mean of $U(t)$ is obtained as

$$\begin{aligned} \overline{\langle x_A \rangle} &= \frac{F\tau_\gamma}{8\gamma\delta r_2} e^{-2r_1u_t} \left[4r_2 e^{2r_1u_t} [2 - \theta + 2\delta + \delta\theta(u_t - 2)] + e^{\lambda_2u_t} [(1 - 2r_2)(2 - \theta) \right. \\ &\quad \left. + (1 - \theta)\{4\delta^2 + 2\delta(1 - 2r_2)\}] - e^{\lambda_1u_t} [(1 + 2r_2)(2 - \theta) + (1 - \theta)\{4\delta^2 + 2\delta(1 + 2r_2)\}] \right], \\ \overline{\langle x_B \rangle} &= \frac{F\tau_\gamma}{4\gamma r_2} e^{-\lambda_1u_t} \left[1 + 2(\delta - r_2)(1 - \theta) - e^{2r_2u_t} [1 + 2(1 - \theta)(\delta + r_2)] + 2r_2 e^{\lambda_1u_t} [2 + \theta(u_t - 2)] \right], \end{aligned}$$

where the dimensionless parameter $\theta = 2v\gamma/F$ is the relative strength acting on the harmonic trap which confines particle B to that on particle A.

The work done on the particle A and B at time τ are given in Eqs. (7.6) and (7.7), respectively. Both of these quantities are linear in thermal noises. Therefore, it is sufficient to compute the means and correlations of them to write the joint distribution

$P_\tau(W_A, W_B)$, and these are given by

$$\mu_A = \frac{F}{T} \overline{\langle x_A(\tau) \rangle}, \quad (7.19)$$

$$\mu_B = \frac{v^2 \tau^2 \gamma}{2T \tau_\gamma} - \frac{v \gamma}{T \tau_\gamma} \int_0^\tau dt \overline{\langle x_B(t) \rangle}, \quad (7.20)$$

$$C_{AA} = \frac{2F^2}{T^2} [\{1 - G_{11}(\tau)\} \overline{x_A^2(0)} - G_{12}(\tau) \overline{x_A(0)x_B(0)}], \quad (7.21)$$

$$C_{BB} = \frac{v^2 \gamma^2}{T^2 \tau_\gamma^2} \int_0^\tau dt_1 \int_0^\tau dt_2 \overline{\langle M_{21}(t_1) M_{21}(t_2) \rangle}, \quad (7.22)$$

$$C_{AB} = -\frac{Fv\gamma}{T^2 \tau_\gamma} \int_0^\tau dt \overline{\langle M_{21}(t) [M_{11}(\tau) - x_A(0)] \rangle} = 0, \quad (7.23)$$

where the matrix elements $G_{ij}(t) = [G(t)]_{ij}$, $M_{i1}(t) = [M(t)]_{i1}$, and $\mu_r = \overline{\langle W_r \rangle}$, $C_{rl} = \overline{\langle [W_r - \overline{\langle W_r \rangle}] [W_l - \overline{\langle W_l \rangle}] \rangle}$ with $\{i, j\} = \{1, 2\}$ and $\{r, l\} = \{A, B\}$. In Eq. (7.21), $\overline{x_A^2(0)} = [\Sigma]_{11}$ and $\overline{x_A(0)x_B(0)} = [\Sigma]_{12}$. The explicit form of mean and correlation of W_A and W_B are given as

$$\begin{aligned} \mu_A = & \frac{\alpha^2 \tau_\gamma}{8\delta r_2} \left[4r_2 [2(1 + \delta) + \theta(\delta u_\tau - 1 - 2\delta)] + [\{2 - \theta + 2\delta(1 - \theta)\}(1 - 2r_2) \right. \\ & \left. + 4\delta^2(1 - \theta)] e^{-\lambda_1 u_\tau} - [\{2 - \theta + 2\delta(1 - \theta)\}(1 + 2r_2) + 4\delta^2(1 - \theta)] e^{-\lambda_2 u_\tau} \right], \end{aligned} \quad (7.24)$$

$$\begin{aligned} \mu_B = & -\frac{\alpha^2 \theta \tau_\gamma}{2} \left[(1 - \theta) u_\tau + [1 - 2r_2 + 2\delta(1 - \theta) + 2\theta r_2] \frac{(1 - e^{-\lambda_1 u_\tau})}{4r_2 \lambda_1} \right. \\ & \left. - [1 + 2r_2 + 2\delta(1 - \theta) - 2\theta r_2] \frac{(1 - e^{-\lambda_2 u_\tau})}{4r_2 \lambda_2} \right], \end{aligned} \quad (7.25)$$

$$\begin{aligned} C_{AA} = & \frac{\alpha^2 \tau_\gamma}{2\delta r_2} \left[4(1 + \delta)r_2 + [(1 + \delta)(1 - 2r_2) + 2\delta^2] e^{-\lambda_1 u_\tau} - [(1 + \delta)(1 + 2r_2) \right. \\ & \left. + 2\delta^2] e^{-\lambda_2 u_\tau} \right], \end{aligned} \quad (7.26)$$

$$\begin{aligned} C_{BB} = & \frac{\alpha^2 \theta^2 \tau_\gamma}{16\delta r_2^2} \left[8r_2^2 [2\delta(u_\tau - 2) - 1] + [1 - 2r_2 + 4\delta(1 - r_2) + 4\delta^2(1 + 4\delta - 4r_2)] e^{-\lambda_1 u_\tau} \right. \\ & \left. + [1 + 2r_2 + 4\delta(1 + r_2) + 4\delta^2(1 + 4\delta + 4r_2)] e^{-\lambda_2 u_\tau} \right], \end{aligned} \quad (7.27)$$

$$C_{AB} = 0, \quad (7.28)$$

where $u_\tau = \tau/\tau_\gamma$, and $\alpha = F/\sqrt{\gamma T}$ is the relative strength acting on particle A to that of thermal bath.

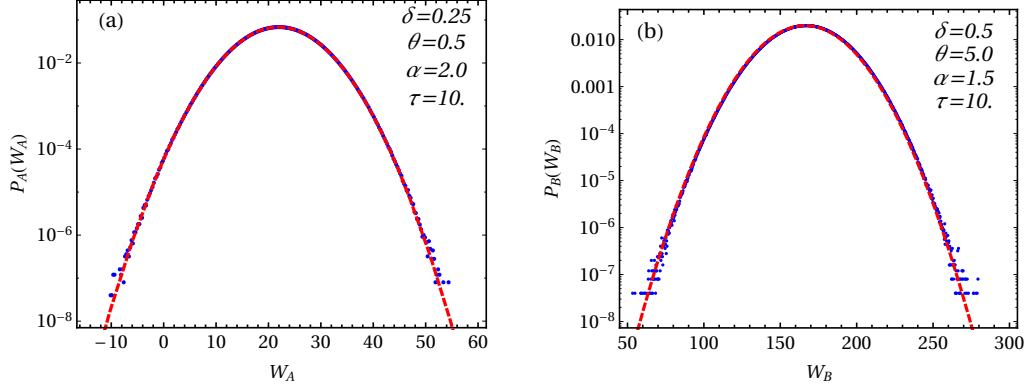


FIGURE 7.2: The probability density function for work done on particle A and B is shown for: (a) $\theta = 0.5$, $\alpha = 2.0$, coupling parameter $\delta = 0.25$ at $\tau = 10$, and (b) $\theta = 5.0$, $\alpha = 1.5$, coupling parameter $\delta = 0.5$ at time $\tau = 10$. In both figures, red dashed lines are the analytical results given in Eq. (7.29), and blue dots are obtained from numerical simulations at the respective times τ . These results are shown for fixed $\tau_\gamma = 1$.

Since the correlation between W_A and W_B is zero: $C_{AB} = 0$, the joint distribution $P_\tau(W_A, W_B)$ can be written in factorize form: $P_\tau(W_A, W_B) = P_A(W_A)P_B(W_B)$, where

$$P_r(W_r) = \frac{1}{\sqrt{2\pi C_{rr}}} \exp \left[-\frac{(W_r - \mu_r)^2}{2C_{rr}} \right], \quad r = A, B. \quad (7.29)$$

For convenience, we have dropped the subscript τ in $P_r(W_r)$.

In order to verify the analytical probability density functions of W_A and W_B , we perform the numerical simulation. The method of the numerical simulation is as follows. We first discretize the overdamped Langevin equations given in Eqs. (7.2)–(7.3) upto an order of time increment $\Delta\tau$. Similarly, we discretize the observable W_B given in Eq. (7.7) upto an order $\Delta\tau$. For each realization, we draw the initial positions $x_A(0)$ and $x_B(0)$ at step $n = 0$ from the joint distribution given in Eq. (7.12), and compute $x_A(\Delta\tau)$ and $x_B(\Delta\tau)$, and then using them we compute $W_B(\Delta\tau)$. In the next increment ($n = 1$), we use $x_A(\Delta\tau)$ and $x_B(\Delta\tau)$, and $W_B(\Delta\tau)$ to compute $x_A(2\Delta\tau)$ and $x_B(2\Delta\tau)$, and $W_B(2\Delta\tau)$, respectively. Similarly, we iterate the process for steps $n = (\tau/\Delta\tau) - 1$ to obtain W_B at time τ . To compute the observable W_A given in Eq. (7.6), we need only boundary terms $x_A(\tau)$ and $x_A(0)$ where τ is the observation time. For R number of realization, we construct the histogram for each W_i . In the chapter, we take dissipation constant $\gamma = 1$, temperature of the bath $T = 1$, time segment $\Delta\tau = 10^{-2}$, and number of realizations $R = 10^7 - 10^8$ for each numerical

simulation.

In Fig. 7.2, we have shown the comparison of the analytical result of the probability density function given in Eq. (7.29), with the numerical simulation. The plots show that there is nice agreement between theory and numerical simulation.

7.4. Transient fluctuation theorem for work done W_A and W_B

For a system initially in equilibrium and then driven away from equilibrium using external driving, the stochastic quantity Ω is observed. Let $P(\Omega)$ be the probability density function of Ω . When Ω satisfies the transient fluctuation theorem (TFT) [34], it obeys the following relation

$$\frac{P(\Omega)}{P(-\Omega)} = e^{\Omega}. \quad (7.30)$$

The above relation states that the probability of getting positive values of Ω is exponentially favourable than that of negative values.

In this section, we analyze TFT for both W_A and W_B . It is clear that TFT may not hold for all parameters [see Eqs. (7.24)–(7.27)]. One may guess that the TFT for work done on one of the particles in the coupled system shown in Fig. 7.1 would hold in the weak coupling limit as both particles may behave independently. However, we show that TFT for work done W_A and W_B may not hold even in the weak coupling limit when the observation time is large. Similar studies in the case of steady state fluctuation theorem for partial entropy production are already been done (see Chapters 2 and 3) [52, 54, 53].

In the weak coupling limit ($\delta \rightarrow 0$) and for small observation time ($u_\tau \ll \delta^{-1}$), the means and correlations given in Eqs. (7.24)–(7.27) reduce to

$$\tilde{\mu}_A = \alpha^2 u_\tau \tau_\gamma + O(\delta), \quad (7.31)$$

$$\tilde{\mu}_B = \frac{\alpha^2 \theta^2 \tau_\gamma}{4} (e^{-u_\tau} + u_\tau - 1) + O(\delta), \quad (7.32)$$

$$\tilde{C}_{AA} = 2\alpha^2 u_\tau \tau_\gamma + O(\delta), \quad (7.33)$$

$$\tilde{C}_{BB} = \frac{\alpha^2 \theta^2 \tau_\gamma}{2} (e^{-u_\tau} + u_\tau - 1) + O(\delta), \quad (7.34)$$

where $u_\tau = \tau / \tau_\gamma$.

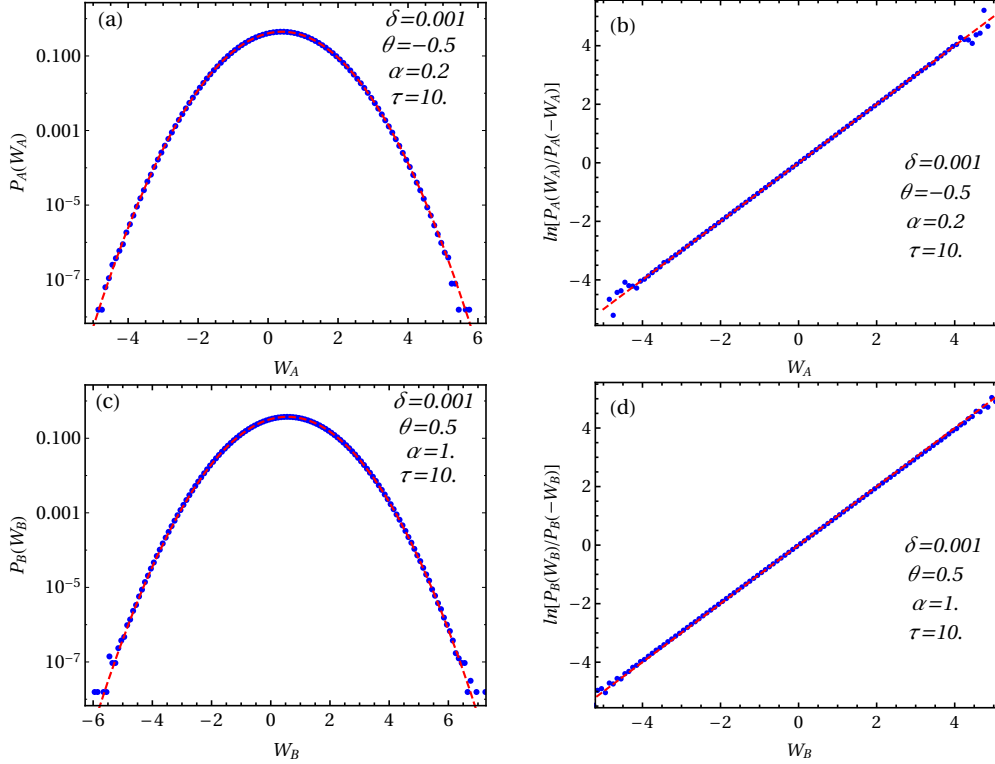


FIGURE 7.3: The probability density function for work done on particle A and B, respectively, is shown for: (a) $\theta = -0.5$ and $\alpha = 0.2$, and (b) $\theta = 0.5$ and $\alpha = 1$. Similarly, the function $\ln[P_i(W_i)/P_i(-W_i)]$ is plotted against W_i for: (b) $\theta = -0.5$ and $\alpha = 0.2$, and (d) $\theta = 0.5$ and $\alpha = 1$. In all figures, red dashed lines are the analytical result obtained from Eq. (7.29) with cumulants given in Eqs. (7.31)–(7.34) whereas blue dots are obtained from numerical simulations. These results are shown for observation time $\tau = 10$ and coupling parameter $\delta = 0.001$ ($\tau \ll \delta^{-1}$) at fixed $\tau_\gamma = 1$. In figures (b) and (d), red dashed lines have slope unity which indicate that probability density functions for both work done (W_A and W_B) satisfy TFT in the weak coupling limit ($\delta \ll 1$) for small observation time ($\tau \ll \delta^{-1}$).

Using above equations, one can see that $\tilde{C}_{AA} = 2\tilde{\mu}_A$ and $\tilde{C}_{BB} = 2\tilde{\mu}_B$ in the limit $\delta \rightarrow 0$. Therefore, TFT for both work done (W_A and W_B) is satisfied in the weak coupling limit for small observation time ($\mu_\tau \ll \delta^{-1}$).

In Figs. 7.3 (a) and 7.3(c), the comparison between the analytical probability density function for work done on particle A and B given in Eq. (7.29) in which the cumulants $(\mu_A, \mu_B, C_{AA}, C_{BB}) \rightarrow (\tilde{\mu}_A, \tilde{\mu}_B, \tilde{C}_{AA}, \tilde{C}_{BB})$ are given in Eqs. (7.31)–(7.34), with the numerical simulation is shown for coupling strength $\delta = 0.001$, $\tau_\gamma = 1$, and observation time $\tau = 10 \ll \delta^{-1}$. TFT for work done on particle A and B is shown in Figs. 7.3(b) and 7.3(d) for respective parameters. In all plots, blue points are obtained from numerical simulations and red dashed lines are the analytical results. In Figs. 7.3(b) and 7.3(d), red dashed lines have slope unity. Therefore, in the weak

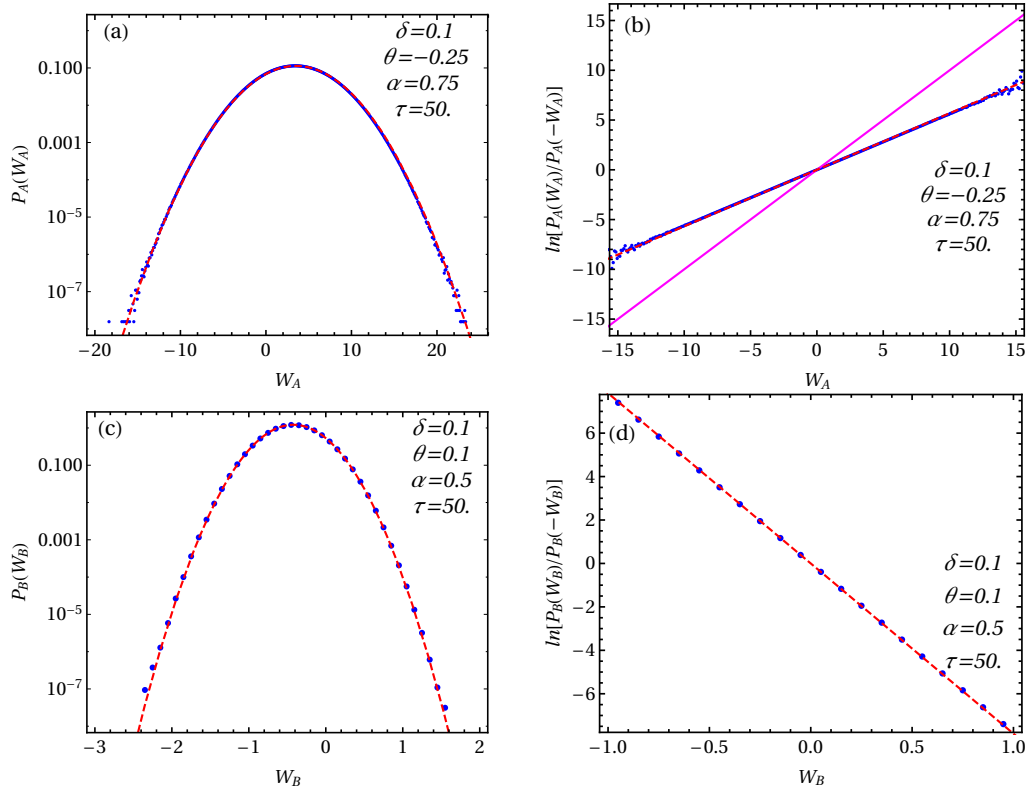


FIGURE 7.4: The probability density function for work done on particle A and B is shown in (a) for $\theta = -0.25$ and $\alpha = 0.75$ and (c) for $\theta = 0.1$ and $\alpha = 0.5$, respectively. Similarly, the function $\ln[P_i(W_i)/P_i(-W_i)]$ is plotted against W_i in (b) for $\theta = -0.25$ and $\alpha = 0.75$ and (d) for $\theta = 0.1$ and $\alpha = 0.5$, respectively. In all figures, red dashed lines are the analytical result obtained from Eq. (7.29) with cumulants given in Eqs. (7.35)–(7.38) whereas blue dots are obtained from numerical simulations. These results are shown for observation time $\tau = 50$ and coupling parameter $\delta = 0.1$ ($\tau \gg \lambda_2^{-1}$) at fixed $\tau_\gamma = 1$. Figures (b) and (d) indicate that probability density function for both work done (W_A and W_B) do not satisfy TFT even in the weak coupling limit ($\delta \ll 1$) for large observation time ($\tau \gg \lambda_2^{-1} \sim \delta^{-1}$).

coupling limit ($\delta \ll 1$) and small observation time $u_\tau \ll \delta^{-1}$, TFT is satisfied.

We see that $\lambda_1 > \lambda_2 > 0$. Thus, in the large time limit ($u_\tau \gg \lambda_2^{-1}$), the cumulants for both work done (W_A and W_B) simplify to

$$\bar{\mu}_A = \frac{\alpha^2 \tau_\gamma}{2\delta} [2(1 + \delta) + \theta(\delta u_\tau - 2\delta - 1)], \quad (7.35)$$

$$\bar{\mu}_B = \frac{\alpha^2 \theta \tau_\gamma}{4\delta} [2 - \theta - 2\delta(1 - \theta)(u_\tau - 2)], \quad (7.36)$$

$$\bar{C}_{AA} = \frac{2(1 + \delta)\alpha^2 \tau_\gamma}{\delta}, \quad (7.37)$$

$$\bar{C}_{BB} = \frac{\alpha^2 \theta^2 \tau_\gamma}{2\delta} [2\delta(u_\tau - 2) - 1], \quad (7.38)$$

where $u_\tau = \tau/\tau_\gamma$. Notice that the above given results are true for all coupling parameter δ .

In Figs. 7.4(a) and 7.4(c), we have shown a comparison of analytical probability density function for work done on particle A and particle B, respectively, given in Eq. (7.29) in which cumulants $(\mu_A, \mu_B, C_{AA}, C_{BB}) \rightarrow (\bar{\mu}_A, \bar{\mu}_B, \bar{C}_{AA}, \bar{C}_{BB})$ are given as Eqs. (7.35)–(7.38), with the numerical simulation for coupling strength $\delta = 0.1$, $\tau_\gamma = 1$, and time $\tau = 50 \gg \delta^{-1}$. The variations of function $\ln[P_i(W_i)/P_i(-W_i)]$ are shown against W_i in Figs. 7.4(b) and 7.4(d) where magenta solid line in Fig. 7.4(b) has slope unity. Thus, in the weak coupling limit ($\delta \rightarrow 0$), $\lambda_2 \sim \delta$, the deviation from TFT can be seen for both work done (W_A and W_B) for large observation time limit $u_\tau \gg \delta^{-1}$.

In above two cases, we have studied the TFT for W_A and W_B in the weak coupling limit ($\delta \rightarrow 0$) and showed that TFT would hold in the limit $u_\tau \ll \delta^{-1}$ whereas deviation can be seen in the large observation time $u_\tau \gg \delta^{-1}$. This is because in the small time limit, the effect from the other particle will not affect the TFT of the work done on the observed particle. However, when the time of observation is large ($u_\tau \gg \delta^{-1}$), the effect from the other particle may appear as the term coupling (δ) times relative separation ($x_A - x_B$) becomes relevant [see Eqs. (7.2) and (7.3)] which leads to the deviation from TFT of the work done on the observed particle even in the weak coupling limit.

7.5. Transient fluctuation theorem for total work done on coupled system

In the above section, we have analyzed TFT for work done on particle A and B. In this section, we study the TFT for the total work done on both particles.

Total work done on particle A and B is given by

$$W = W_A + W_B, \quad (7.39)$$

Since W_A and W_B have Gaussian distribution, therefore, W also has Gaussian distribution with mean $\mu = \overline{W}$ and variance $C = \overline{[W - \overline{W}]^2}$ given as

$$\mu = \mu_A + \mu_B, \quad (7.40)$$

$$C = C_{AA} + C_{BB}, \quad (7.41)$$

where $C = 2\mu$ and

$$\begin{aligned} \mu = & \frac{\alpha^2 \tau_\gamma}{4\delta} \left[4(1 + \delta) - [1 + 2\delta(2 - u_\tau)]\theta^2 - e^{-(1+2\delta)u_\tau/2} \left\{ [4 - \theta + 4\delta(1 - \theta^2)] \right. \right. \\ & \left. \left. \times \cosh \left[\sqrt{1 + 4\delta^2} u_\tau / 2 \right] + \frac{[4 - \theta^2 + 2\delta\{2 - \theta^2 + 4\delta(1 - \theta^2)\}]}{\sqrt{1 + 4\delta^2}} \sinh \left[\sqrt{1 + 4\delta^2} u_\tau / 2 \right] \right\} \right]. \end{aligned} \quad (7.42)$$

Therefore, the probability density function for total work done W is given by

$$P(W) = \frac{1}{\sqrt{2\pi C}} \exp \left[-\frac{(W - \mu)^2}{2C} \right]. \quad (7.43)$$

Using the above relation, one can see that $P(W)/P(-W) = e^W$, i.e. TFT for total work done on both particles is satisfied. Therefore, it is clear that when degrees of freedom (DOFs) having same time of relaxation are coupled and driven out of equilibrium, total work done on all DOFs obeys the TFT for all parameters.

Figure 7.5(a) and 7.5(b) show the comparison of the analytical results for the probability density function for W given in Eq. (7.43) and the function $\ln[P(W)/P(-W)]$ with the numerical simulation, and they have nice agreement. Figure 7.5(b) indicates that the total work done W obeys the transient fluctuation theorem.

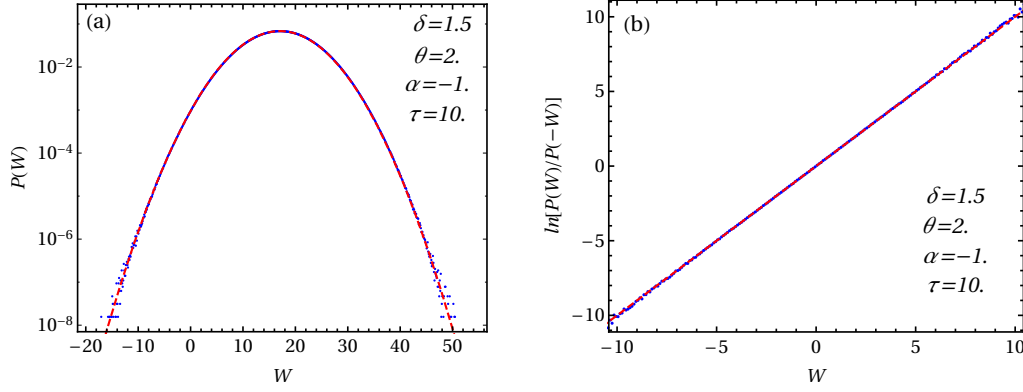


FIGURE 7.5: (a) The distribution function given in Eq. (7.43) is compared with the numerical simulation. (b) The function $\ln[P(W)/P(-W)]$ is plotted against the $W = W_A + W_B$. In both figures, parameters are $\delta = 1.5$, $\theta = 2.0$, $\alpha = -1.0$ and $\tau = 10$, and red dashed line is the analytical result whereas blue dots are obtained from the numerical simulation. The red dashed line in (b) has unit slope. These results are shown for $\tau_\gamma = 1$.

7.6. Probability density function for stochastic efficiency $p_\tau(\eta)$

In the following, we understand the statistics of the stochastic efficiency of the isothermal machine. Therefore, substituting $P_A(W_A)$ and $P_B(W_B)$ given in Eq. (7.29), in the integral Eq. (7.11), the probability density function for stochastic efficiency $p_\tau(\eta)$ can be obtained as [99, 103]

$$p_\tau(\eta) = \frac{e^{I(\eta, \tau)}}{\sqrt{(2\pi)^2 C_{AA} C_{BB}}} \frac{e^{-K_1 K_2^2} + K_2 \sqrt{\pi K_1} \operatorname{erf}(K_2 \sqrt{K_1})}{K_1}, \quad (7.44)$$

where

$$I(\eta, \tau) = -\frac{1}{2} \frac{(\eta \mu_B + \mu_A)^2}{\eta^2 C_{BB} + C_{AA}}, \quad (7.45)$$

$$K_1 = \frac{\eta^2 C_{BB} + C_{AA}}{2 C_{AA} C_{BB}}, \quad (7.46)$$

$$K_2 = \frac{C_{AA} \mu_B - \eta C_{BB} \mu_A}{C_{AA} + \eta^2 C_{BB}}. \quad (7.47)$$

In Eq. (7.44), $\operatorname{erf}(u)$ is the error function given by

$$\operatorname{erf}(u) = \frac{2}{\sqrt{\pi}} \int_0^u dx e^{-x^2}. \quad (7.48)$$

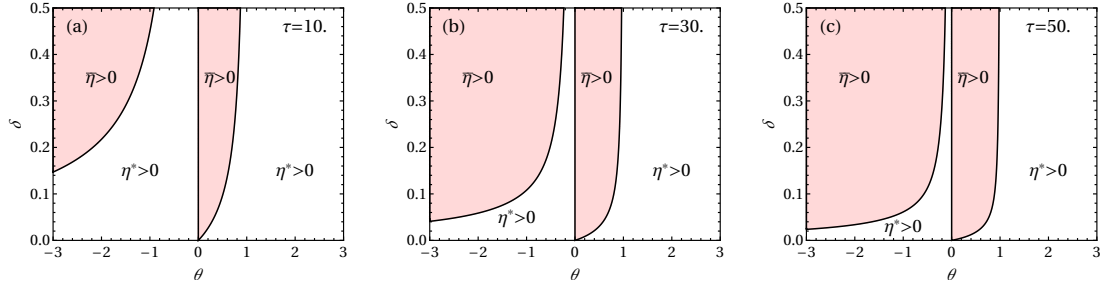


FIGURE 7.6: Phase diagrams in (θ, δ) plane are shown using $\bar{\eta}$ and η^* given in Eq. (7.49), for time: (a) $\tau = 10$, (b) $\tau = 30$, and (c) $\tau = 50$ where $\bar{\eta}$ and η^* are the efficiencies at which the function $I(\eta, \tau)$ given in Eq. (7.45), achieves maximum and minimum value, respectively. The shaded regions correspond to the areas where efficiencies $\bar{\eta}$ and η^* remain positive and negative, respectively. The above phase diagrams are shown for given $\tau_\gamma = 1$.

Notice that μ_i and C_{ij} given in Eqs. (7.24)–(7.28) for all time (see $\bar{\mu}_i$ and \bar{C}_{ij} in Eqs. (7.35)–(7.38) for large time) do not scale linearly with the observation time. Consequently, the probability density function for stochastic efficiency does not have large deviation form [136] for this model system.

It can be seen that the function $I(\eta, \tau)$ has two extrema, i.e. at $\bar{\eta}$ and η^* where

$$\bar{\eta} = -\frac{\mu_A}{\mu_B}, \quad \eta^* = \frac{\mu_B C_{AA}}{\mu_A C_{BB}}. \quad (7.49)$$

Moreover, $I(\eta, \tau)|_{\eta=\bar{\eta}} = 0$. The function $I(\eta, \tau)$ has a maximum and a minimum at $\eta = \bar{\eta}$ and $\eta = \eta^*$, respectively. Note that both $\bar{\eta}$ and η^* do not depend on the parameter α (relative strength acting on particle A, i.e. $\alpha = F/\sqrt{\gamma T}$). The efficiency $\bar{\eta}$ can have any sign depending on parameters τ , δ , and θ . To understand the nature of $\bar{\eta}$, we have plotted phase diagram in (θ, δ) plane as shown in Fig. 7.6 for different observation times τ at fixed $\tau_\gamma = 1$. In Fig. 7.6, light red shaded regions correspond to areas where efficiency $\bar{\eta}$ is positive. Notice that C_{AA} and C_{BB} are positive [see Eq. (7.49)]. Therefore, $\bar{\eta}$ and η^* have opposite sign. Hence, the unshaded regions in Fig. 7.6 represent the areas where η^* is positive otherwise negative.

Figure 7.7 shows the comparison of analytical results of the probability density function $p_\tau(\eta)$ given in Eq. (7.44) with the numerical simulation results for both signs of θ . While in Fig. 7.7(a) the comparison is shown for parameters $\theta = -1$, $\alpha = 0.5$, and coupling parameter $\delta = 0.3$ at $\tau = 10, 30$ and 50 , the parameters

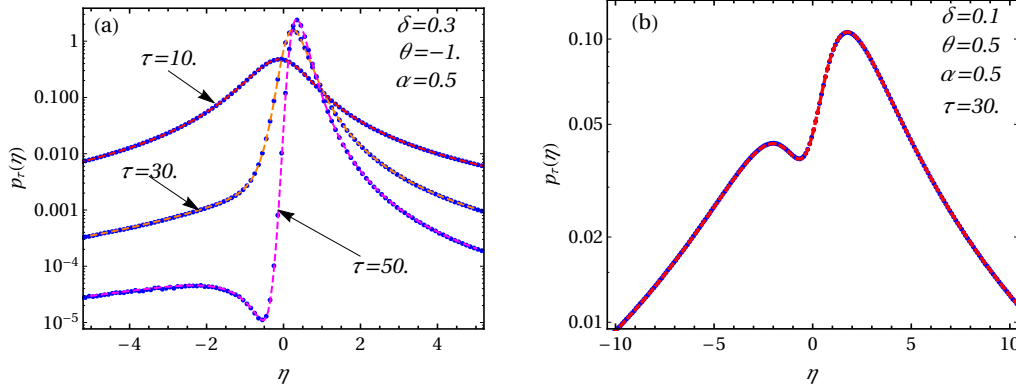


FIGURE 7.7: The probability density function for stochastic efficiency $p_\tau(\eta)$ is plotted against the stochastic efficiency η : (a) for $\theta = -1$, $\alpha = 0.5$, coupling parameter $\delta = 0.3$ at three different time $\tau = 10, 30$ and 50 where red ($\tau = 10$), orange ($\tau = 30$) and magenta ($\tau = 50$) dashed lines represent the analytical results given by Eq. (7.44), and (b) for $\theta = 0.5$, $\alpha = 0.5$, coupling parameter $\delta = 0.1$ at time $\tau = 30$ where red dashed lines represent the analytical result given in Eq. (7.44). In both figures, blue dots are obtained from numerical simulations at the respective times τ . These results are shown for fixed $\tau_\gamma = 1$.

$\theta = 0.5$, $\alpha = 0.5$, and coupling parameter $\delta = 0.1$ at $\tau = 30$ are taken in Fig. 7.7(b). In Fig. 7.7(a), red ($\tau = 10$), orange ($\tau = 30$) and magenta ($\tau = 50$) dashed lines are the analytical result given by Eq. (7.44) whereas blue dots are obtained from numerical simulations at corresponding times τ . Similarly, red dashed lines correspond to the analytical result given by Eq. (7.44) and blue dots are obtained from numerical simulation in Fig. 7.7(b). Figure 7.7 shows that there is a nice agreement between theory and numerical simulation. From Fig. 7.7(a), it is clear that the peak of the density function $p_\tau(\eta)$ shifts from negative to positive side as time τ is increased from $\tau = 10$ to $\tau = 30$ as shown in Figs. 7.6(a)—7.6(b).

In the above, we have given efficiencies $\bar{\eta}$ and η^* where $I(\eta, \tau)$ has extrema. It can be seen that in the weak coupling limit ($\delta \rightarrow 0$) and small time limit ($u_\tau \ll \delta^{-1}$), these efficiencies reduce to

$$\bar{\eta} = -\frac{4}{\theta^2} \frac{u_\tau}{e^{-u_\tau} + u_\tau - 1}, \quad (7.50)$$

$$\eta^* = 1. \quad (7.51)$$

Clearly, here the most probable efficiency $\bar{\eta}$ is negative. This is because in the small

coupling limit ($\delta \rightarrow 0$) and small observation time ($u_\tau \ll \delta^{-1}$), both of the particles behave independently (see Fig. 7.3), and the machine will not do work against the load force F irrespective the value of θ (in most probable sense). In Fig. 7.8(a), we have plotted the probability density function for the stochastic efficiency $p_\tau(\eta)$ in the weak coupling limit and small time of observation where red dashed lines represents the analytical results given by Eq. (7.44) in which $(\mu_A, \mu_B, C_{AA}, C_{BB}) \rightarrow (\tilde{\mu}_A, \tilde{\mu}_B, \tilde{C}_{AA}, \tilde{C}_{BB})$ as given in Eqs. (7.31)–(7.34) and blue dots correspond to the numerical simulation results. Similarly, one can obtain $\bar{\eta}$ and η^* in the large time limit ($u_\tau \gg \lambda_2^{-1}$) from Eqs. (7.35)–(7.38)

$$\bar{\eta} = -\frac{2[\delta\{\theta(u_\tau - 2) + 2\} - \theta + 2]}{\theta[2\delta(\theta - 1)(u_\tau - 2) - \theta + 2]}, \quad (7.52)$$

$$\eta^* = \frac{2(\delta + 1)[2\delta(\theta - 1)(u_\tau - 2) - \theta + 2]}{\theta[2\delta(u_\tau - 2) - 1][\delta\{\theta(u_\tau - 2) + 2\} - \theta + 2]}. \quad (7.53)$$

We have also compared the large time ($u_\tau \gg \lambda_2^{-1}$) analytical results for the probability density function $p_\tau(\eta)$ given in Eq. (7.44) in which $(\mu_A, \mu_B, C_{AA}, C_{BB}) \rightarrow (\tilde{\mu}_A, \tilde{\mu}_B, \tilde{C}_{AA}, \tilde{C}_{BB})$ as given in Eqs. (7.35)–(7.38), with the numerical simulations in Fig. 7.8(b). These comparisons indicate that there is a nice agreement between theory and numerical simulations.

In the large time limit ($u_\tau \gg \lambda_2^{-1}$), when $\theta = 1$, we see that

$$\bar{\eta} = -2(1 + \delta u_\tau), \quad (7.54)$$

$$\eta^* = \frac{2(1 + \delta)}{(1 + \delta u_\tau)[2\delta(u_\tau - 2) - 1]}. \quad (7.55)$$

However, Eqs. (7.52) and (7.53) reduce to $\bar{\eta} \rightarrow 1/(1 - \theta)$ and $\eta^* \rightarrow 0$ for $\theta \neq 1$ as $u_\tau \rightarrow \infty$. Therefore, the machine will not perform work against the load force F (in most probable sense) when $\theta \geq 1$ in the large time limit as $\bar{\eta} < 0$.

Finally, we emphasize that for all cases shown above, probability density function for the stochastic efficiency $p_\tau(\eta) \rightarrow \eta^{-2}$ as $|\eta| \rightarrow \infty$. Similar behaviour of $p_\tau(\eta)$ has been observed earlier in different model systems [46, 100, 99, 103, 55].

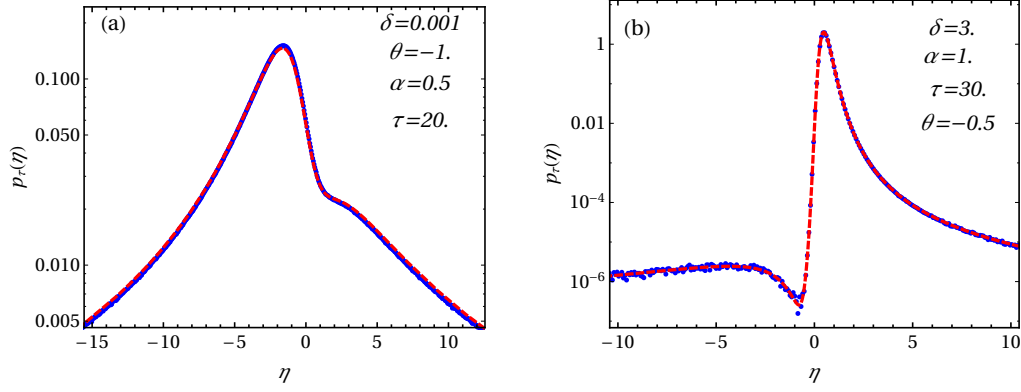


FIGURE 7.8: The probability density functions for stochastic efficiency $p_\tau(\eta)$ are plotted against the stochastic efficiency η for weak coupling ($\delta \ll 1$) and for small observation time ($\tau \ll \delta^{-1}$) [see (a)] at $\theta = -1$, $\alpha = 0.5$, $\delta = 0.001$, and $\tau = 20$, and for large observation time $\tau \gg \lambda_2^{-1}$ [see (b)] at $\theta = -0.5$, $\alpha = 1$, $\delta = 3$, and $\tau = 30$. In both figures, blue dots are obtained from numerical simulations and red dashed lines are the analytical probability density function with respective cumulants. We set $\tau_\gamma = 1$ for both above plots.

7.7. Summary

We considered a machine composed of two Brownian particles (say particle A and B) interacting harmonically with a spring of stiffness k . Particle B is confined in a harmonic trap of stiffness k_0 . The whole system is in contact of a heat reservoir of a constant temperature T . For simplicity, we defined a dimensionless coupling parameter δ as the ratio of spring constant and trap stiffness: $\delta = k/k_0$. For $t \leq 0$, the harmonic trap was kept stationary. Thus, the system obeyed the equilibrium Boltzmann's distribution at $t = 0$. A constant load $F = \alpha\sqrt{\gamma T}$ is attached to particle A and the minimum of the harmonic confinement is dragged with a constant velocity $v = F\theta/(2\gamma)$ for $t \geq 0$. The joint distribution of both work done is computed. Transient fluctuation theorem (TFT) is studied for work done on particle A and B in the weak coupling limit $\delta \ll 1$ for both small ($u_\tau \ll \delta^{-1}$) and large observation time ($u_\tau \gg \delta^{-1}$). It is shown that the TFT would hold in the small time limit whereas deviation can be seen even in the weak coupling limit ($\delta \ll 1$) for large time. Interestingly, the total work done on both particles satisfies TFT for all parameters. Further, we computed the stochastic efficiency which is defined as the work done against the load on particle A to the work done on the particle B by dragging the

harmonic confinement. The exact distribution for the stochastic efficiency is evaluated for all time τ and the coupling parameter δ . We have given the phase diagrams in (θ, δ) plane for different observation times τ which shows the region where the efficiency at which the probability density function is maximum, attains the positive value. Moreover, we have shown that the probability density function of the stochastic efficiency $p_\tau(\eta)$ does not have large deviation form [136] for this model system. The analytical results are also supported by the numerical simulations and they have an excellent match.

In the probability density function for the stochastic efficiency, there are two maxima and one minimum. For example, consider Fig. 6.8 in which one can find two regions: (1) $\eta \leq 1$ and (2) $\eta > 1$. In the region (1), there are two subregions: (I) $\eta \leq 0$ and (II) $0 < \eta \leq 1$. In the subregion (I), the engine dissipates the whole energy into the bath and does not perform the work against the external load, and there exists a global maximum where a large number of events corresponding to that contribute to the probability density function at $\eta = \bar{\eta}$. In the subregion (II), the engine performs the work against the load as well as dissipates the energy in the heat bath. At $\eta = 1$, the entire work done by the drive force is converted in the lifting of the load, and the probability density function attains a local minimum value. On the other hand [in region (2)], the engine absorbs the energy from the heat bath and performs work against the load force, therefore, we see the efficiency greater than one. As one moves from region (1) to (2), the probability density function *surprisingly* increases with η and attains a local maximum value. This increase in the density function in this region is quite unclear to us, and it will remain an open question for the future discussions.

Appendix A

Simulation technique

To obtain the probability density function for a stochastic observable Ω , i.e. $P_\tau(\Omega)$, in the numerical simulation, we first discretize the Langevin equations up to an order of time segment $\Delta\tau$.

In this thesis (except Chapter 7), in general, the observable Ω depends upon the Gaussian noise quadratically, and has the following integral form

$$\Omega = \int_0^\tau [\sqrt{\sigma}\zeta(t) + y(t)]v(t), \quad (\text{A.1})$$

where the integral follows the Stratonovich rule of integration, τ is the observation time, $\zeta(t)$ is the Gaussian noise with mean zero and correlation $\langle \zeta(t)\zeta(t') \rangle = \delta(t - t')$, σ is some constant, and $y(t)$ and $v(t)$ are the system variables. In all chapters (except Chapter 7), we computed observables in the steady state of the system. Thus, the initial condition for $y(t)$ and $v(t)$ are drawn from the steady state of the system.

The functional Ω given in Eq. (A.1), is discretized as following

$$\Omega = \sum_{n=0}^{(\tau/\Delta\tau)-1} [\sqrt{\sigma/\Delta\tau}\tilde{\zeta}_A^{\Delta\tau}(t_n) + y(t_n)][v(t_n + \Delta\tau) + v(t_n)]\frac{\Delta\tau}{2}, \quad (\text{A.2})$$

where $t_n = n\Delta\tau$, and $\tilde{\zeta}_A^{\Delta\tau}(t_n)$ is the Gaussian random variable of mean zero and variance one at time step t_n .

Using above equation, we construct the histogram for Ω , i.e. $P_\tau(\Omega)$, for R number of realizations.

Bibliography

- [1] Bruce Alberts et al. *Molecular Biology of the Cell*. 6th ed. Garland Science, 2014.
- [2] Christian P. Amann, Tim Schmiedl, and Udo Seifert. "Communications: Can one identify nonequilibrium in a three-state system by analyzing two-state trajectories?" In: *The Journal of Chemical Physics* 132.4 (2010), p. 041102. DOI: [10.1063/1.3294567](https://doi.org/10.1063/1.3294567).
- [3] Ken Sekimoto (auth.) *Stochastic Energetics*. 1st ed. Lecture Notes in Physics 799. Springer-Verlag Berlin Heidelberg, 2010. ISBN: 3642054102,9783642054105.
- [4] A. Baule and E. G. D. Cohen. "Steady-state work fluctuations of a dragged particle under external and thermal noise". In: *Phys. Rev. E* 80 (1 2009), p. 011110. DOI: [10.1103/PhysRevE.80.011110](https://doi.org/10.1103/PhysRevE.80.011110). URL: <https://link.aps.org/doi/10.1103/PhysRevE.80.011110>.
- [5] Giuliano Benenti, Keiji Saito, and Giulio Casati. "Thermodynamic Bounds on Efficiency for Systems with Broken Time-Reversal Symmetry". In: *Phys. Rev. Lett.* 106 (23 2011), p. 230602. DOI: [10.1103/PhysRevLett.106.230602](https://doi.org/10.1103/PhysRevLett.106.230602).
- [6] A. Bérut et al. "Stationary and Transient Fluctuation Theorems for Effective Heat Fluxes between Hydrodynamically Coupled Particles in Optical Traps". In: *Phys. Rev. Lett.* 116 (6 2016), p. 068301. DOI: [10.1103/PhysRevLett.116.068301](https://doi.org/10.1103/PhysRevLett.116.068301). URL: <https://link.aps.org/doi/10.1103/PhysRevLett.116.068301>.
- [7] Gili Bisker et al. "Hierarchical bounds on entropy production inferred from partial information". In: *Journal of Statistical Mechanics: Theory and Experiment* 2017.9 (2017), p. 093210. URL: <http://stacks.iop.org/1742-5468/2017/i=9/a=093210>.

- [8] V. Blickle et al. "Thermodynamics of a Colloidal Particle in a Time-Dependent Nonharmonic Potential". In: *Phys. Rev. Lett.* 96 (7 2006), p. 070603. DOI: [10.1103/PhysRevLett.96.070603](https://doi.org/10.1103/PhysRevLett.96.070603). URL: <https://link.aps.org/doi/10.1103/PhysRevLett.96.070603>.
- [9] Valentin Blickle and Clemens Bechinger. "Realization of a micrometre-sized stochastic heat engine". In: *Nat. Phys.* 8 (2 2012), p. 143. DOI: [10.1038/nphys2163](https://doi.org/10.1038/nphys2163).
- [10] F. BONETTO, J. L. LEBOWITZ, and L. REY-BELLET. "FOURIER'S LAW: A CHALLENGE TO THEORISTS". In: *Mathematical Physics 2000*, pp. 128–150. DOI: [10.1142/9781848160224_0008](https://doi.org/10.1142/9781848160224_0008). eprint: http://www.worldscientific.com/doi/pdf/10.1142/9781848160224_0008. URL: http://www.worldscientific.com/doi/abs/10.1142/9781848160224_0008.
- [11] Massimo Borrelli et al. "Fluctuation relations for driven coupled classical two-level systems with incomplete measurements". In: *Phys. Rev. E* 91 (1 2015), p. 012145. DOI: [10.1103/PhysRevE.91.012145](https://doi.org/10.1103/PhysRevE.91.012145).
- [12] Carlos Bustamante, David Keller, and George Oster. "The Physics of Molecular Motors". In: *Acc. Chem. Res.* 34.6 (2001), pp. 412–420. DOI: [10.1021/ar0001719](https://doi.org/10.1021/ar0001719).
- [13] Carlos Bustamante, Jan Liphardt, and Felix Ritort. "The Nonequilibrium Thermodynamics of Small Systems". In: *Physics Today* 58.7 (2005), pp. 43–48. DOI: [10.1063/1.2012462](https://doi.org/10.1063/1.2012462). eprint: <https://doi.org/10.1063/1.2012462>. URL: <https://doi.org/10.1063/1.2012462>.
- [14] A. Bérut, A. Petrosyan, and S. Ciliberto. "Energy flow between two hydrodynamically coupled particles kept at different effective temperatures". In: *EPL (Europhysics Letters)* 107.6 (2014), p. 60004. URL: <http://stacks.iop.org/0295-5075/107/i=6/a=60004>.
- [15] Herbert B Callen. *Thermodynamics and an Introduction to Thermostatistics*. 2nd ed. Wiley, 1985.
- [16] D. M. Carberry et al. "Fluctuations and Irreversibility: An Experimental Demonstration of a Second-Law-Like Theorem Using a Colloidal Particle Held in an Optical Trap". In: *Phys. Rev. Lett.* 92 (14 2004), p. 140601. DOI: [10.1103/](https://doi.org/10.1103/)

- PhysRevLett . 92 . 140601. URL: <https://link.aps.org/doi/10.1103/PhysRevLett.92.140601>.
- [17] Hyun-Myung Chun and Jae Dong Noh. “Hidden entropy production by fast variables”. In: *Phys. Rev. E* 91 (5 2015), p. 052128. DOI: [10.1103/PhysRevE.91.052128](https://doi.org/10.1103/PhysRevE.91.052128).
- [18] S. Ciliberto. “Experiments in Stochastic Thermodynamics: Short History and Perspectives”. In: *Phys. Rev. X* 7 (2 2017), p. 021051. DOI: [10.1103/PhysRevX.7.021051](https://doi.org/10.1103/PhysRevX.7.021051). URL: <https://link.aps.org/doi/10.1103/PhysRevX.7.021051>.
- [19] S. Ciliberto, R. Gomez-Solano, and A. Petrosyan. “Fluctuations, Linear Response, and Currents in Out-of-Equilibrium Systems”. In: *Annual Review of Condensed Matter Physics* 4.1 (2013), pp. 235–261. DOI: [10.1146/annurev-conmatphys-030212-184240](https://doi.org/10.1146/annurev-conmatphys-030212-184240). eprint: <https://doi.org/10.1146/annurev-conmatphys-030212-184240>. URL: <https://doi.org/10.1146/annurev-conmatphys-030212-184240>.
- [20] S Ciliberto, S Joubaud, and A Petrosyan. “Fluctuations in out-of-equilibrium systems: from theory to experiment”. In: *Journal of Statistical Mechanics: Theory and Experiment* 2010.12 (2010), P12003. URL: <http://stacks.iop.org/1742-5468/2010/i=12/a=P12003>.
- [21] S. Ciliberto et al. “Heat Flux and Entropy Produced by Thermal Fluctuations”. In: *Phys. Rev. Lett.* 110 (18 2013). DOI: [10.1103/PhysRevLett.110.180601](https://doi.org/10.1103/PhysRevLett.110.180601).
- [22] E G D Cohen. “Properties of nonequilibrium steady states: a path integral approach”. In: *Journal of Statistical Mechanics: Theory and Experiment* 2008.07 (2008), P07014. URL: <http://stacks.iop.org/1742-5468/2008/i=07/a=P07014>.
- [23] D Collin et al. “Verification of the Crooks fluctuation theorem and recovery of RNA folding free energies”. In: *Nat. Phys.* 437 (7056 2005), p. 231. DOI: [10.1038/nature04061](https://doi.org/10.1038/nature04061).

- [24] Gavin E. Crooks. “Entropy production fluctuation theorem and the nonequilibrium work relation for free energy differences”. In: *Phys. Rev. E* 60 (3 1999), pp. 2721–2726. DOI: [10.1103/PhysRevE.60.2721](https://doi.org/10.1103/PhysRevE.60.2721).
- [25] Gavin E. Crooks. “Nonequilibrium Measurements of Free Energy Differences for Microscopically Reversible Markovian Systems”. In: *Journal of Statistical Physics* 90.5 (1998), pp. 1481–1487. ISSN: 1572-9613. DOI: [10.1023/A:1023208217925](https://doi.org/10.1023/A:1023208217925).
- [26] Gavin E. Crooks. “Path-ensemble averages in systems driven far from equilibrium”. In: *Phys. Rev. E* 61 (3 2000), pp. 2361–2366. DOI: [10.1103/PhysRevE.61.2361](https://doi.org/10.1103/PhysRevE.61.2361).
- [27] Abhishek Dhar. “Heat transport in low-dimensional systems”. In: *Advances in Physics* 57.5 (2008), pp. 457–537. DOI: [10.1080/00018730802538522](https://doi.org/10.1080/00018730802538522). eprint: <https://doi.org/10.1080/00018730802538522>. URL: <https://doi.org/10.1080/00018730802538522>.
- [28] F Douarche, S Ciliberto, and A Petrosyan. “Estimate of the free energy difference in mechanical systems from work fluctuations: experiments and models”. In: *Journal of Statistical Mechanics: Theory and Experiment* 2005.09 (2005), P09011. URL: <http://stacks.iop.org/1742-5468/2005/i=09/a=P09011>.
- [29] F. Douarche et al. “Work Fluctuation Theorems for Harmonic Oscillators”. In: *Phys. Rev. Lett.* 97 (14 2006), p. 140603. DOI: [10.1103/PhysRevLett.97.140603](https://doi.org/10.1103/PhysRevLett.97.140603). URL: <https://link.aps.org/doi/10.1103/PhysRevLett.97.140603>.
- [30] Douarche, F. et al. “An experimental test of the Jarzynski equality in a mechanical experiment”. In: *Europhys. Lett.* 70.5 (2005), pp. 593–599. DOI: [10.1209/epl/i2005-10024-4](https://doi.org/10.1209/epl/i2005-10024-4). URL: <https://doi.org/10.1209/epl/i2005-10024-4>.
- [31] Massimiliano Esposito. “Stochastic thermodynamics under coarse graining”. In: *Phys. Rev. E* 85 (4 2012), p. 041125. DOI: [10.1103/PhysRevE.85.041125](https://doi.org/10.1103/PhysRevE.85.041125). URL: <https://link.aps.org/doi/10.1103/PhysRevE.85.041125>.

- [32] Denis J. Evans, E. G. D. Cohen, and G. P. Morriss. “Probability of second law violations in shearing steady states”. In: *Phys. Rev. Lett.* 71 (15 1993), pp. 2401–2404. DOI: [10.1103/PhysRevLett.71.2401](https://doi.org/10.1103/PhysRevLett.71.2401).
- [33] Denis J. Evans and Gary Morriss. *Statistical Mechanics of Nonequilibrium Liquids*. 2nd ed. Cambridge University Press, 2008. DOI: [10.1017/CB09780511535307](https://doi.org/10.1017/CB09780511535307).
- [34] Denis J. Evans and Debra J. Searles. “Equilibrium microstates which generate second law violating steady states”. In: *Phys. Rev. E* 50 (2 1994), pp. 1645–1648. DOI: [10.1103/PhysRevE.50.1645](https://doi.org/10.1103/PhysRevE.50.1645).
- [35] Denis J. Evans and Debra J. Searles. “The Fluctuation Theorem”. In: *Advances in Physics* 51.7 (2002), pp. 1529–1585. DOI: [10.1080/00018730210155133](https://doi.org/10.1080/00018730210155133). eprint: <https://doi.org/10.1080/00018730210155133>. URL: <https://doi.org/10.1080/00018730210155133>.
- [36] Jean Farago. “Injected Power Fluctuations in Langevin Equation”. In: *Journal of Statistical Physics* 107.3 (2002), pp. 781–803. ISSN: 1572-9613. DOI: [10.1023/A:1014538214117](https://doi.org/10.1023/A:1014538214117). URL: <https://doi.org/10.1023/A:1014538214117>.
- [37] Hans C Fogedby and Alberto Imparato. “A bound particle coupled to two thermostats”. In: *Journal of Statistical Mechanics: Theory and Experiment* 2011.05 (2011), P05015. URL: <http://stacks.iop.org/1742-5468/2011/i=05/a=P05015>.
- [38] Hans C Fogedby and Alberto Imparato. “Heat flow in chains driven by thermal noise”. In: *Journal of Statistical Mechanics: Theory and Experiment* 2012.04 (2012), P04005. URL: <http://stacks.iop.org/1742-5468/2012/i=04/a=P04005>.
- [39] G. Gallavotti and E. G. D. Cohen. “Dynamical Ensembles in Nonequilibrium Statistical Mechanics”. In: *Phys. Rev. Lett.* 74 (14 1995), pp. 2694–2697. DOI: [10.1103/PhysRevLett.74.2694](https://doi.org/10.1103/PhysRevLett.74.2694).
- [40] Giovanni Gallavotti. “Extension of Onsager’s Reciprocity to Large Fields and the Chaotic Hypothesis”. In: *Phys. Rev. Lett.* 77 (21 1996), pp. 4334–4337. DOI: [10.1103/PhysRevLett.77.4334](https://doi.org/10.1103/PhysRevLett.77.4334). URL: <https://link.aps.org/doi/10.1103/PhysRevLett.77.4334>.

- [41] N. Garnier and S. Ciliberto. “Nonequilibrium fluctuations in a resistor”. In: *Phys. Rev. E* 71 (6 2005), p. 060101. DOI: [10.1103/PhysRevE.71.060101](https://doi.org/10.1103/PhysRevE.71.060101). URL: <https://link.aps.org/doi/10.1103/PhysRevE.71.060101>.
- [42] Pierre Gaspard. “Fluctuation theorem for nonequilibrium reactions”. In: *J. Chem. Phys.* 120.19 (2004), pp. 8898–8905. DOI: [10.1063/1.1688758](https://doi.org/10.1063/1.1688758). eprint: <https://doi.org/10.1063/1.1688758>. URL: <https://doi.org/10.1063/1.1688758>.
- [43] Jeff Gelles and Robert Landick. “RNA Polymerase as a Molecular Motor”. In: *Cell* 93.1 (1998), pp. 13–16. ISSN: 0092-8674. DOI: [http://dx.doi.org/10.1016/S0092-8674\(00\)81140-X](http://dx.doi.org/10.1016/S0092-8674(00)81140-X).
- [44] Jan Gieseler et al. “Dynamic relaxation of a levitated nanoparticle from a non-equilibrium steady state”. In: *Nature Nanotechnology* 9 (2014), pp. 358–364. DOI: [10.1038/nnano.2014.40](https://doi.org/10.1038/nnano.2014.40).
- [45] D.T. Gillespie. *Markov Processes: An Introduction for Physical Scientists*. Academic Press, 1992. ISBN: 9780122839559. URL: <https://books.google.co.in/books?id=blinSGpXHtEC>.
- [46] Todd R Gingrich et al. “Efficiency and large deviations in time-asymmetric stochastic heat engines”. In: *New Journal of Physics* 16.10 (2014), p. 102003.
- [47] A. Gomez-Marin and J. M. Sancho. “Heat fluctuations in Brownian transducers”. In: *Phys. Rev. E* 73 (4 2006), p. 045101. DOI: [10.1103/PhysRevE.73.045101](https://doi.org/10.1103/PhysRevE.73.045101). URL: <https://link.aps.org/doi/10.1103/PhysRevE.73.045101>.
- [48] J. R. Gomez-Solano, A. Petrosyan, and S. Ciliberto. “Heat Fluctuations in a Nonequilibrium Bath”. In: *Phys. Rev. Lett.* 106 (20 2011), p. 200602. DOI: [10.1103/PhysRevLett.106.200602](https://doi.org/10.1103/PhysRevLett.106.200602).
- [49] J. R. Gomez-Solano et al. “Steady-state fluctuation relations for systems driven by an external random force”. In: *EPL (Europhysics Letters)* 89.6 (2010), p. 60003.
- [50] Deepak Gupta. “Exact distribution for work and stochastic efficiency of an isothermal machine”. In: *Journal of Statistical Mechanics: Theory and Experiment* 2018.7 (2018), p. 073201. URL: <http://stacks.iop.org/1742-5468/2018/i=7/a=073201>.

- [51] Deepak Gupta and Sanjib Sabhapandit. “Entropy production for partially observed system in a harmonic trap”. In: *ArXiv e-prints* (Oct. 2017). arXiv: [1710.11339](https://arxiv.org/abs/1710.11339) [[cond-mat.stat-mech](https://arxiv.org/abs/1710.11339)].
- [52] Deepak Gupta and Sanjib Sabhapandit. “Fluctuation theorem for entropy production of a partial system in the weak-coupling limit”. In: *EPL* 115.6 (2016), p. 60003. DOI: [10.1209/0295-5075/115/60003](https://doi.org/10.1209/0295-5075/115/60003).
- [53] Deepak Gupta and Sanjib Sabhapandit. “Fluctuation theorem for partial entropy production in a coupled Brownian particle system”. In: ().
- [54] Deepak Gupta and Sanjib Sabhapandit. “Partial entropy production in heat transport”. In: *Journal of Statistical Mechanics: Theory and Experiment* 2018.6 (2018), p. 063203. URL: <http://stacks.iop.org/1742-5468/2018/i=6/a=063203>.
- [55] Deepak Gupta and Sanjib Sabhapandit. “Stochastic efficiency of an isothermal work-to-work converter engine”. In: *Phys. Rev. E* 96 (4 2017), p. 042130. DOI: [10.1103/PhysRevE.96.042130](https://doi.org/10.1103/PhysRevE.96.042130). URL: <https://link.aps.org/doi/10.1103/PhysRevE.96.042130>.
- [56] R J Harris and G M Schütz. “Fluctuation theorems for stochastic dynamics”. In: *Journal of Statistical Mechanics: Theory and Experiment* 2007.07 (2007), P07020. URL: <http://stacks.iop.org/1742-5468/2007/i=07/a=P07020>.
- [57] Takahiro Hatano and S Sasa. “Steady-State Thermodynamics of Langevin Systems”. In: *Phys. Rev. Lett.* 86 (16 2001), pp. 3463–3466. DOI: [10.1103/PhysRevLett.86.3463](https://doi.org/10.1103/PhysRevLett.86.3463).
- [58] Kerson Huang. *Statistical Mechanics, 2nd Edition*.
- [59] A. Imparato et al. “Work and heat probability distribution of an optically driven Brownian particle: Theory and experiments”. In: *Phys. Rev. E* 76 (5 2007), p. 050101. DOI: [10.1103/PhysRevE.76.050101](https://doi.org/10.1103/PhysRevE.76.050101). URL: <https://link.aps.org/doi/10.1103/PhysRevE.76.050101>.
- [60] C. Jarzynski. “Equilibrium free-energy differences from nonequilibrium measurements: A master-equation approach”. In: *Phys. Rev. E* 56 (5 1997), pp. 5018–5035. DOI: [10.1103/PhysRevE.56.5018](https://doi.org/10.1103/PhysRevE.56.5018).

- [61] C. Jarzynski. “Nonequilibrium Equality for Free Energy Differences”. In: *Phys. Rev. Lett.* 78 (14 1997), pp. 2690–2693. DOI: [10.1103/PhysRevLett.78.2690](https://doi.org/10.1103/PhysRevLett.78.2690).
- [62] Christopher Jarzynski. “Equalities and Inequalities: Irreversibility and the Second Law of Thermodynamics at the Nanoscale”. In: *Annual Review of Condensed Matter Physics* 2.1 (2011), pp. 329–351. DOI: [10.1146/annurev-conmatphys-062910-140506](https://doi.org/10.1146/annurev-conmatphys-062910-140506). eprint: <https://doi.org/10.1146/annurev-conmatphys-062910-140506>. URL: <https://doi.org/10.1146/annurev-conmatphys-062910-140506>.
- [63] A. M. Jayannavar and Mamata Sahoo. “Charged particle in a magnetic field: Jarzynski equality”. In: *Phys. Rev. E* 75 (3 2007), p. 032102. DOI: [10.1103/PhysRevE.75.032102](https://doi.org/10.1103/PhysRevE.75.032102). URL: <https://link.aps.org/doi/10.1103/PhysRevE.75.032102>.
- [64] J. I. Jiménez-Aquino. “Entropy production theorem for a charged particle in an electromagnetic field”. In: *Phys. Rev. E* 82 (5 2010), p. 051118. DOI: [10.1103/PhysRevE.82.051118](https://doi.org/10.1103/PhysRevE.82.051118). URL: <https://link.aps.org/doi/10.1103/PhysRevE.82.051118>.
- [65] J. I. Jiménez-Aquino, R. M. Velasco, and F. J. Uribe. “Dragging of an electrically charged particle in a magnetic field”. In: *Phys. Rev. E* 78 (3 2008), p. 032102. DOI: [10.1103/PhysRevE.78.032102](https://doi.org/10.1103/PhysRevE.78.032102). URL: <https://link.aps.org/doi/10.1103/PhysRevE.78.032102>.
- [66] J. I. Jiménez-Aquino, R. M. Velasco, and F. J. Uribe. “Fluctuation relations for a classical harmonic oscillator in an electromagnetic field”. In: *Phys. Rev. E* 79 (6 2009), p. 061109. DOI: [10.1103/PhysRevE.79.061109](https://doi.org/10.1103/PhysRevE.79.061109). URL: <https://link.aps.org/doi/10.1103/PhysRevE.79.061109>.
- [67] S Joubaud, N B Garnier, and S Ciliberto. “Fluctuation theorems for harmonic oscillators”. In: *Journal of Statistical Mechanics: Theory and Experiment* 2007.09 (2007), P09018. URL: <http://stacks.iop.org/1742-5468/2007/i=09/a=P09018>.
- [68] S. Joubaud, N. B. Garnier, and S. Ciliberto. “Fluctuations of the total entropy production in stochastic systems”. In: *EPL (Europhysics Letters)* 82.3 (2008), p. 30007. URL: <http://stacks.iop.org/0295-5075/82/i=3/a=30007>.

- [69] M. Kahlen and J. Ehrich. “Hidden slow degrees of freedom and fluctuation theorems: An analytically solvable model”. In: *ArXiv e-prints* (Mar. 2018). arXiv: [1803.04740](https://arxiv.org/abs/1803.04740) [[cond-mat.stat-mech](https://arxiv.org/archive/cond)].
- [70] N.G. Van Kampen. *Stochastic Processes in Physics and Chemistry*. 3rd ed. Elsevier, 2007.
- [71] Kyogo Kawaguchi and Yohei Nakayama. “Fluctuation theorem for hidden entropy production”. In: *Phys. Rev. E* 88 (2 2013), p. 022147. DOI: [10.1103/PhysRevE.88.022147](https://doi.org/10.1103/PhysRevE.88.022147).
- [72] Kazuhiko Kinoshita et al. “A rotary molecular motor that can work at near 100% efficiency”. In: *Phil. Trans. R. Soc.* 355.1396 (2000), pp. 473–489. ISSN: 0962-8436. DOI: [10.1098/rstb.2000.0589](https://doi.org/10.1098/rstb.2000.0589).
- [73] Sudeesh Krishnamurthy et al. “A micrometre-sized heat engine operating between bacterial reservoirs”. In: *Nat. Phys.* 12 (12 2016), p. 1134. DOI: [10.1038/nphys3870](https://doi.org/10.1038/nphys3870).
- [74] R. Kubo. *Statistical Mechanics - An Adv. Course With Probs and Solns*. 7th ed. North-Holland, 1988.
- [75] R Kubo. “The fluctuation-dissipation theorem”. In: *Reports on Progress in Physics* 29.1 (1966), p. 255.
- [76] Anupam Kundu, Sanjib Sabhapandit, and Abhishek Dhar. “Large deviations of heat flow in harmonic chains”. In: *Journal of Statistical Mechanics: Theory and Experiment* 2011.03 (2011), P03007.
- [77] Jorge Kurchan. “Fluctuation theorem for stochastic dynamics”. In: *Journal of Physics A: Mathematical and General* 31.16 (1998), p. 3719.
- [78] E.M. Lifshitz L D Landau. *Statistical Physics, Third Edition, Part 1: Volume 5*. 3rd ed. Course of Theoretical Physics, Volume 5. Butterworth-Heinemann, 1980. ISBN: 0750633727,9780080230399,9780750633727,0080230393.
- [79] D. Lacoste and K. Mallick. “Fluctuation theorem for the flashing ratchet model of molecular motors”. In: *Phys. Rev. E* 80 (2 2009), p. 021923. DOI: [10.1103/PhysRevE.80.021923](https://doi.org/10.1103/PhysRevE.80.021923).

- [80] Lahiri, S. and Jayannavar, A. M. "Total entropy production fluctuation theorems in a nonequilibrium time-periodic steady state". In: *Eur. Phys. J. B* 69.1 (2009), pp. 87–92. DOI: [10.1140/epjb/e2009-00017-7](https://doi.org/10.1140/epjb/e2009-00017-7). URL: <https://doi.org/10.1140/epjb/e2009-00017-7>.
- [81] A. W. C. Lau, D. Lacoste, and K. Mallick. "Nonequilibrium Fluctuations and Mechanochemical Couplings of a Molecular Motor". In: *Phys. Rev. Lett.* 99 (15 2007), p. 158102. DOI: [10.1103/PhysRevLett.99.158102](https://doi.org/10.1103/PhysRevLett.99.158102).
- [82] Joel L. Lebowitz and Herbert Spohn. "A Gallavotti–Cohen-Type Symmetry in the Large Deviation Functional for Stochastic Dynamics". In: *Journal of Statistical Physics* 95.1 (1999), pp. 333–365. ISSN: 1572-9613. DOI: [10.1023/A:1004589714161](https://doi.org/10.1023/A:1004589714161).
- [83] J. S. Lee, Chulan Kwon, and Hyunggyu Park. "Everlasting initial memory threshold for rare events in equilibration processes". In: *Phys. Rev. E* 87 (2 2013), p. 020104. DOI: [10.1103/PhysRevE.87.020104](https://doi.org/10.1103/PhysRevE.87.020104).
- [84] Stefano Lepri, Roberto Livi, and Antonio Politi. "Thermal conduction in classical low-dimensional lattices". In: *Physics Reports* 377.1 (2003), pp. 1–80. ISSN: 0370-1573. DOI: [https://doi.org/10.1016/S0370-1573\(02\)00558-6](https://doi.org/10.1016/S0370-1573(02)00558-6). URL: <http://www.sciencedirect.com/science/article/pii/S0370157302005586>.
- [85] Ying Li et al. "How the nature of an observation affects single-trajectory entropies". In: *The Journal of Chemical Physics* 128.7 (2008), p. 074102. DOI: [10.1063/1.2828505](https://doi.org/10.1063/1.2828505).
- [86] Umberto Marini Bettolo Marconi et al. "Fluctuation–dissipation: Response theory in statistical physics". In: *Physics Reports* 461.4 (2008), pp. 111–195. ISSN: 0370-1573. DOI: <https://doi.org/10.1016/j.physrep.2008.02.002>. URL: <http://www.sciencedirect.com/science/article/pii/S0370157308000768>.
- [87] I Martinez et al. "Brownian Carnot engine". In: *Nat. Phys.* 12 (1 2016), p. 67. DOI: [10.1038/nphys3518](https://doi.org/10.1038/nphys3518).

- [88] O. Mazonka and C. Jarzynski. “Exactly solvable model illustrating far-from-equilibrium predictions”. In: *eprint arXiv:cond-mat/9912121* (Dec. 1999). eprint: [cond-mat/9912121](https://arxiv.org/abs/cond-mat/9912121).
- [89] J. Mehl et al. “Role of Hidden Slow Degrees of Freedom in the Fluctuation Theorem”. In: *Phys. Rev. Lett.* 108 (22 2012), p. 220601. DOI: [10.1103/PhysRevLett.108.220601](https://doi.org/10.1103/PhysRevLett.108.220601).
- [90] Jakob Mehl, Thomas Speck, and Udo Seifert. “Large deviation function for entropy production in driven one-dimensional systems”. In: *Phys. Rev. E* 78 (1 2008), p. 011123. DOI: [10.1103/PhysRevE.78.011123](https://doi.org/10.1103/PhysRevE.78.011123). URL: <https://link.aps.org/doi/10.1103/PhysRevE.78.011123>.
- [91] Jae Dong Noh. “Fluctuations and correlations in nonequilibrium systems”. In: *Journal of Statistical Mechanics: Theory and Experiment* 2014.1 (2014), P01013.
- [92] Yoshitsugu Oono and Marco Paniconi. “Steady state thermodynamics”. In: *Progress of Theoretical Physics Supplement* 130 (1998), pp. 29–44. ISSN: 0375-9687.
- [93] Arnab Pal and Sanjib Sabhapandit. “Work fluctuations for a Brownian particle driven by a correlated external random force”. In: *Phys. Rev. E* 90 (5 2014), p. 052116. DOI: [10.1103/PhysRevE.90.052116](https://doi.org/10.1103/PhysRevE.90.052116).
- [94] Arnab Pal and Sanjib Sabhapandit. “Work fluctuations for a Brownian particle in a harmonic trap with fluctuating locations”. In: *Phys. Rev. E* 87 (2 2013), p. 022138. DOI: [10.1103/PhysRevE.87.022138](https://doi.org/10.1103/PhysRevE.87.022138).
- [95] P. S. Pal, Sourabh Lahiri, and A. M. Jayannavar. “Transient exchange fluctuation theorems for heat using a Hamiltonian framework: Classical and quantum regimes”. In: *Phys. Rev. E* 95 (4 2017), p. 042124. DOI: [10.1103/PhysRevE.95.042124](https://doi.org/10.1103/PhysRevE.95.042124). URL: <https://link.aps.org/doi/10.1103/PhysRevE.95.042124>.
- [96] Jong-Min Park, Hyun-Myung Chun, and Jae Dong Noh. “Efficiency at maximum power and efficiency fluctuations in a linear Brownian heat-engine model”. In: *Phys. Rev. E* 94 (1 2016), p. 012127. DOI: [10.1103/PhysRevE.94.012127](https://doi.org/10.1103/PhysRevE.94.012127).

- [97] Patrick Pietzonka, Eva Zimmermann, and Udo Seifert. “Fine-structured large deviations and the fluctuation theorem: Molecular motors and beyond”. In: *EPL (Europhysics Letters)* 107.2 (2014), p. 20002.
- [98] M. Poletti and M. Esposito. “Effective fluctuation and response theory”. In: *ArXiv e-prints* (Mar. 2018). arXiv: [1803.03552](https://arxiv.org/abs/1803.03552) [[cond-mat.stat-mech](https://arxiv.org/abs/1803.03552)].
- [99] Matteo Poletti and Massimiliano Esposito. “Effective Thermodynamics for a Marginal Observer”. In: *Phys. Rev. Lett.* 119 (24 2017), p. 240601. DOI: [10.1103/PhysRevLett.119.240601](https://doi.org/10.1103/PhysRevLett.119.240601). URL: <https://link.aps.org/doi/10.1103/PhysRevLett.119.240601>.
- [100] K. Proesmans, B. Cleuren, and C. Van den Broeck. “Stochastic efficiency for effusion as a thermal engine”. In: *EPL (Europhysics Letters)* 109.2 (2015), p. 20004.
- [101] Karel Proesmans and Christian Van den Broeck. “Stochastic efficiency: five case studies”. In: *New Journal of Physics* 17.6 (2015), p. 065004.
- [102] Karel Proesmans, Bart Cleuren, and Christian Van den Broeck. “Power-Efficiency-Dissipation Relations in Linear Thermodynamics”. In: *Phys. Rev. Lett.* 116 (22 2016), p. 220601. DOI: [10.1103/PhysRevLett.116.220601](https://doi.org/10.1103/PhysRevLett.116.220601).
- [103] Karel Proesmans et al. “Brownian Duet: A Novel Tale of Thermodynamic Efficiency”. In: *Phys. Rev. X* 6 (4 2016), p. 041010. DOI: [10.1103/PhysRevX.6.041010](https://doi.org/10.1103/PhysRevX.6.041010).
- [104] A Puglisi et al. “Entropy production and coarse graining in Markov processes”. In: *Journal of Statistical Mechanics: Theory and Experiment* 2010.05 (2010), P05015.
- [105] Saar Rahav and Christopher Jarzynski. “Fluctuation relations and coarse-graining”. In: *Journal of Statistical Mechanics: Theory and Experiment* 2007.09 (2007), P09012.
- [106] Marco Ribezzi-Crivellari and Felix Ritort. “Free-energy inference from partial work measurements in small systems”. In: *Proceedings of the National Academy of Sciences* 111.33 (2014), E3386–E3394. DOI: [10.1073/pnas.1320006111](https://doi.org/10.1073/pnas.1320006111).

- [107] Hannes Risken. *The Fokker-Planck Equation: Methods of Solutions and Applications*. 2nd ed. 1989. 3rd printing. Springer Series in Synergetics. Springer, Sept. 1996.
- [108] F. Ritort. "Work Fluctuations, Transient Violations of the Second Law and Free-Energy Recovery Methods: Perspectives in Theory and Experiments". In: *Poincaré Seminar 2003, Progress in Mathematical Physics, Volume 38*. ISBN 978-3-7643-7116-6. Birkhäuser Verlag, 2004, p. 193. Ed. by J. Dalibard, B. Duplantier, and V. Rivasseau. 2004, p. 193. DOI: [10.1007/978-3-0348-7932-3_9](https://doi.org/10.1007/978-3-0348-7932-3_9).
- [109] Sanjib Sabhapandit. "Heat and work fluctuations for a harmonic oscillator". In: *Phys. Rev. E* 85 (2 2012), p. 021108. DOI: [10.1103/PhysRevE.85.021108](https://doi.org/10.1103/PhysRevE.85.021108).
- [110] Sanjib Sabhapandit. "Work fluctuations for a harmonic oscillator driven by an external random force". In: *EPL (Europhysics Letters)* 96.2 (2011), p. 20005.
- [111] Arnab Saha and A. M. Jayannavar. "Nonequilibrium work distributions for a trapped Brownian particle in a time-dependent magnetic field". In: *Phys. Rev. E* 77 (2 2008), p. 022105. DOI: [10.1103/PhysRevE.77.022105](https://doi.org/10.1103/PhysRevE.77.022105). URL: <https://link.aps.org/doi/10.1103/PhysRevE.77.022105>.
- [112] Arnab Saha, Sourabh Lahiri, and A. M. Jayannavar. "Entropy production theorems and some consequences". In: *Phys. Rev. E* 80 (1 2009), p. 011117. DOI: [10.1103/PhysRevE.80.011117](https://doi.org/10.1103/PhysRevE.80.011117). URL: <https://link.aps.org/doi/10.1103/PhysRevE.80.011117>.
- [113] M Sahoo, S Lahiri, and A M Jayannavar. "Fluctuation theorems and atypical trajectories". In: *Journal of Physics A: Mathematical and Theoretical* 44.20 (2011), p. 205001. URL: <http://stacks.iop.org/1751-8121/44/i=20/a=205001>.
- [114] O.-P. Saira et al. "Test of the Jarzynski and Crooks Fluctuation Relations in an Electronic System". In: *Phys. Rev. Lett.* 109 (18 2012), p. 180601. DOI: [10.1103/PhysRevLett.109.180601](https://doi.org/10.1103/PhysRevLett.109.180601).
- [115] Keiji Saito and Abhishek Dhar. "Generating function formula of heat transfer in harmonic networks". In: *Phys. Rev. E* 83 (4 2011), p. 041121. DOI: [10.1103/PhysRevE.83.041121](https://doi.org/10.1103/PhysRevE.83.041121).

- PhysRevE. 83.041121. URL: <https://link.aps.org/doi/10.1103/PhysRevE.83.041121>.
- [116] Shin ichi Sasa. "Possible extended forms of thermodynamic entropy". In: *Journal of Statistical Mechanics: Theory and Experiment* 2014.1 (2014), P01004. URL: <http://stacks.iop.org/1742-5468/2014/i=1/a=P01004>.
- [117] D. J. Searles and D. J. Evans. "Fluctuation Theorem for Heat Flow". In: *International Journal of Thermophysics* 22.1 (2001), pp. 123–134. ISSN: 1572-9567. DOI: [10.1023/A:1006759703505](https://doi.org/10.1023/A:1006759703505).
- [118] Debra J. Searles and Denis J. Evans. "Ensemble dependence of the transient fluctuation theorem". In: *The Journal of Chemical Physics* 113.9 (2000), pp. 3503–3509. DOI: [10.1063/1.1287424](https://doi.org/10.1063/1.1287424).
- [119] U. Seifert. "Fluctuation theorem for a single enzym or molecular motor". In: *EPL (Europhysics Letters)* 70.1 (2005), p. 36. URL: <http://stacks.iop.org/0295-5075/70/i=1/a=036>.
- [120] U. Seifert. "Stochastic thermodynamics: principles and perspectives". In: *The European Physical Journal B* 64.3 (2008), pp. 423–431. ISSN: 1434-6036. DOI: [10.1140/epjb/e2008-00001-9](https://doi.org/10.1140/epjb/e2008-00001-9).
- [121] Udo Seifert. "Entropy Production along a Stochastic Trajectory and an Integral Fluctuation Theorem". In: *Phys. Rev. Lett.* 95 (4 2005), p. 040602. DOI: [10.1103/PhysRevLett.95.040602](https://doi.org/10.1103/PhysRevLett.95.040602).
- [122] Udo Seifert. "Stochastic thermodynamics, fluctuation theorems and molecular machines". In: *Reports on Progress in Physics* 75.12 (2012), p. 126001. URL: <http://stacks.iop.org/0034-4885/75/i=12/a=126001>.
- [123] Ken Sekimoto. "Kinetic Characterization of Heat Bath and the Energetics of Thermal Ratchet Models". In: *Journal of the Physical Society of Japan* 66.5 (1997), pp. 1234–1237. DOI: [10.1143/JPSJ.66.1234](https://doi.org/10.1143/JPSJ.66.1234).
- [124] Ken Sekimoto. "Langevin Equation and Thermodynamics". In: *Progress of Theoretical Physics Supplement* 130 (1998), pp. 17–27. DOI: [10.1143/PTPS.130.17](https://doi.org/10.1143/PTPS.130.17). eprint: [/oupanbackfile/content_public/journal/ptps/130/10.1143/](http://oupanbackfile/content_public/journal/ptps/130/10.1143/)

- <https://doi.org/10.1143/PTPS.130.17>. URL: <http://dx.doi.org/10.1143/PTPS.130.17>.
- [125] Ken Sekimoto and Shin ichi Sasa. “Complementarity Relation for Irreversible Process Derived from Stochastic Energetics”. In: *Journal of the Physical Society of Japan* 66.11 (1997), pp. 3326–3328. DOI: [10.1143/JPSJ.66.3326](https://doi.org/10.1143/JPSJ.66.3326). eprint: <https://doi.org/10.1143/JPSJ.66.3326>. URL: <https://doi.org/10.1143/JPSJ.66.3326>.
- [126] Naoto Shiraishi and Takahiro Sagawa. “Fluctuation theorem for partially masked nonequilibrium dynamics”. In: *Phys. Rev. E* 91 (1 2015), p. 012130. DOI: [10.1103/PhysRevE.91.012130](https://doi.org/10.1103/PhysRevE.91.012130).
- [127] Naoto Shiraishi, Keiji Saito, and Hal Tasaki. “Universal Trade-Off Relation between Power and Efficiency for Heat Engines”. In: *Phys. Rev. Lett.* 117 (19 2016), p. 190601. DOI: [10.1103/PhysRevLett.117.190601](https://doi.org/10.1103/PhysRevLett.117.190601).
- [128] T Speck and U Seifert. “Integral fluctuation theorem for the housekeeping heat”. In: *Journal of Physics A: Mathematical and General* 38.34 (2005), p. L581. URL: <http://stacks.iop.org/0305-4470/38/i=34/a=L03>.
- [129] T. Speck et al. “Distribution of entropy production for a colloidal particle in a nonequilibrium steady state”. In: *EPL (Europhysics Letters)* 79.3 (2007), p. 30002. URL: <http://stacks.iop.org/0295-5075/79/i=3/a=30002>.
- [130] Mitsuhiro Sugawa et al. “F1-ATPase conformational cycle from simultaneous single-molecule FRET and rotation measurements”. In: *Proc. Natl. Acad. Sci.* 113 (May 2016), E2916. DOI: [10.1073/pnas.1524720113](https://doi.org/10.1073/pnas.1524720113).
- [131] Peter Talkner, Michele Campisi, and Peter Hänggi. “Fluctuation theorems in driven open quantum systems”. In: *Journal of Statistical Mechanics: Theory and Experiment* 2009.02 (2009), P02025.
- [132] Tooru Taniguchi and E. G. D. Cohen. “Inertial Effects in Nonequilibrium Work Fluctuations by a Path Integral Approach”. In: *Journal of Statistical Physics* 130.1 (2008), pp. 1–26. ISSN: 1572-9613. DOI: [10.1007/s10955-007-9398-6](https://doi.org/10.1007/s10955-007-9398-6). URL: <https://doi.org/10.1007/s10955-007-9398-6>.

- [133] Tooru Taniguchi and E. G. D. Cohen. “Nonequilibrium Steady State Thermodynamics and Fluctuations for Stochastic Systems”. In: *Journal of Statistical Physics* 130.4 (2008), pp. 633–667. ISSN: 1572-9613. DOI: [10.1007/s10955-007-9471-1](https://doi.org/10.1007/s10955-007-9471-1). URL: <https://doi.org/10.1007/s10955-007-9471-1>.
- [134] Tooru Taniguchi and E. G. D. Cohen. “Onsager-Machlup Theory for Nonequilibrium Steady States and Fluctuation Theorems”. In: *Journal of Statistical Physics* 126.1 (2007), pp. 1–41. ISSN: 1572-9613. DOI: [10.1007/s10955-006-9252-2](https://doi.org/10.1007/s10955-006-9252-2). URL: <https://doi.org/10.1007/s10955-006-9252-2>.
- [135] H. Touchette and E. G. D. Cohen. “Fluctuation relation for a Lévy particle”. In: *Phys. Rev. E* 76 (2 2007), p. 020101. DOI: [10.1103/PhysRevE.76.020101](https://doi.org/10.1103/PhysRevE.76.020101). URL: <https://link.aps.org/doi/10.1103/PhysRevE.76.020101>.
- [136] Hugo Touchette. “The large deviation approach to statistical mechanics”. In: *Physics Reports* 478.1–3 (2009), pp. 1–69. ISSN: 0370-1573. DOI: [http://dx.doi.org/10.1016/j.physrep.2009.05.002](https://doi.org/10.1016/j.physrep.2009.05.002).
- [137] Shoichi Toyabe et al. “Experimental demonstration of information-to-energy conversion and validation of the generalized Jarzynski equality”. In: *Nat. Phys.* 6 (12 2010), p. 988. DOI: [10.1038/nphys1821](https://doi.org/10.1038/nphys1821).
- [138] E. H. Trepagnier et al. “Experimental test of Hatano and Sasa’s nonequilibrium steady-state equality”. In: *Proceedings of the National Academy of Sciences of the United States of America* 101.42 (2004), pp. 15038–15041. DOI: [10.1073/pnas.0406405101](https://doi.org/10.1073/pnas.0406405101). eprint: <http://www.pnas.org/content/101/42/15038.full.pdf>. URL: <http://www.pnas.org/content/101/42/15038.abstract>.
- [139] Matthias Uhl, Patrick Pietzonka, and Udo Seifert. “Fluctuations of apparent entropy production in networks with hidden slow degrees of freedom”. In: *Journal of Statistical Mechanics: Theory and Experiment* 2018.2 (2018), p. 023203. URL: <http://stacks.iop.org/1742-5468/2018/i=2/a=023203>.
- [140] Gatien Verley, Christian Van den Broeck, and Massimiliano Esposito. “Work statistics in stochastically driven systems”. In: *New Journal of Physics* 16.9 (2014), p. 095001.

- [141] Gatién Verley et al. “Universal theory of efficiency fluctuations”. In: *Phys. Rev. E* 90 (5 2014), p. 052145. DOI: [10.1103/PhysRevE.90.052145](https://doi.org/10.1103/PhysRevE.90.052145).
- [142] Gatién Verley et al. “The unlikely Carnot efficiency”. In: *Nat. Commun.* 5 (2014), p. 4721. DOI: [10.1038/ncomms5721](https://doi.org/10.1038/ncomms5721).
- [143] Paolo Visco. “Work fluctuations for a Brownian particle between two thermostats”. In: *Journal of Statistical Mechanics: Theory and Experiment* 2006.06 (2006), P06006.
- [144] G. M. Wang et al. “Experimental Demonstration of Violations of the Second Law of Thermodynamics for Small Systems and Short Time Scales”. In: *Phys. Rev. Lett.* 89 (5 2002), p. 050601.
- [145] G. M. Wang et al. “Experimental study of the fluctuation theorem in a nonequilibrium steady state”. In: *Phys. Rev. E* 71 (4 2005), p. 046142. DOI: [10.1103/PhysRevE.71.046142](https://doi.org/10.1103/PhysRevE.71.046142). URL: <https://link.aps.org/doi/10.1103/PhysRevE.71.046142>.
- [146] Chun-Shang Wong et al. “Strongly coupled plasmas obey the fluctuation theorem for entropy production”. In: *Nat. Phys.* 14 (2017), pp. 21–24. DOI: [10.1038/nphys4253](https://doi.org/10.1038/nphys4253).
- [147] Mark Waldo Zemansky. *Heat and Thermodynamics*. 5th ed. McGraw-Hill, 1968.
- [148] R. van Zon, S. Ciliberto, and E. G. D. Cohen. “Power and Heat Fluctuation Theorems for Electric Circuits”. In: *Phys. Rev. Lett.* 92 (13 2004), p. 130601. DOI: [10.1103/PhysRevLett.92.130601](https://doi.org/10.1103/PhysRevLett.92.130601). URL: <https://link.aps.org/doi/10.1103/PhysRevLett.92.130601>.
- [149] R. van Zon and E. G. D. Cohen. “Extended heat-fluctuation theorems for a system with deterministic and stochastic forces”. In: *Phys. Rev. E* 69 (5 2004), p. 056121. DOI: [10.1103/PhysRevE.69.056121](https://doi.org/10.1103/PhysRevE.69.056121).
- [150] R. van Zon and E. G. D. Cohen. “Extension of the Fluctuation Theorem”. In: *Phys. Rev. Lett.* 91 (11 2003), p. 110601. DOI: [10.1103/PhysRevLett.91.110601](https://doi.org/10.1103/PhysRevLett.91.110601).

- [151] R. van Zon and E. G. D. Cohen. "Stationary and transient work-fluctuation theorems for a dragged Brownian particle". In: *Phys. Rev. E* 67 (4 2003), p. 046102. DOI: [10.1103/PhysRevE.67.046102](https://doi.org/10.1103/PhysRevE.67.046102).
- [152] Robert Zwanzig. *Nonequilibrium Statistical Mechanics*.